Developmental instability in lateral roots of maize : a multi-scale analysis

Beatriz Moreno-Ortega

▶ **To cite this version:**

Beatriz Moreno-Ortega. Developmental instability in lateral roots of maize : a multi-scale analysis. Vegetal Biology. Montpellier SupAgro, 2016. English. NNT : 2016NSAM0022 . tel-01568026

HAL Id: tel-01568026
https://theses.hal.science/tel-01568026

Submitted on 24 Jul 2017

HAL is a multi-disciplinary open access archive for the deposit and dissemination of scientific research documents, whether they are published or not. The documents may come from teaching and research institutions in France or abroad, or from public or private research centers.

L'archive ouverte pluridisciplinaire **HAL**, est destinée au dépôt et à la diffusion de documents scientifiques de niveau recherche, publiés ou non, émanant des établissements d'enseignement et de recherche français ou étrangers, des laboratoires publics ou privés.

Collège Doctoral du Languedoc-Roussillon

Montpellier SupAgro

THÈSE

Pour obtenir le grade de

Docteur

Délivré par le

Centre international d'études supérieures en sciences agronomiques

Montpellier

Préparée au sein de l'école doctorale GAIA

Et de l'unité de recherche LEPSE

Spécialité : **Biologie, Interactions, Diversité Adaptative des Plantes**

CNU : Physiologie

Présentée par **Beatriz MORENO-ORTEGA**

Instabilité développementale chez les racines latérales du maïs : une analyse multi-échélle

-

Developmental instability in lateral roots of maize: a multi-scale analysis

Soutenue le 12 Décembre 2016 devant le jury composé de

Marie-Béatrice BOGEAT-TRIBOULOT, Chargée de recherche, INRA	Rapporteur
Lionel DUPUY, Chercheur, James Hutton Institute	Rapporteur
Philippe HINSINGER, Directeur de Recherche, INRA	Président du jury
Loïc PAGÈS, Directeur de Recherche, INRA	Examinateur
Bertrand MULLER, Directeur de Recherche, INRA	Directeur de thèse
Yann GUÉDON, Chercheur, CIRAD	Co-encadrant

Resumé

Dans l'optique d'une seconde Révolution Verte, visant, à la différence de la première, à accroître les rendements des cultures dans un contexte de faible fertilité, les stratégies mises en place par les plantes pour une assimilation optimale des nutriments du sol se trouvent au cœur du problème. Afin de le résoudre et d'identifier les variétés idéales parmi la diversité génétique des plantes cultivées, les systèmes racinaires, leur développement et leur architecture, sont appelés à jouer le premier rôle. La variabilité au sein des racines latérales semble s'avérer une caractéristique cruciale pour l'optimisation de l'exploration du sol et de l'acquisition de ses ressources mobiles et immobiles, mais ce phénomène est encore mal appréhendé.

Le travail présenté dans cette thèse se concentre sur les racines latérales du maïs (*Zea mays L.*) dans un effort pour révéler les processus à l'origine des variations intrinsèques dans le développement racinaire. Il s'appuie en particulier sur le phénotypage des racines latérales à une échelle sans précédent, suivant la croissance journalière de milliers d'entre elles à haute résolution spatiale, pour caractériser précisément les variations spatio-temporelles entre et au sein des individus racinaires. Les profils individuels de vitesse de croissance ont été analysés à l'aide d'un modèle statistique qui a identifié trois principales tendances temporelles dans les vitesses de croissance menant à la definition de trois classes de racines latérales avec une vitesse et durée de croissance distinctes. Des différences de diamètre à l'émergence de ces racines (dont l'origine remonte au stade du *primordium*) conditionnent probablement la tendance ultérieure de croissance mais ne suffisent pas à déterminer le destin de la racine. Finalement, ces classes racinaires sont distribuées aléatoirement le long de la racine primaire, ce qui suggère qu'aucune stimulation ou inhibition locale n'existe entre racines voisines.

Pour expliquer l'origine des variations observées dans la croissance, ce travail a été complété par une caractérisation multi-échelle de groupes de racines latérales présentant une croissance distincte, à un niveau cellulaire, anatomique et moléculaire. Un effort particulier a été dirigé à l'analyse des profils de longueur de cellules dans des apex racinaires pour lequel nous avons introduit un modèle de segmentation pour identifier des zones développementales. Grâce à cette méthode, une forte modulation dans la longueur des zones de division et d'élongation a été mise en évidence, en lien avec les variations de la croissance des racines latérales. Le rôle régulateur de l'auxine sur l'équilibre entre les processus de prolifération et d'élongation cellulaire a été montré avec l'utilisation de lignées mutantes. En fin de compte, les variations de la croissance entre racines latérales sont remontées jusqu'à l'allocation d'assimilats carbonés et la capacité de transport de la racine, ce qui suggère l'existence d'un mécanisme de rétroaction qui pourrait jouer un rôle déterminant dans la mise en place de tendances contrastées dans la croissance des racines latérales.

Mots clés: système racinaire, racine latérale, *Zea mays*, pattern de croissance, meristème racinaire

Summary

In the perspective of a second Green Revolution, aiming, unlike the first one, to enhance yields of crops in a low fertility context, the strategies used by plants for an optimal uptake of soil nutrients are at the core of the problem. To solve it and identify ideal breeds among the genetic diversity of crops, plant root systems, their development and their architecture, are called upon to play the leading role. The variability among secondary roots appears as a crucial feature for the optimality of soil exploration and acquisition of mobile and immobile resources, but this phenomenon remains poorly understood.

The work presented in this thesis focuses on the lateral roots of maize (*Zea mays L.*) and attempts to unravel the processes at the origin of intrinsic variations in lateral root development. It relies notably on the phenotyping of individual lateral roots at an unprecedented scale, tracking the daily growth of thousands of them at a high spatial resolution, in order to characterize precisely the spatio-temporal variations existing both between and within root individuals. Individual growth rate profiles were analyzed with a statistical model that identified three main temporal trends in growth rates leading to the definition of three lateral root classes with contrasted growth rates and growth duration. Differences in lateral root diameter at root emergence (originating at the *primordium* stage) were likely to condition the followed growth trend but did not seem enough to entirely determine lateral root fate. Lastly, these lateral root classes were randomly distributed along the primary root, suggesting that there is no local inhibition or stimulation between neighbouring lateral roots.

In order to explain the origin of the observed differences in growth behaviour, we complemented our study with a multi-scale characterization of groups of lateral roots with contrasted growth at a cellular, anatomical and molecular level. A particular focus is set on the analysis of cell length profiles in lateral root apices for which we introduced a segmentation model to identify developmental zones. Using this method, we evidenced strong modulations in the length of the division and elongation zones that could be closely related to variations in lateral root growth. The regulatory role of auxin on the balance between cellular proliferation and elongation processes is demonstrated through the analysis of mutant lines. Ultimately, variations in lateral root growth are traced back to the allocation of carbon assimilates and the transport capacity of the root, suggesting that a feedback control loop mechanism could play a determinant role in the setting out of contrasted lateral root growth trends.

Keywords: root system, lateral root, Zea mays, growth pattern, root meristem

Acknowledgements

Je remercie les membres de mon jury de thèse, Marie-Béatrice Bogeat-Triboulot et Lionel Dupuy, rapporteurs de cette thèse, et Philippe Hinsinger et Loïc Pagès, examinateurs de cette thèse, pour le regard critique qu'ils porteront sur ce travail.

Je tiens à remercier mon directeur de thèse Bertrand Muller de m'avoir fait confiance pour réaliser une thèse sous sa direction avec un sujet si passionnant comme le sont les racines. Merci de ta disponibilité et tes conseils avisés toujours donnés dans la bonne humeur. J'ai admiré au cours de ces années ton dévouement pour la recherche et ta volonté infatigable. Merci également à Yann Guédon, mon co-encadrant, pour la pédagogie et la patience démontrées au cours de ses explications portant sur des traitements statistiques qui m'étaient souvent inconnus. Merci encore d'avoir partagé ton expertise et pour tes apports considérables à ce travail.

Tous mes remerciements aussi aux membres de mon comité de thèse Laurent Laplaze, Philippe Nacry et Xavier Draye qui ont su apporter à chaque fois un œil nouveau et encourageant sur mes recherches. Merci aussi à Christine Granier pour son rôle de médiation lors du dernier comité. Je n'oublie pas de remercier Marc Bouvy pour sa réactivité et son soutien qui m'ont aidé, à un moment critique, à retrouver la confiance nécessaire pour accomplir ce travail.

Je tiens à remercier les différentes personnes de l'équipe LEPSE qui ont contribué, chacune à leur façon, à ce travail. Un grand merci d'abord à Anaëlle pour m'avoir aidé à faire mes premiers pas avec R et, de façon plus général, pour avoir été une excellente collègue de bureau dans tous les sens du terme. Je remercie aussi Nathalie pour sa sympathie et toutes ses réponses à mes questions d'imagerie, rédaction, ou encore sur les procédures administratives dans les occasions où je n'arrivais pas à me dépatouiller toute seule. Thanks also to Joanna for sharing ideas and experiences inside and outside the lab (and for your recipe of orange soup….so delicious!). Merci également à tous les autres doctorants et chercheurs de l'équipe: Maryline, Aude, Emilie, Garance, Diane, Cecilio, Santiago, Llorenç, Denis, Christine, Andrea, Cecilia et Oscar pour contribuer à la bonne ambiance de l'équipe et à créer des moments de détente au cours des (parfois) longues journées de travail.

Je remercie spécialement mes stagiaires Guillaume, Emilie et Clara pour leur investissement et leur aide précieuse lors des expériences qui sont à l'origine de cette thèse. Merci à Cris pour les heures passées à construire les rhizotrons (et aussi à les monter, remplir, etc.) sans lesquels je pouvais dire adieu à mes expériences, et surtout pour m'arracher des rires avec ses histoires fantastiques. Un très grand merci à Gaëlle pour son abondante contribution au travail de paillasse et pour les livres qu'elle m'a fait découvrir. Merci à Myriam pour être toujours attentive à ce qui se passe dans les chambres de culture. Merci à Alex et Tony pour leur bonne compagnie et leurs échanges en matière de musique pendant les sessions d'imagerie que nous avons partagées. Merci enfin à tous ceux qui ont pris part aux expériences et/ou récoltes de façon

plus ponctuelle et que je n'ai pas encore remercié. Je pense particulièrement à Emilie (IRD) avec qui j'ai travaillé coude-à-coude à l'occasion de la Journée des Sciences…c'était un grand honneur! Je dirige un dernier remerciement aux «geeks» du LEPSE, en particulier à Jo, pour leur aide dans les situations de panne (et panique) informatique…ainsi qu'à Marie-Claude et Marie-Françoise qui m'ont toujours bien accueillie au bureau de secrétariat et aidé de bon gré dans mes démarches administratives.

J'ai eu la chance de faire des brèves mais belles collaborations avec d'autres équipes au cours de ces années. La première à Louvain-la-Neuve dans l'équipe ELIA dirigé par Xavier Draye, à qui je dois remercier pour avoir donné naissance avec Guillaume Lobet à SmartRoot, l'élégant logiciel dont je me suis servie pour obtenir toutes mes données de croissance racinaire. Je remercie aussi Benjamin et Clémentine pour leur accueil et les échanges sur les coutumes belgo-louvanistes. Merci aussi à Dimitris que j'ai croisé fortuitement à Louvain pour les bons souvenirs que je garde de cette rencontre. En second lieu, je remercie les membres de l'équipe DIADE à Montpellier pour leur appui dans les expériences d'anatomie racinaire. Merci Laurent pour son accueil et Daniel pour son aide avec le microtome. Un grand merci tout spécialement à Sixtine pour les moments passés à penser racines, écrire à quatre mains, échanger du code ou s'occuper des rhizotrons…à la fois agréables et productifs!

De plus, j'ai été amené durant la dernière période de ma thèse à travailler dans les murs de l'équipe Virtual Plants. Merci à tous les doctorants et non-permanents, même ceux qui ne sont plus là, en particulier Guillaume (Cerutti), Guillaume (Bâty), Jerôme, Eugenio, Ibrahim, Simon, Jean-Phi et Hadrien pour ce mélange extraordinaire de compétences et d'origines que vous formez. Vous me laissez des bons souvenirs que j'aurai du mal à oublier après mon départ! Merci aussi à tous les chercheurs avec qui j'ai pu échanger, en particulier Christophe (Pradal) et Fred pour son intérêt pour mes racines. Un grand merci aussi à Laurence pour son efficacité et la sympathie qu'elle a toujours montrée à mon égard.

J'aimerais aussi remercier tous mes proches qui ont vécu cette thèse en même temps que moi. Un grand merci à mes «colocs» Guillaume, Aline, Jonathan et David pour vos encouragements et pour toutes les soirées passés ensemble (de jeux, plage ou randonnée selon la saison) et à Cédric, mon prof de guitare, pour me faire déconnecter du travail et développer mon sens musical doucement mais surement. Merci à Camille, Guillaume (et Antoine) pour les relectures sur l'introduction, les soirées plancha et les conversations pleines d'enthousiasme pour l'avenir. Gracias a mis amigos Guille, Miguel, Espe y Paco por haberme proporcionado risas y apoyo en cada visita a Sevilla. Gracias a mis padres y mi hermana María por vuestro apoyo constante a pesar de la distancia. Un último pensamiento de gratitud hacia mi familia de Vitoria en especial a mi tía Yolanda por sus palabras alentadoras de cara a la lectura de la tesis.

Enfin, merci à Guillaume et son soutien sans faille. Ce travail ne serait pas le même sans toi.

Frequently Used Acronyms

D	Root diameter
DAS	Days after sowing
D_P	Diameter of the root central pith
DR5	Auxin responsive promoter
D_{ST}	Diameter of the root stele
DZ	Division zone of the root apex
$ER_{harvest}$	Root elongation rate at harvesting
EZ	Elongation zone of the root apex
gFW	Grams of fresh weight
Glc	Glucose
Glc_{conc}	Glucose concentration
L_{GZ}	Length of the root growing zone
$L_{harvest}$	Root lenght at harvesting
LR	Lateral root
LRI	Lateral root initiation
LRP	Lateral root primordium
m.a.d.	Mean absolute deviation
MZ	Mature zone of the root apex
N_{XP}	Number of xylem poles
N_{XV}	Number of xylem vessels
PCA	Principal component analysis
RCJ	Root cap junction
s.d.	Standard deviation
SMS-LM	Semi-Markov Switching Linear Model

Table Of Contents

CHAPTER I. INTRODUCTION

1 Which role for roots in global food production?

1.1 Challenges for global agriculture

Feeding the world's growing population is a major challenge today for global agriculture. Undernourishment already affected more than 1 billion people out of the total world population reaching 7 billion human beings in 2009 (FAO, 2009). The food insecurity is expected to continue and intensify in forthcoming decades. Recent estimates suggest that current crop production must be roughly doubled by 2050 to keep pace with rising food demands from current trends in population growth, dietary changes and bioenergy use (Foley *et al*., 2011). However, current yield trends are insufficient to meet projected food demands (Ray *et al*., 2013). On top of that, climate change is expected to affect negatively crop yields by increasing temperatures and water stress (St.Clair and Lynch, 2010).

Theoretically, there are two ways to increase global crop production. One way would be to increase the cropland area, a strategy known as *agricultural expansion* (Foley *et al*., 2011). But agricultural expansion may have severe implications for environment, most of all the replacement of natural ecosystems. Today, the land area dedicated to agriculture (including croplands and pastures) occupies 38% of the Earth terrestrial surface, representing the largest use of land on the planet. Much of the rest is covered by deserts, mountains, cities, and other regions unsuitable for agriculture, which places tropical forests as main targets for this practice. It is estimated that 80% of new croplands are replacing tropical forests. Yet, deforestation of tropical forests dangerously attempts against biodiversity, and is responsible of about 12% of total anthropogenic CO_2 emissions contributing to climate change (Foley *et al*., 2011). Therefore, it becomes clear that expanding agriculture in tropical regions cannot be done without harmful consequences for the global environment.

The other way to increase worldwide food production would consist in making existing lands more productive, a process referred as *agricultural intensification* (Foley *et al*., 2011). The 'Green Revolution' is a good example of production increase through agriculture intensification, which has been responsible of most of the yield increases of the past 50 years (Foley *et al*., 2011; St.Clair and Lynch, 2010). Reasons accounting for yield increases during this period were mainly the use of fertilizers, irrigation and mechanization of labor. The Green Revolution recipe was complemented by crop varieties adapted to the use of agricultural inputs, for instance, dwarf varieties with stalks that could withstand an increase in seed weight without logging (Borlaug, 2007; St.Clair and Lynch, 2010).

However, the benefits of this revolution have not been evenly distributed. The analysis of geographical patterns of major cereal crops productivity reveals large areas where yields are

still limited by suboptimal availability of water and nutrients (Mueller *et al*., 2012; York *et al*., 2013). Taking the example of maize (**Figure I-1**)**,** high-yield areas concentrate in Western Europe, Northern America and some developing countries including China or Brazil, whereas less developed nations often present yields lower than 30% of their potential (Mueller *et al*., 2012). The explanation is simple: poor farmers cannot afford to invest in fertilizers, seeds and irrigation infrastructure required to sustain yields. In consequence, the adoption of high-input agriculture has been minimal in those countries.

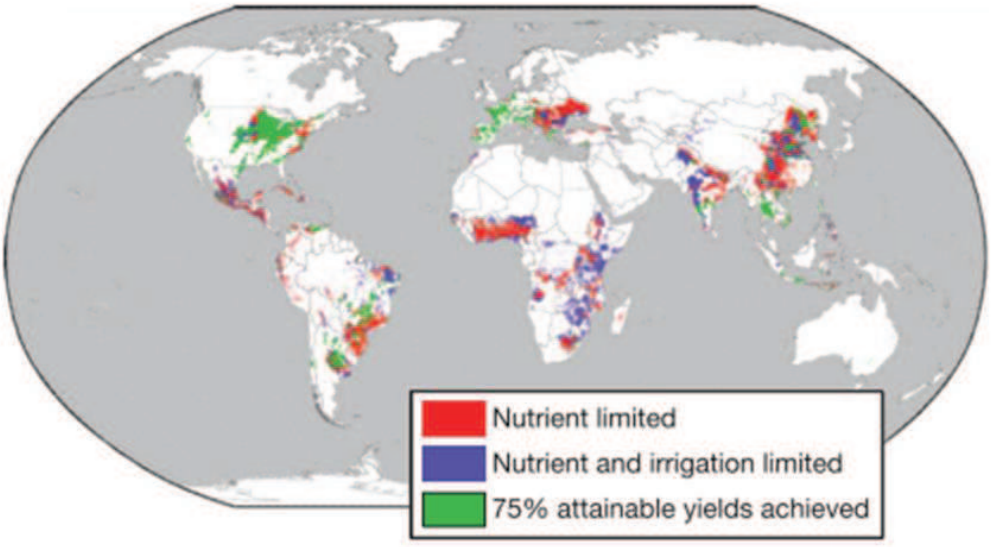

Figure I-1 Maize yield gaps. The factors that limit increasing maize crop yields to 75% of their attainable yields vary depending on planet areas and involve nutrient deficiencies and/or water limitation. Adapted from (Mueller *et al*., 2012).

In the other extreme, high-input agricultures experience diverse complications derived from the application of Green Revolution principles. Intensive irrigation has led to the depletion of natural groundwater reserves. An important fraction of nitrogen-based fertilizers is leached into the soil thereby causing water pollution (Lynch and Brown, 2012). Denitrification of nitrogen fertilizers by soil bacteria produces nitrous oxide, a major greenhouse gas. Phosphorus-based fertilizers can lead to the accumulation in soil of toxic elements such as cadmium, contained in the phosphate rock. Another worrisome problem is the increased depletion rate of non-renewable resources, such as limited phosphate deposits. These "side-effects" places the high-input agricultural system as a major force of the global environmental degradation that we experiment today.

This kind of agriculture is also heavily dependent on energy derived from fossil fuels. Taken alone, the production of ammonia fertilizers is responsible of about 5% of the global natural gas consumption (Abram and Forster, 2005). The high energy inputs required for the

production, application and distribution of fertilizers make modern agriculture vulnerable to fluctuations in fuel prices, increasing the risks of food shocks in poor communities (Bren d'Amour *et al*., 2016). In any way, finite oil reserves make high-input agriculture a non viable solution in the long term (Hopkins, 2008).

In conclusion, in spite of the important increase in crop yields achieved through the Green Revolution, it appears that the current agriculture is neither equitable, nor environmentally or energetically sustainable and needs to be transformed.

1.2 Roots for a second Green Revolution

In which direction should the efforts be addressed to improve food security? One opportunity would consist in improving food production per unit area in developing nations, where current yields are far from potential yields mainly due to low soil fertility and drought. However, the application of fertilizers at a broader scale does not constitute a feasible solution mainly because of their cost and limited availability (Lynch, 2007). What we need, in words of Jonathan Lynch, is "a second Green Revolution, which would boost yields at low fertility" (Lynch, 2007). If the Green Revolution focused on developing crops able to respond to fertilizer inputs, the second Green Revolution aims at developing crops with superior growth in low-fertility soils (**Figure I-2**).

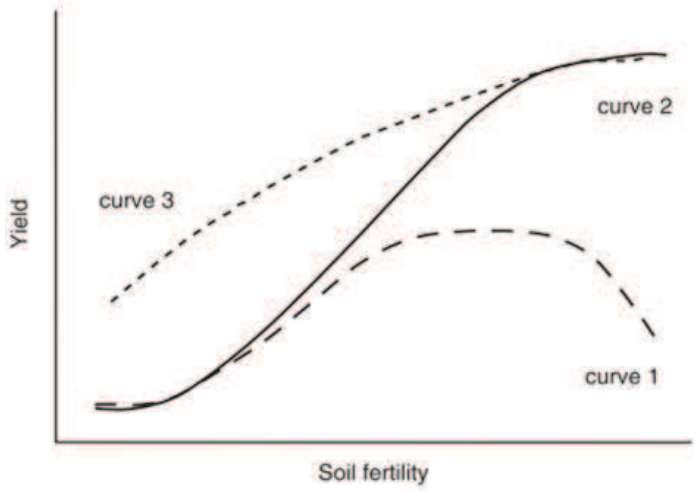

Figure I-2 Crop yield response to nutrient availability. Curve 1 represents the response of wheat and rice to nitrogen availability before the Green Revolution; yields declined at high N fertility because of lodging. Curve 2 shows the enhanced yield in high-fertility soils of dwarf (non-lodging) genotypes of wheat and rice used at the Green Revolution. Curve 3 shows enhanced crop yields across fertility levels that is the goal of the second Green Revolution (Lynch, 2007).

Since crop tolerance to low-fertility presents significant genetic variation, the idea is to exploit this potential by selecting crop traits that improve productivity in suboptimal nutrient

conditions. These new crops would have not only improved productivity in low-input systems but also decreased input requirements in high-input systems (Lynch and Brown, 2012). In complement to this breeding program, management practices to enhance and conserve soil fertility are recommended.

In this context, root traits represent an excellent target for breeding because of (i) their direct implication in the acquisition of soil resources and because (ii) they have been rarely used as selection criteria, offering a valuable pool of phenotypic variation (Lynch, 2007). Several root traits have the potential to improve the acquisition of soil resources. For example, bean genotypes with longer and denser root hairs acquire more P than plants with shorter ones (Haling *et al*., 2013), demonstrating that root hair length is important for P acquisition. Analogously, maize plants with shallower seminal roots presented greater growth in low-phosphorous soils in comparison to deep-rooted genotypes (Zhu *et al*., 2005), suggesting that the growth angle of axial roots could be an important trait for the efficiency of P uptake. Conversely, steep-angled genotypes showed higher tolerance to drought conditions, reaching deeper water resources (Ho *et al*., 2005). In conclusion, plant breeding based on root system variation is a promising avenue to generate varieties with higher efficiency of resource acquisition and thereby yields, especially under poor soil conditions.

2 Root systems and their phenotypic variation

2.1 Components of phenotypic variation: Phenotypic plasticity and developmental instability

The ability of a plant root system to acquire soil resources depends on its architecture, *i.e*. the spatial location and structure of the root axes within the soil (Fitter *et al*., 1991; Pagès *et al*., 2013a) and on its uptake properties, referring to the ability of each root segment to take up resources from soil (Clarkson, 1985).

The reasons why root architecture is important for resource uptake efficiency are multiple. First, resources are not uniformly distributed in the soil and cannot be reached with equal facility by the root system. For instance, phosphorus is more present in upper soil layers while water can be both present at depth through water table or at the surface following rains and nitrate is more associated with nitrification patches (Hodge, 2004). Moreover, nitrate can move rapidly in the soil thanks to its high diffusion coefficient while phosphate (the common form of inorganic phosphorus in soils) is poorly diffusive and demands that roots come very close to it to absorb (Nye and Tinker 1977; Fitter *et al*., 2002). Second, root systems are costly in terms of carbon assimilates. Root mass is classically 1/10 to 1/2 of total plant mass (Gregory *et al*., 1997) and it is estimated that every gram of C present in the root mass has to

be accompanied by 0.2 to 1 g of respired C (Nielsen *et al*., 1994). Any investment into the root system is at the expense of other part of the plant, in particular reproductive organs and yield. Thus, optimal resource uptake efficiencies would be achieved by absorbing the necessary resources with as little root mass as possible.

Root system architecture is known to change in situations where plants are challenged by the external or internal environment (*e.g*. nutrient availability (Zhang and Forde, 2000) or carbon status (Farrar and Jones, 1986)), a response that could affect the fitness of the plant in a resource-limited environment (Fitter *et al*., 1991). The modulation of root architecture in response to the environment is usually termed 'phenotypic plasticity' and is recognized to be a valuable adaptive trait (Crick and Grime, 1987; Drew, 1975; Giehl *et al*., 2014; Hodge, 2004, 2006). Since the root system is responsible for the acquisition of a large number of mineral resources, being able to adjust to their space-varying availability in the soil is a guarantee of survival for the plant. For instance, barley plants grown in a soil with a heterogeneous supply of phosphorus or nitrate showed a preferential development of their roots in rich areas (**Figure I-3**). This way, the plant is likely to obtain a given amount of the resource with a lower "cost" than if the root system had developed with no spatial preference. Phenotypic plasticity also has a genetic component because the response of an individual to the environment depends on its genotype (Forde, 2009).

However, there is an additional component of phenotypic variations that cannot be related to environmental or genetic causes. Maybe the clearest manifestation of this phenomenon is the large variation of lateral root lengths observed in genetically identical plants, showing up to 10-fold differences for neighboring roots, even in homogeneous conditions. These apparently unpredictable variations in root growth trajectories have been described in a diverse range of species either annuals or perennials, dicots or monocots (Freixes *et al*., 2002; Pagès, 1995). Unpredictable phenotypic variations also appear in other stages of root development such as lateral root initiation and growth duration, and have a significant impact on the final architecture of the root system.

These variations in root development have first been referred as 'developmental instability' (Forde, 2009; Mather, 1953) and have often been neglected or treated as an unwanted source of 'noise' in studies of root development. Yet, this so-called instability is an important component when building a root system including root system models, where it is impossible to achieve realistic shapes without introducing a stochastic component in root angles or growth rates of lateral roots (Pagès, 2011), as illustrates **Figure I-4**. Hereafter, we will use the term 'stochastic' as synonymous of 'unpredictable', as it is employed in (Forde, 2009) to designate a process that cause a developing trait to deviate from its expected path under a given genotypic and environmental conditions.

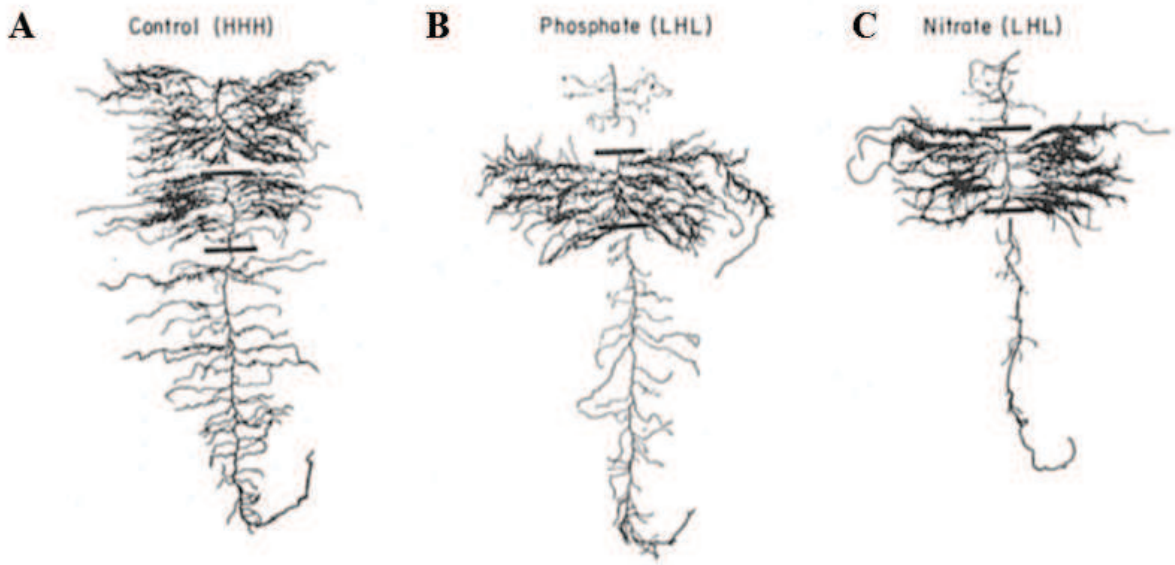

Figure I-3 Illustration of root environmental plasticity. (**A**) Control plants of barley (HHH) received a high nutrient solution to all parts of the root system. (**B**, **C**) The other plants (HLH) received the high nutrient solution only in the middle zone, the top and the bottom being supplied with a solution deficient in the specified nutrient. Adapted from (Drew, 1975).

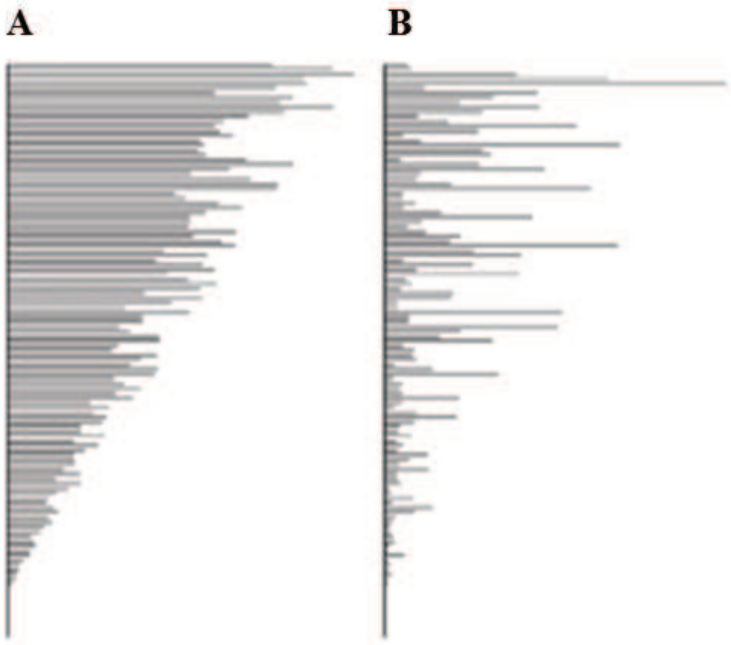

Figure I-4 Illustration of root developmental instability. Simulated root systems obtained by varying a parameter controlling the variance of the distribution of lateral root diameters, linearly related to growth rates in the model described in (Pagès, 2011). Example in (**A**) has a low variance (V=0.5) compared to example in (**B**) (V=3). Adapted from (Pagès, 2011).

2.2 Root developmental instability as a foraging strategy to optimize efficiency of resource uptake

The importance of developmental instability for the function of the root system is still poorly understood. The principal function of a root system is to acquire resources in a heterogeneous soil environment, with an unforeseeable distribution in both space and time. Since it is impossible for the growing root system to know beforehand where the resources are located, it is necessary to sample the soil for the detection of resource-rich patches: a foraging strategy is therefore required (Forde, 2009). Just as the random-walk strategy used by ant colonies searching for food patches, an indiscriminate exploration of the soil appears to be the preferred strategy to locate the unseen target. Once it is found, appropriate responses can be adopted for its exploitation, such as root proliferation in the rich zone for roots, or "telling others" by lying down pheromones in the case of ants (Forde, 2009).

The benefits obtained by exploring more soil volume must be balanced by the metabolic costs associated with the construction and maintenance of new root segments. The total cost is essentially depending on the root mass, approximately proportional to the root volume (when root tissue density is constant) (Pagès, 2014). An efficient exploration strategy should consequently explore a volume of soil with as little total root mass as possible. In this respect, it has been shown that variations in growth among lateral roots contribute to improve the efficiency of soil exploration. Lateral roots of variable lengths allow exploring a larger volume of soil than if the same cumulative root length had been produced in a deterministic way. A major reason for that is the minimization of the overlap between rhizosphere volumes of root axes so that they do not compete for the same resources (Pagès, 2011). It thus appears that some instability in root development is required for an efficient exploration of the soil. The existence of an "optimal" degree of instability, and the mechanisms at its origin are still to be determined.

2.3 Origins of root developmental instability

Developmental instability can manifest at different stages of lateral root development: (i) the initiation of the lateral root *primordium*, (ii) the development of this *primordium* (from initiation to emergence) and (iii) the elongation of the lateral root. This section aims at identifying the specific events where experimental evidence of developmental variations exists by an analysis of the existing literature on lateral root development (especially on *Arabidopsis* plant model) and to eventually propose mechanisms that could be at its origin.

2.3.1 Initiation of lateral root *primordia*

Lateral roots typically arise from pairs of pericycle founder cells (Malamy, 2005). In the radial plane, only pericycle cells adjacent to protoxylem poles can become lateral root founder cells. However, founder cell fate affects only a limited number of these cells, and their exact location in the vertical axis is difficult to predict. The analysis of lateral root spacing in *Arabidopsis* revealed 25-fold variations in the distance between successive founder cells for the col-0 accession (Dubrovsky *et al*., 2006), showing no regular pattern in lateral root spacing for this species. Significantly, no correlation was observed between this distance and the growth rate of adjacent lateral roots (Dubrovsky *et al*., 2006), suggesting that lateral root spacing have no influence on lateral root growth. The timing between two initiation events was also highly variable, ranging from 2 to 14 hours in the same experiment, indicating that neither the time elapsed from the preceding lateral root initiation nor between-lateral root distance were determinant for specifying the site of new initiations.

Despite the highly variable behavior of lateral root initiation, a certain level of structuration could be identified. For instance, the average distance between lateral roots appears to be constant for each *Arabidopsis* accession, suggesting a genetic component in the regulation of root branching (Dubrovsky *et al*., 2006; Forde, 2009). The average between-lateral distance was also found to be significantly dependent on the species in the study of (Pagès, 2014), consisting of an analysis of the branching pattern in a large panel of dicotyledonous species. In addition, the variation in parental root structure (e.g. stele diameter and number of protoxylem poles) seemed to affect the average density of lateral roots in *Banana* (Draye, 2002), indicating some predictability of the branching pattern in function of the structure of the parent root. Adding a layer of complexity, the branching pattern has also been observed to be correlated with the internal nutritional status of the plant (e.g. carbon availability of the primary root (Freixes *et al*., 2002)) and to respond locally to a variety of external stimuli (Forde and Lorenzo, 2001).

At the cellular level, the initiation of lateral root *primordia* has been proposed to be regulated by local auxin maxima. The DR5 auxin reporter expression shows roughly periodic peaks in the protoxylem cells along the elongation zone of the primary root (in a region called the 'oscillation zone') that have been proposed to provide the competence to the adjacent pericycle cells to become founder cells of lateral root *primordia* (Moreno-Risueno *et al*., 2010; De Smet *et al*., 2007). Remarkably, the frequency of DR5 signal followed a Gaussian distribution with a mean period similar to that of lateral root initiation sites (Laskowski, 2013; Moreno-Risueno *et al*., 2010). Thus, the pattern of DR5 expression appears to evidence a determinant role of auxin in the selection of founder cells and the definition of the sites of future lateral roots, at least in the *Arabidopsis* plant model.

Remarkably, the cellular patterns of lateral root initiation can substantially vary between individual *primordia*. Typically, two longitudinally adjacent pericycle cells undergo a first asymmetric division giving rise to two central short cells flanked by two longer cells (Lucas *et al*., 2013). The resulting figure is referred as the longitudinal bi-cellular type of lateral root initiation (Dubrovsky *et al*., 2000), illustrated in **Figure I-5A**. However, there is evidence that a longitudinal uni-cellular type of lateral root initiation also occur (even if rarely) in *Arabidopsis* (Dubrovsky *et al*., 2000); see **Figure I-5B**. Concerning the number of adjacent pericycle files involved in the formation of the lateral root *primordium* (i.e. those in direct contact with the protoxylem), it can range from one to three (see **Figure I-5C** for illustration), indicating that two nascent lateral organs may already differ in the number of pericycle cells recruited both longitudinally and radially to form the original group of founder cells. It is possible that cellular differences in the perception or sensitivity to auxin are at the origin of the different patterns of lateral root initiation.

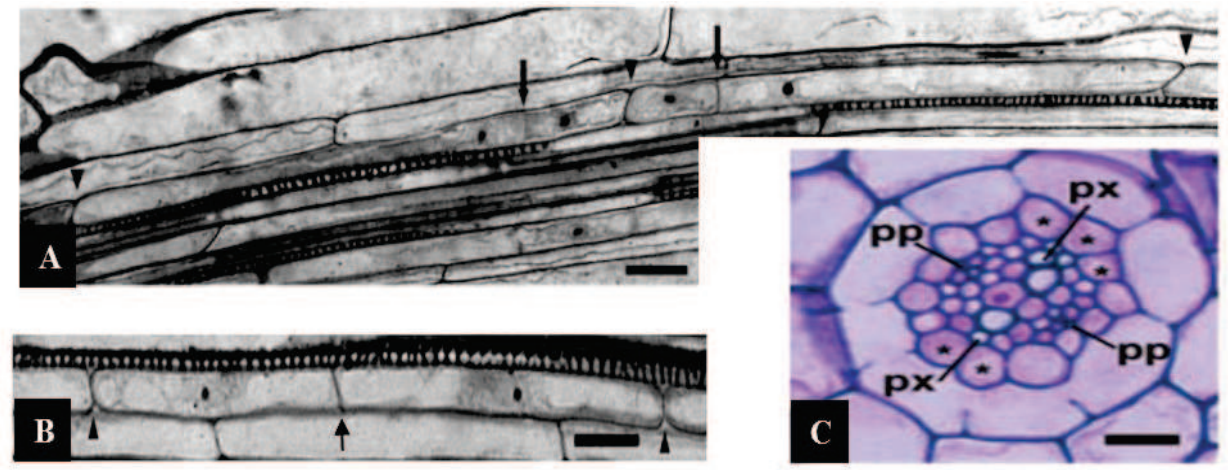

Figure I-5 Longitudinal and radial variants in the number of pericycle founder cells involved in lateral root initiation (LRI) in *Arabidopsis*. (**A**) The longitudinal bi-cellular type of LRI is characterized by synchronous asymmetrical cell divisions in two adjacent cells of the same file. (**B**) The longitudinal uni-cellular type of LRI occurs when only one pericycle cell becomes a founder cell for the entire longitudinal extent of the *primordium*. (**A**, **B**) *Arrowheads* indicate end cell walls of pericycle founder cells (convex); *arrows* indicate position of cell walls resulting from the anticlinal division of founder cells (not-convex). (**C**) The number of pericycle files that are in direct contact with the protoxylem (*asterisks*) can be one (not shown), two, or three. *pp* protophloem, *px* protoxylem. Bars= 20 µm (**A**, **B**), 10 µm (**C**). Adapted from (Dubrovsky *et al*., 2001).

2.3.2 Development of lateral root *primordia*

The morphogenesis of lateral root *primordia* has been extensively studied in *Arabidopsis* (Dubrovsky *et al*., 2001; Lucas *et al*., 2013). After founder cell specification, a coordinated sequence of periclinal and anticlinal divisions follows leading to the formation of a small

dome-shaped organ. The activation of the cell division program seems to be genetically separable from the acquisition of founder cell identity (Dubrovsky *et al*., 2008).

Several developmental stages (from I to VII) are defined in function of the increasing number of cell layers of the lateral root *primordium* (Malamy and Benfey, 1997). Interestingly, the pattern of cell divisions in lateral root *primordium* development is not unique as revealed by the variable number of cells among different *primordia* at the same stage (Lucas *et al*., 2013), showed in **Figure I-6**. The overlap observed in the ranges of cell number between two consecutive developmental stages strongly suggests that cell divisions in lateral root *primordia* do not follow a stereotypical sequence.

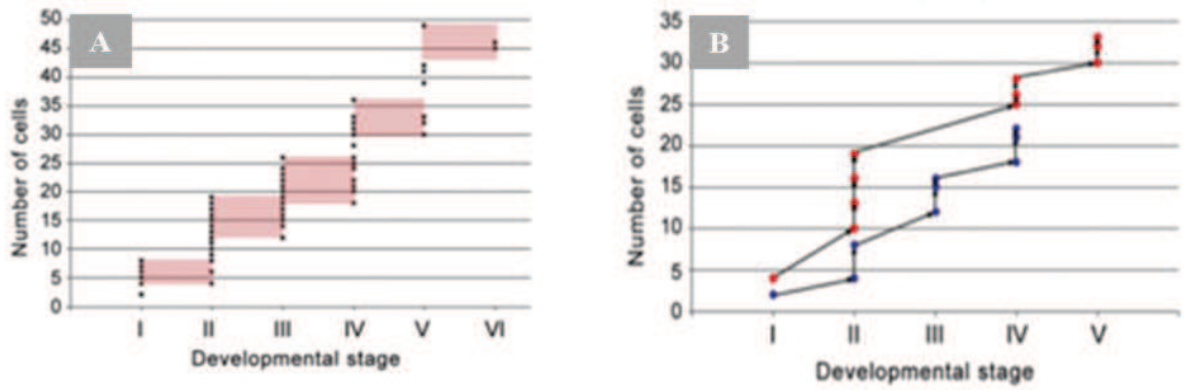

Figure I-6 The pattern of cell divisions in lateral root *primordium* (LRP) development is not stereotypical. (**A**) Number of cells in LRP median slices as a function of the developmental stage. Overlaps between stages are highlighted in red. (**B**) Developmental paths of two distinct LRP (red or blue dots). Adapted from (Lucas *et al*., 2013).

Although the shape of the lateral root *primordium* in this study was considered as highly regular (Lucas *et al*., 2013), significant deformations have been found quite often in *Arabidopsis* plants (19% of 756 *primordia* analysed) such as a lack of symmetry in relation to the *primordium* axis or a flattened surface of the dome (Szymanowska-Pulka, 2013).

Lastly, developing lateral root *primordia* must pass through several parental tissues to emerge. However, not all *primordia* reach this step (Dubrovsky *et al*., 2006; Lucas *et al*., 2008). The emergence of the lateral root *primordium* requires a coordinated separation of outward, adjacent cell layers to minimize the damage of parental tissues (Péret *et al*., 2009). Remarkably, abnormal shapes reported in the study of Szymanowska-Pulka (2013) were usually observed in *primordia* that had not emerged outside the parent root surface, suggesting that both the shape and emergence of the lateral root *primordium* is affected by the overlying tissues of the parent root (Lucas *et al*., 2013; Szymanowska-Pulka, 2013). The

coordination between the progression and emergence of the lateral root *primordium* was confirmed in *lax3 Arabidopsis* mutant, where the inhibition of lateral root *primordium* emergence was accompanied by an increased proportion of stage I *primordia* (Swarup *et al.*, 2008). This mutant failed to express several cell-wall remodeling enzymes necessary for the loosening and separation of overlying tissues during lateral root *primordium* emergence. Lateral root *primordium* morphogenesis therefore appears to be orchestrated by mechanical signals between the developing organ and the parental tissues.

The idea has already been put forward that auxin could play a determinant role in lateral root *primordium* morphogenesis, supported by the observation of aberrant root morphologies in a number of auxin-related *Arabidopsis* mutants (Szymanowska-Pulka, 2013). Combined with recent experimental evidence of auxin distribution being sensitive to mechanical stresses (Nakayama *et al.*, 2012), these findings evoke a mechano-induced, auxin-regulated *primordium* development.

2.3.3 Elongation of lateral roots

As previously mentioned, large variations in root length and growth rate are found between lateral roots even of similar ages. The range of these variations within a given species depends on the branching order (Pagès *et al.*, 1993). For instance, in peach trees, growth rates of first-order laterals (i.e. those directly attached to the primary root) located at 20-40 cm from the base ranged from 0 to 6 mm d^{-1} for the longest roots, while for second-order lateral roots the maximal growth rates were up to about 3 mm d^{-1} as illustrated in **Figure I-7**. A decreasing trend in growth rate from lower to higher branch orders has also been reported for other species (Riedacker *et al.*, 1982; Varney *et al.*, 1991). Interestingly, the extent of growth differences between successive branching orders is not the same for one species to another. For example, greater reductions in growth rate with branching order have been observed for maize (Varney *et al.*, 1991) or oak (Riedacker *et al.*, 1982), characterized by highly hierarchized root systems (Pagès *et al.*, 1993). Therefore, branching order appears as an important factor structuring root growth variations.

A spatial gradient in first-order lateral root growth has also been underlined, with growth rates that decrease from the base to the apex of the taproot (for peach (Pagès *et al.*, 1993); for pea (Yorke, J. S., Sagar, 1969); and for sunflower (Aguirrezabal *et al.*, 1994)). This suggests a preference for the plant to fulfill the growth demand of the branching organs located closer to the base, a phenomenon commonly observed in shoots where it is referred as ‘basitony’ (Pagès *et al.*, 1993).

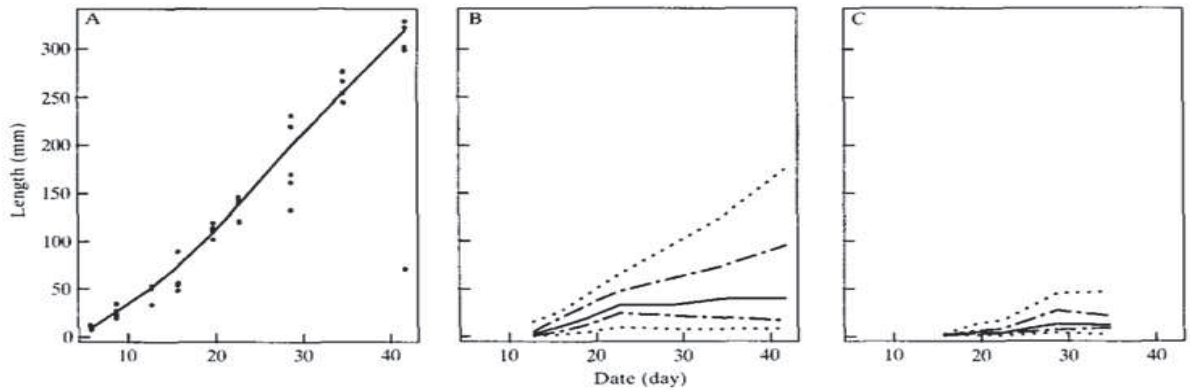

Figure I-7 Evolution of the length of taproots (A) and first (B) and second-order (C) lateral roots of peach trees with time. For the first (**B**) and second (**C**) orders, lines represent the evolution of the 5, 25, 50, 75 and 95% quantiles of root length. Adapted from (Pagès *et al*., 1993).

Variations in growth rates are also linked to root morphological characteristics (Fitter, 1987). In this regard, many authors have reported a positive correlation between growth rates and root diameter in species as diverse as barley (Hackett and Rose, 1972) and oak (Pagès, 1995). This correlation reflects the tendency of thicker roots to elongate faster than thinner ones. Still, large variations in growth rate exist between roots of a given diameter so the apical root diameter must be viewed as an indicator of the potential rather than the actual growth rate of the root, as illustrates **Figure I-8**. The relationship between diameter and growth rate can be interpreted by considering that a larger root tip may contain more dividing cells (Pagès, 1995) that result in a higher rate of organ growth when these cells fully elongate.

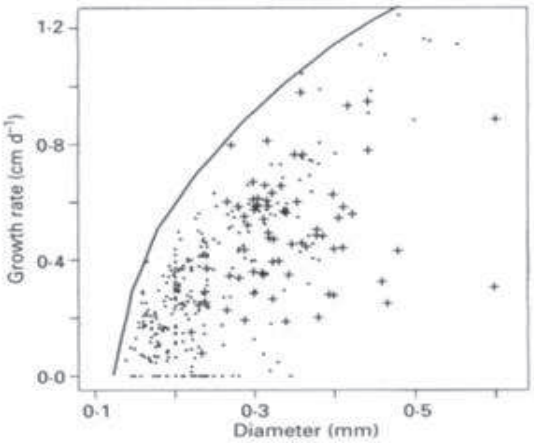

Figure I-8 Relationship between the apical diameter and root growth rate. The hand-drawn line (upper limit of the scatter plot) illustrates a potential growth rate allowed by a given diameter. Early growth points are highlighted (+), representing the growth of young roots during the first 2 days after emergence. Adapted from (Pagès, 1995).

In addition, root growth can be affected by the environment and the plant nutritional status. For example, the growth rate of primary roots in plants exposed to different irradiance is related to their apical sugar content (Freixes *et al.et al.*, 2002; Muller *et al.*, 1998; Willaume and Pagès, 2011), suggesting that the primary root growth is limited by the availability of carbon assimilates. It would therefore be of great interest to investigate the importance of the availability of carbohydrates in the variation of lateral root growth.

At the organ scale, the length of the growing zone of the root (comprising the meristem and the elongation zone) is an important factor to explain the heterogeneity of growth rates. To a lesser extent, growth rates are impacted by the rate of elementalgrowth, reflecting the rate of cell elongation per unit of length in the growing zone (Baskin, 2013; Beemster and Baskin, 1998). For an idealized growing zone within which the growth process is maintained constant, the root growth rate is equal to the product of the length of the growing zone and its rate of elemental growth. Real root growing zones are more complex and the rate of elemental growth might vary spatially along this zone (Baskin, 2013). The exact computation of the rate of root growth would then require integrating both variables. However, approximating it by the maximal rate of elemental growth multiplied by the length of the growing zone was already enough to explain 95% of growth rate variations in the case of poplar lateral roots grown in hydroponics (Bizet, 2014).

Moreover, within a root, growth rates may vary with time during the whole life of the root (Pagès, 1995). Both increasing or decreasing growth trajectories has been described (Beemster and Baskin, 1998; Pagès, 1995). The adjustment in growth rates may allow growing organs to adapt to environmental changes (Baskin, 2013), as illustrated by the response of a *Pinea* roots to various levels of water-deficit stress in

Figure I-9 (Triboulot *et al.*, 1995).

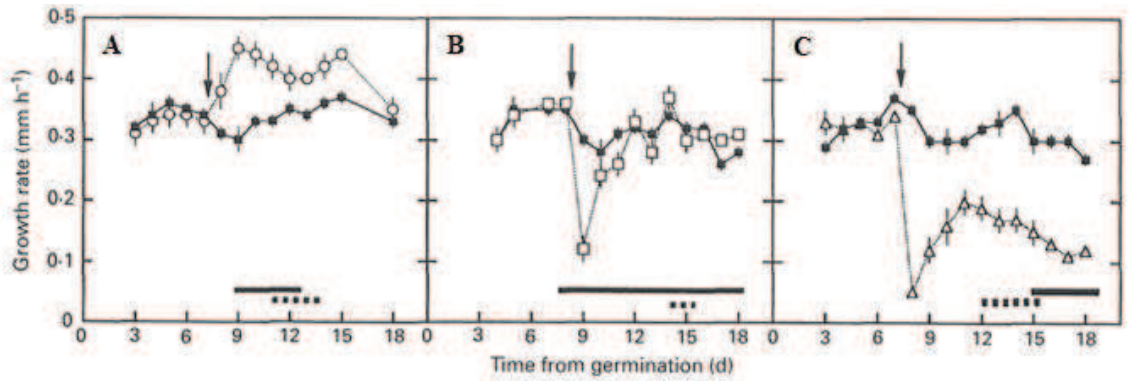

Figure I-9 Growth response of *Pinus pinaster* primary roots to several osmotic stresses: (**A**) 0.15 MPa; (**B**) 0.45 MPa and (**C**) 0.66 MPa. White symbols indicate means of seedlings receiving the treatment; black

symbols are used for control seedlings. The arrow indicates the onset of the stress treatments. Adapted from (Triboulot *et al*., 1995).

Based on the previously described relationship in which the root growth rate is the integral of elemental growth over the span of the growing zone, there are two ways in which a root can change its growth rate: by changing (either or both) the length of the growing zone or the intensity of growth. For example, a change in the intensity of cell elongationcan be achieved by making cell walls looser or tighter (Baskin, 2013).

Changes in the boundary of the growing zone have frequently been reported in response to various stresses; including water deficit (Triboulot *et al*., 1995) or P deficiency (Ma *et al*., 2003). Likewise, a reduction in the length of the growing zone occurs in *Arabidopsis* roots treated with auxin (Rahman *et al*., 2007) or cytokinins (Dello Ioio *et al*., 2007). In contrast, responses in which elemental growth rates varies without a change in the length of the growing zone are rare. Similarly to elemental growth rates, cell division rates appear to be approximately constant in a wide range of contexts, meaning that the variations in root growth rates are essentially related to the variation in the length of the growing zone (Baskin, 2000).

The emerging picture is that the flexibility of the length of the growing zone constitutes a major regulatory process of organ growth. It has been recently proposed that changing the rates of cellular processes (division or elongation) might entail unwanted changes to other linked cellular activities, affecting negatively the plant homeostasis (Baskin, 2013). In contrast, local changes in the number of dividing cells (and hence in the length of the meristem if we consider a constant meristematic cell length) might be more easy to control, without affecting the canonical programs of cell division and expansion that remain the same for each cell (Baskin, 2013). This highlights the importance of three spatial boundaries for determining the rate of root growth: (i) where the zone of elongation begins, (ii) where it ends, and (iii) where cell division ends (Baskin, 2013). How these boundaries are regulated and positioned at the root individual scale remains to be elucidated.

2.4 Signaling clues involved in lateral root development

The reason why a lateral root ceases elongating or not is unknown although few hormonal checkpoints that determine *primordia* and lateral root fate have yet been identified. Auxin is clearly involved in the recruitment of pericycle cells at the early stages of *primordia* initiation (Boerjan *et al*., 1995). Meristem activation also depends on auxin as shown by the *alf3* mutation that arrest root elongation just at emergence and is restored by exogenous application of auxin (Celenza *et al*., 1995). Moreover, the activation of the young lateral root just near emergence was recently shown to be inhibited by abcisic acid, in an auxin-independent pathway (De Smet *et al*., 2003). Information on hormones and genes involved in

the response of root architecture to abiotic stresses is scarce. The *Arabidopsis* ANR1 MADS box is needed for the increase of lateral root elongation in nitrate rich patches (Zhang and Forde, 1998) and this response is absent in an auxin resistant mutant. The LIN1 gene was shown to be associated with the early cessation of lateral root elongation in case of high sucrose to nitrogen concentration in the medium (Malamy and Ryan, 2001).

Beside this incomplete molecular and hormonal network, there is now growing evidence that sugars have important signaling properties not only on the regulation carbon metabolism enzymes (Xu *et al*., 1996) but also on processes such as stress responses, growth and morphogenesis (Rolland *et al*., 2002). The action of sugars as morphogens is suggested by independent information such as the correlation between local sugar concentration and mitotic activities in vicia faba embryo (Borisjuk *et al*., 1998), the differential regulation of D-type cyclins by sugars (Riou-Khamlichi *et al*., 2000) and the sugar controlled expression of spatially distinct genes potentially involved in apical meristem functioning (Pien *et al*., 2001). Heterotrophic roots strongly depend on the continuous supply of C skeleton and earlier work by Farrar and Jones (1986) showed how root architecture can be strongly altered by the carbon status of the plant.

Bingham and Stevenson (1993) suggested this effect is probably caused by a signal (rather than a substrate) effect of sugars. Consistently, elongation rates of both primary and secondary roots (Freixes *et al*., 2002; Muller *et al*., 1998) as well as *primordia* density (Bingham I. J., 1998; Freixes *et al*., 2002) are strongly related with local sugar concentration. Moreover, the relationship between lateral root elongation rate and local hexose concentration accounted for differences in elongation rate among lateral roots within a single plant (Freixes *et al*., 2002). Carbohydrates could act through their effect on cell division. Indeed, in excised roots, the passage through G1-S and G2-M steps is controlled by carbohydrate provision (Van't Hof, 1968). Moreover, the proliferative fraction of root cells (ie those engaged in the cell cycle) increases with root elongation rate as sucrose concentration supplied to the medium increases (Scandeg and McLeod, 1976). In Vicia faba seeds, the mitotic activity is strongly related to the hexoses content of the medium in which the embryo is bathing and the relationship accounts for spatial differences (Borisjuk *et al*., 1998). Finally, D-type cyclin shows a sugar-dependence expression (Riou-Khamlichi *et al*., 2000).

2.5 Modelling root growth variations

2.5.1 Various modelling approaches of the root growth variations

Modelling root growth variations is a main objective included in the models of the root system architecture, since growth variations influence both the colonized volume and the colonization density within this volume. In particular, functional structural plant models (FSPMs) provide a frame to simulate root growth combining a representation of the 3D structure of the plant root system with a description of physiological or environmental processes operating at different scales of space and time (Sievänen *et al*., 2014).

In the first 3D models of the root system architecture (e.g. Rootmap by Diggle (1988); Sarah by Pagès and Aries (1988); Simroot by Lynch *et al*. (1997)), the branching order was the key parameter modulating growth rates. It was assumed that all roots having the same branching order had the same constant growth rate (given as a fixed parameter). Thus, they did not represent the existing growth variability within each branching order. This modelling strategy was justified by the fact that several species exhibit a marked hierarchy between branching orders, especially among cereals. For example, seminal and nodal roots have high and continuous growth rate during the season, while roots of high branching order have both a slow and ephemeral growth activity. These models considered implicitly that additional growth rate variations originated from the heterogeneous soil conditions.

Later on, in more recent models, Pagès *et al*. proposed to include stochastic patterns of root growth in their models (Pagès *et al*.(1989) on maize; Pagès *et al*.(1992) on peach tree). The main reason to represent this variability was that the lateral roots branched on the same primary root tend to exhibit large variations in their growth patterns, and this fact could be observed even in homogeneous media. The point was supported by many references on different species, reported by various authors, as presented in **section 2.1**. Thus, instead of giving fixed growth characteristics to the roots at each branching order, growth attributes were drawn in distributions for each root during the simulation. A different distribution was given for each branching order. Lognormal distributions were used to account for the right-skewness of the length distributions of roots. There are usually a large number of short roots and a low number of long roots.

A different approach was followed by Jourdan *et al*. to simulate the root development of palm trees (Jourdan and Rey, 1997; Jourdan *et al*., 1995). The original point was to define several types of roots instead of using branching orders. These types were categories which group the roots with homogeneous developmental characteristics. In their model (Jourdan and Rey, 1997), a given root (belonging to a given type) can give rise (by branching) to different root types according to a stochastic process. The formalism is that of Markov processes, using a matrix of transition probabilities as model parameters. In this model, each root type is given a set of growth and branching parameters as well as a set of transition probabilities towards

other types. This model is very flexible, but it requires a large number of parameters, if the number of considered root types is large.

Similarly, the generic model RootTyp (Pagès *et al*., 2004) considered root types instead of root branching orders. However, in the RootTyp model, a root type represents a category of roots whose growth rate and branching density follow given distributions (whose characteristics are given as model parameters). During the simulation of the root system, each root is given a type according to its origin (seminal, adventitious, lateral branch) and to the type of its parent root (for lateral roots). The stochastic aspects of this model come from the growth attributes which are drawn from distributions, one for each type, and from the fact that lateral roots can be of different types. For example, it is possible to simulate that among the lateral roots of a nodal cereal root, 80% will be short roots with a given distribution of growth characteristics, and 20% will be long roots with another distribution of growth characteristics. The overall growth distribution of these lateral roots is the mixture of these growth distributions with the pre-defined proportions.

In order to reduce the complexity of the model and the number of parameters, Pagès *et al*. (2013a) proposed a simpler model (called Archisimple) in which the number of root types was restricted. The roots can be either seminals, adventitious or laterals. In this case, stochastic growth was rendered as the result of the stochastic attribution of apical diameter to each root at emergence. Both the potential growth rate and the growth duration were assumed to be linked to diameter. For the lateral roots, diameter was drawn using a Gaussian distribution whose mean and standard deviation depended on the diameter of the parent root. All roots in the root system shared the same set of parameters. This model was calibrated on several different species coming from various plant families (among monocots and dicots).

In a slightly different way, Pagès *et al*. (2013b) suggested to consider two successive steps during root development to quantify and simulate growth variations among the lateral roots. The first step is the definition of a growth potential during the development of the *primordium*. This first step is eventually reflected by the apical diameter of the root at emergence. It depends on the size of the mother root. Therefore, each root transmits a growth potential to its laterals. The second step is the root elongation phase. During this phase, each root has a given daily probability of stopping growth which increases with age and decreases with diameter. In their paper, Pagès *et al*. (2013b) showed the important consequences of this stochastic approach on the architecture of the overall root system.

2.5.2 Towards a spatio-temporal analysis of root growth and root system architecture

In parallel, branching patterns of shoots have been investigated for a long time (*e.g*. Guédon *et al*., 2001) focusing mainly on the spatial dimension. More recently, the development of

trees over several years have been investigated (Costes and Guédon, 2012; Guédon *et al*., 2007; Taugourdeau *et al*., 2015) taking account of both the spatial and temporal dimensions and incorporating in some cases the influence of climatic factors and inter-individual heterogeneity (Chaubert-Pereira *et al*., 2009; Taugourdeau *et al*., 2011).One strength of these spatio-temporal analyses of the development of the aerial part of plants was the identification of unexpected developmental patterns such as the ontogenetic growth component of temperate trees structured as a succession of stationary phases separated by jumps of high amplitude instead of trends corresponding to gradual changes of the growth level (Guédon *et al*., 2007). With such spatio-temporal analyses of plant phenotyping data, it was also possible to compare genotypes (Costes and Guédon, 2012; Dambreville *et al*., 2015; Lièvre *et al*., 2016) and to quantify the influence of the environment (Chaubert-Pereira *et al*., 2009; Dambreville *et al*., 2015; Taugourdeau *et al*., 2011, 2015) on a renewed basis. Such spatio-temporal analysis frameworks could be transposed to root phenotyping data in order to identify developmental patterns and to assess the influence of genotypic or environmental factors on such patterns. The first results obtained concerned mainly root branching (Jourdan *et al*., 1995; Lucas *et al*., 2008).

3 Objectives of this thesis

Looking at the spectrum of lateral root fates within a root system, it is legitimate to wonder which processes have been carried out differently between a short and early arrested root and a long vigorous one. In particular, are lateral roots with such contrasted growth trajectories different in terms of vascular structure, meristematic activity, metabolic state or even genetic expression?

The purpose of this thesis was to investigate specifically the origin of growth rate variations among first-order lateral roots by (i) a detailed characterization of the lateral root growth rate profiles in maize root systems and (ii) the analysis of several potential determinants of lateral root growth variations at the organ, cellular and molecular scales. In the context of this work, the availability of auxin and carbohydrates were selected as major molecular candidates potentially regulating the variations in growth rate among lateral roots.

Maize plants (*Zea mays spp*.) provided a convenient experimental model for different reasons.

(1) Wide variations in first-order lateral root growth can be observed and quantified in maize root systems using 2D rhizotrons;
(2) Maize lateral root diameters are large enough to be measured upon imaging with a high resolution scan;

(3) Maize has an important agronomical interest, having the highest worldwide production of all the cereals, with 817 million tones being produced in 2009 (FAOSTAT).

The organization of chapters is the following:

Chapter II describes a phenotyping pipeline used to generate spatio-temporal data of lateral root development and the approach used to analyze them, relying on recent progresses in statistics for spatio-temporal data (Cressie and Wikle, 2011), pattern recognition and machine learning (Bishop, 2006; Grenander and Miller, 2006). Besides, the spatial positioning of lateral roots along the primary root is investigated to evidence the potential local dependencies between root growth and root spacing. Results on maize are presented in parallel with results obtained on pearl millet (*Pennisetum glaucum*) on the basis of similar phenotyping data. In both cases, they are put in relation to data of root anatomy. At the end of this chapter, the framework developed for the analysis of growth profiles is extended to different experimental conditions supposed to affect the amount of either carbohydrates or auxin available for lateral roots.

Chapter III presents an analysis of cell length data in root apices in a set of lateral roots with contrasting growth, in the reference genotype B73xUH007 but also in two auxin signaling mutants. It proposes a segmentation method that aims at identifying homogeneous developmental zones in individual root apices based on the epidermal cell length profiles.

Chapter IV investigates several factors that may be at the origin of instability in lateral root development. All results in this chapter essentially refer to the B73xUH007 genotype. We present quantitative measures of the differences encountered among a representative population of lateral roots across several complementary scales:

1. Early lateral root development (*primordium* stage);
2. Anatomical lateral root structure and how it changes along the root axis;
3. Cell length patterning within the growing zone of lateral roots;
4. Carbohydrate content and how it is distributed along lateral root apices;
5. Gene expression on lateral root apices, particularly of genes responding to auxin or carbohydrates availability.

Finally, **Chapter V** provides a general discussion of key findings obtained in this thesis. We combine all the different scales and discuss the possible contribution of each studied process to the observed variation in lateral root growth in an attempt to give an integrated view of lateral root development and its variations.

Authors contributions

Beatriz Moreno-Ortega[1,2], Loïc Pagès[3], Philippe Nacry[4], Xavier Draye[5], Yann Guédon[2] and Bertrand Muller[1]

[1]INRA, UMR LEPSE, 34060 Montpellier, France

[2]CIRAD, UMR AGAP and Inria, Virtual Plants, 34095 Montpellier, France

[3]INRA, Centre d'Avignon, UR 1115 PSH, Site Agroparc, 84914 Avignon Cedex 9, France

[4]INRA, UMR BPMP, 34060 Montpellier, France

[5]UCL, Laboratory of Crop Physiology and Plant Breeding (ECOP-GC), Belgium

Acknowledgements

I would like to thank Loïc Pagès for providing a clear chronological description of the approches used in root system modelling that we included in this introduction. This work was supported by the European Union in the frame of the EURoot project and the French National Institute for Agricultural Reseach (INRA, Environment and Agronomy division).

Chapter References

Abram, A., and Forster, D. L. (2005). *A Primer on Ammonia, Nitrogen Fertilizers, and Natural Gas Markets*.

Aguirrezabal, L. A. N., Deleens, E., and Tardieu, F. (1994). Root elongation rate is accounted for by intercepted PPFD and source-sink relations in field and laboratory-grown sunflower. *Plant, Cell Environ*. 17, 443–450. doi:10.1111/j.1365-3040.1994.tb00313.x.

Baskin, T. I. (2000). On the constancy of cell division rate in the root meristem. *Plant Mol. Biol*. 43, 545–554. doi:10.1023/A:1006383921517.

Baskin, T. I. (2013). Patterns of root growth acclimation: Constant processes, changing boundaries. *Wiley Interdiscip. Rev. Dev. Biol*. 2, 65–73. doi:10.1002/wdev.94.

Beemster, G. T., and Baskin, T. I. (1998). Analysis of cell division and elongation underlying the developmental acceleration of root growth in Arabidopsis thaliana. *Plant Physiol*. 116, 1515–1526. doi:10.1104/pp.116.4.1515.

Bingham I. J. (1998). Relationships between tissue sugar content, phloem import and lateral root initiation in wheat. *Physiol. Plant*. 103, 107–113.

Bingham, I. J., and Stevenson, E. A. (1993). Control of root growth: effects of carbohydrates on the extension, branching and rate of respiration of different fractions of wheat roots. *Physiol. Plant*. 88, 149–158. doi:10.1111/j.1399-3054.1993.tb01772.x.

Bizet, F. (2014). Division et élongation cellulaire dans l'apex de la racine : diversité de réponses au déficit hydrique. 1–100.

Boerjan, W., Cervera, M. T., Delarue, M., Beeckman, T., Dewitte, W., Bellini, C., et al. (1995). Superroot, a recessive mutation in Arabidopsis, confers auxin overproduction. *Plant Cell* 7, 1405–19. Available at: http://www.pubmedcentral.nih.gov/articlerender.fcgi?artid=160963&tool=pmcentrez&rendertype=abstract.

Borisjuk, L., Walenta, S., Weber, H., Mueller-Klieser, W., and Wobus, U. (1998). High-resolution histographical mapping of glucose concentrations in developing cotyledons of Vicia faba in relation to mitotic activity and storage processes: Glucose as a possible developmental trigger. *Plant J*. 15, 583–591. doi:10.1046/j.1365-313X.1998.00214.x.

Borlaug, N. (2007). Feeding a hungry world. *Science* 318, 359. doi:10.1126/science.1151062.

Bren d'Amour, C., Wenz, L., Kalkuhl, M., Steckel, J. C., and Creutzig, F. (2016). Teleconnected food supply shocks. *Environ*. *Res*. *Lett*. 11, 035007. doi:10.1088/1748-9326/11/3/035007.

Celenza, J., Grisafi, P. L., and Fink, G. R. (1995). A pathway for lateral root formation in Arabidopsis thaliana. 2131–2142.

Chaubert-Pereira, F., Caraglio, Y., Lavergne, C., and Guédon, Y. (2009). Identifying ontogenetic, environmental and individual components of forest tree growth. *Ann*. *Bot*. 104, 883–896. doi:10.1093/aob/mcp189.

Clarkson, D. T. (1985). Factors Affecting Mineral Nutrient Acquisition by Plants. *Annu*. *Rev*. *Plant Physiol*. 36, 77–115. doi:10.1146/annurev.pp.36.060185.000453.

Costes, E., and Guédon, Y. (2012). Deciphering the ontogeny of a sympodial tree. *Trees - Struct*. *Funct*. 26, 865–879. doi:10.1007/s00468-011-0661-8.

Crick, J. C., and Grime, J. P. (1987). Morphological plasticity and mineral nutrient capture in two herbaceous species of contrasted ecology. *New Phytol*. 107, 403–414. doi:10.1111/j.1469-8137.1987.tb00192.x.

Dambreville, A., Lauri, P. É., Normand, F., and Guedon, Y. (2015). Analysing growth and development of plants jointly using developmental growth stages. *Ann*. *Bot*. 115, 93–105. doi:10.1093/aob/mcu227.

Diggle, A. J. (1988). ROOTMAP-a model in three-dimensional coordinates of the growth and structure of fibrous root systems. *Plant Soil* 105, 169–178. doi:10.1007/BF02376780.

Draye, X. (2002). Consequences of root growth kinetics and vascular structure on the distribution of lateral roots. *Plant, Cell Environ*. 25, 1463–1474. doi:10.1046/j.0016-8025.2002.00924.x.

Drew, M. C. (1975). Comparison of the effects of a localized supply of phosphate, nitrate, ammonium and potassium on the growth of the seminal root sytem, and the shoot, in barley. 479–490.

Dubrovsky, J. G., Doerner, P. W., Colón-Carmona, A., and Rost, T. L. (2000). Pericycle cell proliferation and lateral root initiation in Arabidopsis. *Plant Physiol*. 124, 1648–1657. doi:10.1104/pp.124.4.1648.

Dubrovsky, J. G., Gambetta, G. A., Hernández-Barrera, A., Shishkova, S., and González, I. (2006). Lateral root initiation in Arabidopsis: developmental window, spatial patterning, density and predictability. *Ann*. *Bot*. 97, 903–915. doi:10.1093/aob/mcj604.

Dubrovsky, J. G., Rost, T. L., Colón-Carmona, a, and Doerner, P. (2001). Early primordium morphogenesis during lateral root initiation in Arabidopsis thaliana. *Planta* 214, 30–36. doi:10.1007/s004250100598.

Dubrovsky, J. G., Sauer, M., Napsucialy-Mendivil, S., Ivanchenko, M. G., Friml, J., Shishkova, S., et al. (2008). Auxin acts as a local morphogenetic trigger to specify lateral root founder cells. *Proc. Natl. Acad. Sci. U. S. A.* 105, 8790–4. doi:10.1073/pnas.0712307105.

FAO (2009). *The state of food and agriculture: Livestock in balance*. doi:10.1016/S0140-6736(75)92740-3.

Farrar, J. F., and Jones, C. L. (1986). Modification of Respiration and Carbohydrate Status of Barley Roots By Selective Pruning. *New Phytol.* 102, 513–521. doi:10.1111/j.1469-8137.1986.tb00827.x.

Fitter, A. H. (1987). An Architectural Approach To The Comparitice Ecology Of Plant Root Systems. *New Phytol.* 106, 61–77. doi:10.1111/j.1469-8137.1987.tb04683.x.

Fitter, A. H., Stickland, T. R., Harvey, M. L., and Wilson, G. W. (1991). Architectural analysis of plant root systems 1. Architectural correlates of exploitation efficiency. *New Phytol.* 118, 375–382. doi:10.1111/j.1469-8137.1991.tb00018.x.

Foley, J. A., Ramankutty, N., Brauman, K. a., Cassidy, E. S., Gerber, J. S., Johnston, M., et al. (2011). Solutions for a cultivated planet. *Nature* 478, 337–342. doi:10.1038/nature10452.

Forde, B. G. (2009). Is it good noise? The role of developmental instability in the shaping of a root system. *J. Exp. Bot.* 60, 3989–4002. doi:10.1093/jxb/erp265.

Forde, B. G., and Lorenzo, H. (2001). The nutritional control of root development. *Plant Soil* 232, 51–68. doi:10.1023/A:1010329902165.

Freixes, S., Thibaud, M.-C., Tardieu, F., and Muller, B. (2002). Root elongation and branching is related to local hexose concentration in Arabidopsis thaliana seedlings. *Plant, Cell Environ.* 25, 1357–1366. doi:10.1046/j.1365-3040.2002.00912.x.

Giehl, R. F. H., Gruber, B. D., and Von Wirén, N. (2014). It's time to make changes: Modulation of root system architecture by nutrient signals. *J. Exp. Bot.* 65, 769–778. doi:10.1093/jxb/ert421.

Gregory, P., Palta, J., and Batss, G. (1997). Root systems and root : mass ratio - carbon allocation under current and projected atmospheric conditions in arable crops. *Plant Soil* 187, 221–228. doi:10.1007/BF00017089.

Guédon, Y., Barthélémy, D., Caraglio, Y., and Costes, E. (2001). Pattern analysis in branching and axillary flowering sequences. *J. Theor. Biol.* 212, 481–520. doi:10.1006/jtbi.2001.2392.

Guédon, Y., Caraglio, Y., Heuret, P., Lebarbier, E., and Meredieu, C. (2007). Analyzing growth components in trees. *J. Theor. Biol.* 248, 418–47. doi:10.1016/j.jtbi.2007.05.029.

Hackett, C., and Rose, D. A. (1972). A model of the extension and branching of a seminal root of Barley, and its use in studying relations between root dimensions I. The model. *Aust. J. Biol. Sci.* 25, 669–680. doi:10.1071/BI9720669.

Haling, R. E., Brown, L. K., Bengough, A. G., Young, I. M., Hallett, P. D., White, P. J., et al. (2013). Root hairs improve root penetration, root-soil contact, and phosphorus acquisition in soils of different strength. *J. Exp. Bot.* 64, 3711–3721. doi:10.1093/jxb/ert200.

Ho, M. D., Rosas, J. C., Brown, K. M., and Lynch, J. P. (2005). Root architectural tradeoffs for water and phosphorus acquisition. *Funct. Plant Biol.* 32, 737–748. doi:10.1071/FP05043.

Hodge, A. (2004). The plastic plant: root responses to heterogeneous supplies of nutrients. *New Phytol.* 162, 9–24. doi:10.1111/j.1469-8137.2004.01015.x.

Hodge, A. (2006). Plastic plants and patchy soils. *J. Exp. Bot.* 57, 401–11. doi:10.1093/jxb/eri280.

Hopkins, R. (2008). *The transition handbook. From oil dependency to local resilience.*

Dello Ioio, R., Linhares, F. S., Scacchi, E., Casamitjana-Martinez, E., Heidstra, R., Costantino, P., et al. (2007). Cytokinins determine Arabidopsis root-meristem size by controlling cell differentiation. *Curr. Biol.* 17, 678–82. doi:10.1016/j.cub.2007.02.047.

Jourdan, C., and Rey, H. (1997). Modelling and simulation of the architecture and development of the oil-palm (Elaeis guineensis Jacq.) root system: I. The model. *Plant Soil* 190, 217–233. doi:10.1023/A:1004218030608.

Jourdan, C., Rey, H., and Guédon, Y. (1995). Architectural analysis and modelling of the branching process of the young oil-palm root system. *Plant Soil* 177, 63–72. doi:10.1007/BF00010338.

Laskowski, M. (2013). Lateral root initiation is a probabilistic event whose frequency is set by fluctuating levels of auxin response. *J. Exp. Bot.* 64, 2609–17. doi:10.1093/jxb/ert155.

Lièvre, M., Granier, C., and Guédon, Y. (2016). Identifying developmental phases in the Arabidopsis thaliana rosette using integrative segmentation models. *New Phytol.* 210, 1466–1478. doi:10.1111/nph.13861.

Lucas, M., Guédon, Y., Jay-Allemand, C., Godin, C., and Laplaze, L. (2008). An auxin transport-based model of root branching in Arabidopsis thaliana. *PLoS One* 3, e3673. doi:10.1371/journal.pone.0003673.

Lucas, M., Kenobi, K., von Wangenheim, D., Voβ, U., Swarup, K., De Smet, I., et al. (2013). Lateral root morphogenesis is dependent on the mechanical properties of the overlaying tissues. *Proc. Natl. Acad. Sci. U. S. A.* 110, 5229–34. doi:10.1073/pnas.1210807110.

Lynch, J. P. (2007). Roots of the Second Green Revolution. *Aust. J. Bot.* 55, 493–512. doi:10.1071/BT06118.

Lynch, J. P., and Brown, K. M. (2012). New roots for agriculture: exploiting the root phenome. *Philos. Trans. R. Soc. Lond. B. Biol. Sci.* 367, 1598–604. doi:10.1098/rstb.2011.0243.

Lynch, J. P., Nielsen, K. L., Davis, R. D., and Jablokow, a G. (1997). SimRoot: Modellig and visualization of root systems. *Plant Soil* 188, 139–151.

Ma, Z., Baskin, T. I., Brown, K. M., and Lynch, J. P. (2003). Regulation of root elongation

under phosphorus stress involves changes in ethylene responsiveness. *Plant Physiol*. 131, 1381–1390. doi:10.1104/pp.012161.

Malamy, J. E. (2005). Intrinsic and environmental response pathways that regulate root system architecture. *Plant, Cell Environ*. 28, 67–77. doi:10.1111/j.1365-3040.2005.01306.x.

Malamy, J. E., and Benfey, P. N. (1997). Organization and cell differentiation in lateral roots of Arabidopsis thaliana. *Development* 124, 33–44. doi:VL - 124.

Malamy, J. E., and Ryan, K. S. (2001). Environmental Regulation of Lateral Root Initiation in Arabidopsis 1. *Plant Physiol*. 127, 899–909. doi:10.1104/pp.010406.A.

Mather, K. (1953). Genetical control of stability in development. *Heredity (Edinb)*. 7, 297–336. doi:10.1038/hdy.1953.41.

Moreno-Risueno, M. A., Van Norman, J. M., Moreno, A., Zhang, J., Ahnert, S. E., and Benfey, P. N. (2010). Oscillating gene expression determines competence for periodic Arabidopsis root branching. *Science* 329, 1306–11. doi:10.1126/science.1191937.

Mueller, N. D., Gerber, J. S., Johnston, M., Ray, D. K., Ramankutty, N., and Foley, J. A. (2012). Closing yield gaps through nutrient and water management. *Nature* 490, 254–257. doi:10.1038/nature11420.

Muller, B., Stosser, M., and Tardieu, F. (1998). Spatial distributions of tissue expansion and cell division rates are related to irradiance and to sugar content in the growing zone of maize roots. *Plant, Cell Environ*. 21, 149–158. doi:10.1046/j.1365-3040.1998.00263.x.

Nakayama, N., Smith, R. S., Mandel, T., Robinson, S., Kimura, S., Boudaoud, A., et al. (2012). Mechanical regulation of auxin-mediated growth. *Curr*. *Biol*. 22, 1468–1476. doi:10.1016/j.cub.2012.06.050.

Nielsen, K. L., Lynch, J. P., Jablokow, A. G., and Curtis, P. S. (1994). Carbon cost of root systems: an architectural approach. *Plant Soil* 165, 161–169. doi:10.1007/BF00009972.

Pages, L. (2014). Branching patterns of root systems: quantitative analysis of the diversity among dicotyledonous species. *Ann*. *Bot*. doi:10.1093/aob/mcu145.

Pagès, L. (1995). Growth patterns of the lateral roots of young oak (Quercus robur) tree seedlings Relationship with apical diameter. *New Phytol*. 130, 503–509. doi:doi: 10.1111/j.1469-8137.1995.tb04327.x.

Pagès, L. (2011). Links between root developmental traits and foraging performance. *Plant*. *Cell Environ*. 34, 1749–60. doi:10.1111/j.1365-3040.2011.02371.x.

Pagès, L., and Aries, F. (1988). SARAH : modèle de simulation de la croissance, du développement et de l'architecture des systèmes racinaires. *Agron*. *EDP Sci*. 8, 889–896.

Pagès, L., Bécel, C., Boukcim, H., Moreau, D., Nguyen, C., and Voisin, A. S. (2013a). Calibration and evaluation of ArchiSimple, a simple model of root system architecture. *Ecol*. *Modell*. doi:10.1016/j.ecolmodel.2013.11.014.

Pagès, L., Chadoeuf, J., and Kervella, K. (1992). Modélisation stochastique de la croissance et du développement du système racinaire de jeunes pêchers. *Agronomie* 12, 447–458. doi:10.1051/agro:19920603.

Pagès, L., Jordan, M., and Picard, D. (1989). A simulation model of the three-dimensional

architecture of the maize root system. *Plant Soil* 154, 147–154. doi:10.1007/BF02370279.

Pagès, L., Kervella, J., and Chadoeuf, J. (1993). Development of the Root System of Young Peach Trees (Prunus persica L. Batsch): A Morphometrical Analysis. *Ann. Bot.* 71, 369–375.

Pagès, L., Vercambre, G., Drouet, J. L., Lecompte, F., Collet, C., and Le Bot, J. (2004). Root Typ: A generic model to depict and analyse the root system architecture. *Plant Soil* 258, 103–119. doi:10.1023/B:PLSO.0000016540.47134.03.

Pagès, L., Xie, J., and Serra, V. (2013b). Potential and actual root growth variations in root systems: Modeling them with a two-step stochastic approach. *Plant Soil* 373, 723–735. doi:10.1007/s11104-013-1820-z.

Péret, B., De Rybel, B., Casimiro, I., Benková, E., Swarup, R., Laplaze, L., et al. (2009). Arabidopsis lateral root development: an emerging story. *Trends Plant Sci.* 14, 399–408. doi:10.1016/j.tplants.2009.05.002.

Pien, S., Wyrzykowska, J., McQueen-Mason, S., Smart, C., and Fleming, a (2001). Local expression of expansin induces the entire process of leaf development and modifies leaf shape. *Proc. Natl. Acad. Sci. U. S. A.* 98, 11812–11817. doi:10.1073/pnas.191380498.

Rahman, A., Bannigan, A., Sulaman, W., Pechter, P., Blancaflor, E. B., and Baskin, T. I. (2007). Auxin, actin and growth of the Arabidopsis thaliana primary root. *Plant J.* 50, 514–528. doi:10.1111/j.1365-313X.2007.03068.x.

Ray, D. K., Mueller, N. D., West, P. C., and Foley, J. a (2013). Yield Trends Are Insufficient to Double Global Crop Production by 2050. *PLoS One* 8, e66428. doi:10.1371/journal.pone.0066428.

Riedacker, A., Dexheimer, J., Tavakol, R., and Alaoui, H. (1982). Modifications expérimentales de la morphogénèse et des géotropismes dans le système racinaire de jeunes chênes. *Can. J. Bot.* 60, 765–778. doi:10.1139/b82-100.

Riou-Khamlichi, C., Menges, M., Healy, J. M., and Murray, J. a (2000). Sugar control of the plant cell cycle: differential regulation of Arabidopsis D-type cyclin gene expression. *Mol. Cell. Biol.* 20, 4513–21. doi:10.1128/MCB.20.13.4513-4521.2000.

Rolland, F., Moore, B., and Sheen, J. (2002). Sugar Sensing 2002 Rolland. 185–205. doi:10.1105/tpc.010455.S186.

Scandeg, D., and McLeod, R. (1976). Effect of Sucrose Concentration on Cell Proliferation and Quiescence in the Apical Meristem of Excised Roots of Pisum Sativum L. 29, 391–404. doi:10.1080/00087114.1976.10796515.

Sievänen, R., Godin, C., De Jong, T. M., and Nikinmaa, E. (2014). Functional-structural plant models: A growing paradigm for plant studies. *Ann. Bot.* 114, 599–603. doi:10.1093/aob/mcu175.

De Smet, I., Signora, L., Beeckman, T., Inzé, D., Foyer, C. H., and Zhang, H. (2003). An abscisic acid-sensitive checkpoint in lateral root development of Arabidopsis. *Plant J.* 33, 543–555. doi:10.1046/j.1365-313X.2003.01652.x.

De Smet, I., Tetsumura, T., De Rybel, B., Frey, N. F. D., Laplaze, L., Casimiro, I., et al. (2007). Auxin-dependent regulation of lateral root positioning in the basal meristem of

Arabidopsis. *Development* 134, 681–690. doi:10.1242/dev.02753.

St.Clair, S. B., and Lynch, J. P. (2010). The opening of Pandora's Box: climate change impacts on soil fertility and crop nutrition in developing countries. *Plant Soil* 335, 101–115. doi:10.1007/s11104-010-0328-z.

Swarup, K., Benková, E., Swarup, R., Casimiro, I., Péret, B., Yang, Y., et al. (2008). The auxin influx carrier LAX3 promotes lateral root emergence. *Nat. Cell Biol.* 10, 946–954. doi:10.1038/ncb1754.

Szymanowska-Pulka, J. (2013). Form matters: Morphological aspects of lateral root development. *Ann. Bot.* 112, 1643–1654. doi:10.1093/aob/mct231.

Taugourdeau, O., Caraglio, Y., Sabatier, S., and Guédon, Y. (2015). Characterizing the respective importance of ontogeny and environmental constraints in forest tree development using growth phase duration distributions. *Ecol. Modell.* 300, 61–72. doi:10.1016/j.ecolmodel.2014.12.022.

Taugourdeau, O., Chaubert-Pereira, F., Sabatier, S., and Guédon, Y. (2011). Deciphering the developmental plasticity of walnut saplings in relation to climatic factors and light environment. *J. Exp. Bot.* 62, 5283–5296. doi:10.1093/jxb/err115.

Triboulot, M., Pritchard, J., and Tomos, D. (1995). Stimulation and inhibition of pine root growth by osmotic stress. *New Phytol.* 130, 169–175. doi:10.1111/j.1469-8137.1995.tb03038.x.

Van't Hof, J. (1968). Control of cell progression through the mitotic cycle by carbohydrate provision. I. Regulation of cell division in excised plant tissue. *J. Cell Biol.* 37, 773–780.

Varney, G., Canny, M., Wang, X., and McCully, M. (1991). The branch roots of Zea. I. First Order Branches, Their Number, Sizes and Division into classes. *Ann. Bot.* 67, 357–364.

Willaume, M., and Pagès, L. (2011). Correlated responses of root growth and sugar concentrations to various defoliation treatments and rhythmic shoot growth in oak tree seedlings (Quercus pubescens). *Ann. Bot.* 107, 653–662. doi:10.1093/aob/mcq270.

Xu, J., Avigne, W., McCarty, D., and Koch, K. (1996). A Similar Dichotomy of Sugar Modulation and Developmental Expression Affects Both Paths of Sucrose Metabolism: Evidence from a Maize Invertase Gene Family. *Plant Cell* 8, 1209–1220. doi:10.1105/tpc.8.7.1209.

York, L. M., Nord, E. a, and Lynch, J. P. (2013). Integration of root phenes for soil resource acquisition. *Front. Plant Sci.* 4, 355. doi:10.3389/fpls.2013.00355.

Yorke, J. S., Sagar, G. R. (1969). distribution of secondary root growth potential in the root system of Pisum sativum. *Can. J. Bot.* 48, 699–704.

Zhang, H., and Forde, B. G. (1998). An Arabidopsis MADS box gene that controls nutrient-induced changes in root architecture. *Science* 279, 407–409. doi:10.1126/science.279.5349.407.

Zhang, H., and Forde, B. G. (2000). Regulation of Arabidopsis root development by nitrate availability. *J. Exp. Bot. MP Spec. Issue* 51, 51–59. doi:10.1093/jexbot/51.342.51.

Zhu, J., Kaeppler, S. M., and Lynch, J. P. (2005). Mapping of QTLs for lateral root branching and length in maize (Zea mays L.) under differential phosphorus supply. *Theor. Appl.*

Genet. 111, 688–695. doi:10.1007/s00122-005-2051-3.

CHAPTER II. LATERAL ROOT GROWTH PATTERN IN MAIZE

This chapter is composed of two parts. The first part is an article in a pre-submission format. It presents a work done in collaboration with the group of L. Laplaze at the "DIversité-Adaptation-DEveloppement des plantes" (DIADE) research unit. The main goal of this paper is to provide a framework of analysis able to integrate the spatio-temporal variations observed in lateral root growth. This framework has been developed in parallel on two cereal species, maize (my PhD) and pearl millet (PhD of Sixtine Passot, DIADE). The use of common protocols for the generation and analysis of the phenotyping data of these two phylogenetically related species helped to improve the robustness of the approach presented here. The results and discussion sections are presented before the materials and methods section following submission guidelines of the focused journal.

The second part consists in an extension of the previous approach to new experimental conditions on maize plants, in order to evaluate the influence of particular environmental or genotypic effects on lateral root growth. Various experimental conditions and genotypes were used. However, due to time constraints, only results related to two different modalities are presented. The first one consists in a shading treatment applied to maize plants since seed germination and the second one in the use of a mutant with inhibited auxin signaling, respectively dedicated to investigate the roles of carbohydrates and auxin in lateral root growth. Results on growth dynamics presented here are discussed in the general discussion (Chapter V) in the light of the anatomical, cellular, and molecular results presented in Chapters III and IV.

1 Spatio-temporal analysis of early root system development in two cereals, pearl millet and maize, reveals three types of lateral roots and a stationary random branching pattern along the primary root

Authors contributions

Sixtine Passot contributed to all the experiments concerning pearl millet, except histological sections, analyzed the data and wrote the manuscript;
Beatriz Moreno-Ortega contributed to all the experiments concerning maize, except histological sections, analyzed the data and wrote the manuscript;
Daniel Moukouanga performed histological sections for pearl millet and maize and contributed to plant culture for pearl millet;

Crispulo Balsera contributed to rhizotron preparation and plant culture for both species;
Soazig Guyomarc'h contributed to plant culture for pearl millet;
Mikael Lucas contributed to plant culture for pearl millet;
Guillaume Lobet updated SmartRoot and added specific functions for this study,
Laurent Laplaze designed the study and wrote the manuscript;
Bertrand Muller designed the study and wrote the manuscript;
Yann Guédon designed and implemented the statistical models, analyzed the data and wrote the manuscript.

Abstract

Recent progress in root phenotyping focused mainly on increasing throughput for genetic studies while the identification of root developmental patterns has been comparatively underexplored. We introduce a new phenotyping pipeline for producing high-quality spatio-temporal root system development data and identifying developmental patterns within these data. This pipeline combines the SmartRoot image analysis system with statistical models. Semi-Markov switching linear models were applied to cluster lateral roots based on their growth rate profiles. Applied to maize and pearl millet, this revealed three types of lateral roots with similar characteristics in both species. Correlation between these lateral root types and anatomical traits was strong for pearl millet and weak for maize. Potential dependencies in the succession of lateral root types along the primary root were then analyzed using variable-order Markov chains. The succession of lateral root types along the primary roots was neither influenced by the shootward neighbor root type nor by the distance from this root. This stationary random branching pattern was remarkably conserved despite the high variability of root systems in both pearl millet and maize. Precise recording and analysis of lateral roots spatio-temporal developmental patterns thus revealed strong similarities between two cultivated cereals that are stronger than what anatomical comparisons would suggest.

1.1 Introduction

Cereal breeding has long ignored the belowground part of the plant but it is now acknowledged that root system represents an opportunity for improving plant efficiency and tolerance to abiotic stresses (Bishopp and Lynch, 2015). A better knowledge of root system structure and function is thus needed to open the way to root system improvement. Phenotyping, as the measure of plant traits in a given environment and in a reproducible manner, is one key approach to access this knowledge.

Recent progress in plant phenotyping platforms, including plant handling automation and computer assisted data acquisition, has allowed an increase in phenotyping throughput (Fahlgren *et al*., 2015b). It was critical for association studies and gene discovery that benefit

from the large number of plants studied in automated phenotyping systems. Beside increasing throughput, another strategy chosen in some phenotyping systems is to improve data dimensionality and structure (Dhondt *et al*., 2013). These systems increase the amount of data collected on a single plant, either by measuring several traits that can be of different nature, in control or special conditions, or by measuring the same trait at multiple time points to focus on physiological processes (Fahlgren *et al*., 2015a). Root architecture phenotyping presents specific challenges as compared with phenotyping of aerial parts of plants. The root system is by nature hidden and root phenotyping systems have to make a compromise between the relevance of growth conditions and trait measurement feasibility. Most root phenotyping pipelines focus on the high throughput measurement of selected root traits on a large number of plants, with the objective of detecting QTL usable in breeding (Kuijken *et al*., 2015). For example, Atkinson *et al*. (2015) reported a phenotyping platform where root systems grew in 2D on a filter paper for a few days for QTL detection. Systems considering the 3 dimensions of root systems exist too (Iyer-Pascuzzi *et al*., 2010) but their objective are generally focused on QTL detection (Topp *et al*., 2013). The development of individual root axes during long periods of time is rarely studied, whereas temporal analyses are more developed for the aerial parts (see *e.g*. Lièvre *et al*., 2016). This kind of studies has been hampered by the difficulty of collecting individual root growth data. In addition, the analysis of structured data such as root growth rate profiles is more challenging than the analysis of simple root traits.

The variability in lateral root length among neighbor roots borne by the same root axis is a widely observed feature of root systems. It is proposed that this variability contributes to root system efficiency (Forde, 2009; Pagès, 2011). It is observed in annual as in perennial species (in oak (Pagès, 1995), in banana (Lecompte *et al*., 2005), in rubber tree (Thaler and Pagès, 1996b), in sunflower (Aguirrezabal *et al*., 1994)) and even in the model species *Arabidopsis thaliana* (Freixes *et al*., 2002). It is also observed in monocots such as maize, where some studies reported a high variability among lateral root length (Jordan *et al*., 1993; Varney *et al*., 1991; Wu *et al*., 2016). However, most of these descriptions did not consider growth dynamically. When they did (Pagès, 1995; Thaler and Pagès, 1996b), they generally considered that the variability of growth rate profiles forms a continuum but did not investigate a possible structuring into distinct classes. On the other hand, different lateral root types have been described among cereals, but these classifications were based on anatomical traits or diameter. Four types were reported in maize (Varney *et al*., 1991), three in pearl millet (Passot *et al*., 2016) and rice (Gowda *et al*., 2011; Henry *et al*., 2016) and five in wheat, barley and triticale (Watt *et al*., 2008).

Here, we designed a phenotyping pipeline for producing high-quality spatio-temporal root system development data. This pipeline incorporates the SmartRoot image analysis system (Lobet *et al*., 2011) able to reconstruct consistent spatio-temporal data on the basis of

successive snapshots of root system architecture. Our ultimate goal was the identification and characterization of root developmental patterns on the basis of these spatio-temporal data. To this end, we adopted a two-step approach. Lateral root growth rate profiles were first analyzed. This first temporal step relies on a model-based clustering of these longitudinal data using semi-Markov switching linear models; see Lièvre *et al.* (2016) for another application of similar statistical models. One strength of these statistical models is the capability to model growth phase lengths combining complete and censored growth rate profiles (since some lateral roots were still growing at the end of the experiment entailing growth phase censoring). This first step led us to identify lateral root types on the basis of growth rate profiles. The second spatial step thus consisted in analyzing the primary root branching pattern where the lateral roots were summarized by their types. The proposed root system phenotyping pipeline was used on two contrasted cereals, pearl millet (*Pennisetum glaucum*) and maize (*Zea mays*). Commonalities and differences between these two species regarding the growth patterns of lateral roots and the branching patterns along the primary root was investigated as well as their relation to anatomical (vessel numbers and dimensions) and morphological (apical diameter) features.

1.2 Results

In order to analyze early root system development and architecture in pearl millet and maize, daily images of growing root systems were recorded for 15 and 21 days respectively in a rhizotron system. The ability of SmartRoot (Lobet *et al.*, 2011) to cross-link information corresponding to different time points was then used to build consistent spatio-temporal data of root system development and architecture on the basis of the corresponding series of images. We chose to decompose the analysis of these spatio-temporal data into two steps:

1. *temporal analysis*: we first analyzed growth rate profiles of lateral roots using dedicated statistical models for these specific longitudinal data characterized by the short length of profiles and the high censoring level since many lateral roots were still growing at the last date of measurement. Lateral roots were classified in three types as a byproduct or these longitudinal data analysis.

2. *spatial analysis*: The intervals between consecutive lateral roots and the succession of lateral root types along the primary root were then analyzed.

1.2.1 Model-based clustering of lateral root growth rate profiles reveals three growth patterns for pearl millet and maize lateral roots

Model building

After data curation, our dataset was composed of growth rate profiles of 1254 and 3050 lateral roots from 8 pearl millet and 13 maize plants respectively. These lateral roots were followed up to 10 and 17 days respectively after their emergence from the primary roots. The exploratory analysis of these growth rate profiles highlighted a strong longitudinal organization with growth rates either increasing or decreasing with lateral root age (**Figure II-1**). The growth rate profiles were essentially divergent from the time origin and the growth rate dispersion increased with the lateral root age. Hence, lateral roots can be roughly ordered according to their growth rate profiles.

This raises the question of a stronger structuring of these longitudinal data than a simple ranking of the lateral root growth rate profiles. We thus chose to investigate a model-based clustering approach for these longitudinal data. This raised two types of difficulties: (i) the growth rate profiles were longitudinally limited (up to 10 successive growth rates for pearl millet and up to 17 successive growth rates for maize) and (ii) the censoring level was high with a high proportion of lateral roots still growing at the end of the experiment. We thus designed a statistical model for clustering growth rate profiles, using only profiles lasting at least 5 days (corresponding to 652 lateral roots for pearl millet and 2029 for maize), based on the following assumptions:

- A growth rate profile is modeled by a single growth phase either censored or followed by a growth arrest.

- Changes in growth rate within a growth phase are modeled by a linear trend. This strong parametric assumption was a consequence of the short length of growth rate profiles. Hence, linear trend models should be viewed as instrumental models for clustering growth rate profiles rather than models for fitting each growth rate profile.

The proposed statistical model was composed of growth states, each corresponding to a lateral root growth rate profile type. A distribution representing the growth phase duration (in days) and a linear model representing changes in growth rate during the growth phase were associated with each of these growth states. Growth states were systematically followed by a growth arrest state. The overall model is referred to as a Semi-Markov Switching Linear Model (SMS-LM; see **Materials and Methods** and **Appendix II-1** for a formal definition and **Figure II-2** and **Supplementary Figure II-1** for an illustration in pearl millet and maize, respectively). This kind of integrative statistical model makes it possible to consistently estimate growth phase duration distributions combining complete and censored growth phases.

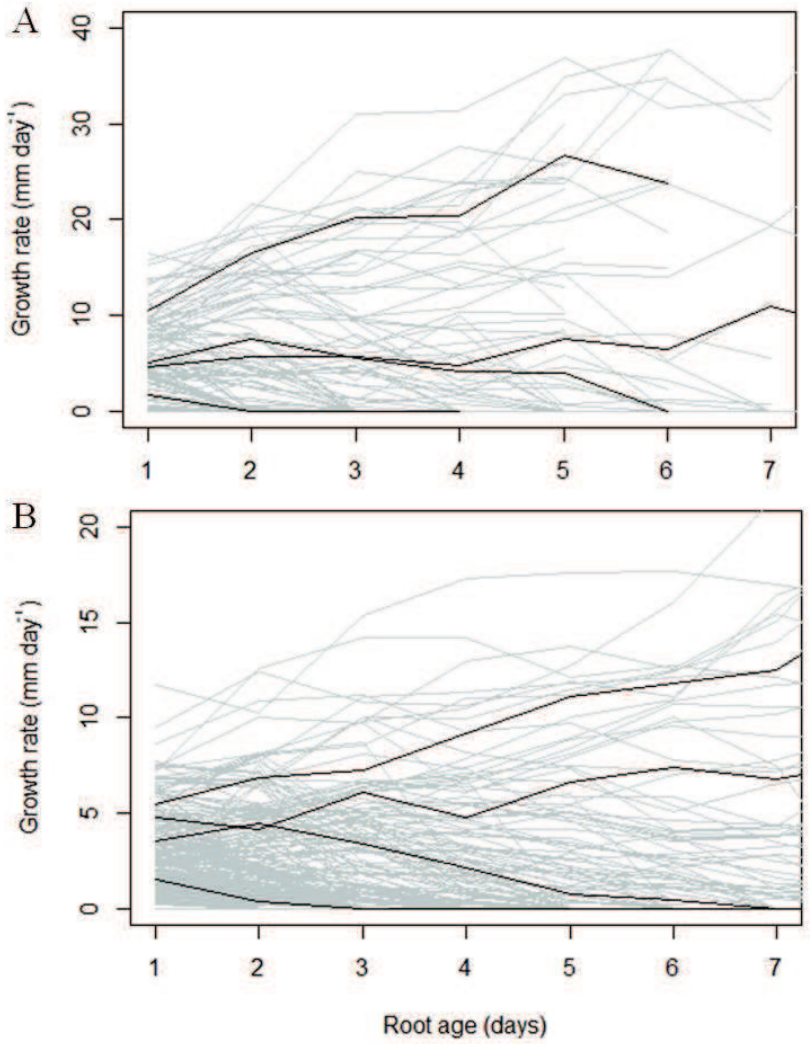

Figure II-1 Growth rate profiles for individual lateral roots of one pearl millet (**A**) and one maize (**B**) plant. A selection of individual growth profiles have been highlighted (black lines) showing contrasted behaviors. Root age refers to the number of days following emergence.

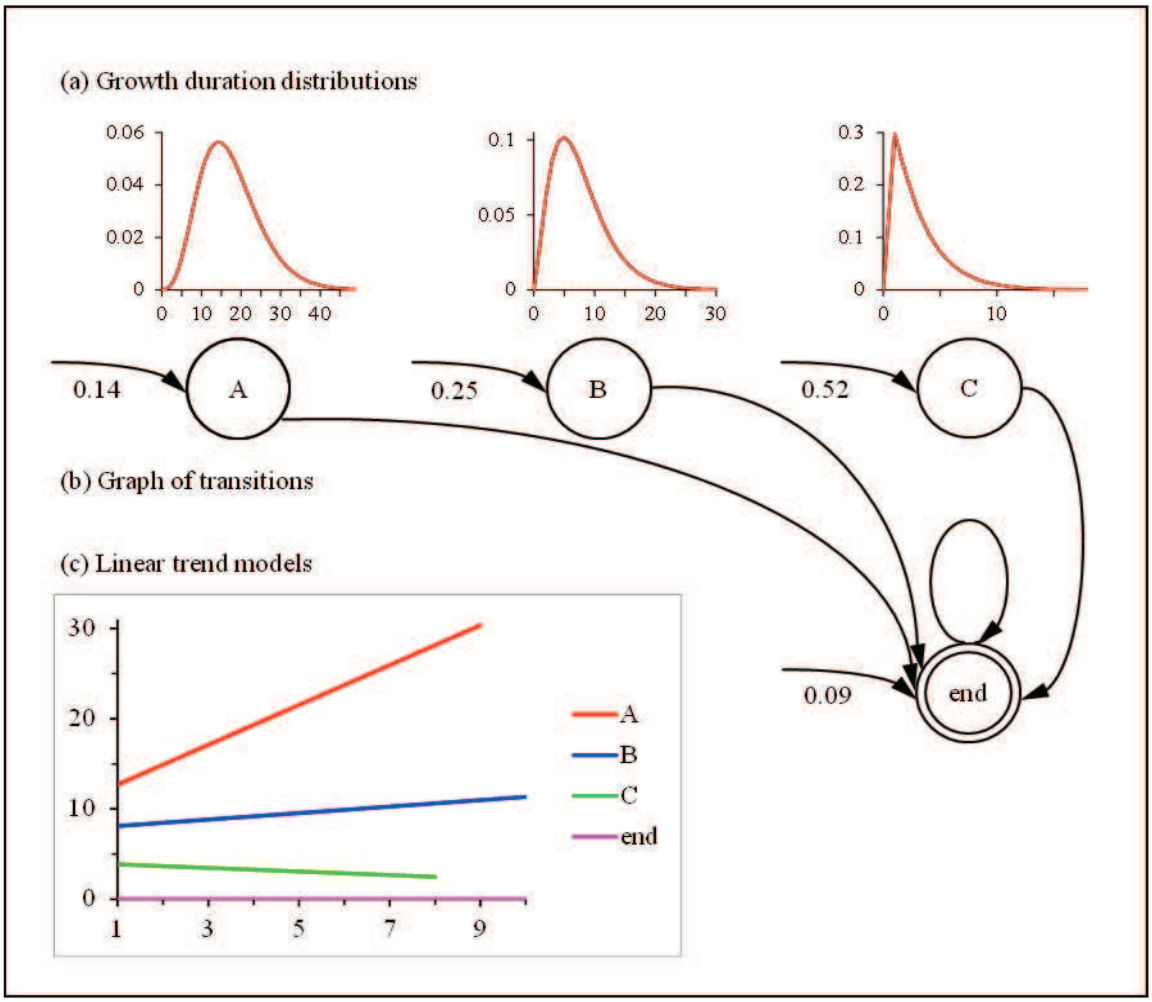

Figure II-2 Four-state semi-Markov switching linear model estimated on the basis of pearl millet lateral root growth rate series: (a) Growth duration distributions; (b) Graph of transitions. The possible transitions between states are represented by arcs with the attached probabilities noted nearby when < 1. The arcs entering in states indicate initial states and the attached initial probabilities are noted nearby. (c) Linear trend models estimated for each state.

Selection of the number of lateral root types

We next had to define the number of growth states (*i.e.* the number of lateral root types). Because of the specific structure of the model where each state can be visited at most once, the usual model selection criteria such as the Bayesian information criterion do not apply. We thus had to design an empirical model selection method for selecting the number of growth states. This method detailed in **Appendix II-2** combines the following criteria:

1. Posterior probabilities of the optimal assignment of each lateral root growth rate profile to a growth state (followed or not by the growth arrest state at a given age) *i.e.*

weight of the optimal assignment among all the possible assignments of a given growth rate profile,

2. Comparison of location and dispersion measures of growth rate profiles for each lateral root type deduced from the optimal assignment of each lateral root growth rate profile,
3. Overlap between growth rate profiles for consecutive lateral root types.

We selected for both species 3 lateral root types that correspond to the best compromise between (i) the proportion of ambiguously assigned lateral roots, (ii) the relative dispersion of growth rate profiles for the most vigorous root type and (iii) the overlap between growth rate profiles for consecutive types.

Growth phases are similar in both species

Growth phase duration distributions for the three growth states estimated within the SMS-LMs are shown in **Figure II-3a** for pearl millet and **Figure II-3b** for maize. The estimated growth phase duration distributions were very similar for the two species for each type (A, B or C), with mean growth durations of 17.3 and 15.2 days for type A, 7.6 and 6.8 days for type B and 3.2 and 3.0 days for type C for pearl millet and maize, respectively, and standard deviations equal to 7.6 and 7.7 for type A, 4.6 and 5.0 for type B, and 2.6 and 2.4 for type C. The censoring level is defined as the proportion of growth phase incompletely observed for a given lateral root type. The censoring level was computed for each growth state as a by-product of the estimation of the corresponding growth phase duration distribution within SMS-LM. This censoring level takes into account all the possible assignments of growth rate profiles of length ≥ 5 incorporated in the training sample. We obtained 96% of censoring for state A, 54% for state B and 14% for state C in the case of pearl millet and 80% for state A, 36% for state B and 10% for state C in the case of maize. The growth rate profile length frequency distribution are superimposed to the estimated growth phase duration distributions shown in **Figure II-3** to illustrate the censoring level for each species. The higher censoring level for pearl millet compared to maize was a direct consequence of the shorter growth rate profiles in average for pearl millet since the growth phase duration distributions were similar for the two species. It should be noted that the growth rate profile lengths were similar for the different lateral root types of a given species (see the corresponding cumulative distributions functions in **Supplementary Figure II-2**).

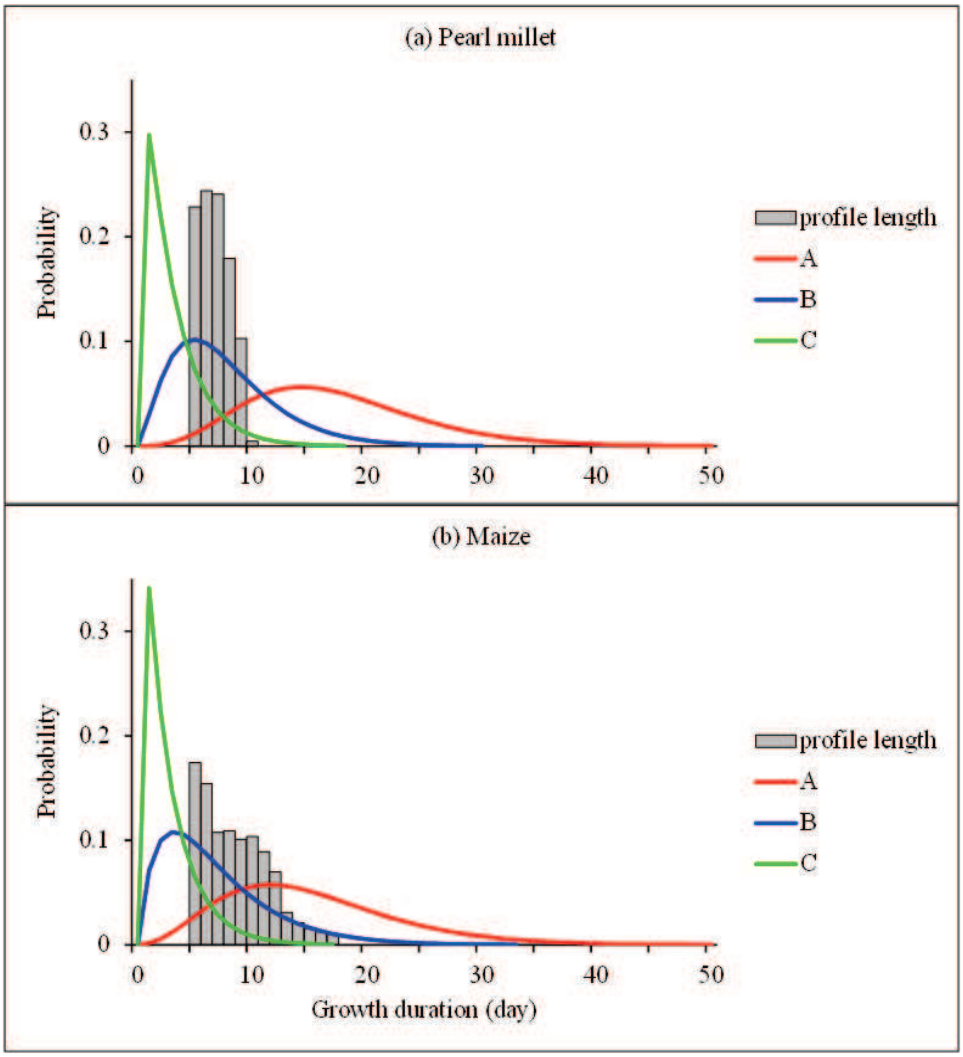

Figure II-3 Growth duration distributions estimated within the 4-state semi-Markov switching linear model: (**a**) pearl millet; (**b**) maize. The growth rate profile length frequency distributions are drawn for illustrating the censoring level.

Classification of individual growth rate profiles

Only growth rate profiles of length ≥ 5 were used for the building of SMS-LMs. Growth rate profiles of length < 5 were then assigned *a posteriori* to classes using the previously estimated SMS-LM.

Daily median growth rate and associated mean absolute deviation for each class are shown in **Figure II-4 a** and **b** for pearl millet and maize respectively. In both species, daily median growth rate were divergent between the three types of lateral roots. Median growth profiles for type B and type C reached 0 mm day^{-1} by 7-8 and 3-4 days respectively, while type A median growth rate stayed positive and did not decrease in both species. The main difference between the two species, apart from different absolute growth rates, concerned type B lateral

roots, where median growth rate stayed nearly constant up to day 5 in pearl millet whereas it started to decrease straight after emergence in maize, and type A lateral root, where median growth rate kept on increasing in pearl millet whereas it stabilizes after a few days in maize. Variability existed around these median profiles for each type. Mean absolute deviations were rather similar between the two species for types B and C. Because the temporal sequences were longer in maize, we could observe a regular increase of mean absolute deviation with root age for type A, up to reaching nearly the same level as median growth rate at day 13. This is due to the presence in this class of lateral roots whose growth rate started to decrease at later stages while some lateral roots continued to increase their growth rate.

The growth rate profiles of all the lateral roots of a selected pearl millet and a selected maize plant colored according to the class they were assigned to, are presented in **Figure II-5**. This shows the variability of growth rate profiles within a class, the overlap between classes and the censoring level of growth rate profiles. Growth characteristics of the three lateral root types were very similar between maize and pearl millet. The main differences between maize and pearl millet root growth rate profiles concerned the absolute values of growth rates which were higher in pearl millet as compared to maize.

1.2.2 Comparison of apical diameter profiles and growth rate profiles for the three classes of lateral roots identified in maize

The optimal assignment of lateral roots to classes computed using the estimated 4-state semi-Markov switching linear model was used to compute median apical diameter profiles and associated mean absolute deviations per lateral root type. The median apical diameter profiles for the different lateral root types were far more stationary than the median growth rate profiles (**Figure II-6**). Apical diameter profiles clearly distinguish type A from type B or C lateral roots but not type B from type C lateral roots (see the overlaps between apical diameter distributions for the successive ages in **Supplementary Table II-3**). Type B and C lateral root apical diameter decreased with time and converged towards median apical diameter around 230 μm corresponding to a high proportion of arrested roots.

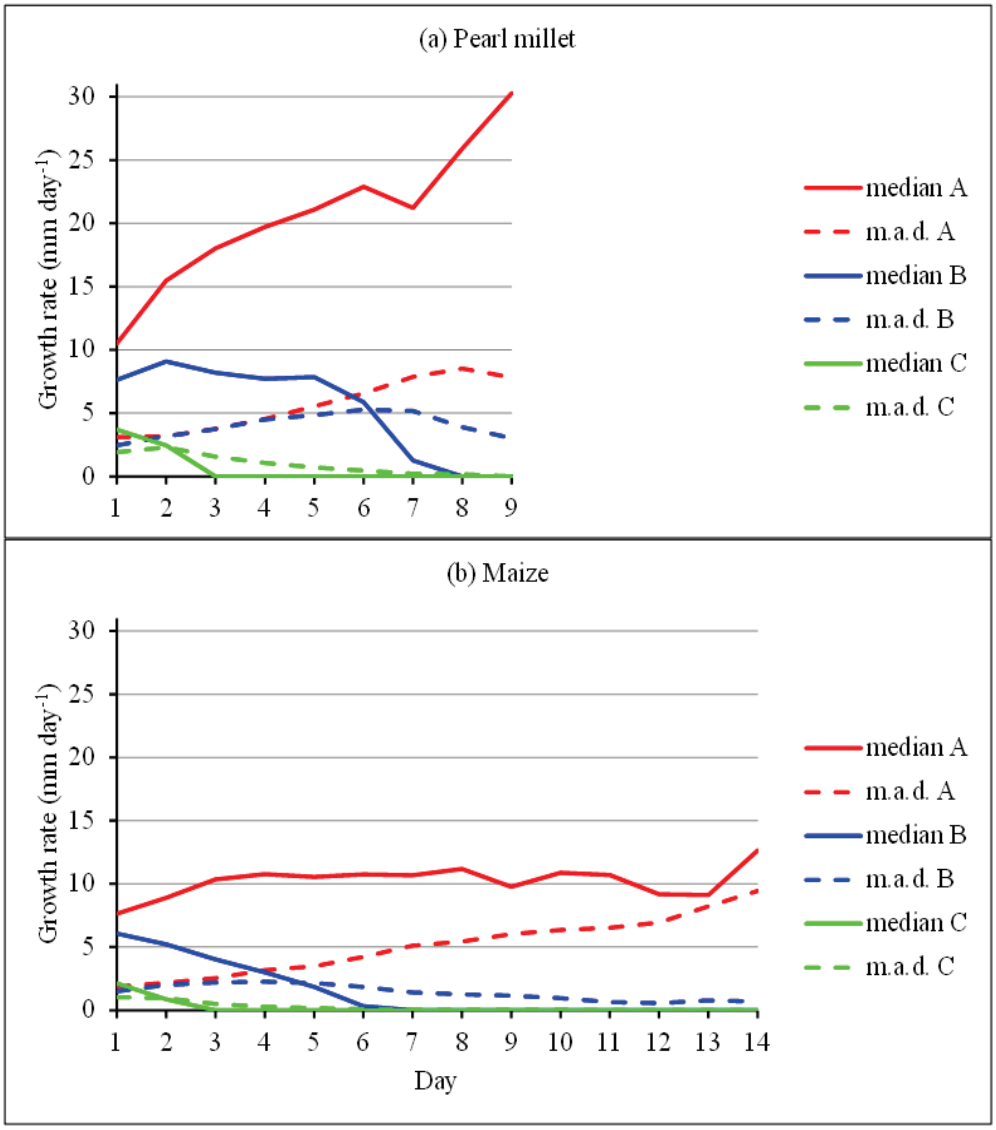

Figure II-4 Daily median growth rate (and associated mean absolute deviation −m.a.d.−) for (**a**) pearl millet and (**b**) maize.

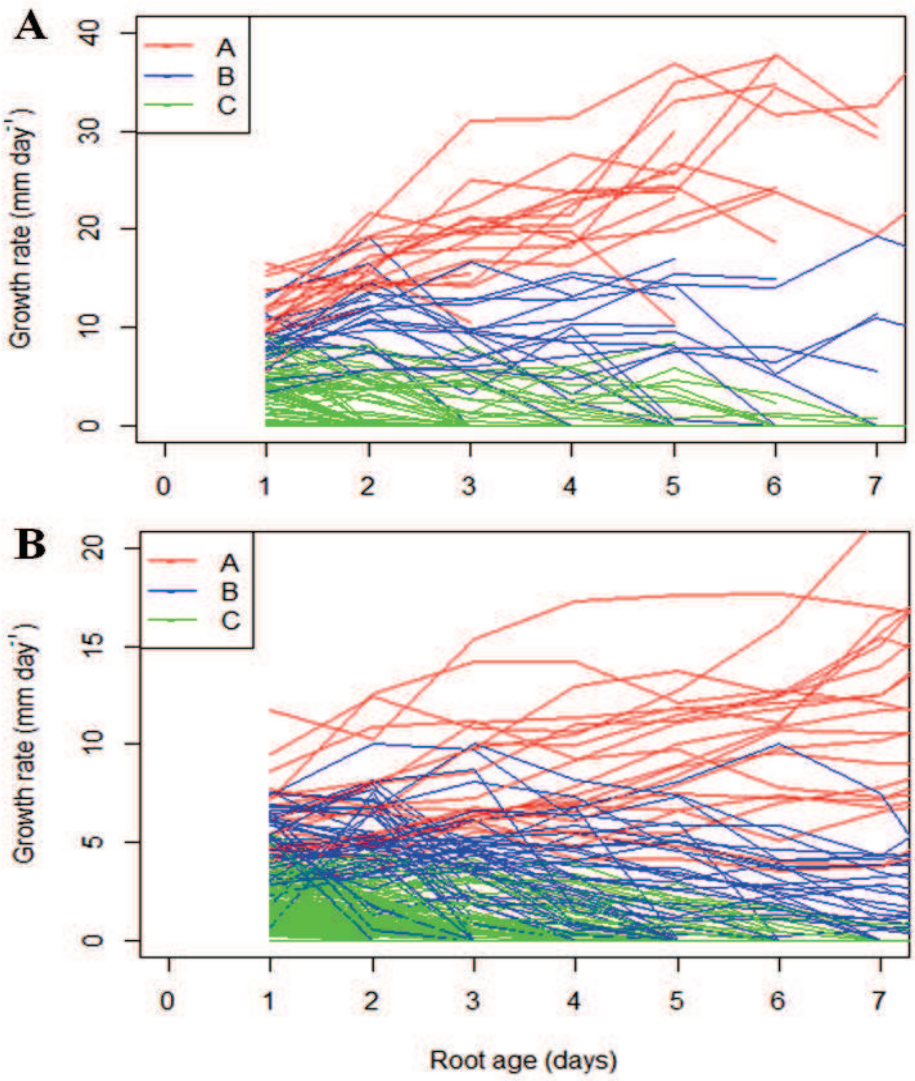

Figure II-5 Growth rate profiles of individual lateral roots of a pearl millet (**A**) and maize (**B**) plant classified with SMS-LM. Colors represent the different types identified with the model.

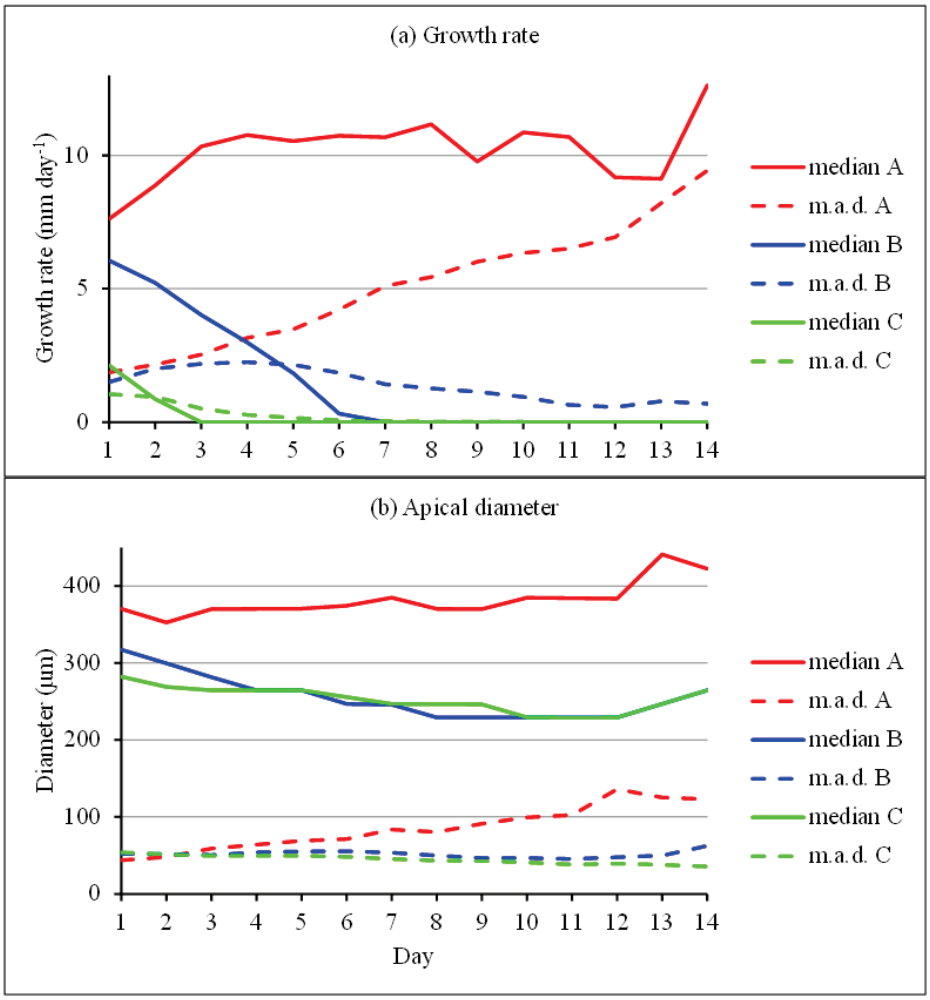

Figure II-6 Maize: (**a**) daily median growth rate and (**b**) apical diameter (and associated mean absolute deviations −m.a.d.−) in the case of 3 groups.

1.2.3 Linking root growth profile with root anatomy

Previous studies have shown that different lateral root types can be defined in maize and pearl millet based on their anatomy (Passot *et al.*, 2016; Varney *et al.*, 1991). To explore the links between root kinetics and root anatomy, we performed root cross sections in 15 maize lateral roots and 35 pearl millet lateral roots with contrasting growth rate profiles. The roots originated from 3 maize plants and 5 pearl millet plants, having grown for 16 days after germination and 12 to 15 days after germination respectively.

Lateral roots were assigned to one of the 3 classes defined previously, based on their growth rate profile. We measured 2 anatomical traits previously shown to be contrasting among individual roots (Passot *et al.*, 2016), stele diameter and central pith diameter. For

pearl millet, the ABC classification of growth rate profiles was mirrored by a ranking of both stele diameter and pith diameter, although there was some overlap between classes (**Figure II-7**). By contrast, no clear trend could be detected in maize, in particular due to the low number (1) of type A roots, the large spread of anatomical dimensions in type B roots and the comparatively large anatomical dimensions of the type C roots. Globally, a consistent tendency was observed between stele diameter and pith diameter that encompassed both species. These results suggest a correlation between anatomical traits and growth profile for pearl millet, but not for maize lateral roots. The small sample size for maize roots could explain the lack of observable relationship.

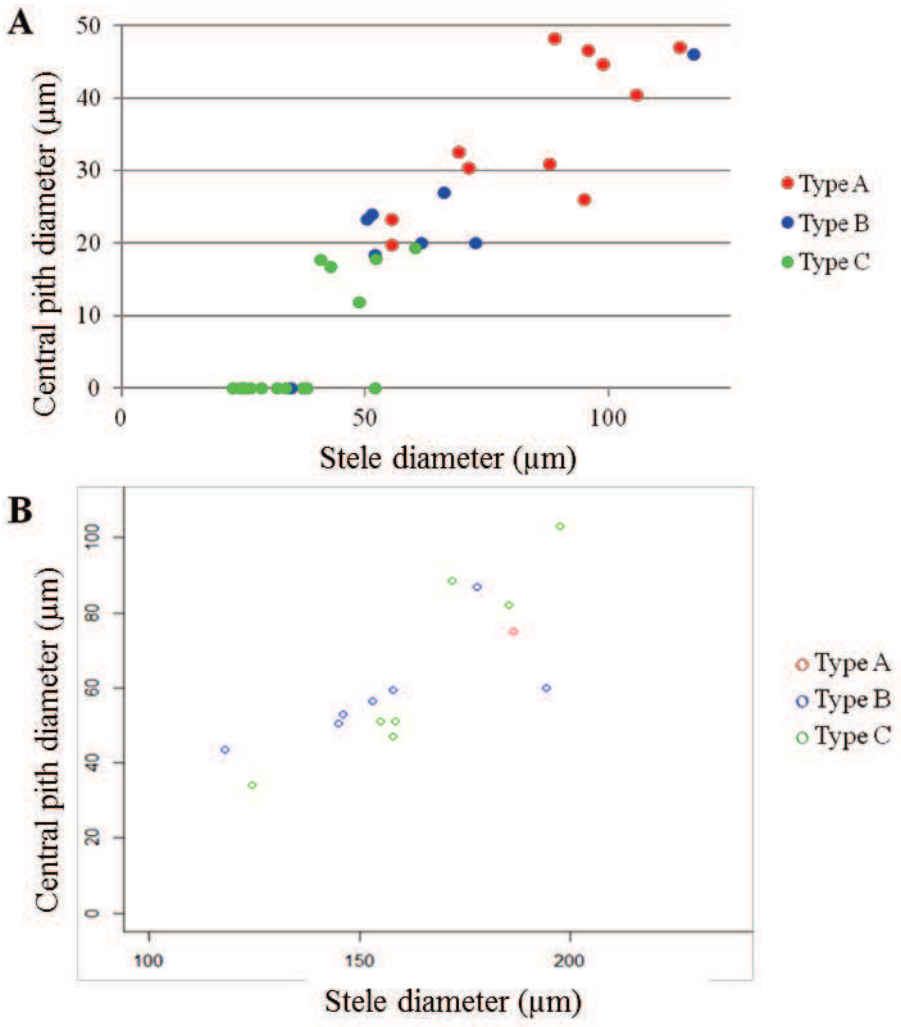

Figure II-7 Relationship between stele and central pith diameter of lateral roots in pearl millet (**A**) and maize (**B**). Colors indicate the estimated type based on the SMS-LM.

1.2.4 Analyzing the primary root branching pattern

In order to explore whether lateral root type repartition along the primary root was random or somehow structured, we analyzed the distribution of lateral root types (A, B and C) along the primary root. We first evaluated the impact of the root type on the length of the interval between a lateral root and its nearest neighbor in the rootward direction (Baskin *et al*., 2010). No difference was found between the mean interval length for the three root types in both species (ANOVA, p-value = 0.83 and 0.7 for pearl millet and maize respectively) (**Table II-1**). The same type of analysis was conducted separating intervals into 9 groups, depending on the types of the two lateral roots delimiting the interval (**Supplementary Table II-5**). No effect of the lateral root types was found on the interval lengths (ANOVA, p-value = 0.52 and 0.39 for pearl millet and maize respectively). Hence, our results indicate that there is no influence of root types on interval lengths between two successive lateral roots.

Table II-1 Length of the interval between successive lateral roots, classified according to the lateral root delimiting the interval in the shootward direction. No significant differences between the means were found (ANOVA, p = 0.83 and p = 0.70 for pearl millet and maize respectively).

Lateral root type in the shootward direction	A		B		C	
	Pearl millet	Maize	Pearl millet	Maize	Pearl millet	Maize
Sample size	165	237	296	814	785	1950
Mean (cm)	0.22	0.16	0.21	0.16	0.21	0.17
Standard deviation (cm)	0.27	0.16	0.27	0.15	0.19	0.15

We then questioned whether lateral root type sequences were random or somehow structured. We first computed the Spearman rank autocorrelation function for these sequences. The autocorrelation function for positive lags was within the confidence interval corresponding to the randomness assumption for most of the plants, indicating that the distribution of the different lateral root types along the primary root was stationary and

suggesting no marked dependencies between successive lateral root types. This finding was consistent with the growth rate profile length frequency distributions being similar for the three types (**Supplementary Table II-4**). Since growth rate profile lengths directly depend on the emergence time of each lateral root and are thus related to the lateral root position on the primary root, this suggests that the proportions of the 3 types along the primary root were essentially stationary. We further analyzed primary root branching sequences applying a statistical modeling approach. To this end, we modeled potential dependencies between successive lateral root types described from the collar to the root tip. Three-state variable-order Markov chains, each state corresponding to a lateral root type, were built. The memories of variable-order Markov chains were selected (Csiszár and Talata, 2006) for each primary root branching sequence and for samples of branching sequences corresponding to each species. For all plants and for both species, a zero-order Markov chain was selected. This confirmed that the type of a lateral root was independent of the type of the previous lateral roots. Hence, our results indicate that there is no influence of the lateral root growth pattern on the distance to or on the growth pattern of the next lateral root.

We checked whether the length of the interval between successive lateral roots and the lateral root type proportions varied or not among individual plants. The mean interval lengths were not equal in all plants (ANOVA, $p < 10^{-5}$ for pearl millet and $p < 10^{-6}$ for maize). Plants were thus classified according to Tukey's Honest Significant Difference. Two overlapping groups were found, both for pearl millet and maize (**Figure II-8**), with average interval length ranging from 0.31 to 0.21 cm in pearl millet, and from 0.25 to 0.14 cm in maize.

Significant differences among plants were also found for lateral root type proportions both for pearl millet and maize (Kruskal-Wallis test, $p < 10^{-10}$ and $p < 10^{-15}$ respectively, **Figure II-9**). For pearl millet, the 8 plants were separated into 3 significantly different groups with two overlapping. The proportion of type A roots ranged from 0.06 to 0.21 between these groups. The 13 maize plants were separated into 6 groups, with some overlaps between groups, type A root proportion ranging from 0 to 0.2. These results indicated that both species show significant inter-individual differences in terms of interval lengths and lateral root type proportions. However, and despite individual differences between plants in terms of lateral root type proportions, the stationary random branching pattern was markedly conserved in all plants. As all plants among species are supposed to be genetically homogeneous, we hypothesize that small environmental variations, either during the grain filling and maturation period or during the experiment itself, could explain differences in lateral root type proportions. The link between interval length and lateral root type proportions in each plant is explored in **Supplementary Result II-1**.

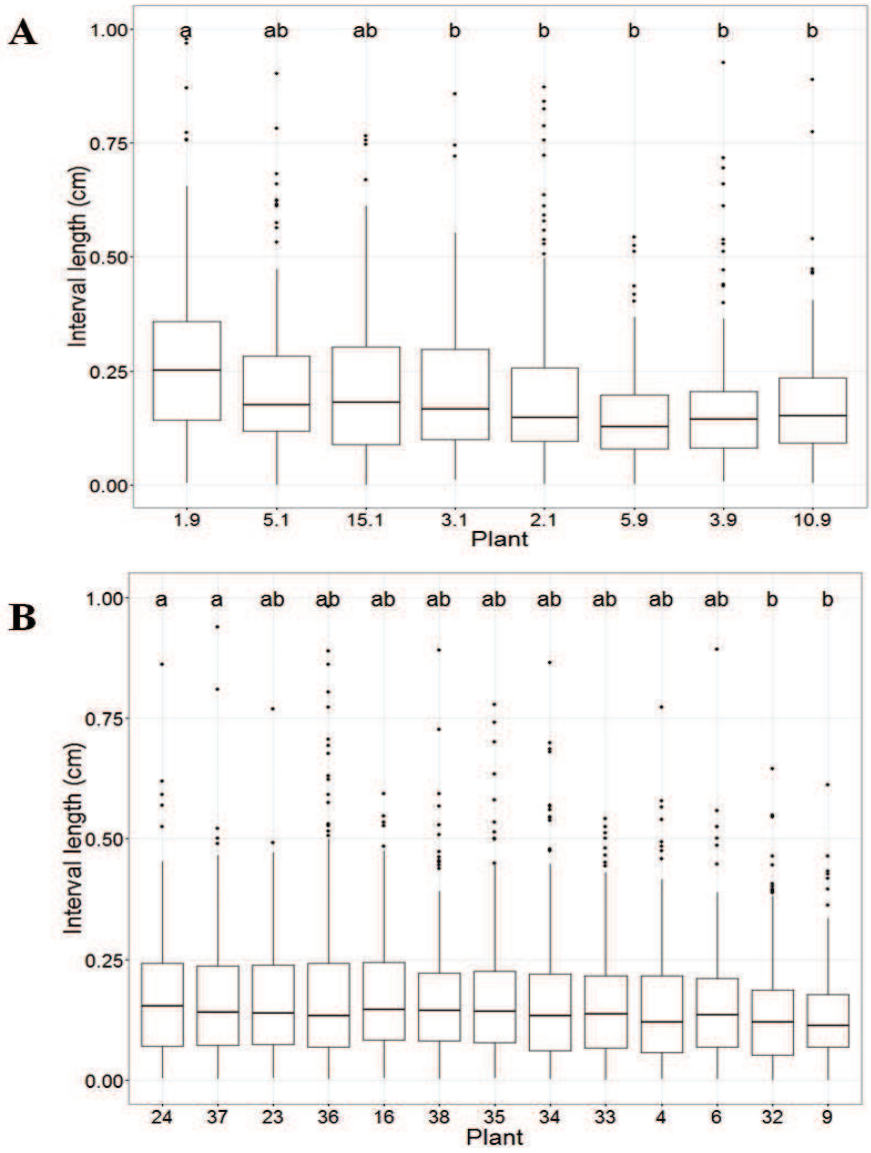

Figure II-8 Distribution of interval lengths between successive lateral roots for each plant in pearl millet (**A**) and maize (**B**) species and plant group assignation according to Tukey's Honest Significant Difference test. Outliers above 1 cm were curtailed. Numbers along the x – axis refer to plant ID.

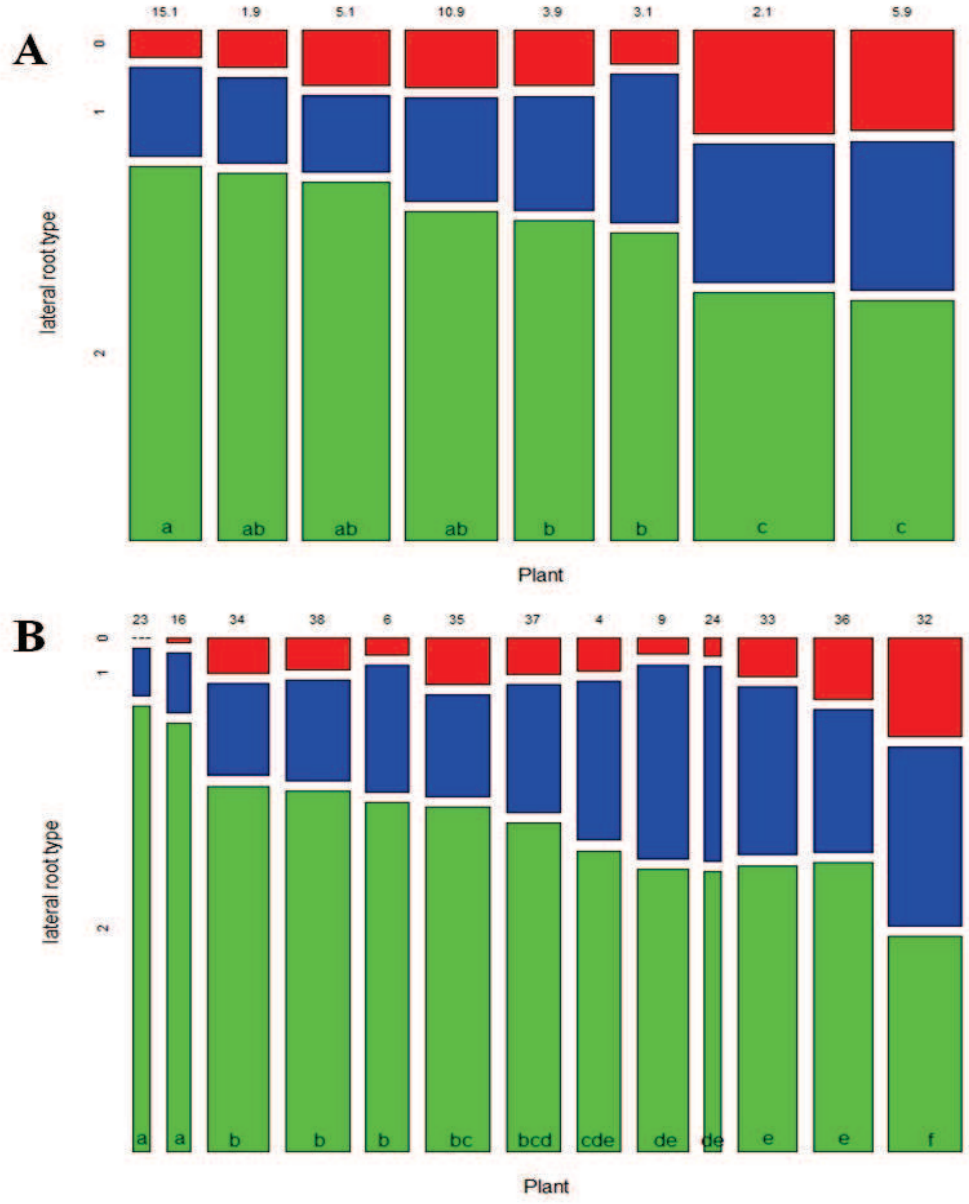

Figure II-9 Proportion of root types for each plant in pearl millet (**A**) and maize (**B**) species and plant group assignation according to Kruskal-Wallis test. Tile areas are proportional to the number of roots in each category. Total lateral root number per plant ranged from 119 to 248 for pearl millet and from 82 to 352 for maize and are proportional to tile width. Numbers above tiles refer to plant ID.

1.3 Discussion

1.3.1 An original methodology to classify lateral roots

In this study, we designed a pipeline for semi-automated analysis of lateral root growth profiles and primary root branching pattern and applied it to explore the diversity of lateral roots in two cereals, maize and pearl millet. Previous efforts to classify the diversity of lateral roots in cereal species into classes have been reported (Henry *et al*., 2016; Passot *et al*., 2016; Rebouillat *et al*., 2009; Varney *et al*., 1991; Watt *et al*., 2008) but these classes were often based on anatomical traits, mainly root diameters and vasculature. A first difficulty comes with the fact that some morphological traits change along lateral roots, typically root diameter (Wu *et al*., 2016), which was confirmed in our own data in maize. A different classification method, based on growth rates, was reported in rice (Rebouillat *et al*., 2009), where root growth rates were very contrasted among lateral roots but assignment to classes was based on expert knowledge. Here we assigned lateral roots to classes based on their growth profiles using a statistical model. Our approach revealed 3 similar classes of lateral roots in two different cereal species. Although absolute growth rates were different between lateral roots of the two species, general shapes of the three median growth rate profiles as well as relative proportion of the three lateral root types were similar between species. Growth durations in the three classes were also remarkably similar between the two species. In previous studies, three anatomical types of lateral roots were identified in pearl millet (Passot *et al*., 2016) and here these types were found to be partially related to the classes based on growth rate profiles. Link between growth rate profiles and anatomy was less clear in maize but maize root diameters were positively linked to growth rate profiles, confirming a general, but not systematical trend (Pagès, 1995). However, diameter of internal root structures was larger for maize than for pearl millet, meaning that the relationship between root diameter and growth rate profiles is not transposable between species.

1.3.2 Origin and roles for the three lateral root types

The identification of 3 types of lateral roots raises questions on the origin of this variability and the potential functions of these three types. In rice, fast-growing lateral roots are also thicker and additional periclinal cell divisions in the endodermal cell layer producing additional mesodermal cell layers during the process of primordia establishment have been reported in these large lateral roots (Rebouillat *et al*., 2009). Variability among the size of lateral root primordia has been reported in maize (MacLeod, 1990) and could account for differences in apical diameter and root growth rate, at least at emergence. Along these lines, lateral root variability would be determined early in development and would be tightly associated with morphology (diameter) and anatomy (Thaler and Pagès, 1996a). The ranking in root anatomy (stele and central pith diameter) with root classes (based on growth rate

profile) evidenced in pearl millet goes in this direction. Root diameters at emergence were also ranked according to growth rate profiles in maize. Another possibility is that growth rate variability is determined after emergence and is controlled by different factors depending on the plant physiology (as local assimilate availability) and/or environmental sensing (local water and nutrients availability, local soil structure…). According to this hypothesis, root development may be more plastic. This hypothesis is for example supported by root apical meristem loss happening in most lateral roots of field grown maize (Varney and McCully, 1991). In this case, lateral roots are thought to emerge without differences between each other and to lose their elongation potential after emergence, probably due to environmental conditions or internal clues. Our results showed that lateral root growth patterns are only partially determined by their initial growth rate, due to the divergent nature of the growth rate profiles. The parallelism between the change in root diameterand growth arrest in maize is also in favor of a link between structural changes, post-emergence growth and growth rate. These two hypotheses may not be exclusive and growth patterns may result from a combination of these two influences, pre- and post-emergence. Factors influencing initial growth rate, growth maintenance and growth arrest could also be different, therefore rendering the picture more complex and the overall patterns of lateral roots globally more plastic to face a variability of external and internal clues (Malamy, 2005).

The functions of these different lateral root types are not precisely known. Locally, each lateral root type could have a preferential function, like water uptake, absorption of certain nutrients, exudation or mycorrhization. In maize, apical meristem loss was suggested to facilitate water uptake (Varney and McCully, 1991). The three major macroscopic elements (N, P and K) for mineral nutrition are absorbed as ions whose diffusion coefficient in the soil widely differ (recalled by Pagès (2011)) and the different lateral root types could share their efforts into those distinct functions. Moreover, these roots may have also longer term functions. In rice, only one lateral root type is known to participate in higher level of branching (Gowda *et al.*, 2011). In perennials, these long lateral roots contribute to the perennial structure of the plant (Coutts, 1987). The existence of different growth profiles is thus likely to contribute to the economy in root system construction. The different root growth patterns described here could be indeed an important component for the efficiency of soil exploration. The interest of such variations to enhance root foraging capacity was already suggested (Forde, 2009) while their cost/benefit advantage as compared to more homogenous lateral root patterns was demonstrated using simulated root systems (Pagès, 2011). Notably, growth cessation appears as an important strategy to avoid an excessive cost of root system. In our data, root type corresponding to indeterminate lateral root growth represented only 14% and 9% of the lateral roots in pearl millet and maize respectively. In an annual cereal plants, the specific functions of these long roots is unknown, but we can imagine a role in

further widening exploration in the horizontal dimension in opposition to exploration in depth covered by the primary and the limited horizontal exploration by nodal roots.

1.3.3 Positioning of the three lateral root classes is random along the primary root

One benefit of our approach is that it enables architectural analysis. All lateral roots were assigned to classes and precisely positioned on the primary axis. We showed that, both in maize and pearl millet, the longitudinal spacing of lateral roots was highly variable, both within and between root systems. Despite this variability, the average between-lateral-root distance was relatively conserved among plants for each species, being larger for millet than for maize. Our analyses showed that there was no relationship between the length of the interval between two successive lateral roots and the growth class of these lateral roots. This indicates that both fast-growing and slow-growing roots may be close or far from neighboring roots. The absence of relationship between lateral root spacing and growth rate suggests that lateral root initiation and development are regulated independently. Moreover, we found that the succession of lateral root types was random along the primary root, indicating that there were no local dependencies in root type succession. In other word, lateral roots appear to grow independently from each other since no local inhibition or stimulation could be observed. The absence of local dependencies can be related to the homogeneous soil in our experimental system. Indeed, the existence of soil heterogeneity is known to lead to spatial structuring, for example local proliferation of longer roots in response to nitrate-rich soil patches (Drew, 1975; Hodge, 2004). Our modeling approach thus opens up new avenues forthe exploration of the link between local root environment and proportion of the different root types on a stronger basis.

1.3.4 Extending the longitudinal modeling framework for studying the whole growth profile of type A lateral roots

The experiment duration constrained by the rhizotron dimensions made that only the beginning of type A lateral root growth could be observed. Hence, most of the growth rate profiles assigned to type A lateral roots were censored in the corresponding growth state for both species. This makes a marked difference with type B or C lateral roots for which the whole growth profile, up to growth arrest, was observed for many individuals. Hence, it would be interesting to design larger rhizotrons or to change the growth conditions in order to study the whole growth of type A lateral roots and in particular the transition from increasing or stationary growth rate to decreasing growth rate. The proposed modeling framework can directly be extended by adding states in series for modeling successive growth phases for type A lateral roots. Such extension of semi-Markov switching models with states in series was recently developed for modeling successive developmental phase in *Arabidopsis* rosette in Lièvre *et al*. (2016). We may expect a single state with decreasing growth rate following the

current increasing growth rate state A or an intermediate roughly stationary growth state between the increasing and decreasing growth rate states. Although mechanisms of lateral root growth arrest are documented for maize (Varney and McCully, 1991), the future of "indeterminate" lateral roots is not documented. If their growth duration appear to be really longer than what our experimental set up allowed to see, it could interfere with the decay of primary root system reported in cereals, occurring for example within two months in pearl millet (Maiti and Bidinger, 1981).

1.3.5 A new look at lateral roots in future high-throughput phenotyping analyses?

To date, genetic improvement based on structural feature of the root system has essentially concentrated on deep vs. shallow rooting (Saengwilai *et al*., 2014) as well as on structural feature such as the presence of aerenchyma in maize roots, suspected to decrease the carbon construction cost of roots without affecting their function (Zhu *et al*., 2010). Lateral roots have been comparatively overlooked although they represent the best example of the overall structural plasticity of the root system to face the variable and unpredictable nature of the soil encountered (Drew, 1975). Therefore, there could exist a mine of genetic variation to exploit (and not only in cereals) if relevant phenotyping pipelines for lateral roots were available. By combining image analysis and statistical modeling, our pipeline is a first step in that direction. Importantly, the structure of the model is flexible enough to accommodate variation in the structure such as the number of root types. Of course, while some steps such as image analysis are already semi-automated, some others will need to be automated to upscale the pipeline to study larger plant populations. Rhizotron handling and scanning could be automated with robot. Moreover, basic tasks could be automated, such as image reconstitution by stamping top and bottom part of the rhizotron, root system alignment from one day to another in SmartRoot or lateral root growth profile generation. The most limiting step appeared to be root tracing and dataset cleaning. Indeed, we found that data curation was necessary and could have a huge impact on the accuracy of the analysis. Curation minimized aberrant root growth profiles by modifying data without necessarily going back to the original image, in order to keep as many roots as possible. No clear criteria exist on what a "realistic" lateral root growth profile should look like and we therefore hypothesized that growth rate changes were smooth rather than steep to clean our database. Visual checking of aberrant growth profiles tended to confirm that our hypotheses on the sources of errors were often reasonable. This cleaning algorithm could be further improved by checking steep growth rate changes without stopping that were not taken into account in our algorithm.

In our experiment, with apparently uniform conditions among plants, variability in root type proportion appeared between plants, suggesting that the proportion of each root type is very sensitive to small environmental variations, vigor differences between plants and/or

differences among seeds. Our pipeline allows to experiment with large replication number and generates parameters that can be statistically compared among genotypes or environmental conditions, opening the door to high throughput phenotyping with a focus on this yet underexploited source of variation: lateral roots.

1.4 Materials and Methods

1.4.1 Experimental

Root observation boxes, called rhizotrons, were built according to Neufeld *et al.* (1989). The size of the frame was 400 x 700 so that they could be imaged with 2 contiguous A3 images using a scanner. The root system was sandwiched against a plexiglass surface by a layer of viscose that was impermeable to roots, but permeable to water and nutrients. Rhizotrons were made of (back to front) a 5 mm thick extruded polystyrene plate, a 2 cm layer of substrate, a layer of viscose and a 5 mm thick plexiglass plate, all joined together using aluminum U frame held by screws. The substrate used was composed of 30% fine clay, 25% peat fibers, 5% blond peat and 40% frozen black peat (Klasmann-Deilmann France SARL). The substrate was sieved before being used. The rhizotrons were weighed individually before and after filling to determine the weight of the substrate contained in each one and later to manage daily irrigation.

Maize seeds (*Zea mays*, hybrid B73xUH007) were surface sterilized with 6% hypochlorite for five minutes and rinsed in distilled water for one minute. Seeds were then germinated on moistened filter paper in Petri-dishes (20 x 20 cm) and placed vertically in a growth chamber in the dark at 20°C. Pearl millet germination was performed with a similar protocol, except that seeds were also cleaned with ethanol solution (70%) for 5 minutes after the first rinsing and germination temperature was set to 30°C. Germinated seedlings were transferred individually in the rhizotrons. A layer of wet sphagnum on the top of the rhizotrons maintained the seedlings and prevented them from drying. Rhizotrons were placed in a growth room with climatic conditions adapted to each species: a temperature of 28°C during day and 24°C during night for pearl millet and a constant temperature of 20°C for maize, with a 14-hour-photoperiod for both species. Light was provided by 6 mercury lamps (HQI, 250 W, Osram, Munich, Germany) and measured by a light sensor (SKP215; Skye Instruments, Llandrindod Wells, Powys, UK). Temperature and air humidity were recorded (HC2-SH, Rotronic, Bassersdorf, CH) for each growth room. The sphagnum was watered twice a day at the beginning of the experiment and from 6 days after germination onward, rhizotrons were watered daily using a 1/10 Hoagland solution to maintain the humidity of the substrate. The amount of watering was monitored by a daily weighting of the rhizotron.

1.4.2 Imaging and image processing

From the second day of growth, rhizotrons were scanned with an A3 scanner (Epson Expression 10000XL Pro, Japan) at 600 or 720 DPI. The histogram of the gray level intensities was adjusted to optimize the contrast on fine roots. As rhizotrons are twice the size of the scanner, two images (upper part and lower part of the rhizotron) were taken and aligned using the *Align_4* ImageJ plugin (http://www.mecourse.com/landinig/software/software.html) to recover an image of the entire root system, thanks to landmarks visible in both parts. These landmarks were either added intentionally on the rhizotron or were fortuitously present (water drops, mist, the root system itself).

The SmartRoot software (Lobet *et al*., 2011) was used to extract root system architecture at successive dates and root growth parameters because it supports time-lapse images and focuses on the analysis of individual root behavior. SmartRoot needs images where roots appear darker than background. An ImageJ (v.1.47v; Rasband, W.S., U. S. National Institutes of Health, Bethesda, Maryland, USA) macro was developed to automatically invert and adjust the contrast of the rhizotron images by scaling the image intensity histogram on a fixed range. The optimal contrast (min and max values of the intensity range) was determined empirically to reduce the number of errors when using the algorithm for automatic lateral root tracing provided by SmartRoot (see next section) using a subset of scan images, and was applied to the whole set of images using the macro tool.

1.4.3 Image analysis

SmartRoot enables semi-automatic root tracing. The primary root was drawn on the first image. For the next days, the root system traced on the previous day was imported and aligned, in such a way that the primary root elongated progressively, using automatic tracing. Crown and lateral roots were added as they appeared, either manually or using automatic detection. Their length increased progressively on the successive scans, as for the primary root.

When all roots were traced, the data were extracted with the batch export tool of SmartRoot. This tool provides several measurements including the length, the insertion position and the diameter for each root. Because the resolution was not sufficient for pearl millet lateral roots, we only considered root diameter for maize. Data were ordered and the age of lateral roots was computed at each day, age 0 being assigned to the first day of appearance of a lateral root. The root growth rates were extracted by differencing the length between 2 consecutive days. When the images were not evenly spaced in time, the computation of the growth rate was adapted to take into account the variable lengths of the time intervals.

1.4.4 Correction of growth rate profiles

In spite of manual supervision of root tracings, the exported dataset contained some digitalization errors. It was therefore necessary to characterize the implausible data points resulting from such errors and to clean out the dataset to ensure that any later analysis is performed on trustable data. We thus designed a data correction algorithm aiming at identifying implausible growth rate profiles that derive from errors in image analysis. The most typical errors were defaults in alignment, missing data at one time increment or non-visible root tips in the case of roots encountering an obstacle. This kind of errors results in implausible trajectories for the root length at some time-point, which can be better identified by examining growth rate profiles. Depending on the type of error, growth rate profiles were either corrected or truncated before the first implausible growth rate. The proposed data correction algorithm is described in **Appendix II-3**.

1.4.5 Model description

Definition of semi-Markov switching linear models

Semi-Markov switching linear models (SMS-LMs) are two-scale models that generalize hidden semi-Markov chains by incorporating linear regression models as observation models. They are formally defined in **Appendix II-1**. In our context, the succession and duration of growth phases (coarse scale) are represented by a non-observable semi-Markov chain while the growth rate trend within a growth phase (fine scale) are represented by observation linear models attached to each state of the semi-Markov chain. Hence, each state of the semi-Markov chain represents a growth phase. A J-state semi-Markov chain is defined by three subsets of parameters:

1. Initial probabilities $\left(\pi_j; j = 1,\ldots,J\right)$ to model which is the first phase occurring in the series measured,
2. Transition probabilities $\left(p_{ij}; i, j = 1,\ldots,J\right)$ to model the succession of phases,
3. Occupancy distributions attached to non-absorbing states (a state is said to be absorbing if, after entering this state, it is impossible to leave it) to model the growth phase duration in number of days. We used, as possible parametric state occupancy distributions binomial distributions B(d, n, p), Poisson distributions P(d, λ) and negative binomial distributions NB(d, r, p) with an additional shift parameter $d \geq 1$.

A SMS-LM adds observations linear models to the non-observable semi-Markov chain:

4. We chose to model growth rate trends within growth phases using simple linear regression models because of the short length of growth phases (up to 10 successive growth rates for pearl millet and up to 17 successive growth rates for maize).

A SMS-LM composed of parallel transient states followed by a final absorbing state was estimated on the basis of growth rate profiles corresponding to a given species. A state is said to be transient if after leaving this state, it is impossible to return to it. The final absorbing state represented the growth arrest and a degenerate linear model corresponding to a constant null growth rate was associated with this state. Each estimated model was used to compute the most probable state series for each observed growth rate profile (Guédon, 2003). This restored state series can be viewed as the optimal segmentation of the corresponding observed series into at most two sub-series corresponding to a given growth phase either censored or followed by a growth arrest. Because of the transient growth states in parallel, this restoration can be interpreted as a classification of the lateral roots on the basis of their growth rate profiles.

Definition of stationary variable-order Markov chain

Most of the methods for analyzing local dependencies in discrete series rely on high-order Markov chains. However, the number of free parameters of a Markov chain increases exponentially with its order, i.e. with the memory length taken into account. For instance, in the case of three states (corresponding to three lateral root types), the number of free parameters is 2 for a zero-order, 6 for a first-order, 18 for a second-order Markov chain, etc. Since there are no models "in between", this very discontinuous increase in the number of free parameters causes the estimated high-order Markov chains to be generally over-parameterized. This drawback can be overcome by defining sub-classes of parsimonious high-order Markov chains such as variable-order Markov chains (Bühlmann and Wyner, 1999; Ron *et al.*, 1997) where the order is variable and depends on the "context" within the series, instead of being fixed. Stationary variable-order Markov chains are formally defined in **Appendix II-4**.

1.4.6 Root anatomy

Plants were grown in rhizotrons as previously described. Stickers were placed on the viscose tissue previous to the plant transfer, evenly spaced near the position of the future root system to help roots tracking. Lateral root growth rate profiles were extracted before sampling, to determine the type of each root. Selected roots were harvested and fixed overnight in an acetic acid: ethanol solution (1:9) and conserved in 70% ethanol. For maize, two 8 mm long segments were cut from the apex (apical and subapical segments, respectively), as well as one segment at the root base (or basal segment). For short roots (< 8 mm), a single segment (considered basal) was analyzed. For pearl millet, samples were taken indifferently along the root at 12 to 15 DAG. Root segments were gently dried on a filter paper and imbibed in warm (30-45°C) liquid 3% agarose solution (SeaKem GTG Agarose, Lonza). 55 µm-thick sections were obtained from solidified agarose blocks using a vibratome (Microm HM 650V, Thermo Scientific, speed 30, frequency 60). Individual root sections

were then collected, transferred to microscope slides and covered with a coverslip for direct observation.

Images were taken using a Leica DMRB microscope equipped with an epifluorescence filter (excitation range: UV; excitation filter: 460-480 nm). Two pictures were taken for each root section: one under visible light using Nomarsky optics and another using epifluorescence that takes advantage of the natural fluorescence of cell walls with secondary deposits. Images were taken using a Retiga SRV FAST 1394 camera and the QCapture Pro7 software. The RGB images were opened in ImageJ using the Bioformats importer plugin and transformed in gray level 8-bit images. A scale-bar was added to the images according to their magnification. Measurements of the diameter of the root, the stele and the central pith so as the number of xylem poles and vessels were recorded for each root section.

2 Analyzing the modulation of the lateral root growth pattern in different contexts

2.1 Methods

In this section, we present the integrality of the phenotyping experiments on maize root systems performed in this PhD. This includes five independent experiments performed in rhizotrons at the LEPSE research unit and one experiment using the aeroponic platform of the UCL research unit at Louvain-la-Neuve. At the end of each experiment, a number of post-harvesting analyses was done on lateral root samples. In this section we focus on the description of the experimental material and conditions used for these experiments. The experimental protocols associated to post-harvesting analyses will be described in the **Methods** section of **Chapter IV**.

2.1.1 Description of rhizotron experiments and associated post-harvesting analyses

Five experiments in rhizotrons were performed (summarized in **Table II-2**). Rhizotrons were similar to those described in (Neufeld *et al*., 1989) and measured 64 cm high, 38 cm wide and 2 cm thick (internal dimensions). Root systems could develop in a plane between a transparent plexiglass layer placed at the front and a nylon mesh preventing the roots from entering into the substrate (**Figure II-10**). The substrate used was composed of 30% fine clay, 25% peat fibers, 5% blond peat and 40% frozen black peat (Klasmann-Deilmann France SARL). This substrate was sieved before rhizotron filling. During all the experiments, rhizotrons were placed in a growth chamber with controlled environmental conditions, with a constant temperature of 20°C, a vapor pressure deficit of 1 kPa and 14 h light d^{-1}. The

photosynthetically active radiation was 200 µmol m s^{-1} except for shaded plants, for which it was reduced to 100 µmol m s^{-1}.

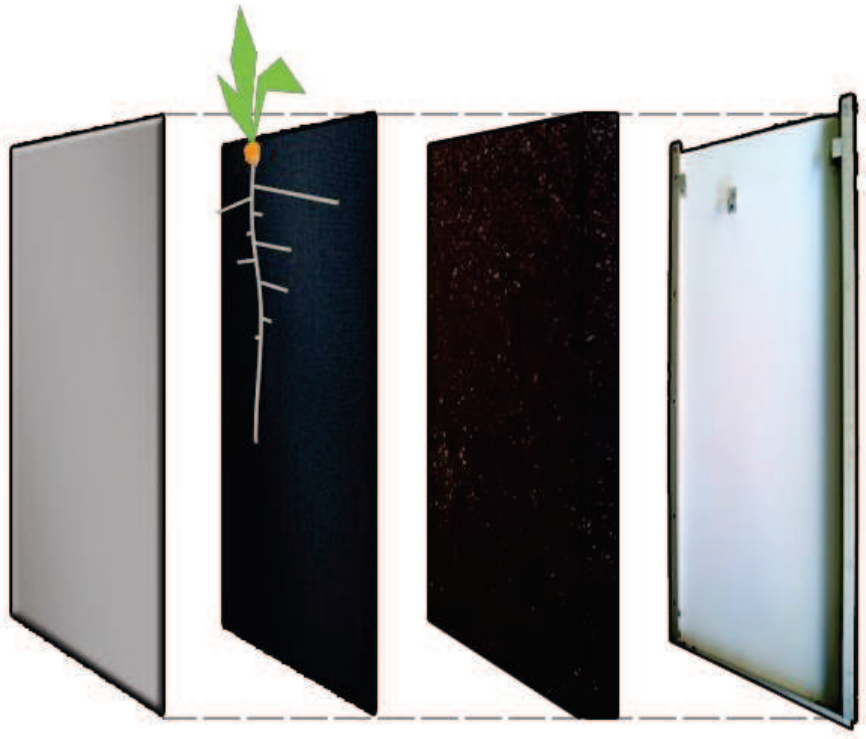

Figure II-10 Illustration of the rhizotron device used for the observation of maize root systems. Root systems are allowed to develop in a plane between a transparent plexiglass layer placed at the front and a nylon fabric preventing the roots from entering into the substrate. Different layers are (from left to right): 5 mm thick plexiglass plate, nylon fabric, 2 cm layer of substrate, 5 mm thick extruded polystyrene plate.

The first experiment (GFBM1) was performed in March 2013 and included 16 plants from the hybrid line B73xUH007 (control conditions, abbreviated "CTRL"), one in each of the 16 available rhizotrons. Scanning of rhizotrons was interrupted 18 DAS when the first primary root reached the bottom of the rhizotron. The harvesting period extended for 14 days from this date. This preliminary experiment allowed us (i) to empirically estimate the duration of a root phenotyping experiment for plants in our growing conditions (around 18 DAS for plants growing at 20°C) and (ii) to collect material to develop different protocols specific to lateral roots. These experimental protocols included: (i) a RNA extraction protocol for the quantification of gene expression; (ii) a microscopy protocol to measure the epidermal cell lengths in root meristems and finally and (iii) a sugar quantification protocol destined to measure the sugar content on lateral roots. Moreover, thanks to this experiment we checked the feasibility of performing a SmartRoot analysis of scanned root systems (correct detection of lateral root diameters, development of R scripts to extract root growth time series, etc).

The second experiment (GFBM2) was performed in May 2013. The aim was to observe the effect of a perturbation in auxin signaling using mutants *rum1* (von Behrens et al., 2011) and *rtcs* (Taramino et al., 2007) referred as "RUM1" and "RTCS", respectively. Because of the slow growth rate of the mutants, the experiment ended 27 DAS. The harvesting period extended for 5 days from this date. A severe problem of contamination reduced the number of usable plants, and only samples for epidermal cell length analysis were collected.

The third experiment (BMEC1) was performed in April 2014. A total of 30 plants from the hybrid B73xUH007 were grown, 2 in each rhizotron. The aim of the experiment was to increase the arrival of carbohydrates (and possibly auxin) to lateral roots attached to the primary root by the excision of seminal and nodal roots, competing for plant resources with the primary root. Seminal and nodal roots were excised in 20 plants, and the remaining 10 were used as control. The excision was performed at 2 different times, when the primary axis was 20 cm long ("Early excision", abbreviated "EXCA") and no lateral root had emerged yet, or when the primary root was 30 cm long ("Late excision", abbreviated "EXCB") and the branching zone was approximately 10 cm long. The gene expression and sugar content were checked for the lateral roots in excised and non-excised plants to evaluate the effect of the excision of competitive roots in lateral root development. In addition, lateral root primordium development along the unbranched zone of the primary root was examined for a subset of plants in this experiment.

The fourth experiment (BMFS1), performed in October 2014 included different modalities: (i) a shading treatment ("OMB", 8 plants) where incident ligth was reduced by 50% in order to reduce the availability of carbohydrates; (ii) the excision of the endosperm at time of seedling transfer ("END", 6 plants) as a complementary way to reduce the availability of carbohydrates; (iii) the excision of nodal and seminal roots (4 plants) as in experiment BMEC; (iv) the auxin signaling mutants *rtcs* (6 plants) and (v) *rum1* (6 plants) as in experiment GFBM2. In this experiment, the observation of the development of lateral roots was limited to a 20 cm long segment of the primary root starting from the seed to simplify the analysis. Molecular analyses of BMFS experiment were focused on sugar quantification in all the previous modalities.

The fifth and last experiment (BMSP) was performed in November 2015 with the aim of characterizing root anatomy in lateral roots of B73xUH007 plants, unexplored up to this moment.

During experiments, maize root systems were imaged and traced to extract root growth profiles as previously described (**sections 1.4.2 and 1.4.3** of this Chapter). FA summary of the post-harvesting analyses performed in each rhizotron experiment is given in **Table II-3**.

As a reminder, the experimental protocols and results associated to these analyses will be presented in **Chapters III** and **IV.**

Table II-2 Summary of *Zea mays sp*. experiments presented in chronological order. Abbrevations are CTRL for B73xUH007 in control conditions; RTCS for *rtcs* mutant, RUM1 for *rum1* mutant; EXCA and EXCB for early and late nodal and seminal excision respectively; OMB for shading; END for endosperm removal.

Experiment #	Experiment name	Date	Genotype	Treatments (number of plants)
1	GFBM1	2013, Mars	B73xUH007	CTRL (16)
2	GFBM2	2013, May	*rtcs*	RTCS (8)
			rum1	RUM1 (8)
3	BMEC1	2014, Apr	B73xUH007	CTRL (10) EXCA (10) EXCB (10)
4	BMFS1	2014, Oct	B73xUH007	CTRL(8) OMB (8) END (6) EXCA (4)
			rtcs	RTCS (6)
			rum1	RUM1 (6)
5	BMSP	2015, Sept	B73xUH007	CTRL (6)

Table II-3 Summary of the different kinds of post-harvesting analyses performed for each experiment. 'LRP' refers to the analysis of lateral root primordia; 'root anatomy' refers to the analysis of lateral root cross-sections; 'epidermal cell lengths' refers to the analysis of cell length measurements on lateral root apices; 'RNA' refers to the gene expression analysis performed on lateral root apices; 'sugar' refers to the quantification of soluble sugars in lateral root apices. See **section 1** of **Chapter IV** for a detailed description of the associated experimental protocols.

Experiment #	Experiment name	Treatments	LRP	Root anatomy	Epidermal cell lengths	RNA	Sugar
1	GFBM1	CTRL			✓		✓
2	GFBM2	RTCS			✓		
		RUM1			✓		
3	BMEC1	CTRL	✓			✓	✓
		EXCA	✓			✓	✓
		EXCB	✓			✓	✓
4	BMFS1	CTRL					✓
		OMB					✓
		END					✓
		EXCA					✓
		RTCS					✓
		RUM1					✓
5	BMSP	CTRL		✓			

2.1.2 Aeroponic experiment in collaboration with UCL

In addition to rhizotron experiments, we studied maize root system development in the aeroponic platform (de Dorlodot et al., 2007) conceived by the UCL research unit in Louvain-la-Neuve, Belgium. A detailed description of this experiment is given in **Supplementary Methods II-1**.

2.2 Results

2.2.1 Model-based analysis of the influence of treatments on lateral root growth rate profiles and apical diameters

In order to investigate the impact of shading and disrupted auxin signaling on growth rate profiles, we used the model-based clustering SMS-LM to classify lateral root growth rate profiles in spite of their high degree of censoring. Basic assumptions of this model were the linearity of the growth trend during the growth phase and the existence of a phase of growth arrest at the end of the initial growth phase. Such model, previously presented in **section 1.4.5** of this Chapter, was initially developed on data from *wild-type* (CTRL) plants and identified three main trends in growth rate profiles. In this section, we extend the application of the SMS-LMs to the growth rate profiles obtained in shaded (OMB) plants and those of the auxin signaling *rtcs* mutant (RTCS). Due to time constraints, the application of the model to the remaining modalities (early and late nodal and seminal excision, endospermal excision and auxin signaling *rum1* mutant) could not be achieved before the end of this PhD.

Shading experiment

Lateral root growth rate profiles of shaded plants were used to build a SMS-LM specific for this treatment. The empirical selection of the number of growth states favored a grouping of lateral growth rate profiles into only two classes in shaded plants, with satisfactory values for the posterior probabilities of the optimal assignment of each lateral growth rate profile and the overlap between the growth rate profiles of the two classes (not shown).

Results are presented in **Figure II-11**. Two decreasing trends in growth rates could be observed for lateral roots of shaded plants (named B and C). Roots assigned to class B had initial growth rates around 5 mm day^{-1} and finished growth on average 6 days after emergence. Roots in class C presented lower initial growth rates (around 2 mm day^{-1}) and shorter growth duration, with a majority of roots being arrested by day 3. Regarding root apical diameters, initial values were around 370 µm for B and 350 µm for C roots. In both cases, root apical diameter tended to decrease with root age, more quickly for C than for B roots, and to stabilize at a value close to 335 µm. Trends in root apical diameters at root ages further than 7 days after emergence for B and C roots were ignored since the vast majority of

roots was already arrested at this time and root apical diameter was not expected to be modified after root arrest.

Finally, we quantified the relative abundance of root elongation categories. This analysis indicated about two thirds (72.6 %) of C roots and one third (27.4 %) of B roots for shaded plants. We also assigned lateral root growth rate profiles using the SMS-LM previously built on the basis of wild-type plants. We obtained 94% of match between the two independent assignments indicating that the definition of B and C lateral root types on the basis of growth rate profiles is very similar for shaded and unshaded plants.

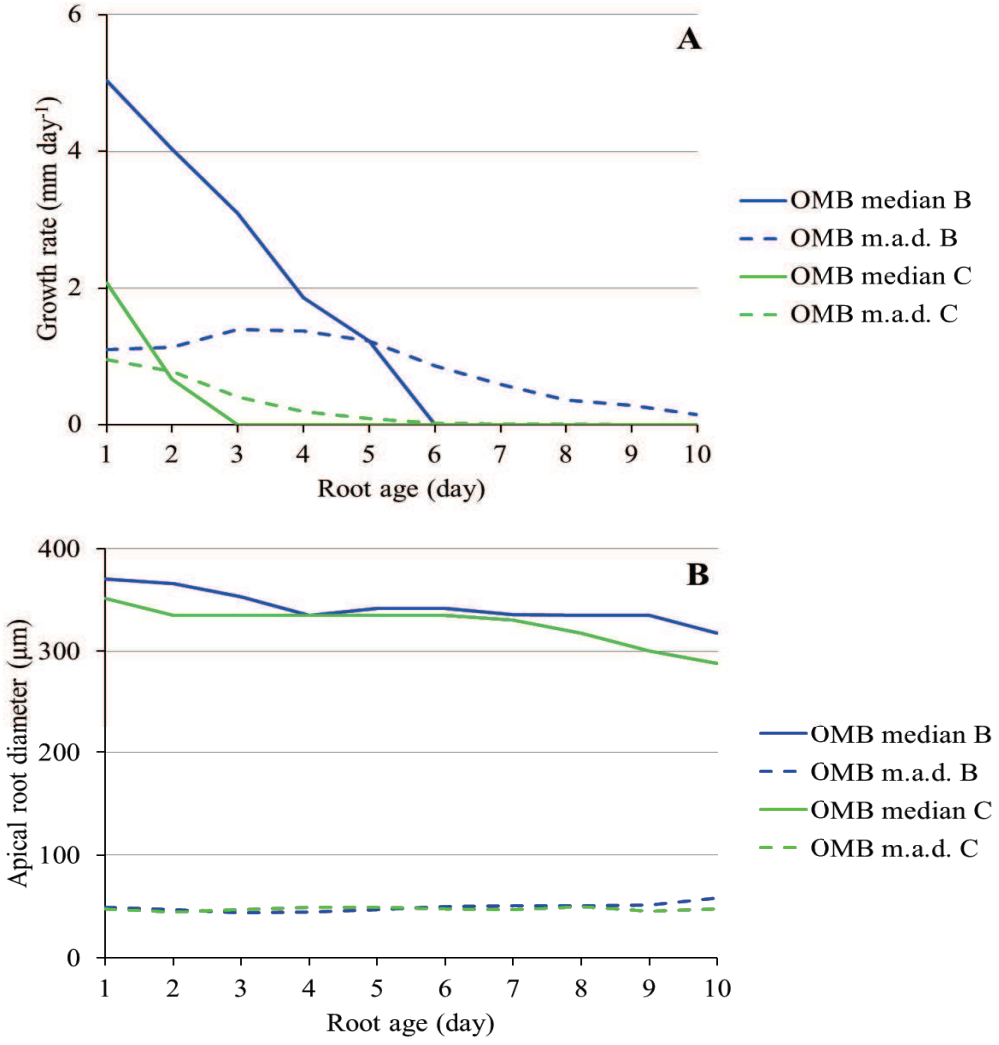

Figure II-11 Shading (OMB) treatment: (**A**) daily median growth rate and (**B**) apical diameter (and associated mean absolute deviations −m.a.d.−).

Auxin signaling *rtcs* mutant

Lateral root growth profiles of *rtcs* plants were used to estimate a SMS-LM specific to this mutant genotype. The selected structure of *rtcs* lateral growth profiles consisted of three root classes (details concerning the empirical selection of the number of root classes are not shown).

The empirical growth trends deduced from the SMS-LM clustering are presented in **Figure II-12A**. Associated trends in apical diameters are shown in **Figure II-12B**. The identified trends in growth rate were either increasing (A) or decreasing (B and C). Growth half-lives for B and C roots were 7 and 4 days, respectively. Initial growth rates were higher for roots with sustained growth in class A, and lower for B and C roots.

A similar ranking for the different root classes was observed in root apical diameter at emergence. Moreover, root apical diameter appeared to decrease and stabilize only for B and C roots, while a continuous increase in root apical diameter was clearly observed for roots with increasing growth rates in class A. The decreasing trend in root apical diameter reached a plateau close to 335 µm for C roots and 400 µm for B roots.

The relative abundance of lateral root types for *rtcs* mutant was 10.0 % for A roots, 35.3 % of B roots and 54.7 % for C roots. We also assigned lateral root growth rate profiles using the SMS-LM previously build on the basis of wild-type plants. We obtained 97% of match between the two independent assignments indicating that the definition of A, B and C lateral root types on the basis of growth rate profiles is very similar for wild-type and *rtcs* plants.

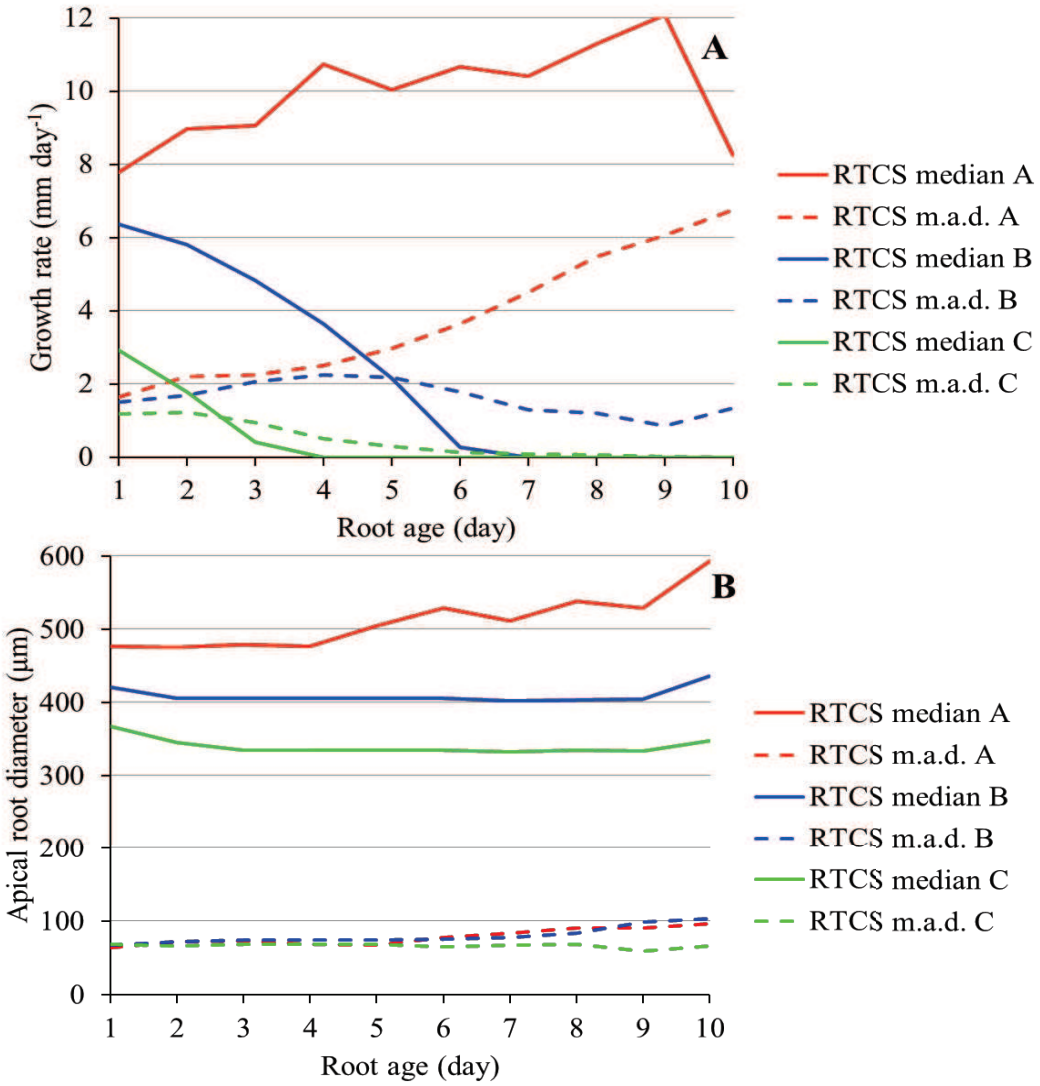

Figure II-12 Maize *rtc*s mutant: (**A**) daily median growth rate and (**B**) apical diameter (and associated mean absolute deviations −m.a.d.−).

2.2.2 Comparison between treatments

We compared the outputs of SMS-LMs for the treatments previously presented, by superimposing median profiles of growth rates on the same graph (**Figure II-13A**). Lateral root growth rate profiles were similar between root classes for the different treatments. This was a consequence of the model building, since linear regression models within SMS-LMs had similar slopes and initial growth rate values for a given root type (**Supplementary Figure II-5**). These similarities legitimate considering the ABC root types comparable in terms of growth characteristics for the three treatments treated here, and to use their proportions to characterize differences in lateral root growth between treatments.

The analysis of root class proportions (**Table II-4**) indicates a complete inhibition of fast-elongating (A) roots in shaded plants. In addition, early arrests (C) were found more frequently (73% compared to 61% in CTRL) in shaded plants. The proportion of slow-growing roots remained stable. We made the assumption that this overall inhibition of lateral root growth could be related to a restriction in the supply of carbohydrates in shaded plants.

In *rtcs* mutant plants, early arrested roots were slightly less represented while slow growing roots proportion increased to 35% of the total lateral root population in this mutant genotype. However, these differences in root type proportions were not significant. Overall, in both shaded and *rtcs* plants, the definition of the lateral root types on the basis of growth rate profiles appears to be well conserved, and the treatment effect is mainly observed through the modulation of the proportion of the lateral root types.

In parallel to growth rate profiles, we compared apical diameter profiles associated to root types across treatments (**Figure II-13B**). Qualitatively, apical root profiles presented some similarities, that is to say, apical diameters decrease for B and C roots identified in all treatments and increase in the case of A roots (when present). A second resemblance is that a ranking of apical diameters could be observed within a treatment, with larger diameters for A than for B and C roots. However, absolute values of apical diameter associated to root types depended on the genotype and growth conditions. For example, initial values for root apical diameter in A roots were around 380 µm for CTRL plants and 480 µm for RTCS plants. A similar gap of 100 µm existed between root diameters of B and C root classes. Shaded plants presented also increased apical diameters (around 50 µm larger) for B and C roots relative to CTRL. But, it must be recalled that OMB plants were grown in one experiment only whereas CTRL plants were systematically present in all experiments.

In summary, both shaded and *rtcs* plants require larger diameters to achieve the same growth behavior. Overall, these results suggest that the relationship between apical diameters and elongation is strongly dependent upon the carbohydrate supply and auxin signaling.

Moreover, the unconstancy of root diameters for root types introduces an unexpected level of complexity when comparing treatments; since the same elongation types can be very different at the anatomical (and maybe molecular) level.

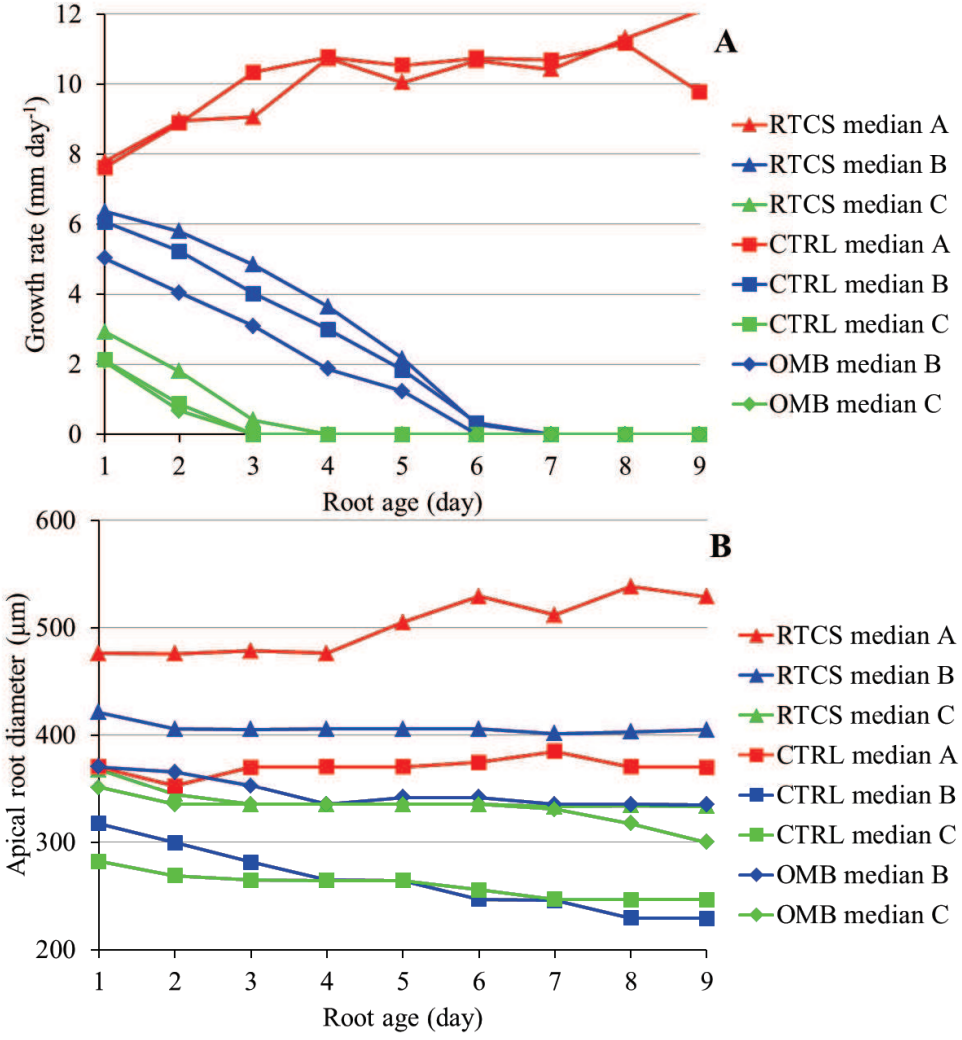

Figure II-13 Maize wild-type, *rtc*s mutant and shading treatment: (A) daily median growth rate and (B) apical diameter (and associated mean absolute deviations −m.a.d.−).

Table II-4 Relative abundance of root types A, B and C for *wild-type* (CTRL), *rtc*s mutant (RTCS) and shading (OMB) treatment.

Treatment	Root type abundance (%)			Number of roots	Number of plants
	A	B	C		
CTRL	9	29	62	2439	20
OMB	0	27	73	514	6
RTCS	10	35	55	710	4

Chapter References

Aguirrezabal, L. A. N., Deleens, E., and Tardieu, F. (1994). Root elongation rate is accounted for by intercepted PPFD and source-sink relations in field and laboratory-grown sunflower. *Plant, Cell Environ*. 17, 443–450. doi:10.1111/j.1365-3040.1994.tb00313.x.

Atkinson, J. A., Wingen, L. U., Griffiths, M., Pound, M. P., Gaju, O., Foulkes, M. J., et al. (2015). Phenotyping pipeline reveals major seedling root growth QTL in hexaploid wheat. *J. Exp. Bot*. doi:10.1093/jxb/erv006.

Baskin, T. I., Peret, B., Balu??ka, F., Benfey, P. N., Bennett, M., Forde, B. G., et al. (2010). Shootward and rootward: Peak terminology for plant polarity. *Trends Plant Sci*. 15, 593–594. doi:10.1016/j.tplants.2010.08.006.

von Behrens, I., Komatsu, M., Zhang, Y., Berendzen, K. W., Niu, X., Sakai, H., et al. (2011). Rootless with undetectable meristem 1 encodes a monocot-specific AUX/IAA protein that controls embryonic seminal and post-embryonic lateral root initiation in maize. *Plant J*. 66, 341–53. doi:10.1111/j.1365-313X.2011.04495.x.

Bishopp, A., and Lynch, J. P. (2015). The hidden half of crop yields. *Nat. Plants* 1, 15117. doi:10.1038/nplants.2015.117.

Bühlmann, P., and Wyner, A. J. (1999). Variable length markov chains. *Ann. Stat*. 27, 480–513. doi:10.1214/aos/1018031204.

Coutts, M. P. (1987). Developmental processes in tree root systems. *Can. J. For. Res*. 17, 761–767.

Csiszár, I., and Talata, Z. (2006). Context tree estimation for not necessarily finite memory processes, Via BIC and MDL. *IEEE Trans. Inf. Theory* 52, 1007–1016. doi:10.1109/TIT.2005.864431.

Dhondt, S., Wuyts, N., and Inzé, D. (2013). Cell to whole-plant phenotyping: The best is yet to come. *Trends Plant Sci*. 18, 1360–1385. doi:10.1016/j.tplants.2013.04.008.

de Dorlodot, S., Forster, B., Pagès, L., Price, A., Tuberosa, R., and Draye, X. (2007). Root system architecture: opportunities and constraints for genetic improvement of crops. *Trends Plant Sci*. 12, 474–81. doi:10.1016/j.tplants.2007.08.012.

Drew, M. C. (1975). Comparison of the effects of a localized supply of phosphate, nitrate,

ammonium and potassium on the growth of the seminal root sytem, and the shoot, in barley. 479–490.

Fahlgren, N., Feldman, M., Gehan, M. A., Wilson, M. S., Shyu, C., Bryant, D. W., et al. (2015a). A versatile phenotyping system and analytics platform reveals diverse temporal responses to water availability in Setaria. *Mol. Plant* 8, 1520–1535. doi:10.1016/j.molp.2015.06.005.

Fahlgren, N., Gehan, M. a, and Baxter, I. (2015b). Lights, camera, action: high-throughput plant phenotyping is ready for a close-up. *Curr. Opin. Plant Biol.* 24, 93–99. doi:10.1016/j.pbi.2015.02.006.

Forde, B. G. (2009). Is it good noise? The role of developmental instability in the shaping of a root system. *J. Exp. Bot.* 60, 3989–4002. doi:10.1093/jxb/erp265.

Freixes, S., Thibaud, M.-C., Tardieu, F., and Muller, B. (2002). Root elongation and branching is related to local hexose concentration in Arabidopsis thaliana seedlings. *Plant, Cell Environ.* 25, 1357–1366. doi:10.1046/j.1365-3040.2002.00912.x.

Gowda, V. R. P., Henry, A., Yamauchi, A., Shashidhar, H. E., and Serraj, R. (2011). Root biology and genetic improvement for drought avoidance in rice. *F. Crop. Res.* 122, 1–13. doi:10.1016/j.fcr.2011.03.001.

Guédon, Y. (2003). Estimating Hidden Semi-Markov Chains From Discrete Sequences. *J. Comput. Graph. Stat.* 12, 604–639. doi:10.1198/1061860032030.

Guédon, Y. (2005). Hidden hybrid Markov / semi-Markov chains. *Comput. Stat. Data Anal.* 49, 663–688. doi:10.1016/j.csda.2004.05.033.

Guédon, Y. (2007). Exploring the state sequence space for hidden Markov and semi-Markov chains. *Comput. Stat. Data Anal.* 51, 2379–2409. doi:10.1016/j.csda.2006.03.015.

Henry, S., Divol, F., Bettembourg, M., Bureau, C., Guiderdoni, E., Périn, C., et al. (2016). Immunoprofiling of Rice Root Cortex Reveals Two Cortical Subdomains. *Front. Plant Sci.* 6, 1–9. doi:10.3389/fpls.2015.01139.

Hodge, A. (2004). The plastic plant: root responses to heterogeneous supplies of nutrients. *New Phytol.* 162, 9–24. doi:10.1111/j.1469-8137.2004.01015.x.

Iyer-Pascuzzi, A. S., Symonova, O., Mileyko, Y., Hao, Y., Belcher, H., Harer, J., et al. (2010). Imaging and analysis platform for automatic phenotyping and trait ranking of plant root systems. *Plant Physiol.* 152, 1148–1157. doi:10.1104/pp.109.150748.

Jordan, M. O., Harada, J., Bruchou, C., and Yamazaki, K. (1993). Maize nodal root ramification: Absence of dormant primordia, root classification using histological parameters and consequences on sap conduction. *Plant Soil* 153, 125–143. doi:10.1007/BF00010551.

Kuijken, R. C. P., van Eeuwijk, F. a, Marcelis, L. F. M., and Bouwmeester, H. J. (2015). Root phenotyping: from component trait in the lab to breeding. *J. Exp. Bot.* 66, 5389–401. doi:10.1093/jxb/erv239.

Lecompte, F., Pagès, L., and Ozier-Lafontaine, H. (2005). Patterns of variability in the diameter of lateral roots in the banana root system. *New Phytol.* 167, 841–850. doi:10.1111/j.1469-8137.2005.01457.x.

Lièvre, M., Granier, C., and Guédon, Y. (2016). Identifying developmental phases in the Arabidopsis thaliana rosette using integrative segmentation models. *New Phytol*. 210, 1466–1478. doi:10.1111/nph.13861.

Lobet, G., Pagès, L., and Draye, X. (2011). A novel image-analysis toolbox enabling quantitative analysis of root system architecture. *Plant Physiol*. 157, 29–39. doi:10.1104/pp.111.179895.

MacLeod, R. D. (1990). Lateral root primordium inception in Zea mays L. *Environ*. *Exp*. *Bot*. 30, 225–234. doi:10.1016/0098-8472(90)90068-F.

Maiti, R. K., and Bidinger, F. R. (1981). Growth and development of the pearl millet plant. *ICRISAT Res*. *Bull*.

Malamy, J. E. (2005). Intrinsic and environmental response pathways that regulate root system architecture. *Plant, Cell Environ*. 28, 67–77. doi:10.1111/j.1365-3040.2005.01306.x.

Neufeld, H. S., Durall, D. M., Rich, P. M., and Tingey, D. T. (1989). A rootbox for quantitative observations on intact entire root systems. *Plant Soil* 117, 295–298. doi:10.1007/BF02220725.

Pagès, L. (1995). Growth patterns of the lateral roots of young oak (Quercus robur) tree seedlings Relationship with apical diameter. *New Phytol*. 130, 503–509. doi:doi: 10.1111/j.1469-8137.1995.tb04327.x.

Pagès, L. (2011). Links between root developmental traits and foraging performance. *Plant*. *Cell Environ*. 34, 1749–60. doi:10.1111/j.1365-3040.2011.02371.x.

Passot, S., Gnacko, F., Moukouanga, D., Lucas, M., Guyomarc'h, S., Moreno Ortega, B., et al. (2016). Characterization of Pearl Millet Root Architecture and Anatomy Reveals Three Types of Lateral Roots. *Front*. *Plant Sci*. 7, 1–11. doi:10.3389/fpls.2016.00829.

Rebouillat, J., Dievart, A., Verdeil, J. L., Escoute, J., Giese, G., Breitler, J. C., et al. (2009). Molecular genetics of rice root development. *Rice* 2, 15–34. doi:10.1007/s12284-008-9016-5.

Ron, D., Singer, Y., and Tishby, N. (1997). The power of amnesia: Learning probabilistic automata with variable memory length. *Mach*. *Learn*. 25, 117–149. doi:10.1007/BF00114008.

Saengwilai, P., Tian, X., and Lynch, J. P. (2014). Low crown root number enhances nitrogen acquisition from low-nitrogen soils in maize. *Plant Physiol*. 166, 581–9. doi:10.1104/pp.113.232603.

Taramino, G., Sauer, M., Stauffer, J. L., Multani, D., Niu, X., Sakai, H., et al. (2007). The maize (Zea mays L.) RTCS gene encodes a LOB domain protein that is a key regulator of embryonic seminal and post-embryonic shoot-borne root initiation. *Plant J*. 50, 649–59. doi:10.1111/j.1365-313X.2007.03075.x.

Thaler, P., and Pagès, L. (1996a). Root apical diameter and root elongation rate of rubber seedlings (Hevea brasiliensis) show parallel responses to photoassimilate availability. *Physio* 97, 365–371.

Thaler, P., and Pagès, L. (1996b). Root apical diameter and root elongation rate of rubber seedlings (Hevea brasiliensis) show parallel responses to photoassimilate availability.

Physiol. *Plant*. 97, 365–371.

Topp, C. N., Iyer-Pascuzzi, A. S., Anderson, J. T., Lee, C.-R., Zurek, P. R., Symonova, O., et al. (2013). 3D phenotyping and quantitative trait locus mapping identify core regions of the rice genome controlling root architecture. *Proc*. *Natl*. *Acad*. *Sci*. *U*. *S*. *A*. 110, E1695–704. doi:10.1073/pnas.1304354110.

Varney, G., Canny, M., Wang, X., and McCully, M. (1991). The branch roots of Zea. I. First Order Branches, Their Number, Sizes and Division into classes. *Ann*. *Bot*. 67, 357–364.

Varney, G. T., and McCully, M. E. (1991). The branch roots of Zea. II. Developmental loss of the apical meristem in field-grown roots. *New Phytol*. 118, 535–546. doi:10.1111/j.1469-8137.1991.tb00993.x.

Watt, M., Magee, L. J., and McCully, M. E. (2008). Types, structure and potential for axial water flow in the deepest roots of field-grown cereals. *New Phytol*. 178, 135–146. doi:10.1111/j.1469-8137.2007.02358.x.

Wu, Q., Pagès, L., and Wu, J. (2016). Relationships between root diameter, root length and root branching along lateral roots in adult, field-grown maize. *Ann*. *Bot*., mcv185. doi:10.1093/aob/mcv185.

Zhu, J., Brown, K. M., and Lynch, J. P. (2010). Root cortical aerenchyma improves the drought tolerance of maize (Zea mays L.). *Plant, Cell Environ*. 33, 740–749. doi:10.1111/j.1365-3040.2009.02099.x.

Appendix and Supplementary material

Appendix II-1: Definition of semi-Markov switching linear models and associated statistical methods

Appendix II-2: Empirical selection of the number of classes of lateral roots.

Appendix II-3: Algorithm for correcting growth rate profiles

Appendix II-4: Definition of stationary variable-order Markov chains and associated statistical methods

Supplementary Figure II-1: Four-state semi-Markov switching linear model estimated on the basis of maize lateral root growth rate series: (a) Growth duration distributions; (b) Graph of transitions. The possible transitions between states are represented by arcs with the attached probabilities noted nearby when < 1. The arcs entering in states indicate initial states and the attached initial probabilities is noted nearby. (c) Linear trend models estimated for each state.

Supplementary Figure II-2: Cumulative distribution functions of the length of growth rate series assigned to each group: (a) pearl millet; (b) maize.

Supplementary Figure II-3: Pearl millet: daily median growth rate (and associated mean absolute deviation −m.a.d.−) for (a) 2 groups, (b) 3 groups and (c) 4 groups.

Supplementary Figure II-4: Cumulative distribution functions of the length of growth rate series assigned to each group: (a) pearl millet; (b) maize.

Supplementary Table II-1: Pearl millet: Overlaps (i.e. 1 – sup norm distance) between growth rate distributions corresponding to consecutive lateral root categories (α-β for 2 categories, A-B and B-C for 3 categories and a-b, b-c, and c-d for 4 categories) extracted from the optimal assignment of each lateral root growth rate profiles using the estimated 3-, 4- and 5-state semi-Markov switching linear models.

Supplementary Table II-2: Maize: Overlaps (i.e. 1 – sup norm distance) between growth rate distributions corresponding to consecutive lateral root categories (α-β for 2 categories, A-B and B-C for 3 categories and a-b, b-c, and c-d for 4 categories) extracted from the optimal assignment of each lateral root growth rate profiles using the estimated 3-, 4- and 5-state semi-Markov switching linear models.

Supplementary Table II-3: Maize: Overlaps (i.e. 1 – sup norm distance) between growth rate distributions and apical diameter distributions corresponding to consecutive lateral root categories (A-B and B-C) extracted from the optimal assignment of each lateral root growth rate profiles using the estimated 4-state semi-Markov switching linear model.

Supplementary Table II-4: Length of the interval between successive lateral roots in pearl millet, classified according to the types of the two lateral roots delimiting the interval. No significant differences between the means were found (ANOVA, $p = 0.52$).

Supplementary Table II-5: Length of the interval between successive lateral roots in maize, classified according to the types of the two lateral roots delimiting the interval. No significant differences between the means were found (ANOVA, $p = 0.39$).

Supplementary Result II-1: Link between interval length and lateral root type proportions.

Supplementary Methods II-1: Aeroponic experiment in collaboration with UCL.

Appendix II-1 – Definition of semi-Markov switching linear models and associated statistical methods

Semi-Markov chains

Let $\{S_t\}$ be a semi-Markov chain with finite-state space $\{0,\ldots,J-1\}$. A *J*-state semi-Markov chain $\{S_t\}$ is defined by the following parameters:

- initial probabilities $\pi_j = P(S_1 = j)$ with $\sum_j \pi_j = 1$;
- transition probabilities
  - nonabsorbing state *i*: for each $j \neq i, p_{ij} = P(S_t = j \mid S_t \neq i, S_{t-1} = i)$ with $\sum_{j \neq i} p_{ij} = 1$ and $p_{ii} = 0$ by convention,
  - absorbing state *i*: $p_{ii} = P(S_t = i \mid S_{t-1} = i) = 1$ and for each $j \neq i, p_{ij} = 0$.

An explicit occupancy distribution is attached to each nonabsorbing state:

$$d_j(u) = P(S_{t+u+1} \neq j, S_{t+u-v} = j, v = 0,\ldots,u-2 \mid S_{t+1} = j, S_t \neq j), \quad u = 1,2,\ldots$$

Since $t = 1$ is assumed to correspond to a state entering, the following relation is verified:

$$P(S_t \neq j, S_{t-v} = j, v = 1,\ldots,t) = d_j(t)\pi_j.$$

We define as possible parametric state occupancy distributions binomial distributions, Poisson distributions and negative binomial distributions with an additional shift parameter *d* ($d \geq 1$) which defines the minimum sojourn time in a given state.

The binomial distribution with parameters *d*, *n* and *p* ($q = 1 - p$), B(*d*, *n*, *p*) where $0 \leq p \leq 1$, is defined by

$$d_j(u) = \binom{n-d}{u-d} p^{u-d} q^{n-u}, \qquad u = d, d+1,\ldots,n.$$

The Poisson distribution with parameters *d* and λ, P(*d*, λ), where λ is a real number ($\lambda > 0$), is defined by:

$$d_j(u) = \frac{e^{-\lambda}\lambda^{u-d}}{(u-d)!}, \qquad u = d, d+1,\ldots$$

The negative binomial distribution with parameters *d*, *r* and *p*, NB(*d*, *r*, *p*), where *r* is a real number ($r > 0$) and $0 < p \leq 1$, is defined by:

$$d_j(u) = \binom{u-d+r-1}{r-1} p^r q^{u-d}, \qquad u = d, d+1, \ldots$$

Semi-Markov switching linear models

A semi-Markov switching model can be viewed as a pair of stochastic processes $\{S_t, X_t\}$ where the "output" process $\{X_t\}$ is related to the "state" process $\{S_t\}$, which is a finite-state semi-Markov chain, by a probabilistic function or mapping denoted by *f* (hence $X_t = f(S_t)$). Since the mapping *f* is such that a given output may be observed in different states, the state process $\{S_t\}$ is not observable directly but only indirectly through the output process $\{X_t\}$. This output process $\{X_t\}$ is related to the semi-Markov chain $\{S_t\}$ by the observation (or emission) models. The output process at time *t* depends only on the underlying semi-Markov chain at time *t*. The output process $\{X_t\}$ is related to the state process $\{S_t\}$, by a linear trend model

$$X_t = \alpha_j + \beta_j t + \varepsilon_j, \qquad \varepsilon_j \sim \mathrm{N}(0, \sigma_j^2).$$

The maximum likelihood estimation of the parameters of a semi-Markov switching linear model requires an iterative optimization technique, which is an application of the EM algorithm. Once a semi-Markov switching model has been estimated, the most probable state series $\mathbf{s}^*$ with its associated posterior probability $P(\mathbf{S} = \mathbf{s}^* \mid \mathbf{X} = \mathbf{x})$ can be computed for each observed series $\mathbf{x}$ using the so-called Viterbi algorithm (Guédon, 2003). In our application context, the most probable state series can be interpreted as the optimal segmentation of the corresponding observed series into at most two sub-series corresponding to a given growth phase either censored or followed by a growth arrest; see Guédon (2003, 2005, 2007) for the statistical methods for hidden semi-Markov chains that directly apply to semi-Markov switching linear models.

Appendix II-2 – Empirical selection of the number of classes of lateral roots

The empirical selection of the number of lateral root classes combines the three following criteria:

1. Posterior probabilities of the optimal assignment of each lateral root growth rate profile to a growth state (followed or not by the growth arrest state at a given age) i.e. weight of the optimal assignment among all the possible assignments of a given growth rate profile. Ambiguous assignments can be explained by two types of alternative assignments that can be combined: (i) assignment to an alternative growth state, (ii) alternative assignment corresponding to a shift (usually a 1-day shift) of the transition from the optimal growth state to the growth arrest state. The posterior probabilities of the optimal assignments are expected to decrease with the increase of the number of growth states.
2. Comparison between location and dispersion measures of growth rate profiles for each lateral root class deduced from the optimal assignment of each lateral root growth rate profile. Because the empirical growth rate distributions for the less vigorous roots at high ages were semi-continuous and highly right-skewed combining zero values for arrested roots with continuous positive values for growing roots, we chose to use robust measures of location and dispersion (i.e. median and mean absolute deviation from the median). We in particular focused on the relative dispersion of growth rate distributions for the most vigorous root class. Relative dispersions are indeed irrelevant in the case of median at zero or close to zero corresponding to a high proportion of arrested roots.
3. Overlap between growth rate profiles for consecutive lateral root classes deduced from the optimal assignment of each lateral root growth rate profile. Since the growth rate profiles were highly divergent at the beginning of growth, we focused on the overlap from age 3. The high overlap in the case of a high proportion of arrested roots in the two classes being compared (less vigorous roots at the highest ages) should indeed not be considered for the selection of the number of root classes.

To assess the separability of growth rate profiles for each lateral root class, we used the sup-norm distances between the growth rate distributions at a given age for consecutive classes (i.e. A and B or B and C in the case of 3 classes):

$$\sup_x |F(x) - G(x)| = 1 - \int \min\{f(x), g(x)\} dx.$$

This distance, which is the maximum absolute difference between the two cumulative distribution functions $F(x)$ and $G(x)$, is also one minus the overlap between the two distributions in our case of non-crossing cumulative distribution functions. This distance is between 0 (full overlap, i.e. identical distributions) and 1 (no overlap). In the case of crossing

cumulative distribution functions (which was rather infrequent in our context), this distance generalizes to

$$\sum_j \sup_{x\in[\tau_j,\tau_{j+1}]} |F(x)-G(x)| = 1-\int \min\{f(x),g(x)\}dx.$$

where sup norm distances computed over each interval $[\tau_j,\tau_{j+1}]$ between two consecutive crossings of cumulative distribution functions are summed.

As expected, the proportion of ambiguously assigned lateral root increased with the number of growth states (i.e. of lateral root classes). For pearl millet, approximately 5% of lateral roots were ambiguously assigned in the case of 2 classes, 19% in the case of 3 classes and 29% in the case of 4 classes; see **Supplementary Figure II-2a**. For maize, approximately 9% of lateral roots were ambiguously assigned in the case of 2 classes, 22% in the case of 3 classes and 33% in the case of 4 classes; see **Supplementary Figure II-2b**. These proportions indeed favor the most parsimonious models but stay reasonably low even for 4-class models confirming the rather strong clustering structure. It should be noted that these posterior probabilities do not represent, in the case of uncensored growth rate profiles, the different growth phase durations in the optimal growth state but only the optimal growth phase duration. They thus provide a more stringent criterion than the posterior probabilities of the optimal assignment of each lateral root growth rate profile to a growth state.

The high dispersion measure with respect to the location measure at the highest ages for the most vigorous lateral roots makes the 2-class models rather irrelevant regarding the definition of growth rate profile classes. This is especially marked for pearl millet comparing daily median growth rate and associated mean absolute deviation of the most vigorous lateral root class between 2 and 3 classes (**Figure II-3 a** and **b**). This is less marked for maize where the most vigorous lateral root class likely combines lateral roots whose growth rate started to decrease with lateral roots whose growth rate continued to increase at the highest ages.

In the case of 3 classes, the overlap between growth rate profiles of classes A and B stays roughly constant from age 3 onward while the overlap between growth rate profiles of classes B and C progressively increases because of the increasing masses of zero corresponding to arrested roots for these two classes; see **Supplementary Tables II-1** and **II-2**. The situation was very different in the case of 4 classes were the overlap between growth rate profiles was high from age 3 for the two classes of the less vigorous lateral roots. These two classes were thus not well separated in terms of growth rate profiles. Combining these three criteria, we selected for both species 3 lateral root classes that correspond to the best compromise between the proportion of ambiguously assigned lateral roots, the relative

dispersion of growth rate profiles for the most vigorous root class and the overlap between growth rate profiles for consecutive classes.

Appendix II-3 – Algorithm for correcting growth rate profiles

Identification of putatively erroneous growth rate

The correction algorithm was based on the observation of growth rate profiles and was decomposed in two steps: the labeling of each day with a qualifier and the correction of the growth rate profile according to the qualifiers. The qualifiers were assigned according to the following rules:

- "stopped" if growth rate ≤ 0.1 mm.day^{-1};
- "growing" if growth rate > 0.1 mm.day^{-1};
- "zombie" if day is labeled "growing" and the previous day is labeled "stopped";
- "stopping" if day is labeled "growing" and the subsequent day is labeled "stopped";
- "rough stopping" if day is labeled "stopping" and growth rate is higher than a threshold representing an improbable growth rate for a root the day preceding it arrest. This threshold was fixed at 10 mm.day^{-1}.

Correction strategy of growth rate profiles

The roots containing problematic labels ("zombie" or "rough stopping") were visually examined to identify possible common sources of error in image analysis.

A frequent case within the zombie category was alternative stopped and zombie states with low growth rate (< 2 mm.day^{-1}). We assumed that this pattern probably arose from slight alignment defaults in SmartRoot tracings for roots that have stopped their growth and we forced the corresponding growth rates to zero. The other frequent source of zombies was the lack of manual elongation at a single day. The result was a zero growth followed by an overestimated growth rate. In these cases, we either corrected the data directly in the SmartRoot tracing if possible, or applied a local smoothing filter on the zombie growth rate, and its two immediate neighbors. All other zombies remaining after these corrections were truncated.

Rough stops were mostly due to the root system becoming progressively denser, therefore increasing the probability for a fast-growing root to encounter another root, hampering correct monitoring of root growth. The roots containing a rough stopping were either examined and corrected individually in the case of pearl millet, where the low number of plants allowed to visually check all the images, or truncated after the last high growth rate in the case of maize.

The intermediate case, where zombie growth rate was comprised between 2 and 10 mm.day^{-1}, were dealt manually in the case of pearl millet and removed from the dataset in the case of maize.

The pearl millet dataset was initially composed of 1256 lateral roots, 9% containing a growth rate classified as zombie and 5% classified as rough stopping. The maize dataset was initially composed of 3896 lateral roots, 18% containing a growth rate classified as zombie and 4% classified as rough stopping.

Appendix II-4 – Definition of stationary variable-order Markov chains and associated statistical methods

Stationary variable-order Markov chains

In the following, we first introduce high-order Markov chains before defining variable-order Markov chains. In the case of a *r*th-order Markov chain $\{S_t; t = 0,1,\ldots\}$, the conditional distribution of S_t given $S_0,\ldots,S_{t-1}$ depends only on the values of $S_{t-r},\ldots,S_{t-1}$ but not further on $S_0,\ldots,S_{t-r-1}$,

$$P(S_t = s_t \mid S_{t-1} = s_{t-1},\ldots,S_0 = s_0) = P(S_t = s_t \mid S_{t-1} = s_{t-1},\ldots,S_{t-r} = s_{t-r})$$

In our context, the random variables represent the lateral root types and can take the three possible values A, B and C. These possible values correspond to the Markov chain states. A *J*-state *r*th-order Markov chain has $J^r(J-1)$ independent transition probabilities if all the transitions are possible. Therefore, the number of free parameters of a Markov chain increases exponentially with the order. Let the transition probabilities of a second-order Markov chain be given by

$$p_{hij} = P(S_t = j \mid S_{t-1} = i, S_{t-2} = h) \quad \text{with} \sum_j p_{hij} = 1.$$

These transition probabilities can be arranged as a $J^2 \times J$ matrix where the row $(p_{hi0},\ldots,p_{hiJ-1})$ corresponds to the transition distribution attached to the [state *h*, state *i*] memory. If for a given state *i* and for all pairs of states (h,h') with $h \neq h'$, $p_{h'ij} = p_{hij}$ for each state *j*, i.e. once S_{t-1} is known, S_{t-2} conveys no further information about S_t, the *J* memories of length 2 [state *h*, state *i*] with $h = 0,\ldots,J-1$ can be grouped together and replaced by the single [state *i*] memory of length 1 with associated transition distribution $(p_{i0},\ldots,p_{iJ-1})$. This illustrates the principle used to build a variable-order Markov chain where the order (or memory length) is variable and depends on the "context" within the sequence. The memories of a Markov chain can be arranged as a memory tree such that each vertex (i.e. element of a tree graph) is either a terminal vertex or has exactly *J* "offspring" vertices. A transition distribution is associated with each terminal vertex of this memory tree.

A stationary Markov chain starts from its stationary distribution and will continue to have that distribution at all subsequent time points. In the case of a variable-order Markov chain, the

stationary distribution − which is the implicit initial distribution− is defined on the possible memories.

Selection of the memories of a stationary variable-order Markov chain

The order of a Markov chain can be estimated using the Bayesian information criterion (BIC). For each possible order *r*, the following quantity is computed

$$\mathrm{BIC}(r) = 2\log(L_r) - d_r \log n \quad \text{(S1)},$$

where L_r is the likelihood of the *r*th-order estimated Markov chain for the observed sequences, d_r is the number of free parameters of the *r*th-order estimated Markov chain and *n* is the cumulative length of the observed series. The principle of this penalized likelihood criterion consists in making a trade-off between an adequate fitting of the model to the data (given by the first term in (S1)) and a reasonable number of parameters to be estimated (controlled by the second term in (S1), the penalty term). In practice, it is infeasible to compute a BIC value for each possible variable-order Markov chain of maximum order $r \leq R$ since the number of hypothetical memory trees is very large. An initial maximal memory tree is thus built combining criteria relative to the maximum order (3 or 4 in our case) and to the minimum count of memory occurrences in the observed series. This memory tree is then pruned using a two-pass algorithm which is an adaptation of the Context-tree maximizing algorithm (Csiszár and Talata, 2006): a first dynamic programming pass starting from the terminal vertices and progressing towards the root vertex for computing the maximum BIC value attached to each sub-tree rooted in a given vertex, is followed by a second tracking pass starting from the root vertex and progressing towards the terminal vertices for building the memory tree.

Supplementary Figure II-1

Four-state semi-Markov switching linear model estimated on the basis of maize lateral root growth rate series: (a) Growth duration distributions; (b) Graph of transitions. The possible transitions between states are represented by arcs with the attached probabilities noted nearby when < 1. The arcs entering in states indicate initial states and the attached initial probabilities is noted nearby. **(c) Linear trend models estimated for each state.**

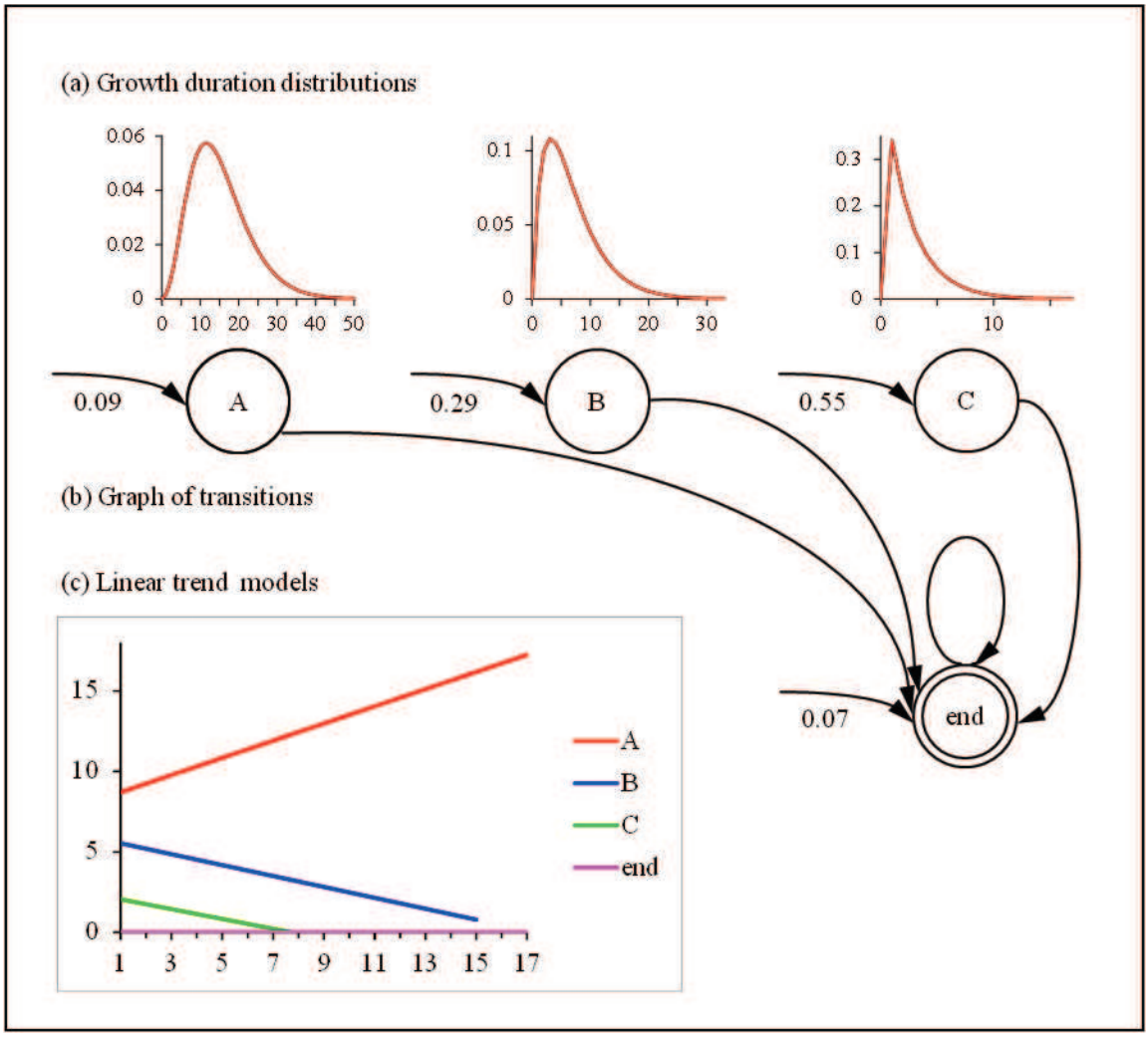

Supplementary Figure II-2

Ranked posterior probabilities of the optimal assignment of each lateral root growth rate series to a group: (a) pearl millet; (b) maize. Limits (dotted lines) between unambiguously and ambiguously explained lateral root growth rate series are positioned on the basis of a curve shape criterion.

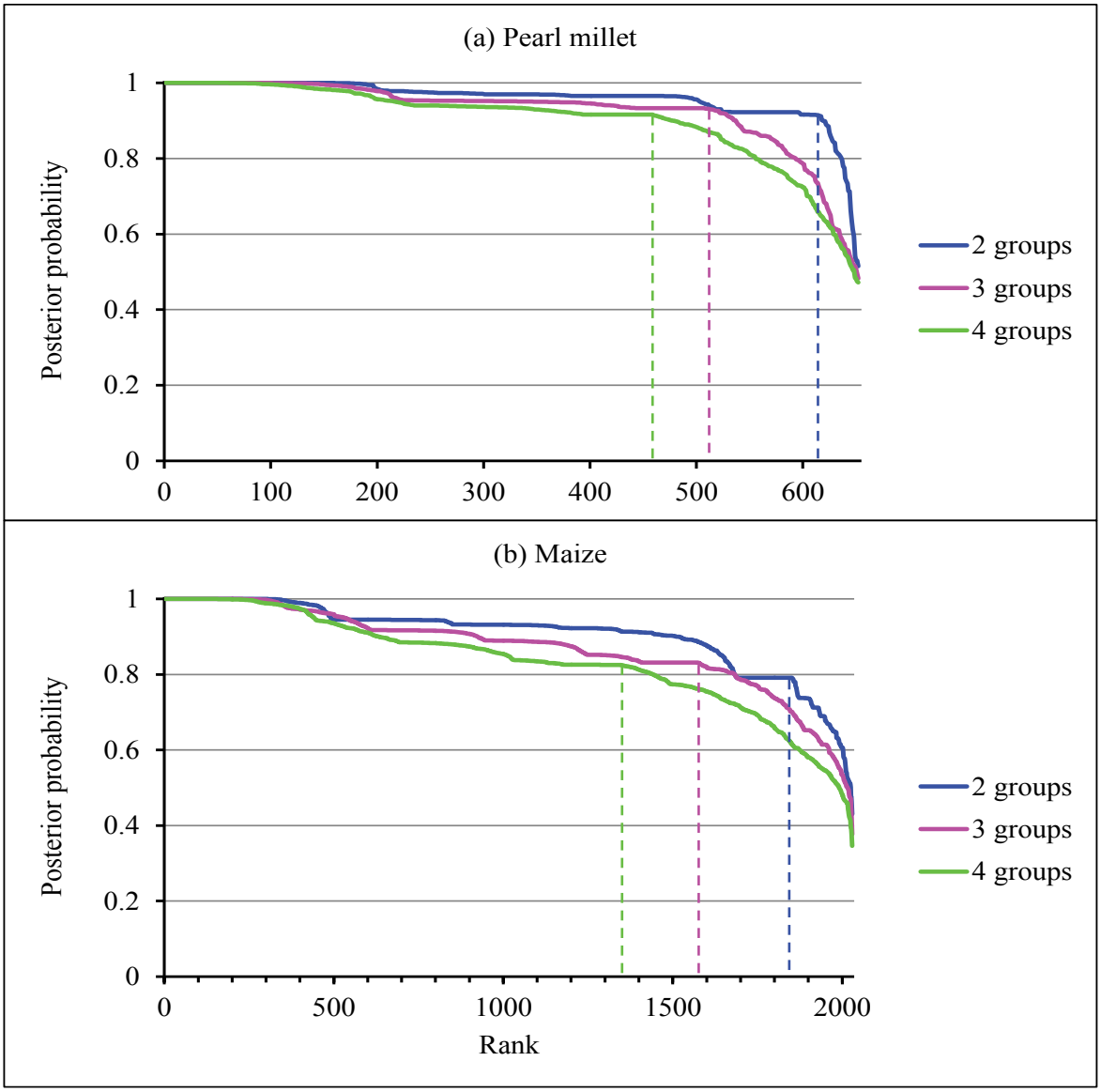

Supplementary Figure II-3

Pearl millet: daily median growth rate (and associated mean absolute deviation −m.a.d.−) for (a) 2 groups, (b) 3 groups and (c) 4 groups.

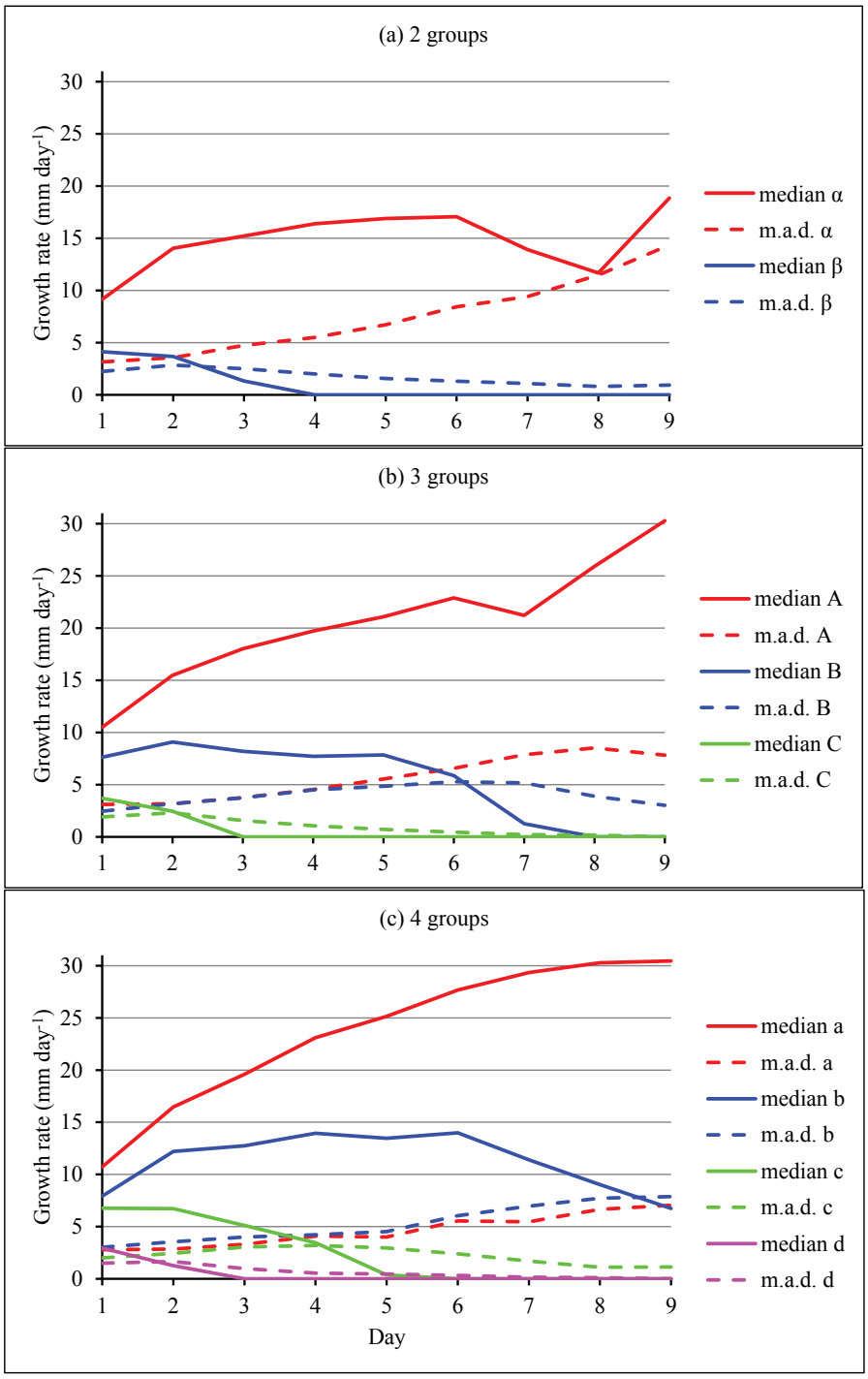

Supplementary Figure II-4

Cumulative distribution functions of the length of growth rate series assigned to each group: (a) pearl millet; (b) maize.

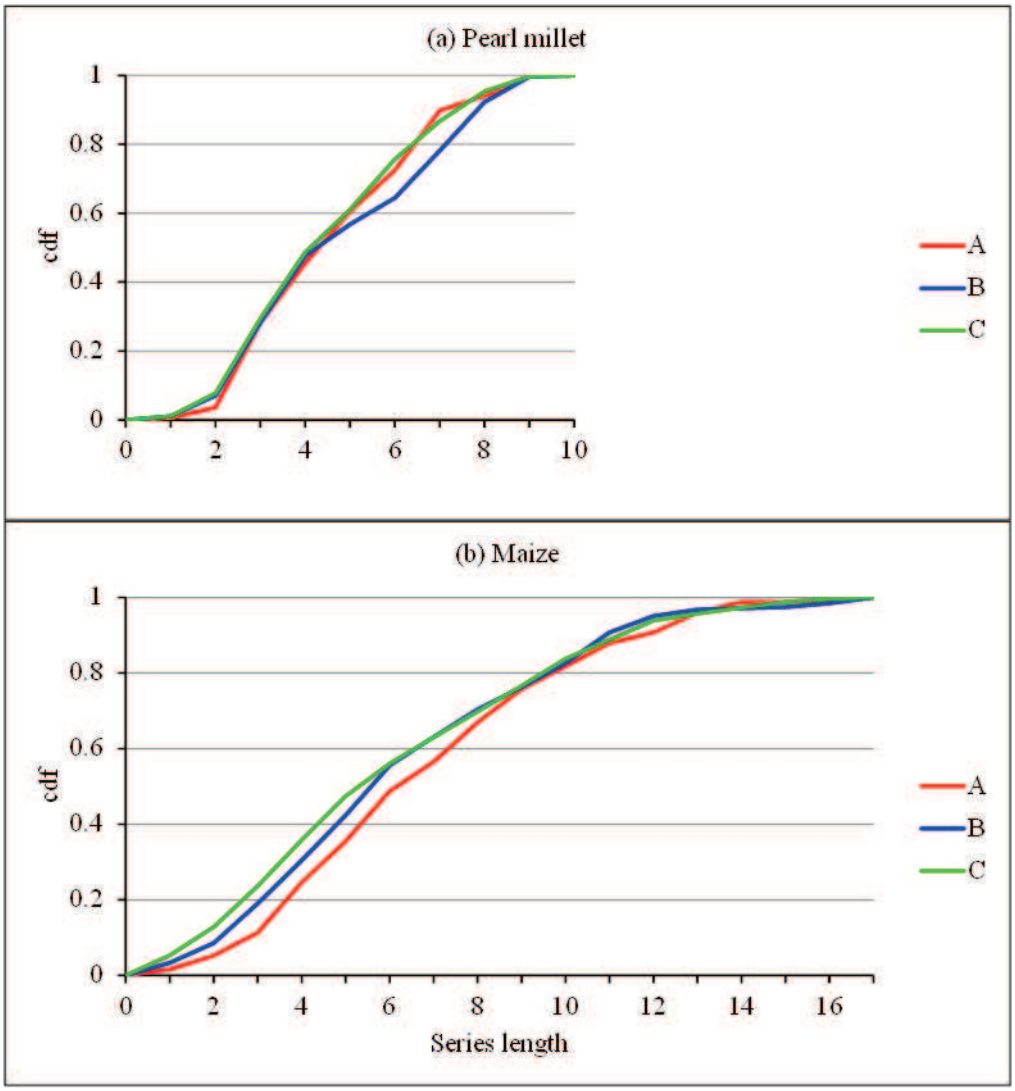

Supplementary Table II-1

Pearl millet: Overlaps (i.e. 1 – sup norm distance) between growth rate distributions corresponding to consecutive lateral root classes (α-β for 2 classes, A-B and B-C for 3 classes and a-b, b-c, and c-d for 4 classes) extracted from the optimal assignment of each lateral root growth rate profiles using the estimated 3-, 4- and 5-state semi-Markov switching linear models.

	2 classes	3 classes		4 classes		
Age	α-β	A-B	B-C	a-b	b-c	c-d
1	0.47	0.55	0.53	0.53	0.67	0.4
2	0.22	0.38	0.32	0.5	0.39	0.27
3	0.16	0.27	0.3	0.37	0.31	0.5
4	0.15	0.23	0.34	0.28	0.25	0.51
5	0.17	0.2	0.39	0.09	0.31	0.65
6	0.25	0.18	0.45	0.19	0.37	0.72
7	0.34	0.28	0.54	0.17	0.45	0.79

Supplementary Table II-2

Maize: Overlaps (i.e. 1 – sup norm distance) between growth rate distributions corresponding to consecutive lateral root classes (α-β for 2 classes, A-B and B-C for 3 classes and a-b, b-c and c-d for 4 classes) extracted from the optimal assignment of each lateral root growth rate profiles using the estimated 3-, 4- and 5-state semi-Markov switching linear models.

	2 classes	3 classes		4 classes		
Age	α-β	A-B	B-C	a-b	b-c	c-d
1	0.29	0.61	0.27	0.78	0.44	0.21
2	0.17	0.46	0.22	0.65	0.3	0.31
3	0.17	0.25	0.32	0.34	0.28	0.47
4	0.24	0.23	0.4	0.25	0.37	0.57
5	0.32	0.19	0.5	0.22	0.48	0.65
6	0.38	0.23	0.55	0.19	0.53	0.7
7	0.4	0.24	0.59	0.16	0.55	0.78
8	0.43	0.25	0.64	0.14	0.57	0.83
9	0.46	0.31	0.71	0.13	0.57	0.9
10	0.48	0.3	0.8	0.14	0.61	0.94
11	0.5	0.29	0.85	0.17	0.65	0.96

Supplementary Table II-3

Maize: Overlaps (i.e. 1 – sup norm distance) between growth rate distributions and apical diameter distributions corresponding to lateral root classes (A-B, B-C and A-C only for apical diameters) extracted from the optimal assignment of each lateral root growth rate profiles using the estimated 4-state semi-Markov switching linear model.

	Growth rate		Apical diameter		
Age	A-B	B-C	A-B	A-C	B-C
1	0.61	0.27	0.65	0.48	0.79
2	0.46	0.22	0.62	0.48	0.85
3	0.25	0.32	0.49	0.45	0.89
4	0.23	0.4	0.47	0.42	0.87
5	0.19	0.5	0.47	0.43	0.77
6	0.23	0.55	0.41	0.37	0.84
7	0.24	0.59	0.38	0.38	0.86
8	0.25	0.64	0.34	0.4	0.84
9	0.31	0.71	0.35	0.39	0.78
10	0.3	0.8	0.33	0.37	0.8
11	0.29	0.85	0.39	0.33	0.62

Supplementary Table II-4

Length of the interval between successive lateral roots in pearl millet, classified according to the types of the two lateral roots delimiting the interval. No significant differences between the means were found (ANOVA, p = 0.52).

Lateral root types	A-A	A-B	A-C	B-A	B-B	B-C	C-A	C-B	C-C
Sample size	23	37	105	48	76	172	93	182	510
Mean (cm)	0.26	0.23	0.21	0.26	0.22	0.20	0.22	0.19	0.22
Standard deviation (cm)	0.22	0.17	0.31	0.52	0.23	0.17	0.19	0.16	0.19

Supplementary Table II-5

Length of the interval between successive lateral roots in maize, classified according to the types of the two lateral roots delimiting the interval. No significant differences between the means were found (ANOVA, p = 0.39).

Lateral root types	A-A	A-B	A-C	B-A	B-B	B-C	C-A	C-B	C-C
Sample size	44	67	138	59	269	502	143	491	1324
Mean (cm)	0.17	0.19	0.14	0.15	0.15	0.16	0.15	0.16	0.17
Standard deviation (cm)	0.19	0.20	0.12	0.11	0.15	0.16	0.11	0.12	0.16

Supplementary Result II-1 – Link between interval length and lateral root type proportions

We tested whether the interval lengths and the proportion of lateral roots types were related, based on the two plant classifications. As the number of plants were small (8 for pearl millet, 13 for maize), we put in parallel the two groupings but could not perform statistical comparison. The following results are therefore only descriptive and should be interpreted with caution.

For pearl millet, two groups could be distinguished. The first group was formed of 3 plants, belonging to interval group a or ab, and to proportion group a or ab. It corresponded to a large interval and a low proportion of type A lateral roots. The second group was formed of 4 plants, belonging to interval group b and to proportion group b or c. It corresponded to a small inter-root interval and higher proportion of type A and type B lateral roots compared to the first group. One plant did not fit in this grouping, as it belonged to group b for interval and to group ab for proportion. This link suggested that more vigorous plants could present a higher lateral root density and proportionally more type A lateral roots.

For maize, no clear similarities between groups were visible (not shown).

Table S1: Comparison of the individual plant classifications based on interval lengths and on lateral root type proportions in pearl millet.

Plant	Interval	Proportion
1.9	a	ab
5.1	ab	
15.1		a
3.1	b	b
2.1		c
5.9		
3.9		b
10.9	b	ab

Supplementary Methods II-1 – Aeroponic experiment in collaboration with UCL

The aim of this collaboration LEPSE-UCL was to characterize root growth dynamics and sugar status of lateral roots upon different treatments targeting the manipulation of carbon sources and sinks, similarly to some of the rhizotron treatments. Plants root systems in the aeroponic platform develop in 3 dimensions, suspended on the air inside an 11 m^3 culture box and are continuously sprayed by a nutrient solution (**Figure S1**). A maximum of 990 plants can be grown at the same time, distributed in the 2 available culture boxes. The acquisition of root system images is facilitated by a high resolution (600 DPI) scanner placed in front of a window practiced in one side of the box. The scanner is programmed to take automatically an image of each root system every two hours. This culture system allows a high-throughput and non-destructive phenotyping of root growth.

Manipulation of carbon sinks included the excision of different kinds of roots (primary root, seminal and/or seminal roots) performed at 6, 10 and/or 14 days after the germination of maize seeds (early, intermediary and late excisions, respectively). Manipulation of carbon sources included a shading applied to one of the two culture boxes, and/or the removal of the endosperm surrounding the embryo from maize seeds. In some cases, various treatments were combined for the same subset of plants. The description of the different treatments applied can be found in **Table S2**. The treatment combinations and the number of plants grown undergoing them are presented in **Table S3**. At the end of this experiment, my mission consisted in the analysis of sugar content at the primary and secondary root tissues from harvested root apices, whereas the UCL took charge of the analysis of root system growth dynamics.

Figure S1 Presentation of the aeroponic platform and UCL people. Topleft: Benjamin Lobet, UCL PhD student, supervising one of the two aeroponic vats with a capacity for growing 500 plants each one. Topright: Bertrand Muller, the LEPSE leader, holding a 5-plants polystyrene strip. Bottomleft: Xavier Draye, the UCL leader, sharing Belgian culture with Montpellier people. Bottomright: Clementine Barthélemy, UCL master student, and me working together in a root sampling session.

Table S2 Description of Zea mays sp. experiments performed at the UCL laboratory of Louvain La Neuve, Belgium.

Genotype	Traitements	Description
B73xUH007	CTRL	Untreated
	EXC_SN	All seminal and nodal roots are excised
	EXC_1S	One seminal roots is excised
	EXC_S	All seminal roots are excised
	EXC_N	All nodal roots are excised
	EXC_P	The primary root is excised
	END	The starch-rich endosperm is removed
B73 inbred	B73	Classical maize inbred line with american origin
rum1	RUM1	Maize mutant lacking seminal and lateral roots
rtcs	RTCS	Maize mutant lacking seminal and nodal roots
DR5-RFP	DR5	GMO allowing to visualize auxin distribution using fluorescence
indifferent	OMB	Shading applied to plants in BOX 2 reducing the light income to 10% of that received by plants exposed to sunlight (BOX 1)

Table S3 Experimental design used at the UCL experiment

Traitement	BOX 1 (control radiance)			Treatment	BOX 2 (shading until day 10-12)		
	Early (day 4)	Intermediary (day 8)	Late (day 12)		Early (day 4)	Intermediary (day 8)	Late (day 12)
CTRL		30		CTRL + OMB		30	
EXC_SN		30		EXC_SN + OMB		30	
EXC_SN + END		30		EXC_SN + END + OMB		30	
EXC_1S	30	30	30	EXC_1S + OMB	30	30	30
EXC_S	30	30	30	EXC_S + OMB	30	30	30
EXC_N	-	-	30	EXC_N + OMB	30	30	30
EXC_P	30	30	30	EXC_P + OMB	30	30	30
B73		30		B73 + OMB		30	
RTCS		30		RTCS + OMB		30	
RUM1		30		RUM1 + OMB		30	
DR5		15		DR5 + OMB		15	
		495				495	

Supplementary Figure II-5

Linear trend models estimated within the semi-Markov switching linear model: *wild-type* (solid line); *rtcs* mutant (long dashed line) and shading treatment (short dashed line).

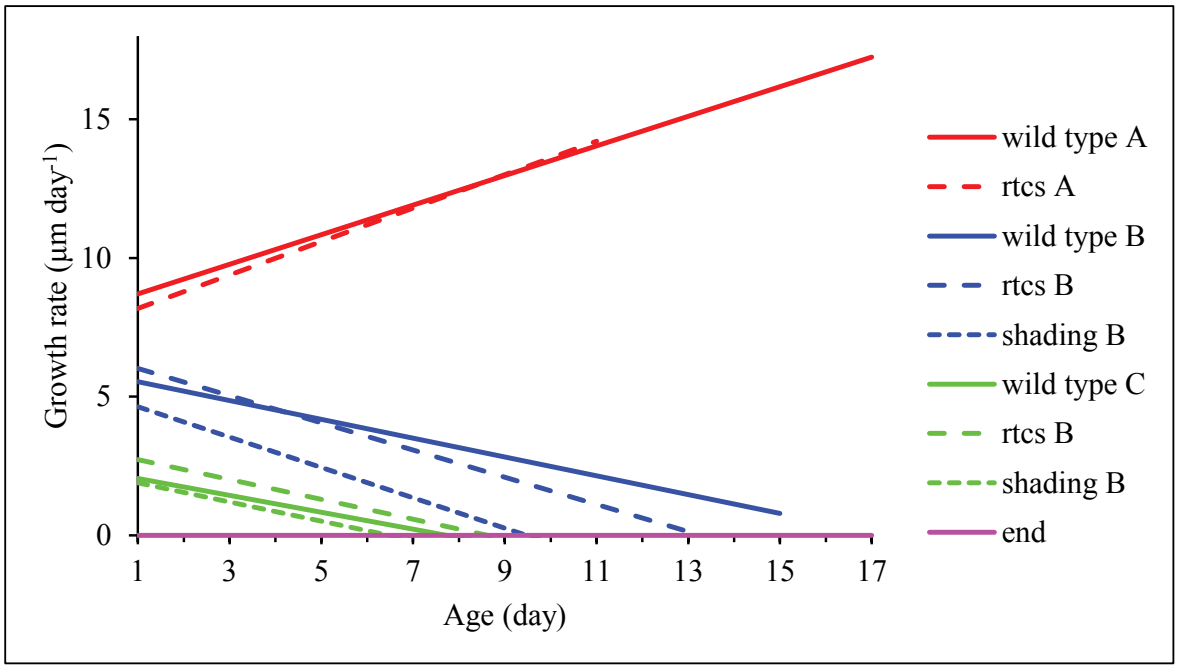

Supplementary References

Csiszár, I., & Talata, Z. (2006). Context tree estimation for not necessarily finite memory processes, Via BIC and MDL. *IEEE Transactions on Information Theory*, *52*(3), 1007–1016. http://doi.org/10.1109/TIT.2005.864431

Guédon, Y. (2003). Estimating Hidden Semi-Markov Chains From Discrete Sequences. *Journal of Computational and Graphical Statistics*, *12*(3), 604–639. http://doi.org/10.1198/1061860032030

Guédon, Y. (2005). Hidden hybrid Markov / semi-Markov chains. *Computational Statistics & Data Analysis*, *49*(May 2006), 663–688. http://doi.org/10.1016/j.csda.2004.05.033

Guédon, Y. (2007). Exploring the state sequence space for hidden Markov and semi-Markov chains. *Computational Statistics and Data Analysis*, *51*(5), 2379–2409. http://doi.org/10.1016/j.csda.2006.03.01

CHAPTER III. IDENTIFYING DEVELOPMENTAL ZONES IN MAIZE LATERAL ROOT CELL LENGTH PROFILES

This chapter consists in a journal article submitted for publication to the Journal of Experimental Botany on the 20th September 2016. It presents a segmentation method for the analysis of cell length data aiming at identifying developmental zones in root apices. This method is applied to a set of lateral roots with contrasting growth trajectories, in the reference genotype B73xUH007 but also in two auxin signaling mutants. This data was obtained from experiments GFBM1 and GFBM2 previously described in section 2.1 of Chapter II.

Authors

Beatriz Moreno Ortega[1,2], Guillaume Fort[1], Bertrand Muller[1], Yann Guédon[2]*

[1]INRA, UMR LEPSE, 34060 Montpellier, France

[2]CIRAD, UMR AGAP and Inria, Virtual Plants, 34095 Montpellier, France

**To whom correspondence should be addressed.*

Beatriz Moreno Ortega (E-mail: ortegab@supagro.inra.fr)

Guillaume Fort (E-mail: g-fort@live.com)

Bertrand Muller (E-mail: bertrand.muller@supagro.inra.fr)

Yann Guédon (E-mail: yann.guedon@cirad.fr)

Abstract

The identification of the limits between the cell division, elongation and mature zones in the root apex is still a matter of controversy when methods based on cellular features, molecular markers or kinematics are compared while methods based on cell length profiles have been comparatively underexplored. A pipeline of analysis methods combining image analysis and segmentation models was developed to identify developmental zones within a root apex on the basis of epidermal cell length profiles. Heteroscedastic piecewise linear models were estimated for maize lateral roots of various lengths of both wild type and auxin mutants. The outputs of these individual root analyses combined with morphological features (first root hair position and root diameter) were then globally analyzed using principal component analysis. Three zones corresponding to the division zone, the elongation zone and the mature zone were identified in most lateral roots while division zone and sometimes elongation zone were missing in arrested roots. Moreover, our results were globally consistent with a tight, auxin-dependent, coordination between cell flux, cell elongation and cell differentiation. The

proposed segmentation models could extend our knowledge of developmental regulations in longitudinally organized plant organs such as roots, monocot leaves or internodes.

Keywords: auxin mutant; lateral root diversity; multiple change-point model, piecewise linear function; principal component analysis; root apex

1 Introduction

Since the pioneering studies of Sachs (1873) and Darwin (1880), the root apex has been one of the most widely used plant organs to study cell division, cell elongation and cell differentiation which occur within successive and essentially distinct zones (Goodwin & Stepka, 1945; Erickson and Sax, 1956). While the longitudinal cellular pattern within the root apex and the naming of the different zones are now the matter of tentative consensus views (Ivanov & Dubrovsky, 2013; Barrio *et al*., 2013), there is still no general agreement regarding the criteria used to define the limits between these zones (Verbelen *et al*., 2006; Ivanov & Dubrovsky, 2013). Historically, the shootward limit of the division zone (DZ) was identified by the presence/absence of mitotic figures in longitudinal sections (Clowes, 1959; Hejnowicz, 1959). By the turn of the last century, molecular markers have revolutionized the histology and, regarding cell division, cyclins which show marked overexpression at precise time points during the cell cycle have been extensively used (Ferreira *et al*., 1994; West *et al*., 2004). However, such type of discrete labelling leads to a probabilistic pattern. This approach has led to the identification of a transition zone (TZ), where a progressive decrease of the occurrence of cell division is observed while cells acquire the capacity to elongate through vacuolization (Baluška *et al*., 1992) and cortical microtubules reorganization (Baluška *et al*., 1996). After TZ, cells move to a rapid elongation zone (EZ) and, to our knowledge, there is no consensus molecular marker for this zone although some members of the expansin gene family show tight association of their expression with elongation rate in monocot leaves (Muller *et al*., 2007) or internodes (Lee & Kende, 2001). Growth cessation at the shootward limit of EZ has been associated with cell wall stiffening (Tomos & Pritchard, 1994), peroxidase activity (though more convincingly in aerial organs, e.g. MacAdam *et al*., 1992) or the burst of reactive oxygen species (Dunand *et al*., 2007) but none of these events were used as marker to locate this limit.

Alternative to cellular features or molecular markers are kinematic studies (Sharp et al., 1988; Muller et al., 1998; Walter et al., 2002). They are based on the non-destructive observation of landmarks (ink, graphite marks or trackable cellular patterns) along the root apex, following protocols and formalisms defined 60 years ago (Erickson & Sax, 1956). These techniques are appropriate for studying the local growth rate and, when combined with cell length profiles, can be used to quantify cell division rate and thus locate the shootward limit of DZ (Erickson

& Sax, 1956; Beemster & Baskin 1998; Muller et al., 1998). However, averaging kinetic profiles for several roots was identified as a source of bias, leading to smooth rapid individual variations and probably to overestimate the size of DZ (van der Weele et al., 2003). Moreover, these techniques require that growth is steady which excludes accelerating, decelerating or stopping roots (Silk, 1992).

The identification of longitudinal cellular patterns in root apices can also be obtained from the observation of cell length profiles alone. Meristematic cells are short in length, the exit from the cell cycle and the entry into EZ are characterized by a rapid increase in cell length while the end of EZ is expected to correspond to cell length reaching a plateau. Different methods were proposed to determine meristem size based on cell length profiles including exploratory visual methods (Casamitjana-Martınez et al., 2003; Mouchel et al., 2004), geometrical approaches (French et al., 2012) and thresholds on the length ratio of the longest to the shortest cells (Hacham et al., 2011). For the identification of the limit between the elongation zone and the mature zone (MZ), the large standard deviation of cell lengths around this limit (Silk et al., 1989) made it difficult to precisely locate it.

One of the aims of this study was thus to provide an accurate segmentation method able to identify root developmental zones in cell length profiles, with minimum a priori biological assumptions. To this end, we sampled lateral roots showing various growth trajectories with acceleration, deceleration and rapid growth arrest (Freixes et al., 2002), likely corresponding to meristem enlargement, shrinking or exhaustion, respectively (Dubrovsky et al., 2003; Sanchez-Calderon et al., 2005). We here introduce heteroscedastic piecewise Gaussian linear models (Hawkins 1976) for identifying root developmental zones. These specific multiple change-point models are distinct from segmented regression or broken-line models (Muggeo, 2003) which are constrained to be homoscedastic (a residual variance common to the different developmental zones). This assumption appeared to be unrealistic in our context. In order to increase the sources of variability in our lateral root samples, and given the impact of auxin on establishment and maintenance of meristem size (Pacifici et al., 2015) and the balance between division and differentiation (Dello Ioio et al., 2008), we used two independent maize mutants altered in auxin signaling. The objectives of this work were thus twofold: (i) design a pipeline of analysis methods combining image analysis and statistical models for identifying development zones in cell length profiles observed in root apices (ii) on this basis, identify emerging properties in terms of coupling/uncoupling between cell division, expansion and differentiation processes and characterize the intrinsic modulation of the root developmental pattern as well as the impact of perturbation in auxin signaling.

2 Material and Methods

2.1 Plant material, growth conditions and lateral root apex harvest

Maize seeds of the hybrid B73xUH007 (referred to as wild type in the sequel) used in this study were produced within the European FP7 project EURoot (http://www.euroot.eu). Seeds of *rtcs* (Taramino et al., 2007) and *rum-1* (Woll et al. 2005) maize auxin signaling mutants were provided by Frank Hochholdinger (University of Bonn, Germany). Germinated seeds were transferred upon emergence of the radicule on the top of 70 x 40 cm rhizotrons adapted from Neufeld et al. (1989). Root systems were allowed to develop between a layer of cellulose acetate tissue in contact with nutrient and water rich compost and a slide of plexiglass. Rhizotrons were installed into 1 m growth chambers under controlled conditions (20/20 °C day/night temperature, 1 kPa VPD and PPFD of 200 µmol photons m^{-2} s^{-1}).

After 2 weeks, a selection of ~ 1 cm long root apices from 42 lateral roots encompassing the diversity of roots present along the primary root was harvested. The lateral roots were sampled in 3 categories depending on length and apparent vigor: (A) long and vigorous; (B) intermediate, apparently decelerating; (C) short (< 1 cm). Type B and type C roots had visually short distances between tip and first root hair position. In the mutants, vigorous lateral roots emerging from curvatures of the primary roots were categorized as A.

2.2 Image analysis and acquisition of lateral root cell length profiles and morphological properties

Root apices were placed in a fixative solution of 1:3 vol/vol acetic acid: 70% ethanol and stored at 4°C. After 2 days, the fixed material was moved to a clearing solution of chloral hydrate (200 g chloral hydrate in 20 ml glycerol and 30 ml water) for at least 4 h (Wu et al., 2011). Roots were mounted in the same solution and imaged within a week. Root apices were observed using a light microscope (Olympus BX61 TRF, Japan) under autofluorescence conditions using UV illumination (360-370 nm) to allow observation of cell walls in epidermal root cells. Individual root apices (**Figure III-1**) were imaged at 10 x magnification by gathering 2-3 contiguous images, until the zone where root hair development was observed.

All image manipulation and data acquisition were performed using the ImageJ image analysis software (Rasband WS. U.S. National Institutes of Health, Bethesda, MD, USA). Cell lengths from all clearly visible files (usually the central 3-4 cell files) of the epidermal tissue were manually measured for each root. Cell length sampling started at the root cap junction and spanned shootward, as much as the quality of the image allowed it, and in all cases after the occurrence of the first root hair. Each cell was assigned to a longitudinal position equal to its orthogonal projection to a virtual line passing through the middle of the root, taking the root cap junction as the origin. The location at which root hair formation begins was estimated for

each root using the most proximal cell showing an incipient root hair bulge. Lateral root diameter profiles were evaluated at 2 independent locations beyond the first root hair. After exploration of cell length profiles, 36 lateral roots were retained for further analyses (18 wild-type, 8 *rtcs* and 10 *rum-1* individuals), the 6 others being rejected because of a too sparse sampling of cells. An average of 160 cell lengths was measured for each selected root, with a minimum of 52 and a maximum of 267.

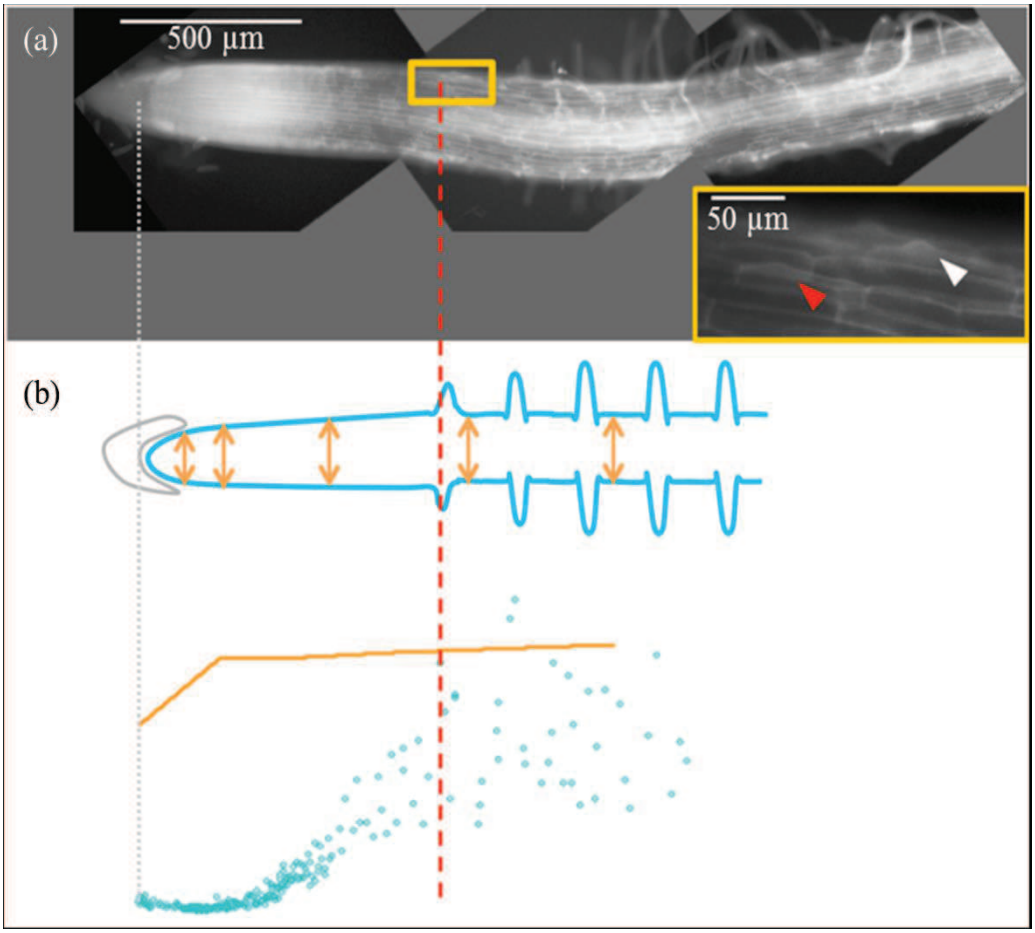

Figure III-1. Acquisition of epidermal cell length profiles and associated measurements. (**a**) Autofluorescence microphotography of a maize lateral root apex obtained as a composite of 3 different microscopy images (black background). Arrowheads in the inbox indicate root hair bulges. The most rootward epidermal cell with a visible root hair bulge is indicated by a red arrowhead. (**b**) Epidermal cell lengths (blue points) have been sampled along the longitudinal axis of the root. The positions of the root cap junction (gray line; origin of the longitudinal axis) and of the most rootward root hair bulge (red line) have been recorded. Root diameter has been sampled at 5 different positions spanning the imaged root (orange arrows) in order to build a longitudinal profile of the root diameter (orange line).

2.3 Multiple change-point models for identifying development zones in lateral root cell length profiles

2.3.1 Definition of heteroscedastic piecewise Gaussian linear models and Gaussian change in the variance models

Multiple change-point models were used to delimit developmental zones within a cell length series **x** of length *T*. We made the assumption of heteroscedastic piecewise Gaussian linear models where the within-zone parameters were the intercept, the slope and the residual variance. The heteroscedasticity assumption (a residual variance different in each zone) was justified by the data characteristics.

We adopted a retrospective or off-line inference approach whose objective was to infer the number of developmental zones *J*, the positions of the $J-1$ change points $\tau_1,\ldots,\tau_{J-1}$ (with the convention $\tau_0=1$ and $\tau_J=T+1$), the *J* within-zone intercepts α_j, slopes β_j and residual variance σ_j^2. For the selection of the number of developmental zones *J*, we used the slope heuristic proposed by Guédon (2015b). The principle of this kind of penalized likelihood criterion consists in making a trade-off between an adequate fitting of the model to the data and a reasonable number of parameters to be estimated.

Once the number of developmental zones J had been selected, the cell length series was optimally segmented into J zones using the dynamic programming algorithm proposed by Auger and Lawrence (1989). This optimal segmentation defines the optimal change points and relies on the estimation of within-segment parameters. It thus defines the optimal piecewise linear function which is not assumed to be continuous at change points. Guédon (2013) generalizes this dynamic programming algorithm to compute the top *N* most probable segmentations. This algorithm was useful since, in some cases, a well-supported alternative segmentation was more consistent with biological assumptions than the optimal segmentation.

The assessment of multiple change-point models relied on two posterior probabilities (see **Supplementary Methods III-1** for formal definitions):

- posterior probability of the selected *J*-developmental-zone model, deduced from the slope heuristic computed for a collection of multiple change-point models i.e. weight of the *J*-developmental-zone model among all the possible models,
- posterior probability of the optimal segmentation in *J* developmental zones i.e. weight of the optimal segmentation among all the possible segmentations in *J* developmental zones.

We used different diagnostic tools (Guédon, 2013) to assess the assumption of the segmentation in developmental zones and in particular two types of posterior probability profiles that summarize all the possible segmentations for a fixed number of developmental

zones: posterior zone probability profiles and posterior segmentation probability profiles. It is often of interest to quantify the uncertainty concerning change-point position. To this end, we computed uncertainty interval for each change point using the smoothing algorithm proposed by Guédon (2013). All these quantities used for diagnostic are formally defined in **Supplementary Methods III-1**.

We conducted a residual analysis to decipher the weights of the change in slope and of the change in residual variance in the determination of change points. To this end, we computed the residual series by subtracting the piecewise linear function corresponding to the selected segmentation from the measured series. We then estimated a Gaussian change in the variance model applying the methodology previously described for heteroscedastic piecewise Gaussian linear models. In a Gaussian change in the variance model, we suppose that $J-1$ change points $\tau_1 < \cdots < \tau_{J-1}$ exist such that the mean is assumed to be constant and the variance is constant between two successive change points:

$$\text{if } \tau_j \leq t < \tau_{j+1}, \quad \begin{cases} E(X_t) = \alpha, \\ \text{Var}(X_t) = \sigma_j^2. \end{cases}$$

In our context of residual analysis, the estimated mean was always very close to 0. Details on the statistical methods for multiple change-point models are given in **Supplementary Methods III-1**.

2.3.2 Illustration of the application of multiple change-point models on selected maize lateral root apices

Three successive zones are expected along the apex of growing roots starting from the tip: the division zone, the elongation zone and the mature zone. We assumed that DZ was characterized by small cells, EZ by cells of gradually increasing length and MZ by large cells. In our modeling framework, the limit between two successive zones corresponds to a marked change in slope and in residual standard deviation.

The example presented in **Figure III-2** illustrates a typical vigorous lateral root where the DZ-EZ and EZ-MZ limits correspond to changes both in slope and in residual standard deviation. The residual analysis (**Figure III-3**) highlights the role played by the change in residual standard deviation for defining limits between consecutive zones since the uncertainty intervals for the DZ-EZ and EZ-MZ limits given by the piecewise linear model estimated on the basis of the measured series and the change in the variance model estimated on the basis of the residual series are very close.

The example presented in **Figure III-4** illustrates a more difficult case where the optimal piecewise linear function deduced from the optimal 2-developmental-zone model can be interpreted as a division zone followed by a mature zone according to our biological assumptions. The missing elongation zone could not be identified in the optimal 3-segment piecewise linear function (the slope in the elongation zone is not significantly different from zero) but rather in the well-supported alternative 3-segment piecewise linear function corresponding to the second segmentation. The difficulty came from the rather sparse sampling of MZ (16 cells in the retained segmentation instead of 62 in *rtcs* A1 shown in **Figure III-2**) in conjunction with the high MZ residual standard deviation. The example (*rtcs* A2) in **Supplementary Figure III-1** illustrates a similar situation but where the optimal 3-segment piecewise linear function is consistent with our biological assumptions.

The example presented in **Figure III-5** illustrates the case of a probably arrested lateral root without DZ for which the determination of the EZ-MZ limit was rather uncertain. The optimal limit was at the shootward end of the uncertainty interval. This limit entailed a jump of −54.4 μm between the two linear functions. We thus retained the limit at 520 μm corresponding to the second segmentation which only entailed a jump of −10.9 μm. Moreover, it was far closer to the first hair position at 210 μm than the limit at 819 μm corresponding to the optimal segmentation. It was also consistent with the residual analysis (see the **Results section**) while in the case of the residual series deduced from the optimal segmentation, the slope heuristic favors the single-zone model (posterior model probability of 0.91). The example in **Supplementary Figure III-2** illustrates a similar situation in the case of a 3-zone lateral root where the third segmentation that differs only from the optimal segmentation by the position of the EZ-MZ limit was far more consistent with an approximate continuity of the selected piecewise linear function and the residual analysis. The optimal segmentation of the residual series deduced either from the optimal segmentation or from the second segmentation of the measured series has the same change points as the second segmentation of the measured series.

These examples illustrate the strategy we adopted for selecting piecewise linear functions combining the inference of multiple change-point models with biological assumptions. We first computed the optimal piecewise linear function for the number of developmental zones given by the slope heuristic. We then identified DZ, EZ and MZ and checked their characteristics according to our biological assumptions (knowing that DZ or DZ and EZ can be absent for arrested roots). If two consecutive zones were merged (e.g., EZ and MZ for the example presented in **Figure III-4**), we explored the well-supported (in terms of posterior probabilities) segmentations with one more zone. If the optimal piecewise linear function was strongly inconsistent regarding the approximate continuity assumption, we explored well-supported alternative segmentations. No other biological assumptions (e.g. position of the EZ-

MZ limit with respect to the first root hair position) were used for selecting piecewise linear functions.

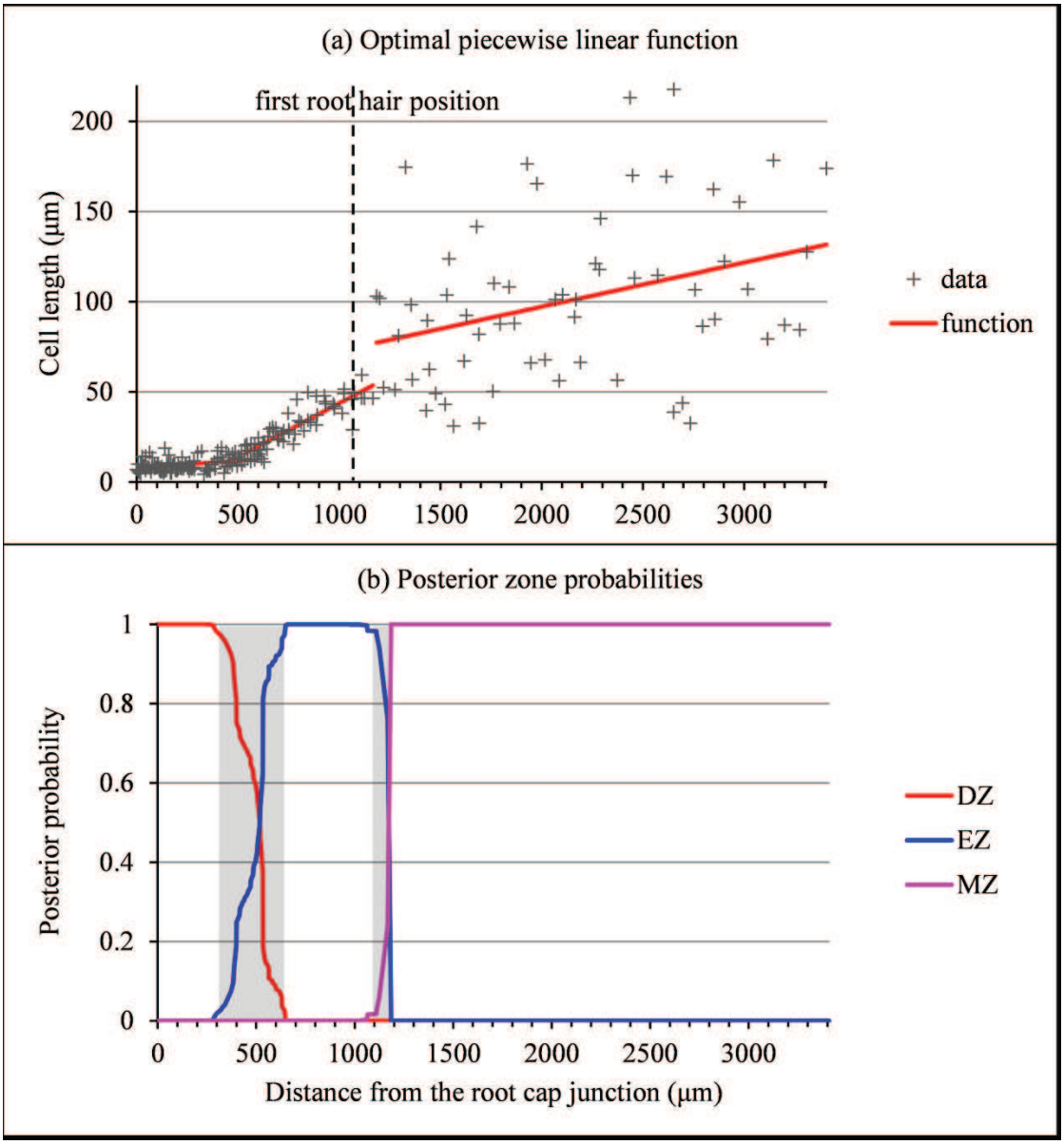

Figure III-2. Outputs of the selected piecewise linear model in the case of a typical vigorous lateral root (*rtcs* A1). (**a**) Optimal 3-zone piecewise linear function and first root hair position; (**b**) Posterior division zone (DZ), elongation zone (EZ) and mature zone (MZ) probabilities. The uncertainty intervals for the DZ-EZ and EZ-MZ limits are in grey.

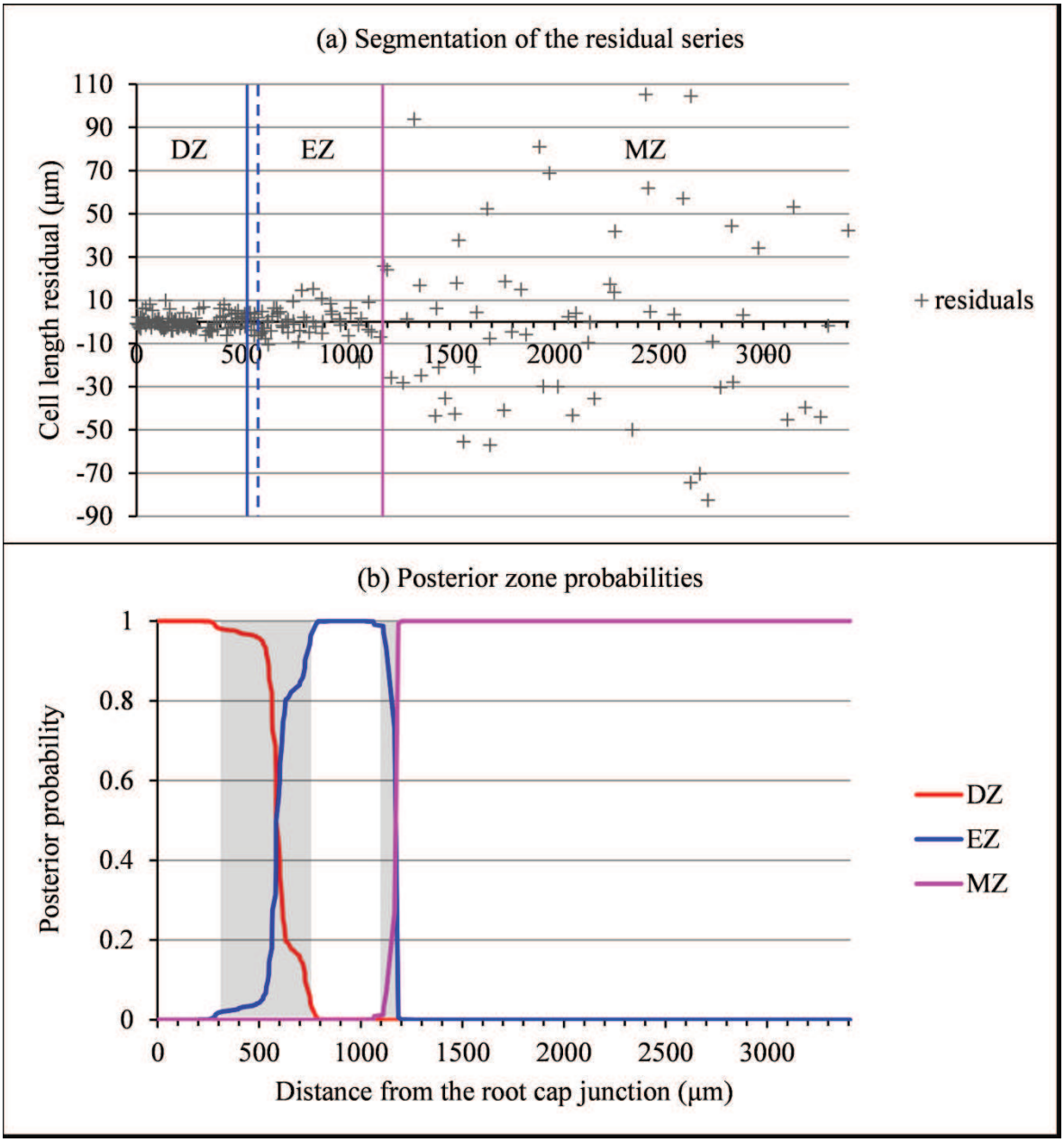

Figure III-3. Residual analysis of the lateral root (*rtcs* A1) presented in **Figure 2**. (**a**) Segmentation in 3 zones of the residual series using a Gaussian change in the variance model with the division zone-elongation zone (DZ-EZ) and elongation zone-mature zone (EZ-MZ) limits (solid lines: estimated on the basis of the original series; dotted lines: estimated on the basis of the residuals series); (**b**) Posterior DZ, EZ and MZ probabilities. The uncertainty intervals for the DZ-EZ and EZ-MZ limits are in grey.

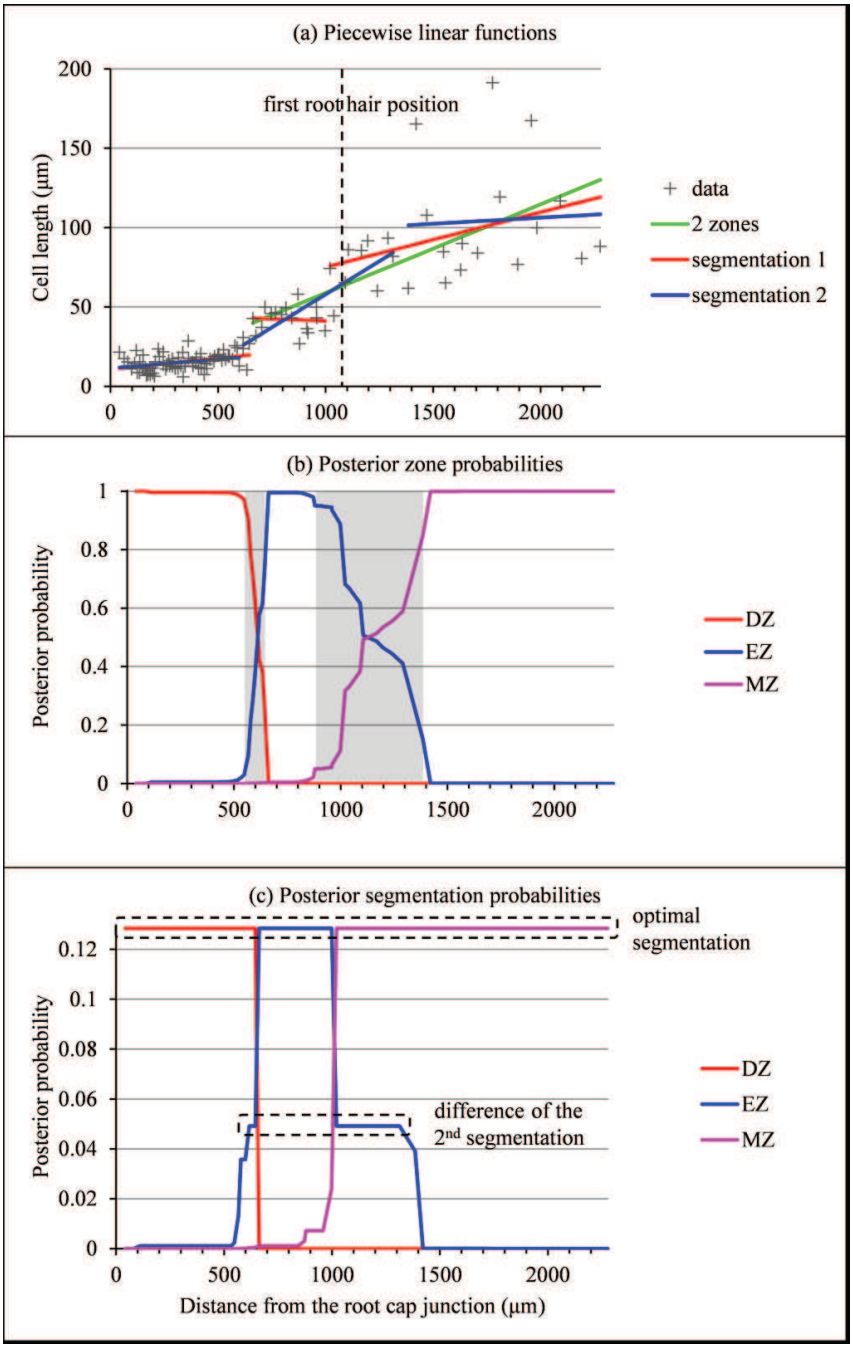

Figure III-4. Outputs of the piecewise linear models in the case of a lateral root (*rtcs* A3) for which the 2-zone model selected by the slope heuristic and the optimal 3-zone piecewise linear function do not fit biological assumptions (lack of EZ and null EZ slope respectively). (a) Optimal 2-zone and 3-zone piecewise linear functions, sub-optimal 3-zone piecewise linear function and first root hair position; (b) Posterior division zone (DZ), elongation zone (EZ) and mature zone (MZ) probabilities; (c) Posterior segmentation probabilities highlighting the difference between the 2nd segmentation and the optimal segmentation in 3 zones.

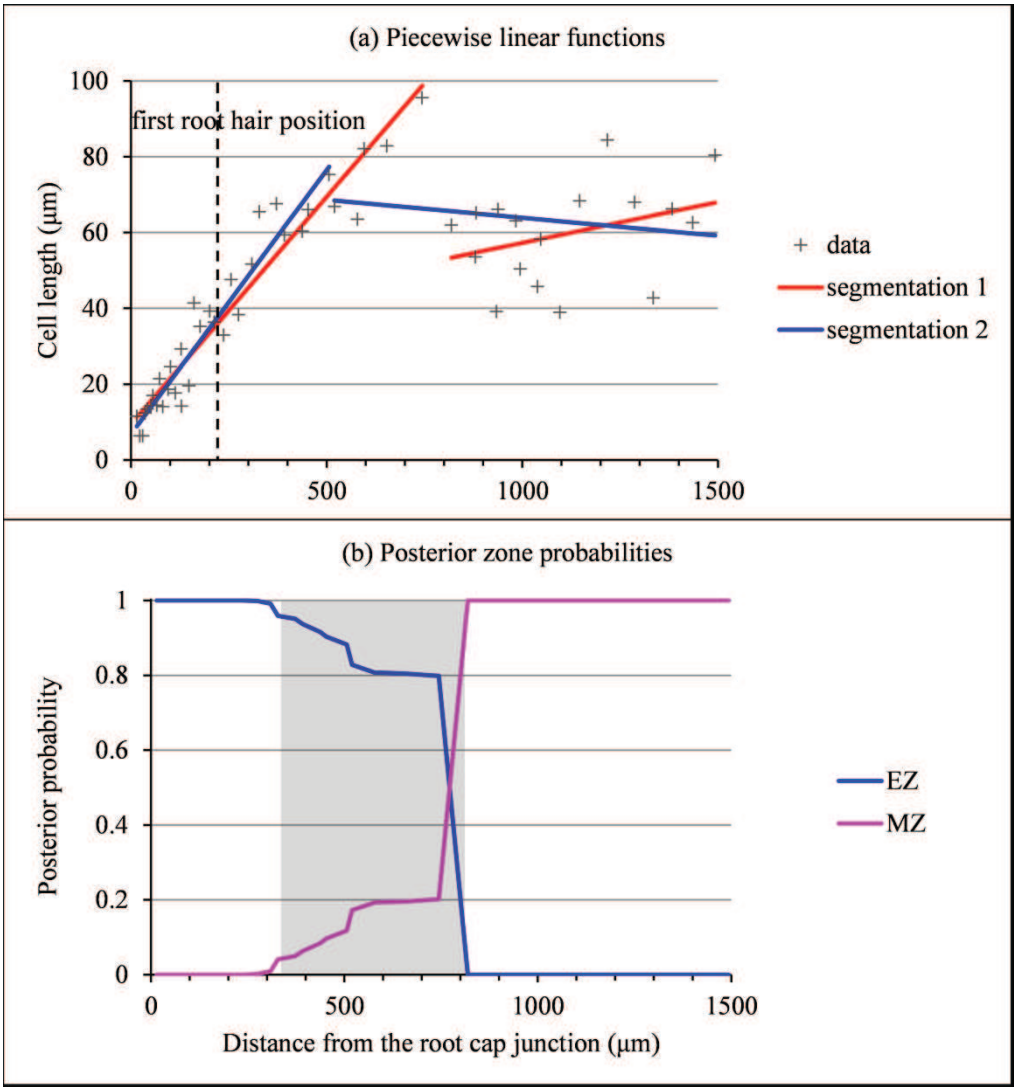

Figure III-5. Outputs of the selected piecewise linear model in the case of a probably arrested lateral root (*rtcs* B15) for which the optimal 2-zone piecewise linear function do not fit biological assumptions (piecewise linear function not approximately continuous). (**a**) Optimal 2-zone piecewise linear function, sub-optimal 2-zone piecewise linear function corresponding to the 2nd segmentation and first root hair position; (**b**) Posterior elongation zone (EZ) and mature zone (MZ) probabilities. The uncertainty interval for the EZ-MZ limit is in grey.

3 Results

We here assumed that the developmental pattern was common for the studied lateral roots even if the most rootward developmental zones (i.e. DZ or DZ and EZ) were missing for some roots. The analysis of this developmental pattern was decomposed in two steps:

1. Identification and characterization of the successive developmental zones along each lateral root. For this individual analysis, we focused in particular on the selection of

the number of developmental zones, on the roles played by the change in slope and the change in residual standard deviation in the determination of the limits between these zones and on the uncertainty concerning these limits.

2. Comparison of the developmental zones of the lateral roots in order to identify commonalities and differences between these zonations.

3.1 Selection of the number of developmental zones

We retained the number of developmental zones given by the slope heuristic and the optimal segmentation for this number of developmental zones for 26 individuals among 36 (**Tables III-1, III-3, III-5** for the wild type and the *rtcs* and *rum-1* mutant respectively). This includes the three 4-zone individuals presented in **Supplementary Table III-1**. For 2 individuals, we retained a well-supported alternative model with one more developmental zone than the model selected by the slope heuristic and for 2 other individuals (see **Figure III-5 and Supplementary Figure III-2**), we retained a well-supported alternative segmentation. For the 6 remaining individuals, we retained a model with one more developmental zone than the model selected by the slope heuristic and the optimal segmentation for this number of developmental zones except for one individual (see **Figure III-4**) for which we retained a well-supported alternative segmentation. All these choices were clearly supported by biological assumptions. **Figure III-2** shows a typical 3-zone individual while **Figure III-6** shows a typical 2-zone (EZ and MZ) individual and a typical single-zone (MZ only) individual corresponding to arrested or almost arrested roots. For these three individuals, the piecewise linear function corresponds to the optimal segmentation in the number of developmental zones given by the slope heuristic.

For three wild-type individuals, four zones were identified where the first two zones correspond to a split of DZ (**Table III-1 and Supplementary Table III-1**). The segmentations in 3 and 4 zones were nested or almost nested in the case of A13 (**Supplementary Figure III-3**). The limit between the two successive zones within DZ corresponded mainly to a change in slope with a negative slope in the first zone followed by a positive slope or a slope non-significantly different from zero in the B32 case in the second zone. When the residual series was extracted using the 4-segment piecewise linear function, the first two zones could only be identified in B32 but not in the two other individuals for which they were merged consistently with the similar residual standard deviations estimated for the two DZ zones for A13 and B33 (**Supplementary Table III-1**).

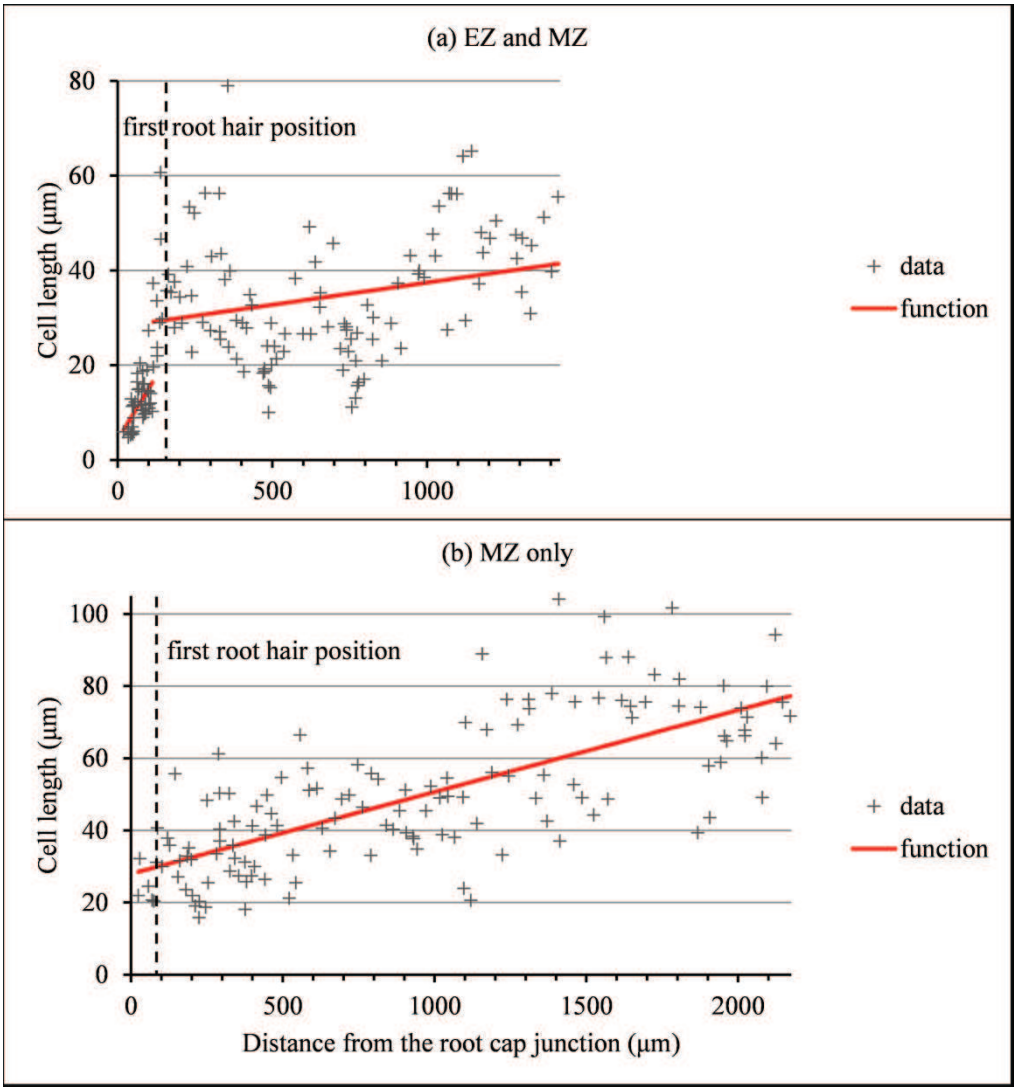

Figure III-6. Outputs of the selected piecewise linear model in the case of 2-zone (EZ and MZ) individual and a single-zone (MZ only) individual corresponding to arrested or almost arrested roots. (a) Wild-type C28: optimal 2-zone piecewise linear function and first root hair position; (b) Wild-type C27: optimal linear function and first root hair position.

Table III-1. Multiple change-point models estimated for wild-type lateral roots. For each lateral root (ordered in decreasing division zone length), the piecewise linear model is described in the first row and the Gaussian change in the variance model estimated on the basis of the residual series is described in the second row. For each multiple change-point model, the standard deviations (s.d.) estimated for each zone −division zone (DZ), elongation zone (EZ) and mature zone (MZ)−, the limits between zones with associated 0.05-uncertainty intervals, the first root hair position (all in μm), the selected segmentation posterior probability −an asterisk indicates that the segmentation is the optimal one−, the selected model posterior probability −an asterisk indicates that the model is the one given by the slope heuristic (SH)−, and the number of zones given by the slope heuristic are given.

						First hair		Posterior probability		SH
		DZ s.d.	DZ-EZ limit	EZ s.d.	EZ-MZ limit	position	MZ s.d.	Segmentation	Model	model
A10	Linear	1.3	855 (761, 855)	5.5	1494 (1121, 1531)	2122	18.2	0.16*	1*	3
	Variance	1.3	855 (766, 855)	5.5	1494 (1188, 1559)		18.1	0.17*	0.54*	3
A31	Linear	2.2	676 (633, 722)	4.6	1368 (1323, 1368)	1692	29.9	0.1*	1*	3
	Variance	2.6	988 (898, 1015)	5.8	1368 (1323, 1368)		29.7	0.1*	0.95*	3
A9	Linear	2	587 (528, 629)	3.5	1219 (1177, 1219)	2318	27.8	0.13*	1*	3
	Variance	2.2	1008 (973, 1018)	7.3	1531 (1440, 2225)		30.4	0.07*	0.95*	3
A8	Linear	0.8	553 (532, 553)	5.4	1100 (1001, 1100)	1862	17	0.13*	0.29	2
	Variance	0.7	553 (532, 553)	4.4	1030 (980, 1100)		15.9	0.16*	0.98*	3
A13	Linear	2	510 (459, 519)	6	973 (952, 973)	1267	37.5	0.24*	0	4
	Variance	2	511 (489, 519)	6	1013 (915, 1013)		37.5	0.25*	0.91*	3
B33	Linear	1.8	439 (387, 439)	8.1	672 (631, 672)	781	33.4	0.21*	0	4
	Variance	1.8	458 (427, 468)	8.4	672 (628, 672)		33.3	0.21*	0.98*	3
B32	Linear	2.2	411 (337, 411)	6.7	716 (672, 716)	929	24.7	0.35*	0	4
	Variance	2.2	411 (337, 515)	6.8	719 (672, 820)		24.9	0.1*	0.02	4
B19	Linear	1.7	366 (344, 380)	4.9	600 (578, 763)	895	32.5	0.17*	1*	3
	Variance	1.8	415 (358, 422)	5.3	600 (568, 600)		32.1	0.21*	0.98*	3
A11	Linear	1.9	328 (255, 379)	3.6	655 (647, 655)	1165	24.1	0.13*	0.96*	3
	Variance	2.2	454 (277, 462)	4.6	678 (654, 678)		24.3	0.1*	0.98*	3
A12	Linear	1.7	320 (314, 320)	5.1	722 (677, 722)	756	25.6	0.5*	1*	3
	Variance	1.7	320 (314, 358)	5.2	729 (677, 729)		25.6	0.26*	1*	3
B34	Linear	1.2	278 (274, 317)	6.3	461 (392, 461)	515	24.6	0.27*	0.85*	3

	Variance	1.2	278 (270, 294)	4	392 (391, 473)		22.2	0.17*	0.13	4
B20	Linear	2.7	232 (227, 243)	10.1	574 (517, 672)	586	25.3	0.14*	1*	3
	Variance	2.7	232 (224, 243)	9.8	591 (349, 591)		25.7	0.2*	0.91*	3
B35	Linear	3	215 (171, 215)	7.2	388 (367, 418)	430	23.2	0.19*	1*	3
	Variance	3.3	257 (207, 285)	12	1157 (388, 1157)		29.9	0.02*	0.72*	3
C25	Linear			3.2	144 (67, 176)	121	11.6	0.37*	0.01	1
	Variance			3.1	144 (67, 697)		11.6	0.44*	0.9*	2
C28	Linear			4.2	115 (106, 115)	166	12.8	0.65*	1*	2
	Variance			4.5	139 (97, 139)		13	0.21*	1*	2
C26	Linear					101	11.5	1*	1*	1
	Variance						11.5	1*	0.27	2
C27	Linear					93	14	1*	1*	1
	Variance						14	1*	0.61*	1
C30	Linear					197	15.9	1*	1*	1
	Variance						15.9	1*	0.95*	1

Table III-2. Piecewise linear functions selected for wild-type lateral roots. For each lateral root (ordered in decreasing division zone length), the parameters of the piecewise linear function (slope x 1000, correlation coefficient for each zone –division zone (DZ), elongation zone (EZ) and mature zone (MZ), n.s. for non-significant− and limits between zones in μm) are given in the first row and the piecewise linear function with associated rootward and shootward confidence intervals at each limit between zones is given in the second row.

	Division zone			Elongation zone			Mature zone		
	Slope	Correlation	DZ-EZ limit	Slope	Correlation	EZ-MZ limit	Slope	Correlation	End point
	Linear function	Confidence intervals		Linear function	Confidence intervals		Linear function		
A10	0.8	0.12 n.s.	855	59.5	0.88	1494	49.6	0.78	2990
	5.4 → 6	(5.5, 6.5	| 5, 9.7)	7.3 → 45.4	(41.8, 48.9	| 45.7, 61)	53.3 → 127.6		
A31	−6	−0.42	676	50.5	0.9	1368	65.9	0.73	3126
	9.3 → 5.7	(4.8, 6.7	| 4.2, 8)	6.1 → 41	(38.9, 43.2	| 47.7, 70.9)	59.3 → 175.2		
A9	−5.3	−0.35	587	42.4	0.91	1219	43.1	0.76	3557
	7.8 → 5.1	(4.2, 6	| 5, 8.3)	6.7 → 33.5	(31.5, 35.4	| 40.2, 65)	52.6 → 153.4		
A8	−3.2	−0.36	553	59.2	0.83	1100	49.4	0.77	2459
	7.7 → 6.7	(6.1, 7.2	| 2.4, 12.8)	7.6 → 40	(36.4, 43.6	| 42.7, 60.7)	51.7 → 118.8		
A13	−3.6	−0.24	510	90.9	0.87	973	30.1	0.35	2582
	7.3 → 5.4	(4.7, 6.2	| 3.9, 9.2)	6.5 → 48.6	(45.1, 52.2	| 69.2, 108)	88.6 → 137		
B33	−0.2	−0.01 n.s.	439	201.8	0.82	672	15.1	0.21 n.s.	2198
	6.4 → 6.3	(5.5, 7	| 4.4, 14.8)	9.6 → 56.6	(49.2, 64	| 68.6, 99.3)	83.9 → 107.1		
B32	−16	−0.53	411	116.3	0.81	716	35.2	0.44	1852
	9.3 → 3.6	(2.5, 4.7	| 6.1, 13.8)	10 → 45.5	(40.7, 50.2	| 60.6, 87.1)	73.8 → 113.8		
B19	11.6	0.42	366	118.8	0.85	600	21.2	0.36	2283
	6.5 → 8.9	(7.8, 9.9	| 7.7, 14.6)	11.2 → 39	(34.9, 43	| 66.6, 107.8)	87.2 → 122.9		
A11	−6.3	−0.25 n.s.	328	83	0.9	655	74.6	0.72	1898
	7.3 → 5.5	(4.3, 6.7	| 3.6, 6.6)	5.1 → 32.3	(30.3, 34.2	| 44.1, 65.7)	54.9 → 147.6		
A12	1.3	0.05 n.s.	320	102.5	0.91	722	13.3	0.33	2967
	5.9 → 6.2	(5.3, 7.1	| 4.5, 9.7)	7.1 → 48.3	(44.2, 52.4	| 59, 79.2)	69.1 → 98.9		
B34	−9.6	−0.4	278	140.1	0.72	461	27.6	0.55	2182
	6.4 → 4.9	(4.1, 5.7	| 1.4, 8.3)	4.8 → 30.5	(26.5, 34.5	| 52.7, 72.2)	62.4 → 109.9		

B20	1 11.3 → 11.5	0.02 n.s. (10, 13	232 | 6.5, 16.6)	201.4 11.6 → 80.4	0.88 (73.5, 87.4	574 | 88.5, 115.9)	15.9 102.2 → 137.2	0.44	2775
B35	−22.1 9.2 → 5.1	−0.32 (3.3, 7	215 | 4.8, 13.2)	183.3 9 → 40.7	0.76 (35.5, 45.9	388 | 55.1, 71.9)	3.2 63.5 → 71	0.09 n.s.	2771
C25				159 5.2 → 25.7	0.75 (18.2, 33.1	144 | 20.9, 28.4)	30.6 24.6 → 80.3	0.82	1961
C28				108.6 6.3 → 16.7	0.53 (13.9, 19.5	115 | 25, 33.4)	9.4 29.2 → 41.4	0.26	1424
C26							28.1 20.3 → 79.2	0.82	2115
C27							22.7 28.5 → 77.2	0.72	2172
C30							27.6 28.7 → 89	0.69	2214

Table III-3. Multiple change-point models estimated for *rtcs* lateral roots. For each lateral root (ordered in decreasing division zone length), the piecewise linear model is described in the first row and the Gaussian change in the variance model estimated on the basis of the residual series is described in the second row. For each multiple change-point model, the standard deviations (s.d.) estimated for each zone −division zone (DZ), elongation zone (EZ) and mature zone (MZ)−, the limits between zones with associated 0.05-uncertainty intervals, the first root hair position (all in μm), the selected segmentation posterior probability −an asterisk indicates that the segmentation is the optimal one−, the selected model posterior probability −an asterisk indicates that the model is the one given by the slope heuristic (SH)−, and the number of zones given by the slope heuristic are given.

						First hair		Posterior probability		SH
		DZ s.d.	DZ-EZ limit	EZ s.d.	EZ-MZ limit	position	MZ s.d.	Segmentation	Model	model
A3	Linear	4.8	617 (548, 645)	12.9	1385 (879, 1385)	1083	40.1	0.05	0	2
	Variance	4.7	634 (553, 704)	13.1	1385 (879, 1385)		38.7	0.19*	0.53*	3
A1	Linear	3.4	535 (321, 644)	6	1185 (1112, 1185)	1078	43.6	0.14*	1*	3
	Variance	3.4	583 (387, 753)	6.3	1185 (1112, 1185)		43.3	0.08*	0.96*	3
A’36	Linear	2.1	506 (474, 506)	6.6	1146 (997, 1167)	965	21.8	0.13*	0.61*	3
	Variance	2.1	506 (465, 506)	6.5	1146 (997, 1215)		21.3	0.15*	0.99*	3
A2	Linear	3.1	323 (16, 342)	11.4	744 (388, 796)	485	28	0.13*	0.01	2
	Variance	3.1	347 (68, 347)	11.8	744 (347, 744)		27.6	0.12*	0.17	2
A’37	Linear	1.3	313 (298, 313)	6.1	707 (549, 803)	692	14.7	0.1*	0.95*	3
	Variance	1.3	313 (288, 313)	3.8	455 (417, 688)		12.3	0.08*	0.94*	3
A’38	Linear	1.4	272 (267, 318)	4.3	505 (426, 505)	563	16.1	0.05*	0	2
	Variance	1.5	295 (285, 311)	4.3	428 (402, 692)		15.5	0.05*	0.88*	3
A’39	Linear			8.8	980 (548, 1103)	634	26.9	0.35*	0.2	1
	Variance			8.6	980 (548, 1103)		26.4	0.39*	0.91*	2
B15	Linear			5.8	520 (328, 819)	210	15.2	0.05	1*	2
	Variance			5.6	596 (101, 596)		15.6	0.36*	0.9*	2

Table III-4. Piecewise linear functions selected for *rtcs* lateral roots. For each lateral root (ordered in decreasing division zone length), the parameters of the piecewise linear function (slope x 1000, correlation coefficient for each zone –division zone (DZ), elongation zone (EZ) and mature zone (MZ), n.s. for non-significant– and limits between zones in µm) are given in the first row and the piecewise linear function with associated rootward and shootward confidence intervals at each limit between zones is given in the second row.

	Division zone			Elongation zone			Mature zone		
	Slope	Correlation	DZ-EZ limit	Slope	Correlation	EZ-MZ limit	Slope	Correlation	End point
	Linear function	Confidence intervals		Linear function	Confidence intervals		Linear function		
A3	11.2	0.34	617	83.4	0.81	1385	7.7	0.05 n.s.	2277
	11.9 → 18.3	(15.7, 20.9	| 17.7, 34.4)	26 → 90.1	(77.7, 102.4	| 63.7, 139.4)	101.5 →108.4		
A1	8.3	0.36	535	59.6	0.88	1185	24.5	0.34	3407
	7.6 → 12	(10.5, 13.6	| 13.3, 18.5)	15.9 → 54.6	(50.8, 58.4	| 57.1, 97.3)	77.2 → 131.6		
A'36	2.3	0.15 n.s.	506	92.2	0.93	1146	25.5	0.3 n.s.	1998
	7.5 → 8.6	(7.8, 9.4	| 7.1, 13.8)	10.4 → 69.4	(63.8, 75	| 51.1, 86.2)	68.6 → 90.3		
A2	27.8	0.64	323	157.5	0.86	744	10.1	0.17 n.s.	2257
	5.6 → 14.6	(13, 16.2	| 10.4, 24.7)	17.5 → 83.8	(73.4, 94.3	| 64.3, 99.5)	81.9 → 97.2		
A'37	20.4	0.63	313	82.2	0.84	707	31.2	0.47	1514
	5.6 → 9.1	(8.3, 9.9	| 7.1, 12.8)	10 → 42.4	(38.2, 46.5	| 41.6, 59.1)	50.4 → 75.5		
A'38	9.7	0.5	272	111.7	0.82	505	28.7	0.49	1621
	6.3 → 9	(8.3, 9.6	| 2.7, 6.8)	4.8 → 30.8	(26.3, 35.3	| 34.2, 51.7)	42.9 → 75		
A'39				66	0.84	980	23.5	0.23 n.s.	1844
				11.1 → 59.7	(53.1, 66.3	| 34.3, 74.4)	54.4 → 74.7		
B15				139.5	0.96	520	−9.5	−0.18 n.s.	1493
				8.9 → 79.3	(73.7, 85	| 54.9, 82)	68.5 → 59.2		

Table III-5. Multiple change-point models estimated for *rum-1* lateral roots. For each lateral root (ordered in decreasing division zone length), the piecewise linear model is described in the first row and the Gaussian change in the variance model estimated on the basis of the residual series is described in the second row. For each multiple change-point model, the standard deviation (s.d.) estimated for each zone −division zone (DZ), elongation zone (EZ) and mature zone (MZ)−, the limits between zones with associated 0.05-uncertainty intervals, the first root hair position (all in μm), the selected segmentation posterior probability −an asterisk indicates that the segmentation is the optimal one−, the selected model posterior probability −an asterisk indicates that the model is the one given by the slope heuristic (SH)−, and the number of zones given by the slope heuristic are given.

						First hair		Posterior probability		SH
		DZ s.d.	DZ-EZ limit	EZ s.d.	EZ-MZ limit	position	MZ s.d.	Segmentation	Model	model
A5	Linear	2.5	787 (771, 812)	8.8	2360 (2090, 2360)	2032	51.7	0.38*	1*	3
	Variance	2.6	842 (787, 842)	9.2	2360 (2185, 2360)		50.8	0.41*	1*	3
A7	Linear	1.8	456 (415, 483)	7	1123 (610, 1123)	1241	19.4	0.1*	0	2
	Variance	1.8	456 (393, 456)	4.1	629 (595, 1040)		12.3	0.03*	0.97*	3
A'41	Linear	4.6	452 (392, 462)	9.8	1246 (787, 1305)	1023	33.2	0.06*	0.74*	3
	Variance	4.5	452 (401, 469)	9.6	1352 (1107, 1352)		34.3	0.12*	0.99*	3
A4	Linear	2.1	399 (379, 442)	6.1	1068 (941, 1181)	869	18.6	0.1*	0.95*	3
	Variance	2.4	542 (507, 542)	7	1187 (1103, 1187)		19.8	0.31*	0.99*	3
A'40	Linear	4.4	385 (343, 385)	12	689 (647, 1132)	885	30	0.05	0.97*	3
	Variance	4.4	385 (310, 385)	11.8	689 (639, 737)		29.7	0.17*	0.97*	3
A6	Linear	2.1	371 (347, 443)	4.7	958 (846, 958)	1700	29.4	0.25*	1*	3
	Variance	2.1	371 (347, 542)	4.7	958 (909, 958)		28.9	0.28*	0.94*	3
A'42	Linear	3.2	295 (178, 346)	5.5	627 (499, 627)	585	20.7	0.14*	0.93*	3
	Variance	2.8	225 (140, 295)	5.2	627 (548, 627)		20.5	0.07*	0.29	2
C22	Linear			5.4	1510 (1289, 1510)	1270	15.2	0.85*	1*	2
	Variance			5.4	1867 (1752, 1867)		17.5	0.33*	1*	2
C24	Linear			4	540 (482, 600)	656	11.6	0.5*	0.94*	2
	Variance			4	540 (482, 600)		11.5	0.46*	0.91*	2
C23	Linear			7.8	732 (456, 873)	421	10.3	0.15*	0	1
	Variance						9.1	1*	0.99*	1

Table III-6. Piecewise linear functions selected for *rum-1* lateral roots. For each lateral root (ordered in decreasing division zone length), the parameters of the piecewise linear function (slope x 1000, correlation coefficient for each zone – division zone (DZ), elongation zone (EZ) and mature zone (MZ), n.s. for non-significant– and limits between zones in µm) are given in the first row and the piecewise linear function with associated rootward and shootward confidence intervals at each limit between zones is given in the second row.

	Division zone			Elongation zone			Mature zone		
	Slope	Correlation	DZ-EZ limit	Slope	Correlation	EZ-MZ limit	Slope	Correlation	End point
	Linear function	Confidence intervals		Linear function	Confidence intervals		Linear function		
A5	−3.2	−0.28	787	65	0.96	2360	21.1	0.22 n.s.	4090
	10.2 → 7.7	(6.9, 8.5	6.6, 12.9)	9.8 → 112	(106.5, 117.6	69, 140)	104.5 → 140.9		
A7	3	0.15 n.s.	456	62	0.85	1123	41	0.58	2109
	6.7 →7.7	(6.9, 8.6	4.3, 10.5)	7.4 → 48.8	(43.7, 53.8	51.7, 91.7)	71.7 → 112.2		
A'41	−6	−0.17 n.s.	452	75	0.84	1246	16.9	0.18 n.s.	2329
	13.7 → 11	(9.1, 12.9	8.4, 16.6)	12.5 → 72.1	(64.9, 79.2	27.6, 91.6)	59.6 → 78		
A4	0	0 n.s.	399	42.3	0.8	1068	6.5	0.08 n.s.	1870
	8.9 → 8.9	(8.1, 9. 8	8.7, 13.1)	10.9 → 39.2	(36.1, 42.3	38.5, 61)	49.8 → 55		
A'40	19.5	0.43	385	139.9	0.71	689	13	0.2 n.s.	2235
	9.9 → 17.4	(15.7, 19.1	12.2, 25.4)	18.8 → 61.3	(52.1, 70.6	58.4, 86.4)	72.4 → 92.6		
A6	−14.7	−0.57	371	43.1	0.83	958	73.7	0.64	2139
	12 → 6.6	(5.6, 7.6	4.34, 8.4)	6.4 → 31.6	(28.8, 34.5	20.1, 59)	39.5 → 126.5		
A'42	26.7	0.57	295	145.3	0.93	627	2.4	0.06 n.s.	2325
	7.3 → 15.2	(13.5, 16.9	8.9, 15.3)	12.1 → 60.3	(55.4, 65.3	51.1, 72.1)	61.6 → 65.7		
C22				11.6	0.61	1510	14.4	0.34	2820
				13.2 → 29.2	(26.6, 31.9	45.5, 65)	55.2 → 74.1		
C24				9.8	0.38	540	13.5	0.67	3247
				15.4 → 20.7	(18.7, 22.7	19.5, 28.4)	23.9 → 60.6		
C23				85.2	0.85	732	22.6	0.64	2008
				8 → 53.5	(47.1, 59.8	34.1, 45.5)	39.8 → 68.7		

3.2 Discontinuity of the selected piecewise linear functions

Contrary to segmented regression models (Muggeo, 2003), the piecewise linear functions are not constrained to be continuous in the framework of multiple change-point models. We thus computed the rootward and shootward confidence intervals at each limit between two consecutive developmental zones (e.g. DZ and EZ confidence intervals at the DZ-EZ limit) in order to assess the approximate continuity of the piecewise linear function selected for each individuals. The piecewise linear functions were most often approximately continuous for the mutants with overlap between confidence intervals for 13 limits among 14 for *rtcs* (**Table III-4**) and for 15 limits among 17 for *rum-1* (**Table III-6**). The situation was substantially different for the wild type with overlap between confidence intervals for 15 limits among 28, the non-overlap concerning mostly EZ-MZ limits (**Table III-2**).

3.3 The limits between developmental zones is explained both by a change in slope and in residual standard deviation

We conducted a residual analysis using the residual series deduced from the selected piecewise linear function for each individual. We checked that the residual series were stationary and selected for each series a Gaussian change in the variance model using the slope heuristic (**Tables III-1, III-3 and III-5**). We found the same number of zones as for the measured cell length series for 31 individuals among 36 while this number of zones corresponds to a well-supported alternative model for 4 other individuals. 54 change points among 59 were co-localized i.e. the uncertainty intervals for a given change point for the piecewise linear model and for the change in the variance model overlapped. It should also be noted that we did not detected any supplementary change point within EZ in the residual series. The residual standard deviation was thus approximately stationary within EZ.

3.4 Consistency of the EZ-MZ limit with the first root hair position

For about half of the individuals (16 among 33), the EZ-MZ limit was consistent with the first root hair position, i.e. the first hair position falls within the uncertainty interval of the EZ-MZ limit or in EZ (**Tables III-1, III-3** and **Supplementary Table III-5**). The situation was contrasting between the wild type and the *rtcs* and *rum-1* mutants since in the mutant case, the EZ-MZ limit was consistent with the first hair position for most of the individuals (7 among 8 for *rtcs* and 7 among 10 for *rum-1*) while this was rather the exception for the wild type (2 among 15 individuals with a least two zones). In particular, the EZ-MZ limit was far from the first hair position in the rootward direction for five wild-type lateral roots of type A.

Among the individuals which were inconsistent regarding the EZ-MZ limit, we focused on the six 3-zone individuals for which the distance between the EZ-MZ limit and the first root hair position was the largest (wild-type A8, A9, A10, A11, A31 and *rum-1* A6 with a distance between 324 and 1099 μm); see **Supplementary Table III-2**. These 6 individuals were also the individuals with the largest MZ slopes (see Tables 2, 4 and 6) and the smallest difference between the MZ slope and the EZ slope among the 3-zone individuals and were characterized by a high overlap between the confidence intervals of the EZ and MZ slopes; see **Supplementary Table III-2**. It should be noted that for most of the other 3-zone individuals (17 among 20), there were no overlap between the confidence intervals of the EZ and MZ slopes (results not shown). For the selected 6 individuals, the limit between EZ and MZ was thus mainly explained by a change in residual standard deviation. Finally, the cell sampling could not fully explain these results since for 3 of these individuals, the number of cells beyond the first hair position was above 30 (**Supplementary Table III-2**). This inconsistency of the EZ-MZ limit with the first hair position for some individuals can be viewed as a consequence of the fact that this limit is only explained by a change in residual standard deviation for these individuals while for most individuals, the EZ-MZ limit is explained by a concomitant change in slope and in residual standard deviation. Overall, when these 6 individuals were omitted, there was a consistent relationship between the EZ-MZ limit and the first root hair position in both the wild type and the two auxin mutant (**Supplementary Figure III-4**). This relationship was shifted in the mutants with first root hairs emerging closer to the root tip compared to the wild type.

3.5 A strong modulation of the developmental pattern was observed among lateral roots

As expected from the sampling strategy, a strong modulation of the developmental pattern was observed among lateral roots (**Tables III-1**, **III-3** and **III-5**). While long roots (A type) showed the longest DZ and EZ, intermediate (B type) roots showed much reduced DZ and EZ and arrested roots (C type) showed a lack of DZ and sometimes even a lack of EZ. **Figure III-6a** illustrates a case where a shrunken and probably inactive elongation zone is followed by a mature zone with irregular cell length. **Figure III-6b** illustrates a lateral root with neither DZ, nor EZ but a MZ with irregularly increasing cell length, possibly the trace of a progressive and irregular deceleration of the root. In both cases, growth arrest was associated with meristem exhaustion. With regard to cell length, the most remarkable property was the clear difference between DZ cell length between the wild type (4-10 μm, see **Table III-2**) and the mutants (6-18 μm; see **Tables III-4 and III-6**).

3.6 Choice of the variables summarizing lateral root development for the meta-analysis

In order to provide a synthetic view of the modulation of the lateral root developmental pattern, we selected a set of variables for a meta-analysis. The lengths of DZ and EZ and the first root hair position were chosen to characterize lateral root development. These three variables are strongly correlated (correlation coefficients between 0.63 and 0.83 for 3-zone lateral roots) which can be interpreted as a longitudinal scaling of lateral root developmental zones. Concerning cell dimension variables, since EZ was the most structuring zone with high estimated correlation coefficients (**Tables III-2**, **III-4** and **III-6**), we chose the predicted cell lengths at the two ends of the linear function estimated in EZ for summarizing the change in cell length along the lateral roots. These two predicted cell lengths will be referred to as DZ cell length and MZ cell length respectively in the following. These two predicted values are positively correlated ($r = 0.63$ for 3-zone lateral roots). There is thus also a scaling effect in the cell length along the roots. The slope within EZ, which is negatively correlated with the EZ length indicating a partial compensation phenomenon, was also incorporated. Finally, we incorporated the first root hair position and the mean root diameter within MZ, in order to explore the relationships between meristem length, growing zone length, root diameter and onset of differentiation.

3.7 Exploration of the diversity of lateral roots using principal components analysis

We applied a principal components analysis (PCA) to the twenty six 3-zone lateral roots (13 wild-type, 6 *rtcs* and 7 *rum-1* individuals) using 6 variables extracted from the analysis of individual lateral roots using multiple change points models (DZ length, EZ length, DZ cell length, MZ cell length, EZ slope) completed by two morphological variables (first root hair position, mean diameter within MZ). We incorporated as supplementary variables in PCA the slope within DZ. This slope is either negative or non-significantly different from zero for the wild type while being positive (**Table III-2**) or non-significantly different from zero for *rtcs* (**Table III-4**). The situation of the *rum-1* mutants is intermediate with both positive, negative slopes and slopes non-significantly different from zero (**Table III-6**). We also incorporated as supplementary variables in PCA the residual standard deviation estimated within each zones. The cell length predicted at the limit between DZ and EZ is strongly correlated with the residual standard deviations estimated in DZ and MZ ($r = 0.8$ and $r = 0.81$ respectively for 3-zone lateral roots) and the cell length predicted at the limit between EZ and MZ is strongly correlated with the

residual standard deviation estimated in each zone (r = 0.58, r = 0.77 and r = 0.58 for DZ, EZ and MZ respectively).

The first axis accounting for 49% of variance corresponded to the longitudinal variables (mainly DZ and EZ lengths but also first root hair position) while the second axis accounting for 29% of variance corresponded to the cell length variables (DZ and MZ cell lengths), longitudinal variables and cell length variables being uncorrelated (**Figure III-6a**). All these five variables were highly structuring; see the distances of their projections to the correlation circle. The residual standard deviations within DZ and EZ incorporated as supplementary variables were highly related to the second axis. The EZ slope was less affected by the difference in cell dimension within EZ (MZ cell length − DZ cell length) than by the EZ length. Hence, the EZ slope increased when the EZ length decreased; see **Figure III-7a**. The auxin signaling mutation effect was related both to DZ cell length and root diameter being higher for the mutants than for the wild type (**Figure III-7**).

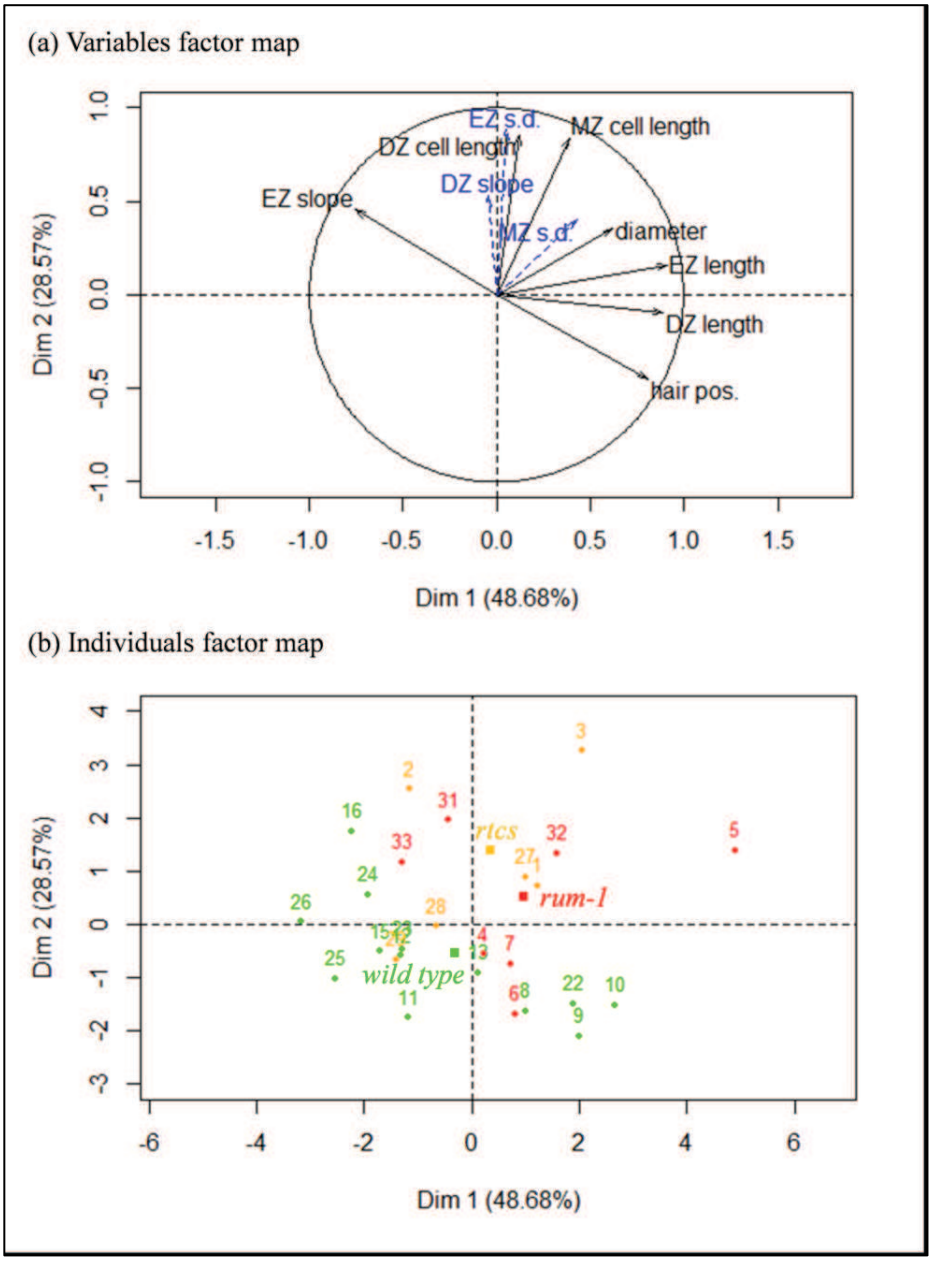

Figure III-7. Principal component analysis applied to the twenty six 3-zone lateral roots: (a) Variables factor map with solid black arrows corresponding to variables (first root hair position abbreviated as hair pos., mean diameter within MZ abbreviated as diameter) used to build the principal components and dotted blue arrows corresponding to supplementary variables (residual standard deviation abbreviated as s.d.); (b) Individuals factor map with wild-type individuals in green, *rtcs* individuals in orange and *rum-1* individuals in red. The genotype centroids are indicated using the same colors.

4 Discussion

4.1 Successive developmental zones in the root apex are well characterized by piecewise linear functions

Heretoscedastic piecewise linear models with at most 4 developmental zones were selected for each lateral root, consistently with the expectation of 3-4 zones for growing roots (*i.e*. DZ, possibly TZ, EZ and MZ). But does the hypothesis of cell length linearity within developmental zones match biological observations? Within EZ, the linearity was clear as shown by the high correlation coefficient estimated for most of the lateral roots. Because EZ corresponds to a zone without cell division, a linear increase in cell length suggests a linearly increasing absolute elongation rate and thus a constant relative elongation rate (Silk, 1992). The consensus view was for decades that relative elongation rate is bell-shaped at the root apex (Erickson & Sax, 1956; Sharp et al., 1988; Muller et al., 1998). It has been convincingly argued that this view was likely biased because of averaging distinct individual roots, temporal integration and curve smoothing (van der Weele et al., 2003). Individual roots observed using fine imaging techniques on the short term (minutes rather than hours) show (for several species so likely a general property) constant growth rate in EZ as well as in DZ and abrupt changes at the DZ-EZ and EZ-MZ limits (van der Weele et al., 2003), results that fit well with the proposed piecewise linear model.

Cell length in DZ was well approximated with a single linear function. For only 3 roots among 36, the optimal model induced a split into 2 zones with negative and positive or nil slope. Such a split is consistent with the concept of a transition zone between a fully proliferative zone with a maximal proportion of cells engaged in the cycle and a transition zone where cells progressively leave the cycle but elongation rate has not yet changed (Dello Ioio et al., 2008; Baluška et al., 2010). Because cell length is the result of an equilibrium between cell division rate and cell elongation rate (Green, 1976), a split into 2 zones with negative and positive slope is consistent with relative elongation rate being constant throughout the meristem (as proposed by van der Weele et al., 2003) but lower and higher than cell division rate in the two domains respectively (Ivanov et al., 2002) due to more or less cells being in the cycle. The fact that the transition zone was identified in only 3 roots could be due to the short size of this zone (Pacifici et al., 2015) in conjunction with changes in slope and in residual standard deviation of small amplitude.

Beyond these 3 roots, DZ slopes were not systematically zero but rather essentially negative in the wild type while being positive in *rtcs* and mixed *in rum-1*. As stated above, a negative slope indicates a proliferative activity being higher than local tissue expansion leading to apparent

decrease in cell size (Green, 1976; Ivanov et al., 2002). Our results thus suggest that (i) expansion and division are not always in perfect equilibrium, (ii) in wild-type roots, this equilibrium is clearly in favor of cell division, (iii) deceleration or slow growth is not associated with a disequilibrium towards expansion but rather to a shortening of the meristem, consistently with other results (e.g. Beemster & Baskin, 1998), and (iv) auxin strongly interferes with this balance, at the benefit of local tissue expansion in the meristem, consistently with the knowledge on the role of this hormone (Pacifici et al., 2015). Finally, if we admit a constant relative elongation rate throughout the meristem (van der Weele et al., 2003), a linear change in cell length suggests that relative cell division rate is also constant, in agreement with independent estimations based of cell cycle duration and mitotic index (Baskin, 2000).

More unexpected was the identified mature zones often displaying significantly positive slopes as one would not expect from a 'classical' mature zone. A first reason could be the mispositioning of the EZ-MZ limit which was likely the case for 6 of the roots, thus drifting the MZ slope towards too high positive values. These 6 roots were those showing the largest distance between the EZ-MZ limit and the first root hair position. Some of these roots were also among those in which cell sampling was the sparser beyond the first root hair which could have negatively impacted the accuracy of the zone detection. A further (and likely interacting) source of confusion could come from the non-stationarity of growth which may have impacted mature cell length. Accelerating roots show higher mature cell length (Beemster & Baskin, 1998) and we can suspect that the reverse is true. In our sample, cell length in MZ was positively correlated with meristem length and thus likely with growth rate. Therefore, we can hypothesize that at least some of the roots with positive slopes result from non-stationary growth. An illustration is given by the type C arrested roots which show clear positive slope although with a wavy pattern (**Figure III-6**) suggesting that deceleration was not uniform.

Once roots with miss-positioned EZ-MZ limit are omitted, all other roots fit well with the 1:1 line between EZ-MZ limit and the first root hair position, in accordance with the biological knowledge regarding the synchronicity of the onset of root hair development and growth cessation (Ma et al., 2003). A distinction could clearly be seen between the wild type and the auxin mutants suggesting that auxin plays also a role (likely in interaction with ethylene, see Ivanchenko et al., 2008; Cho & Cosgrove, 2002) in coupling cell elongation and differentiation.

4.2 Interpretations of the changes in residual standard deviation at the limit between developmental zones

A striking outcome of our analysis was that the limits between developmental zones were explained in most cases by a concomitant change in slope and in residual standard deviation. There are several reasons for the concomitant change slope and in residual standard deviation at the DZ-EZ limit. It is well known that epidermal cells differentiate into 2 distinct types ultimately giving rise to root hairs (trichoblasts) or not (atrichoblasts). In some species including poaceaes (Sinnott & Bloch, 1939), this differentiation is associated with the last division being asymmetrical giving rise to 2 cells of clearly distinct length. Moreover, the DZ-EZ limit is the place where a decreasing proportion of cells remain in the cell cycle while others start to elongate therefore, contributing to standard deviation increase. A last explanation could be linked to endoreduplication. In *Arabidopsis*, endoreduplication starts at the shootward limit of the root meristem with a switch from mitotic cycles to endocycles (Ishida et al., 2009). A detailed analysis of endoreduplication in maize roots remains to be done to validate this hypothesis.

The change in residual standard deviation at the EZ-MZ limit is more challenging to interpret since it occurs after the completion of cell division which is an obvious source of cell length dispersion. Indeed, cells are not supposed to slide from one file to another at a given position from the apex. Could this change in residual standard deviation originate from another round of endoreduplication that would occur shootward from the meristem? This would require that other epidermal cells proceed another round of mitotic cycle which seems unlikely with cells being 40-80 µm long in this region. Strikingly, Dolan et al. (1994) reported large changes in trichoblast vs. non-trichoblast cell length in *Arabidopsis* taking place in pace with the occurrence of the first root hair bulge, exactly like in our situation. In older reports (e.g. Goodwin & Stepka, 1945), a massive increase in epidermal cell length dispersion was already reported at the EZ-MZ limit in cereal roots. How and when this difference in length is generated has not been investigated to our knowledge.

4.3 Comparison between segmented regression models and multiple change-points models

Segmented regression or broken-line models are regression models where the regression function is piecewise linear, i.e. made of straight lines connected at change points (Muggeo, 2003). But the homoscedasticty assumption of these models (a residual standard deviation common to the different developmental zones) is very unrealistic in our context. We thus adopted the framework of multiple change-point models which are latent structure models (Guédon 2013, 2015a) meaning that the outputs of a model are not only the piecewise linear function corresponding to the optimal segmentation but also include the alternative segmentations and more generally

various quantities of interest computed on the basis of all the possible segmentations. Contrary to segmented regression models, the piecewise linear functions corresponding to the selected segmentations are not constrained to be continuous in the context of multiple change-point models. This may be viewed as a shortcoming for biological interpretations but the counterparts of choosing the framework of multiple change-points models are numerous: Heteroscedastic models can be managed which was mandatory in our context. The detection of change points is not constrained by the continuity assumption and the approximate continuity is potentially an emerging property of interest. In multiple-change point models, the inference concerns not only the selection of the number of developmental zones and the estimation of linear function parameters as in standard statistical models such as segmented regression models but also the latent segmentation space (e.g., alternative segmentations). This enables a detailed introspection of each cell length profile with many possibilities to incorporate or assess biological assumptions.

5 Conclusion

The proposed method could successfully handle roots with rather strong modulation of the expected developmental pattern such as arrested roots without DZ or without both DZ and EZ. Our method thus appears both robust and versatile for studying genetic and environmental impacts on root development. It is potentially applicable at high throughput, given the possibility to work on epidermal tissues thus avoiding the tedious preparation of longitudinal sections.

Our results highlight a strong coordination of proliferation and growth processes for a large range of fast, slow growing or arrested lateral roots. As expected, auxin signaling had a great influence on both coordination between division and elongation in the meristem and between cell growth and differentiation. Our method could thus be used for revisiting the coordination of developmental processes among different cell files within a tissue (e.g., trichoblast, atrichoblast…) or, using longitudinal sections or confocal microscopy, the coordination of developmental processes among different tissues (epidermis, cortex, pericycle, stele, etc.). This could extend our knowledge of developmental regulations in longitudinally organized plant organs such as roots, monocot leaves or internodes.

Acknowledgements

This work was supported by the European Union in the frame of the EURoot project and the French National Institute for Agricultural Reseach (INRA, Environment and Agronomy division).

Author contributions

B.M. and Y.G. planned and designed the experiment and the pipeline of analysis, B.M.O. and G.F. performed experiments, Y.G. implemented multiple change-point models, B.M.O. and Y.G. analyzed data, and B.M.O, B.M. and Y.G. wrote the manuscript.

Chapter references

Auger IE, Lawrence CE. 1989. Algorithms for the optimal identification of segment neighborhoods. *Bulletin of Mathematical Biol*ogy 51: 39-54.

Baluška F, Mancuso S, Volkmann D, Barlow PW. 2010. Root apex transition zone: a signalling–response nexus in the root. *Trends in plant science* 15(7): 402-408.

Baluška F, Parker JS, Barlow PW. 1992. Specific patterns of cortical and endoplasmic microtubules associated with cell growth and tissue differentiation in roots of maize (*Zea mays* L.). *Journal of Cell Science* 103(1): 191-200.

Baluška F, Volkmann D, Barlow PW. 1996. Specialized zones of development in roots: view from the cellular level. *Plant Physiology* 112(1): 3-4.

Barrio RA, Romero-Arias JR, Noguez MA, Azpeitia E, Ortiz-Gutiérrez E, Hernández-Hernández V, Cortes-Poza Y, Álvarez-Buylla ER. 2013. Cell patterns emerge from coupled chemical and physical fields with cell proliferation dynamics: the *Arabidopsis thaliana* root as a study system. *PLoS Computational Biology* 9(5): e1003026.

Baskin TI. 2000. On the constancy of cell division rate in the root meristem. *Plant Molecular Biology* 43(5-6): 545-554.

Beemster GTS, Baskin TI. 1998. Analysis of cell division and elongation underlying the developmental acceleration of root growth in *Arabidopsis thaliana*. *Plant Physiology* 116(4): 1515-1526.

Casamitjana-Martinez E, Xu J, Scheres B. 2003. Root-specific CLE19 overexpression and the sol1/2 suppressors implicate a CLV-like pathway in the control of *Arabidopsis* root meristem maintenance. *Medical Engineering & Physics* 25: 75-78.

Cho, HT, Cosgrove DJ. 2002. Regulation of root hair initiation and expansin gene expression in *Arabidopsis*. *The Plant Cell* 14(12): 3237-3253.

Clowes FAL. 1959. Apical meristems of roots. *Biological Reviews* 34(4): 501-527.

Darwin C. 1880. *The Power of Movement in Plants*. Murray, London.

Dunand C, Crèvecoeur M, Penel C. 2007. Distribution of superoxide and hydrogen peroxide in *Arabidopsis* root and their influence on root development: possible interaction with peroxidases. *New Phytologist* 174(2): 332-341.

Dello Ioio R, Nakamura K, Moubayidin L, Perilli S, Taniguchi M, Morita MT, Aoyama T, Costantino P, Sabatini S. 2008. A genetic framework for the control of cell division and differentiation in the root meristem. *Science* 322(5906): 1380-1384.

Dolan L, Duckett CM, Grierson C, Linstead P, Schneider K, Lawson E, Dean C, Poethig S, Roberts K. 1994. Clonal relationships and cell patterning in the root epidermis of *Arabidopsis*. *Development* 120: 2465-2474.

Dubrovsky JG, Gómez-Lomeli LF. 2003. Water deficit accelerates determinate developmental program of the primary root and does not affect lateral root initiation in a Sonoran Desert cactus (*Pachycereus pringlei*, Cactaceae). *American Journal of Botany* 90(6): 823-831.

Erickson RO, Sax KB. 1956. Rates of cell division and cell elongation in the growth of the primary root of *Zea mays*. *Proceedings of the American Philosophical Society* 100(5): 499-514.

Freixes S, Thibaud M-C, Tardieu F, Muller B. 2002. Root elongation and branching is related to local hexose concentration in *Arabidopsis thaliana* seedlings. Plant, Cell & Environment 25(10): 1357-1366.

French AP, Wilson MH, Kenobi K., Dietrich D., Voß U., Ubeda-Tomás S., Pridmore TP, Wells DM, 2012. Identifying biological landmarks using a novel cell measuring image analysis tool: Cell-o-Tape. *Plant Methods* 8(1): 7.

Goodwin RH, Stepka W. 1945. Growth and differentiation in the root tip of *Phleum pratense*. *American Journal of Botany* 32: 36-46.

Green PB. 1976. Growth and cell pattern formation on an axis: critique of concepts, terminology, and modes of study. *Botanical Gazette* 137(3): 187-202.

Guédon Y. 2013. Exploring the latent segmentation space for the assessment of multiple change-point models. *Computational Statistics* 28(6): 2641-2678.

Guédon Y. 2015a. Segmentation uncertainty in multiple change-point models. *Statistics and Computing* 25(2): 303-320.

Guédon Y. 2015b. Slope heuristics for multiple change-point models. In: *30th International Workshop on Statistical Modelling* (IWSM 2015). Friedl H, Wagner H. eds., vol. 2: 103-106.

Hacham Y, Holland N, Butterfield C, Ubeda-Tomás S, Bennett MJ, Chory J, Savaldi-Goldstein S. 2011. Brassinosteroid perception in the epidermis controls root meristem size. *Development* 138(5): 839-848.

Hawkins DM. 1976. Point estimation of the parameters of a piecewise regression model. *Applied Statistics* 25: 51-57.

Hejnowicz Z. 1959. Growth and cell division in the apical meristem of wheat roots. *Physiologia Plantarum* 12(1): 124-138.

Ishida T, Fujiwara S, Miura K, Stacey N, Yoshimura M, Schneider K, Adachi S, Minamisawa K, Umeda M, Sugimoto K. 2009. SUMO E3 ligase HIGH PLOIDY2 regulates endocycle onset and meristem maintenance in *Arabidopsis*. *The Plant Cell* 21(8): 2284-2297.

Ivanchenko MG, Muday GK, Dubrovsky JG. 2008. Ethylene–auxin interactions regulate lateral root initiation and emergence in *Arabidopsis thaliana*. *The Plant Journal* 55(2): 335-347.

Ivanov VB, Dubrovsky JG. 2013. Longitudinal zonation pattern in plant roots: Conflicts and solutions. *Trends in Plant Science* 18: 237-243.

Ma Z, Baskin TI, Brown KM, Lynch JP. 2003. Regulation of root elongation under phosphorus stress involves changes in ethylene responsiveness. *Plant Physiology* 131(3): 1381-1390.

MacAdam J W, Sharp RE, Nelson CJ. 1992. Peroxidase activity in the leaf elongation zone of tall fescue. II. Spatial distribution of apoplastic peroxidase activity in genotypes differing in length of elongation zone. *Plant Physiology*. 99(3): 879-885.

Mouchel CF, Briggs GC, Hardtke CS. 2004. Natural genetic variation in *Arabidopsis* identifies BREVIS RADIX, a novel regulator of cell proliferation and elongation in the root. *Genes & Development* 18(6): 700-714.

Muggeo, VMR. 2003. Estimating regression models with unknown break-points. *Statistics in Medicine* 22(19): 3055–3071.

Muller B, Stosser M, Tardieu F. 1998. Spatial distributions of tissue expansion and cell division rates are related to irradiance and to sugar content in the growing zone of maize roots. *Plant, Cell & Environment*: 21(2): 149-158.

Muller B, Bourdais G, Reidy B, Bencivenni C, Massonneau A, Condamine P, Rolland G, Conéjéro G, Rogowsky P, Tardieu F. 2007. Association of specific expansins with growth in maize leaves is maintained under environmental, genetic, and developmental sources of variation. *Plant Physiology* 143(1): 278-290.

Pacifici E, Polverari L, Sabatini S. 2015. Plant hormone cross-talk: the pivot of root growth. *Journal of Experimental Botany* 66(4): 1113-1121.

Sachs J. 1873. Oder das Wachstum der Haupt und Nebenwurzeln. *Arbeiten des Botanischen Instituts in Würzburg* 3: 395-477.

Sánchez-Calderón L, López-Bucio J, Chacón-López A, Cruz-Ramírez A, Nieto-Jacobo F, Dubrovsky JG, Herrera-Estrella L. 2005. Phosphate starvation induces a determinate developmental program in the roots of *Arabidopsis thaliana*. *Plant and Cell Physiology* 46(1): 174-184.

Silk WK 1992. Steady form from changing cells. *International Journal of Plant Sciences* 153(3): S49-S58.

Silk WK, Lord EM, Eckard KJ. 1989. Growth patterns inferred from anatomical records: empirical tests using longisections of roots of *Zea mays* L. *Plant Physiology* 90(2): 708-713.

Sinnott EW, Bloch R. 1939. Cell polarity and the differentiation of root hairs. *Proceedings of the National Academy of Sciences* 25: 248-252.

Taramino G, Sauer M, Stauffer JL, Multani D, Niu X, Sakai H, Hochholdinger F. 2007. The maize (*Zea mays* L.) RTCS gene encodes a LOB domain protein that is a key regulator of embryonic seminal and post-embryonic shoot-borne root initiation. *The Plant journal* 50(4): 649-659.

Tomos D, Pritchard J. 1994. Biophysical and biochemical control of cell expansion in roots and leaves. *Journal of Experimental Botany* 45(Special Issue): 1721-1731.

Verbelen JP, De Cnodder T, Le J, Vissenberg K, Baluška F. 2006. The root apex of *Arabidopsis thaliana* consists of four distinct zones of growth activities: meristematic zone, transition zone, fast elongation zone and growth terminating zone. *Plant Signaling & Behavior* 1(6): 296-304.

van der Weele CM, Jiang HS, Palaniappan KK, Ivanov VB, Palaniappan K, Baskin TI. 2003. A new algorithm for computational image analysis of deformable motion at high spatial and temporal resolution applied to root growth. Roughly uniform elongation in the meristem and also, after an abrupt acceleration, in the elongation zone. *Plant Physiology* 132(3): 1138-1148.

Walter AH, Spies H, Terjung S. Kusters R, Kirchgeβner N, Schurr U. 2002. Spatio-temporal dynamics of expansion growth in roots: automatic quantification of diurnal course and temperature response by digital image sequence processing. *Journal of Experimental Botany* 53(369): 689-698.

Woll, K, Borsuk LA, Stransky H, Nettleton D, Schnable PS, Hochholdinger F. 2005. Isolation, characterization, and pericycle-specific transcriptome analyses of the novel maize lateral and seminal root initiation mutant *rum1*. *Plant Physiology* 139(3): 1255-126.

Appendix and Supplementary material

Supplementary Methods III-1. Statistical methods for heteroscedastic piecewise Gaussian linear models and Gaussian change in the variance models.

Supplementary Figure III-1. Outputs of the piecewise linear models in the case of a lateral root (*rtcs* A2) for which the 2-zone model selected by the slope heuristic does not fit biological assumptions (lack of EZ). (a) Optimal 2- and 3-segment piecewise linear functions and first root hair position; (b) Posterior segmentation probabilities highlighting the prediction of a 2-zone model by the 6th segmentation in 3 segments.

Supplementary Figure III-2. Outputs of the selected piecewise linear model in the case of a lateral root (*rum-1* A'40) for which the optimal 2-zone piecewise linear function does not fit biological assumptions (piecewise linear function not approximately continuous). (a) Optimal 3-zone piecewise linear function, sub-optimal 3-zone piecewise linear function corresponding to the 3rd segmentation and first root hair position; (b) Posterior division zone (DZ), elongation zone (EZ) and mature zone (MZ) probabilities; The uncertainty intervals for the DZ-EZ and EZ-MZ limits are in grey. (c) Posterior segmentation probabilities highlighting the difference between the 3rd segmentation and the optimal segmentation.

Supplementary Figure III-3. Outputs of the piecewise linear models in the case of a lateral root (wild-type A13) for which 4 zones were identified. (a) Optimal 3- and 4-zone piecewise linear functions and first root hair position; (b) Details of the piecewise linear functions in the division zone; (c) Posterior division zone 1st and 2nd segment (DZ1, DZ2), elongation zone (EZ) and mature zone (MZ) probabilities. The uncertainty intervals for the DZ1-DZ2, DZ2-EZ and EZ-MZ limits are in grey.

Supplementary Figure III-4. Relationships between the EZ-MZ limit and the first root hair position: The linear trends for wild type and mutants, respectively in blue and red, are computed excluding the six outlier individuals (wild-type A8, A9, A10, A11, A31 and *rum-1* A6).

Supplementary Table III-1. Split of the division zone for wild-type A13, B33 and B32. The parameters of the first two segments of the selected piecewise linear function (slope x 1000, correlation coefficient for each segment –n.s. for non-significant– and change-point positions in μm with associated uncertainty intervals) are given in the first row and the first two segments of the selected piecewise linear function with associated rootward and shootward confidence intervals at each limit between zones are given in the second row.

Supplementary Table III-2. Selection of the six 3-zone individuals the most inconsistent regarding the EZ-MZ limit: difference between the MZ slope and the EZ slope (x 1000), overlap between the confidence intervals of the EZ and MZ slopes, distance between the EZ-MZ limit and the first root hair position, numbers of cells between the EZ-MZ limit and the first root hair position and beyond the first root hair position.

Supplementary Methods III-1 – Statistical methods for heteroscedastic piecewise Gaussian linear models and Gaussian change in the variance models

Let θ denote the set of within-zone parameters (and global mean parameter for Gaussian change in the variance models). For heteroscedastic piecewise Gaussian linear models (M_{linear} models), $\theta = \{\alpha_0, \beta_0, \sigma_0^2, \ldots, \alpha_{J-1}, \beta_{J-1}, \sigma_{J-1}^2\}$ while for Gaussian change in the variance models (M_{variance} models), $\theta = \{\alpha, \sigma_0^2, \ldots, \sigma_{J-1}^2\}$. Let $f_J(\mathbf{s}, \mathbf{x}; \hat{\theta})$ denote the likelihood of the segmentation $\mathbf{s}$ in J developmental zones of the observed cell length series $\mathbf{x} = x_1, \ldots, x_T$. The estimation of the $J-1$ change points $\tau_1, \ldots, \tau_{J-1}$, which corresponds to the optimal segmentation $\mathbf{s}^*$ into J developmental zones, is obtained as follows

$$\hat{\tau}_1, \ldots, \hat{\tau}_{J-1} = \arg\max_{\mathbf{s}} \log f_J(\mathbf{s}, \mathbf{x}; \hat{\theta}),$$

with

$$\log f_J(\mathbf{s}, \mathbf{x}; \hat{\theta}) = -\sum_{j=0}^{J-1} \frac{\tau_{j+1} - \tau_j}{2} \left[\log\left\{ \frac{\sum_{t=\tau_j}^{\tau_{j+1}-1} (x_t - \hat{\alpha}_j - \hat{\beta}_j t)^2}{\tau_{j+1} - \tau_j} \right\} + \log(2\pi) + 1 \right] \quad \text{for } M_{\text{linear}} \text{ model,}$$

$$\log f_J(\mathbf{s}, \mathbf{x}; \hat{\theta}) = -\sum_{j=0}^{J-1} \frac{\tau_{j+1} - \tau_j}{2} \left[\log\left\{ \frac{\sum_{t=\tau_j}^{\tau_{j+1}-1} (x_t - \hat{\alpha})^2}{\tau_{j+1} - \tau_j} \right\} + \log(2\pi) + 1 \right] \quad \text{for } M_{\text{variance}} \text{ model.}$$

For this optimization task, the additivity in j of the maximized log-likelihoods for each zone, allows us to use a dynamic programming algorithm (Auger & Lawrence, 1989) whose computational complexity is $O(JT^2)$ in time.

Regarding the inference of multiple change-point models, one key question is to select the number of developmental zones. In a model selection context, the purpose is to estimate J by maximizing a penalized version of the log-likelihood defined as follows

$$\hat{J} = \arg\max_J \{\log f_J(\mathbf{x}) - \text{Penalty}(J)\}.,$$

where

$$f_J(\mathbf{x}) = \sum_{\mathbf{s}} f_J(\mathbf{s}, \mathbf{x}; \hat{\theta})$$

is the log-likelihood of all the possible segmentations in J developmental zones of the observed cell length series $\mathbf{x}$ of length T. The principle of this kind of penalized likelihood criterion consists in making a trade-off between an adequate fitting of the model to the data (expressed by the log-likelihood) and a reasonable number of parameters to be estimated (controlled by the penalty term). The most popular information criteria such as AIC and BIC are not adapted in this particular context since they tend to underpenalize the log-likelihood and thus select a too large number of developmental zones. We thus applied the slope heuristic (SH) given by (Guédon, 2015)

$$\mathrm{SH}_J = 2\left\{\log f_J(\mathbf{x}) - 2\hat{\kappa}\,\mathrm{pen}_{\mathrm{shape}}(J)\right\},$$

where

$$\mathrm{pen}_{\mathrm{shape}}(J) = \log\left\{\frac{L^{J-1}}{(J-1)!}\right\},$$

and $\hat{\kappa}$ is the slope of the linear relationship between $\log f_J(\mathbf{x})$ and $\mathrm{pen}_{\mathrm{shape}}(J)$ for overparameterized models estimated by the data-driven slope estimation method (Baudry *et al.*, 2012). The posterior probability of the J-developmental-zone model M_J, given by

$$P(M_J \mid \mathbf{x}) = \frac{\exp\left(\frac{1}{2}\mathrm{SH}_J\right)}{\sum_{k=1}^{J_{\max}} \exp\left(\frac{1}{2}\mathrm{SH}_K\right)},$$

can be used to assess the relative merits of the models considered.

The posterior probability of the optimal segmentation $\mathbf{s}^*$ given by

$$P(\mathbf{s}^* \mid \mathbf{x}; J) = f_J(\mathbf{s}^*, \mathbf{x}; \hat{\theta}) / \sum_{\mathbf{s}} f_J(\mathbf{s}, \mathbf{x}; \hat{\theta}),$$

can be efficiently computed by the smoothing algorithm proposed by Guédon (2013). The assessment of multiple change-point models thus relies on two posterior probabilities:

- posterior probability of the *J*-developmental-zone model M_J, $P(M_J \mid \mathbf{x})$ deduced from the slope heuristic computed for a collection of multiple change-point models for $J = 1,\ldots,J_{\max}$ i.e. weight of the *J*-developmental-zone model among all the possible models between 1 and $J_{\max}$ developmental zones,
- posterior probability of the optimal segmentation $\mathbf{s}^*$ for a fixed number of developmental zones J $P(\mathbf{s}^* \mid \mathbf{x}; J)$ i.e. weight of the optimal segmentation among all the possible segmentations for a fixed number of developmental zones.

It is often of interest to quantify the uncertainty concerning change-point position. To this end, we computed the posterior change-point probabilities for each change point *j* and each position *t* using the smoothing algorithm proposed by Guédon (2013). We define the α-uncertainty interval for change point *j* as the interval such that

$$\alpha/2 < \sum_{u=1}^{t} P(S_u = j, S_{u-1} = j-1 \mid \mathbf{x}; J) < 1-\alpha/2,$$

with $\sum_{u=1}^{\tau-1} P(S_u = j, S_{u-1} = j-1 \mid \mathbf{x}; J) = 1.$ If there is no overlap between uncertainty intervals for consecutive change points, this α-uncertainty interval for change point *j* can be equivalently defined as

$$\begin{cases} \alpha/2 < P(S_t = j-1 \mid \mathbf{x}; J) < 1-\alpha/2, \\ \alpha/2 < P(S_t = j \mid \mathbf{x}; J) < 1-\alpha/2. \end{cases}$$

where the posterior probability of being in zone *j* at position *t*, $P(S_t = j \mid \mathbf{x}; J)$ can also be computed for each position *t* and each zone *j* using the smoothing algorithm (Guédon, 2013). In this uncertainty interval, $P(S_t = j-1 \mid \mathbf{x}; J)$ is monotonically decreasing as a function of *t* while $P(S_t = j \mid \mathbf{x}; J)$ is monotonically increasing and $P(S_t = j \mid \mathbf{x}; J) = 1 - P(S_t = j-1 \mid \mathbf{x}; J)$; see illustrations in Figs 2b, 3b, 4b, 5b, S2b and S3c.

Other posterior probability profiles of interest can be obtained using the forward-backward dynamic programming algorithm (Guédon, 2013). Rather than summarizing all the possible segmentations as in the posterior zone probability profiles $\{P(S_t = j \mid \mathbf{x}; J);\ j = 1,\ldots,J; t = 1\ldots,L\}$, the idea here is to highlight structural differences between alternative segmentations and the optimal segmentation by computing

$$\left\{ \max_{s_1,\ldots,s_{t-1}} \max_{s_{t+1},\ldots,s_T} P(S_1 = s_1,\ldots,S_{t-1} = s_{t-1}, S_t = j, S_{t+1} = s_{t+1},\ldots,S_T = s_T \mid \mathbf{x}; J);\ j = 1,\ldots,J; t = 1\ldots,T \right\}$$

These posterior segmentation probability profiles are illustrated in Figs 4c, S1b and S2c.

Supplementary Figure III-1

Outputs of the piecewise linear models in the case of a lateral root (*rtcs* A2) for which the 2-zone model selected by the slope heuristic does not fit biological assumptions (lack of EZ). (a) Optimal 2- and 3-zone piecewise linear functions and first root hair position; (b) Posterior segmentation probabilities highlighting the prediction of a 2-zone model by the 6th segmentation in 3 zones.

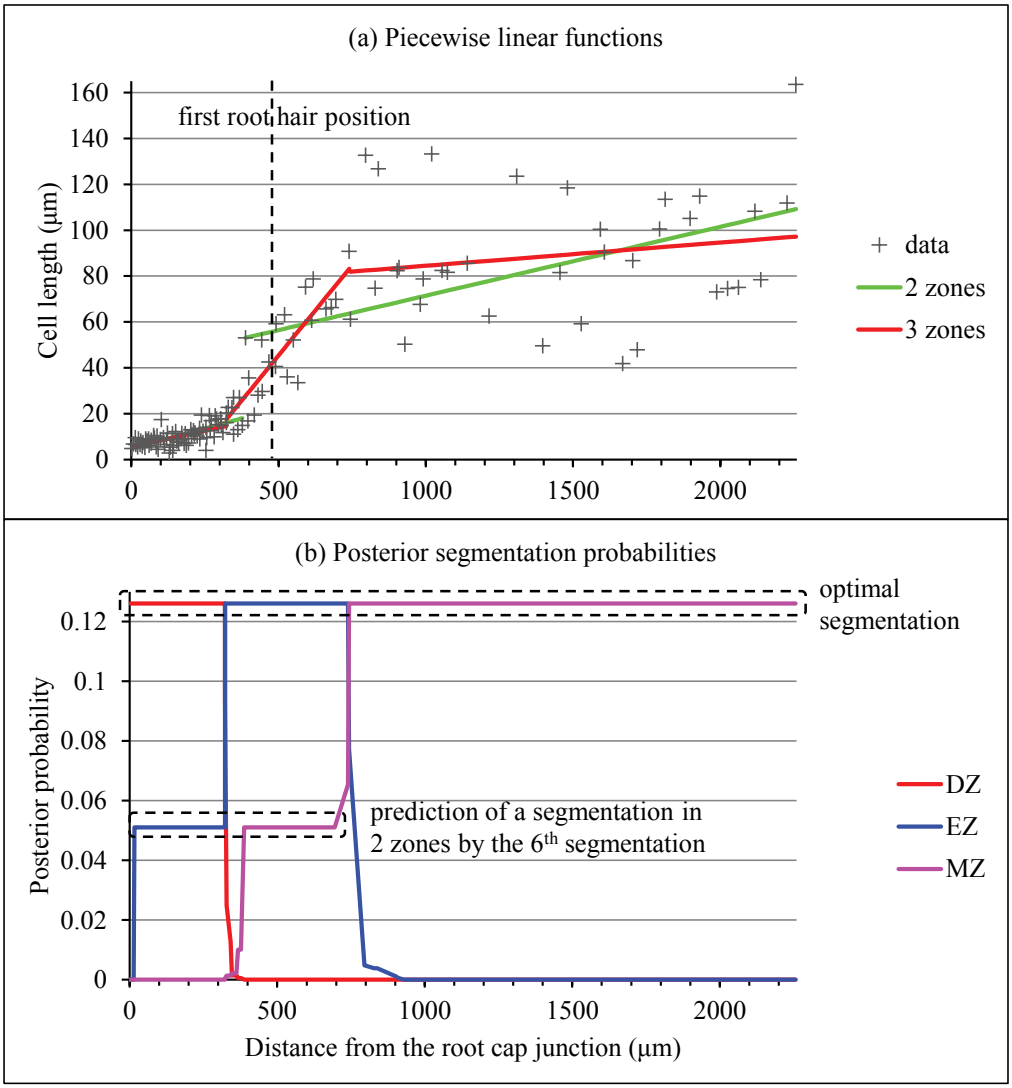

Supplementary Figure III-2

Outputs of the selected piecewise linear model in the case of a lateral root (rum-1 A'40) for which the optimal 2-zone piecewise linear function does not fit biological assumptions (piecewise linear function not approximately continuous). (a) Optimal 3-zone piecewise linear function, sub-optimal 3-zone piecewise linear function corresponding to the 3rd segmentation and first root hair position; (b) Posterior division zone (DZ), elongation zone (EZ) and mature zone (MZ) probabilities; The uncertainty intervals for the DZ-EZ and EZ-MZ limits are in grey. (c) Posterior segmentation probabilities highlighting the difference between the 3rd segmentation and the optimal segmentation.

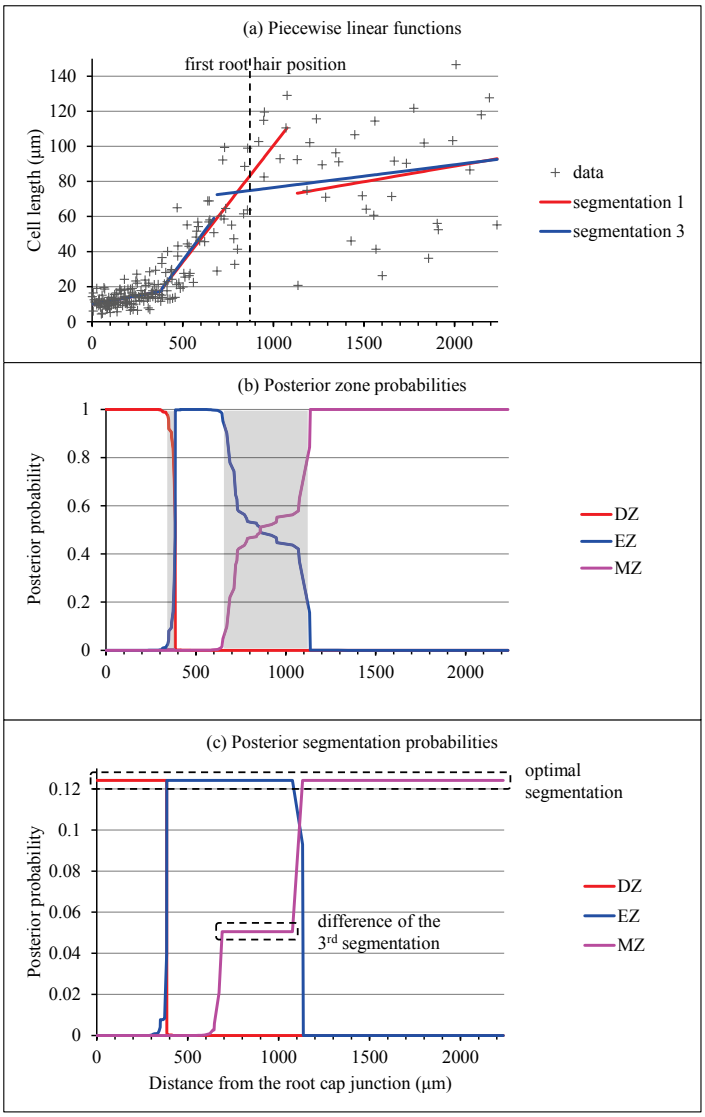

Supplementary Figure III-3

Outputs of the piecewise linear models in the case of a lateral root (wild-type A13) for which 4 zones were identified. (a) Optimal 3- and 4-zone piecewise linear functions and first root hair position; (b) Details of the piecewise linear functions in the division zone; (c) Posterior division zone 1st and 2nd segment (DZ1, DZ2), elongation zone (EZ) and mature zone (MZ) probabilities. The uncertainty intervals for the DZ1-DZ2, DZ2-EZ and EZ-MZ limits are in grey.

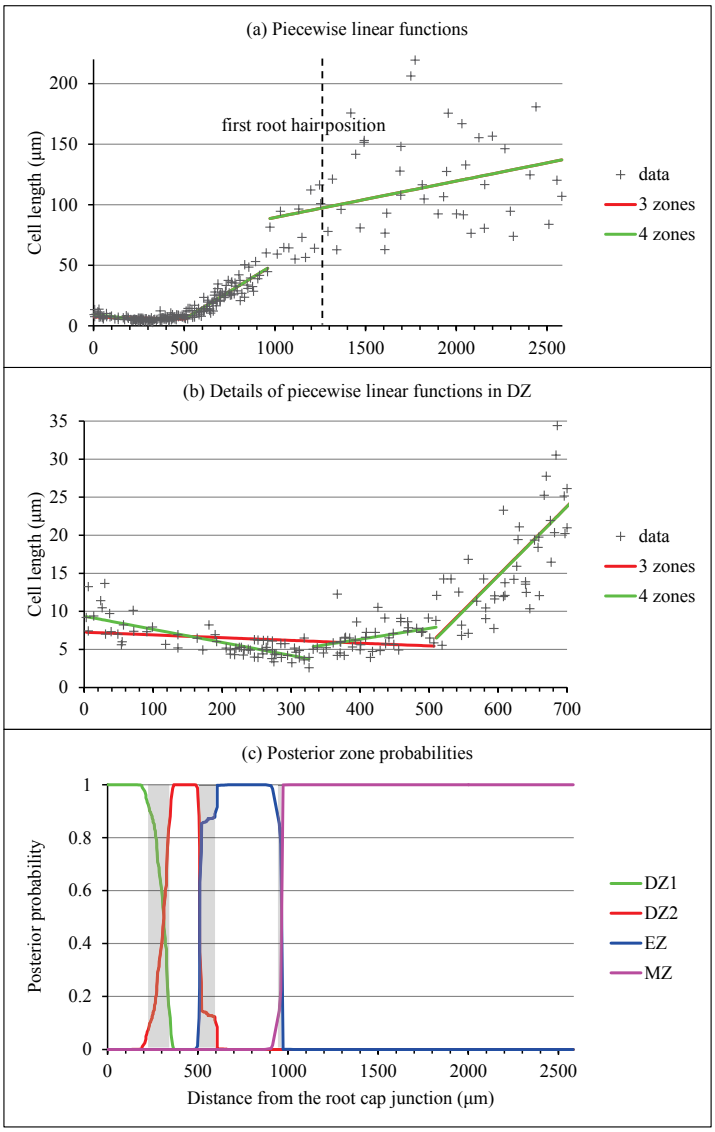

Supplementary Figure III-4

Relationships between the EZ-MZ limit and the first root hair position: The linear trends for wild type and mutants, respectively in blue and red, are computed excluding the six outlier individuals (wild-type A8, A9, A10, A11, A31 and *rum-1* A6).

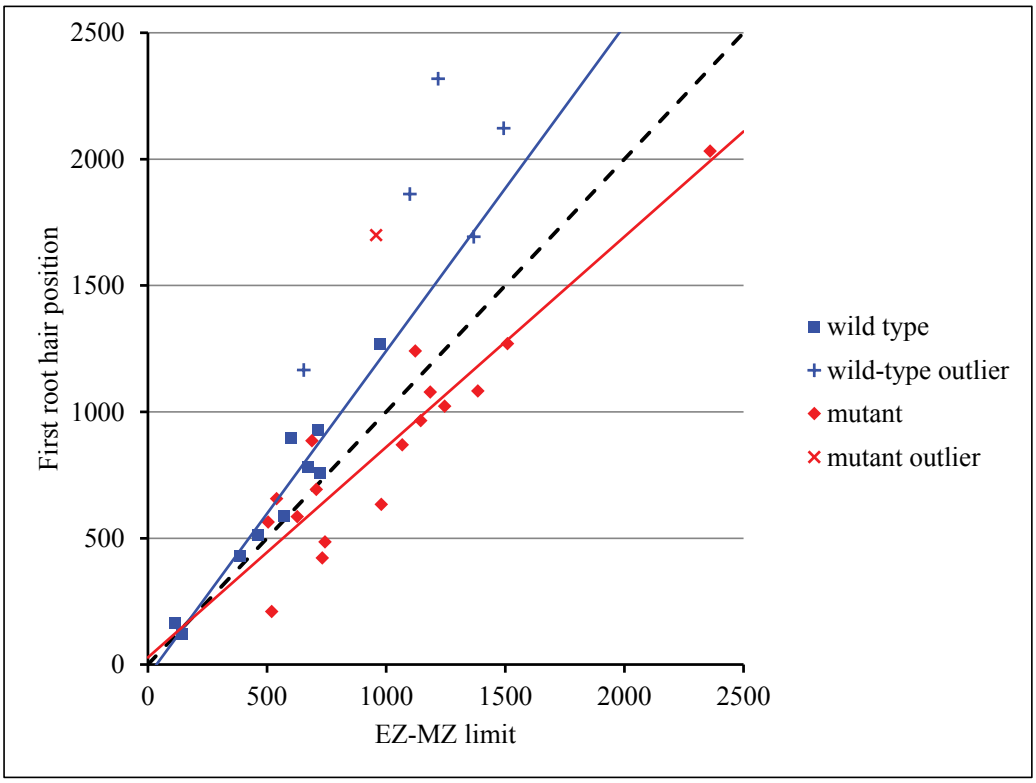

Supplementary Table III-1

Split of the division zone (DZ) for wild-type A13, B33 and B32. The parameters of the first two zones of the selected piecewise linear function (slope x 1000, correlation coefficient for each zone –n.s. for non-significant– and limits between zones in μm with associated 0.05-uncertainty intervals) are given in the first row and the first two zones of the selected piecewise linear function with associated rootward and shootward confidence intervals at each limit between zones are given in the second row.

	Division zone 1				Division zone 2			
	Slope	Correlation	s.d.	DZ1-DZ2 limit	Slope	Correlation	s.d.	DZ-EZ limit
	Linear function		Confidence intervals		Linear function		Confidence intervals	
A13	−17.2	−0.79	1.4	332 (212, 351)	14.3	0.4	1.7	511 (501, 608)
	9.3 → 3.7		(3.1, 4.2	| 4.3, 6.4)	5.4 → 7.9		(6.8, 9	| 3.8, 9.2)
B33	−35.4	−0.59	1.2	146 (131, 186)	13.3	0.67	1.2	439 (428, 439)
	9.3 → 6.2		(4.8, 7.6	| 3.6, 4.6)	4.1 → 8		(7.4, 8.6	| 4, 15.1)
B32	−41.3	−0.54	2.6	201 (139, 210)	6.2	0.24 n.s.	1	411 (340, 411)
	11.1 → 5		(3.6, 6.5	| 4.6, 5.9)	5.3 → 6.6		(5.6, 7.5	| 6.1, 13.8)

Supplementary Table III-2

Selection of the six 3-zone individuals the most inconsistent regarding the elongation zone (EZ)-mature zone (MZ) limit: difference between the MZ slope and the EZ slope (x 1000), overlap between the confidence intervals of the EZ and MZ slopes (in % of EZ slope confidence interval), distance between the EZ-MZ limit and the first root hair position, numbers of cells between the EZ-MZ limit and the first root hair position and beyond the first root hair position.

			Overlap between		Number of cells	
		MZ slope	EZ and MZ slope	First hair position	EZ-MZ limit	Beyond
Genotype	Root	− EZ slope	confidence intervals	− EZ-MZ limit	→ first hair position	first hair position
wild type	A8	−9.8	65.3	762	26	11
wild type	A9	0.7	100	1099	32	35
wild type	A10	−9.9	48.4	628	35	33
wild type	A11	−8.4	100	510	34	16
wild type	A31	15.4	45.7	324	25	45
rum-1	A6	30.6	72	742	24	7

Supplementary References

Auger IE, Lawrence CE. 1989. Algorithms for the optimal identification of segment neighborhoods. Bulletin of Mathematical Biology 51: 39-54.

Baudry J-P. Maugis C, Michel B. 2012. Slope heuristics: overview and implementation. Statistics and Computing 22(2): 455-470.

Guédon Y. 2013. Exploring the latent segmentation space for the assessment of multiple change-point models. Computational Statistics 28(6): 2641-2678.

Guédon Y. 2015. Slope heuristics for multiple change-point models. In: 30th International Workshop on Statistical Modelling (IWSM 2015). Friedl H, Wagner H. eds., vol. 2: 103-106.

CHAPTER IV. EXPLORING THE INTRINSIC ORIGIN OF GROWTH VARIATIONS IN MAIZE LATERAL ROOTS

The current chapter develops experimental approaches to investigate several factors that may be at the origin of instability in lateral root development. All results in this chapter essentially refer to the B73xUH007 genotype and arise from data obtained in the experiments previously described in section 2.1 of Chapter II. We present quantitative measures of the differences encountered among a representative population of lateral roots across several complementary scales:

1. *Early lateral root development (primordium stage);*
2. *Anatomical lateral root structure and how it changes along the root axis;*
3. *Cell length patterning within the growing zone of lateral roots;*
4. *Carbohydrate content and how it is distributed along lateral root apices;*
5. *Gene expression on lateral root apices, particularly of genes responding to auxin or carbohydrates availability.*

Key findings in this chapter will be discussed at the general discussion (Chapter V) providing an integrated view of lateral root development and its variations.

1 Methods

1.1 Observation of lateral root *primordia*

We used a destructive method to visualize lateral root *primordia* including a clearing step followed by an apex-specific staining using Schiff reagent (Fisher Chemical) according to (Bingham I. J., 1998). The apical unbranched zone of individual primary roots (n=4) was harvested and sliced into successive (typically four) 5 cm long segments. Root segments were fixed overnight in a 3:1 v/v 70 % ethanol: acetic acid solution, at 2°C. The material was then hydrolysed in 5 M HCl for 10 minutes at room temperature, stained using Schiff reagent for 20 min, rinsed under tap water for approximately 1 min then rinsed in sterile water for 10 min. Roots were then placed on a microscope slide and digitized using a scanner (EPSON scan Perfection) at 1200 DPI. All the scans corresponding to the same root were aligned to reconstruct the entire unbranched zone (**Figure IV-1**). Finally, the basal diameter and position of each visible lateral organ (lateral root *primordium* or emerged lateral root) were measured using ImageJ software (Rasband WS. U.S. National Institutes of Health, Bethesda, MD, USA).

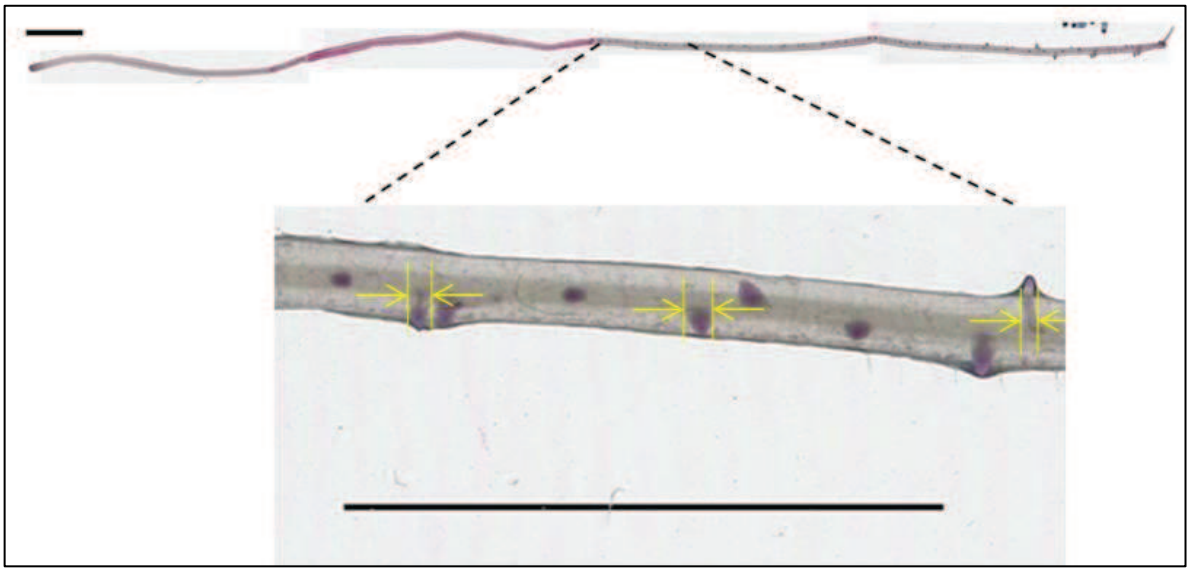

Figure IV-1. Illustration of the rootward 20 cm segment of a maize primary root after Schiff staining. Note the (pink) apex-specific staining and the diversity of lateral root *primordia* basal diameters (yellow bars on the lower image). Scale-bars: 1 cm.

1.2 Root anatomy

1.2.1 Plant material

Lateral roots with contrasted root length were sampled in B73xUH007 plants from the BMSP experiment (see section **2.1.1** of Chapter II). To limit root age differences between sampled lateral roots, we restricted sampling to roots located between 10 and 20 cm from the collet. A total of 22 lateral roots originating from 3 different plants were then imaged using a high resolution scan (EPSON scan Perfection) at 1200 DPI and their length measured. Each of the sampled roots was assigned to an expert growth class ("fast-growing", "slow-growing" or "early-arrested" root) as described in section **1.4** of this Chapter**.** The individual growth profiles associated to each sampled root were obtained by measuring the daily root increments traced by hand on rhizotron slides.

1.2.2 Root cross-sectioning

Sampled lateral roots were fixed overnight in a 1:9 v/v acetic acid/ethanol solution, and further stored in 70% ethanol. From the apex, two 8 mm-long segments (0-8 mm *apical* and 8-16 mm *subapical* segments, respectively) were cut with the help of a millimeter paper as well as one segment at the level of the root base (or *basal* segment). For short roots (< 8 mm), a single segment was taken. This single segment was considered both basal and apical; basal since it was composed of tissue similar in age to the basal segment of long roots, and apical

owing to its proximity to the root apex. Root segments were then gently dried on a filter paper and imbibed in a hot (30-45°C) liquid 3% w/v agarose solution (SeaKem GTG Agarose, Lonza). Fifty-five µm thick sections were obtained from solidified agarose blocks using a vibratome (Microm HM 650V, Thermo Scientific, speed 30, frequency 60). Individual root sections were then collected with a toothpick, transferred to microscope slides and covered with a coverslip for direct observation.

1.2.3 Image acquisition and processing

Root section images were taken using a microscope (Leica DMRB) equipped with an epifluorescence filter (excitation range: UV; observation filter: 460-480 nm). Two pictures were taken for each root section: one under visible light using Nomarsky optics and another using epifluorescence, which takes advantage of the autofluorescence of lignin deposits in cell walls (**Figure IV-2**). Images were taken using a color Retiga SRV FAST 1394 camera running the QCapture Pro7 image acquisition software. The RGB images were opened in ImageJ using the Bioformats importer plugin and transformed into gray level 8-bit images. A scale-bar was added to the images according to their magnification.

1.2.4 Root measurements

The following anatomical traits, abbreviated as shown in the brackets, were manually measured on each root section:

- Root diameter (D) and stele diameter (D_{ST}), defined as the distance between the internal wall of the endodermal cells (**Figure IV-3A**).
- Number of xylem poles (N_{XP}) and xylem vessels (N_{XV}) inside these poles. Xylem elements could easily be distinguished by their strong auto-fluorescence under UV light. In the case of the presence of a central pith (displaying no autofluorescence) , its diameter was measured (D_P) (**Figure IV-3B**).

Since the shape of root cross-sections was often elliptic rather than circular, at least two measurements of D, D_{ST} and D_P were made for each section, and an average value was computed.

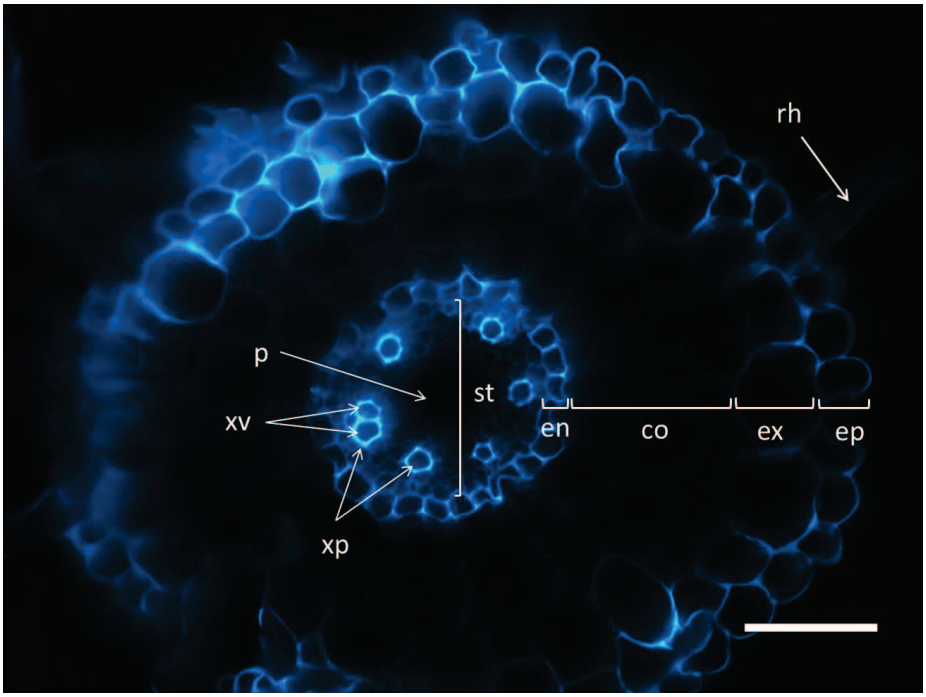

Figure IV-2. Illustration of maize lateral root tissues in an autofluorescence cross-section image. The root tissues, from periphery to the center, are: the epidermis (ep) showing root hair (rh) differentiation; the exodermis (ex); cortex (co) and endodermis (en). The area inside the endodermis corresponds to the stele (st) containing the vascular vessels: the xylem vessels (xv) organized in xylem poles (xp) and the central pith (p). Scale-bar: 100 µm.

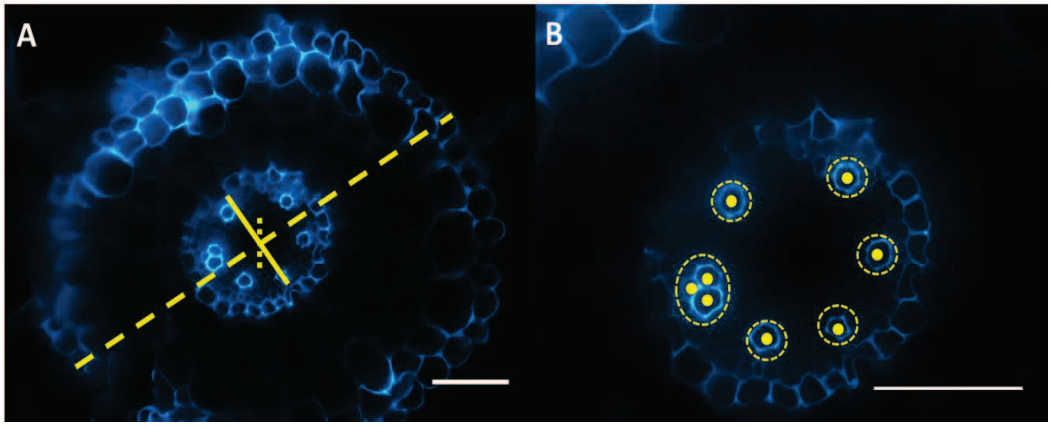

Figure IV-3. Illustration of root anatomical traits measured from root cross-section images. (**A**) The diameters of the root (dashed line), the root stele (filled line) and the root central pith (pointed line) were measured in each cross-section. (**B**) The number of xylem poles (dashed circles) and the number of individual mature xylem vessels (filled circles), 6 and 9 respectively in the example, wer also recorded. Note the lack of auto fluorescence of the root central pith. Scale-bars: 100 µm.

1.3 Epidermal cell length profiles

The extraction of epidermal cell length profiles from cleared root samples was done according to the protocol previously described in **Chapter III**.

1.4 Expert labelling of lateral roots: the A-B-C classification

Protocols used for quantification of sugar content and gene expression in lateral root apices (see **sections 1.5** and **1.6**) required samples with a fresh weight in the range of 10-100 mg. Since the fresh weight of a secondary root tip of 1 cm long rarely reaches 1 mg[1], we needed to pool tens of root tips to constitute a single sample. Moreover, for an efficient root sampling, simple visual (static) criteria had to be established about how the roots should be pooled, avoiding time-loss and technical problems like root drying or RNA degradation once the rhizotron was disarmed for sampling. To address these constraints, we decided to establish an *expert classification of lateral roots* aiming at grouping lateral roots with similar growth profiles.

For the identification of relevant classification criteria and the selection of the number of root classes, we followed root growth in a small number of lateral roots by tracing daily length increments with colored pens on a transparent plastic sheet placed upon the front panel of the rhizotrons. Growth profiles obtained in such a way revealed marked differences both in the initial growth rates and their change with root age (**Figure IV-4A**). However, *qualitatively*, three main growth patterns could be identified: Short roots with short growth duration (about 2 d), long roots with high initial growth rates maintained during a long period (sometimes more than a week), and intermediary roots with high initial growth rates and low growth rates at later stages (**Figure IV-4B**). In addition, lateral roots having similar growth patterns often presented typical profiles of root hair development, with distant root hair differentiation for fast growing roots and much closer hair differentiation for slow growing roots (**Figure IV-4C**).

Based on these observations, we grouped lateral roots into three classes according to two criteria: (i) the *local differences in root length*, likely reflecting mean growth rate differences between neighbouring, close enough roots; and (ii) the *distance between the root hair differentiation* and the root apex, related to the current growth rate of the root at harvesting time. Lateral root classes were defined as follows:

[1] Assuming root density is equal to water density, the theoretical fresh weight of a 1 cm long and 300 µm width lateral root apex is equal to 0.7 mg.

- A first class, designated “fast-growing” or “A” roots, corresponding to long roots, compared to neighbouring roots, showing root hair differentiation distant from the apex,
- A second class, designated “slow-growing” or “B” roots, corresponding to roots with intermediate length, showing root hair differentiation close to the root tip,
- A last class, designated “arrested” or “C” roots, corresponding to very short roots (usually < 1cm), with or without visible root hairs.

We assumed that the so-called A-B-C classification was a good way to cover the whole range of growth behaviours. This expert classification was used each time we needed to harvest lateral root samples for molecular or biochemical analysis. An example of the result of this classification for one maize root system is given in **Figure IV-5**. Roots located near the rootward end of the branching zone were discarded as root length differences were less marked than in older roots, therefore making their assignment to a class less obvious.

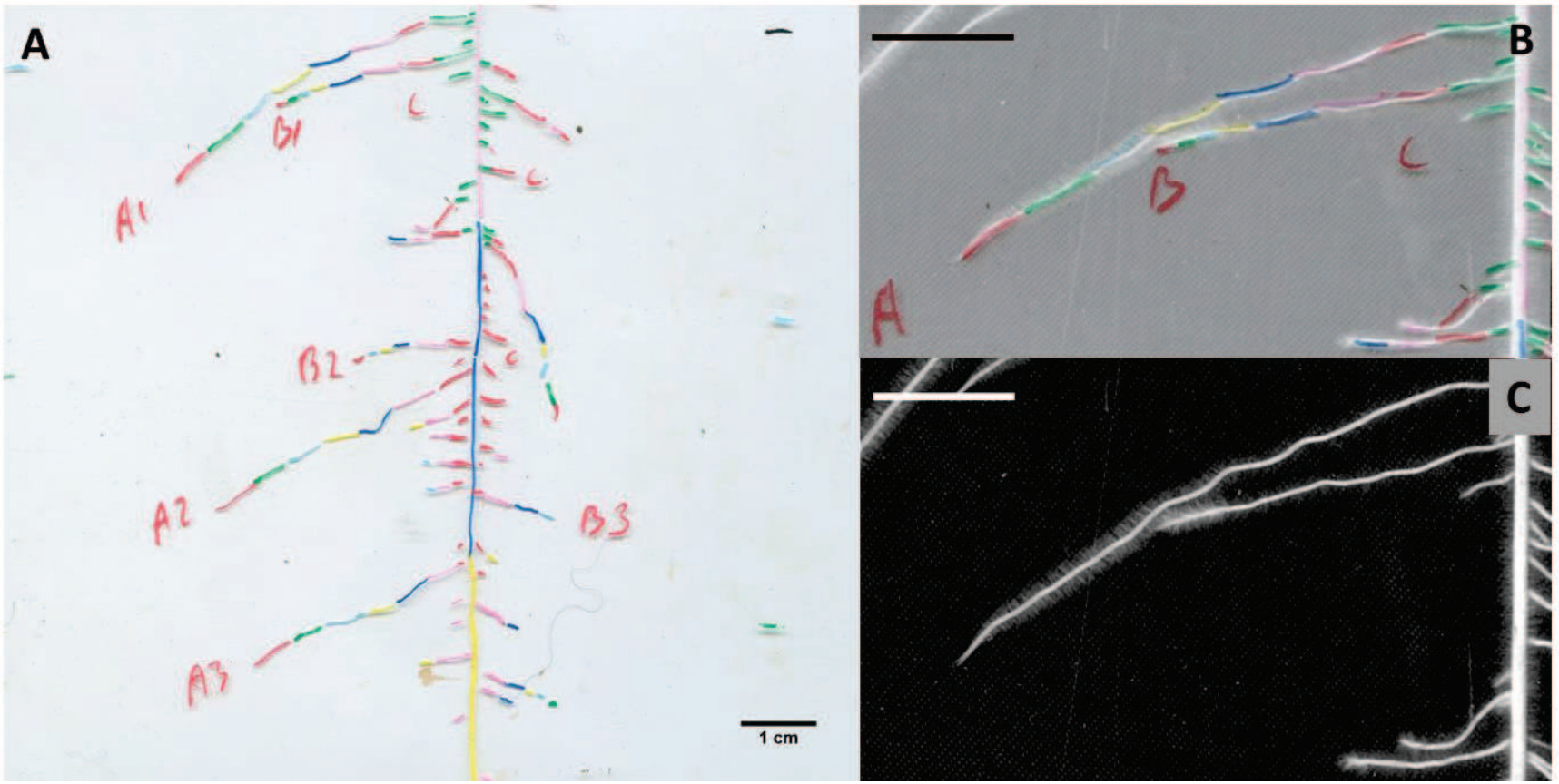

Figure IV-4. Expert identification of main qualitative root growth patterns. (**A-B**) Manual root drawings showing daily root length increments in different colours. Roots annotated "A" grow at a high, apparently constant growth rate during a long period, roots annotated "B" present a gradual decrease in growth rate during the last days of growth, and roots annotated "C" stop their growth soon after emergence (1- 2d). (**C**) Corresponding scanned images showing typical root hair profiles associated with each root type. For the "A" type, root hair development starts at some distance from the root tip, while "B" root presents a much closer differentiation of root hairs. "C" roots do not always present visible root hairs to the naked eye. Scale-bars: 1 cm.

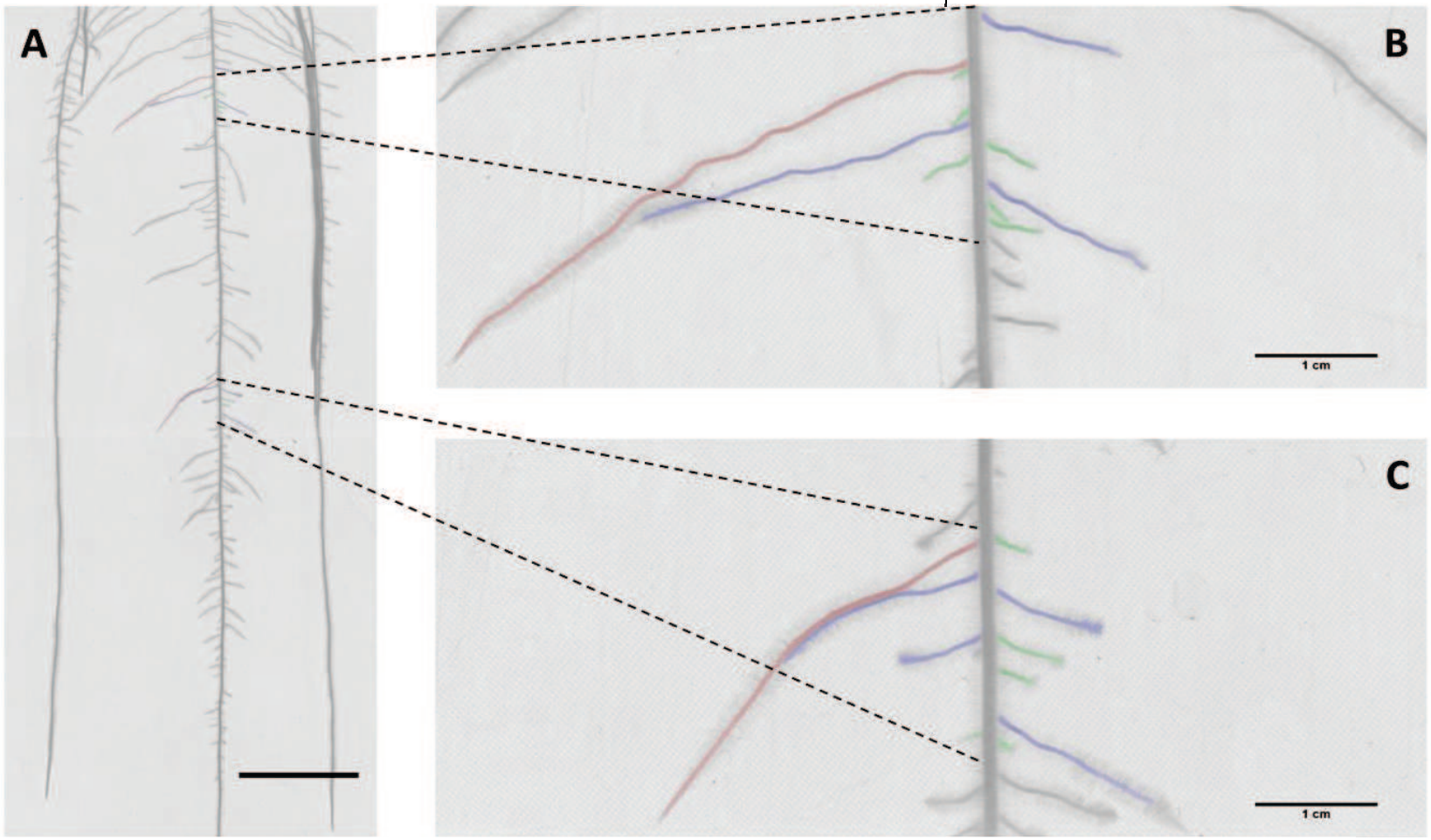

Figure IV-5. Illustration of the A-B-C classification of lateral roots along the primary root of maize. (**A**) Root system of a 15d-old maize plant bearing lateral roots of different lengths. Note that the maximal root length depends on root position along the primary root. (**B**) Sample of 10 relatively old (8d after emergence) lateral roots showing marked differences in length, annotated A (red), B (blue) or C (green). (**C**) Sample of 10 relatively young (4d after emergence) lateral roots showing less marked differences in length, annotated A, B, or C as in (B).

1.5 Sugar content

1.5.1 Root sampling

Two types of root samples were constituted to evaluate the sugar content in root tips (**Figure IV-6**). A*pical samples*, contained pooled root tips (8-10 mm) of the same expert root class (see section **1.4**). *Longitudinal samples*, contained pools of 3 mm lateral root segments from the apex up to 30 mm in the shootward direction. The number of pooled roots depended on the sample type but in all cases aimed at reaching 10 mg per sample, thus ~ 10 lateral roots for *apical samples* and 30 lateral roots for *longitudinal samples*.

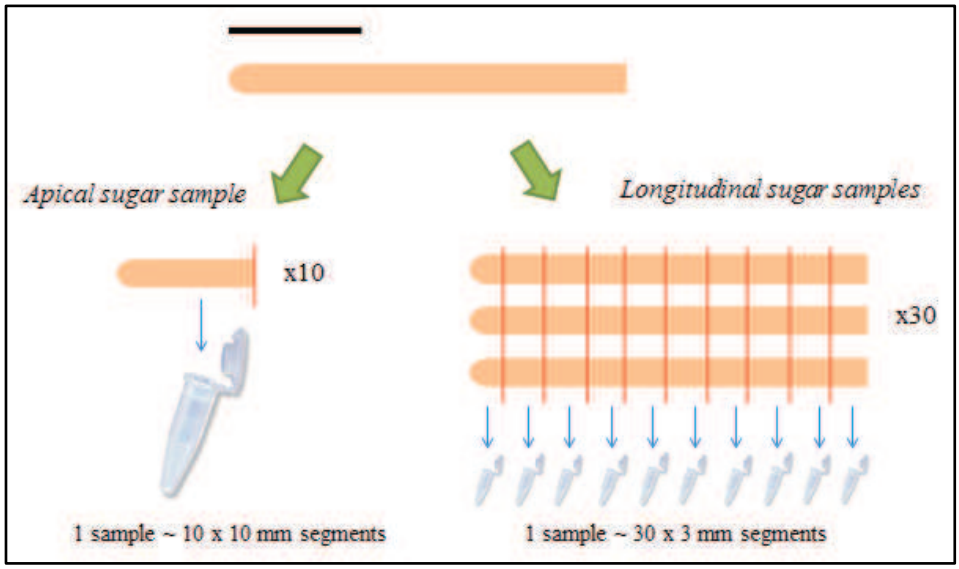

Figure IV-6. Schema describing the two types of samples collected for sugar analysis. Left: Pooling of roots for apical samples. One sample contained about ten pooled 10 mm root apical segments. Right: Pooling of roots for longitudinal samples. One sample contained about thirty pooled 3 mm root segments. Indicative scale-bar: 10 mm.

1.5.2 Sugar content quantification

Sugar content was measured using spectrophotometric analysis of the soluble fraction of ethanol-water extracts as described by (Cross *et al.*, 2006). In all cases, the sucrose content was very close to the detection limit and was thus omitted. Fructose was present, at lower concentration than glucose and most often in a 1:2 proportion of glucose. In the results, we only considered glucose for simplicity and because its measurement was more accurate.

1.6 Gene expression

1.6.1 Total RNA extraction

Apical (8-10 mm long) lateral root samples from each expert class (see **1.4** section) were pooled (~ 10 mg FW) and stored under -80°C. Pooled roots were then ground in liquid nitrogen and RNA was extracted using TRIzol reagent (ThermoFisher) using a modified protocol, and purified using RNase-Free DNase Set (Qiagen) according to the manufacturer's protocol.

1.6.2 Quantitative real-time PCR (qRT-PCR) analysis

Quantitative real-time PCR was performed in a LightCycler 480 (Roche) using the gene-specific oligonucleotides specified in **Table IV-1**. The cDNA for qRT-PCR analysis was synthesized from 1 µg total RNA using Moloney murine leukemia virus reverse transcriptase (Promega) and oligo(dT)15 (Promega) primers. Each qRT-PCR reaction contained 1 µl cDNA sample and 9 µl LightCycler 480 SYBR Green I master kit for PCR (Roche). PCR conditions were as follows: 10 min at 95°C followed by 45 cycles of 5 s at 95°C, 7 s at 65°C, and 8 s at 72°C; the melting curve cycle was 10 s at 95°C, 30 s at 73°C, 0.11°C s-1 increase to 95°C, and then 10 s at 40°C. The primer efficiency of each pair of oligonucleotides was calculated using the following dilution series: 1/5, 1/10, 1/20 and 1/100. The relative expression levels of the transcripts were calculated with reference to the housekeeping gene eukaryotic initiation factor 4 (ZmEIF-4).

Table IV-1 List of oligonucleotide primers used for qRT-PCR experiments and their corresponding PCR efficiency.

Primer name	Sequence (5'→3')	Efficiency
ZmGADPH-F	AGATCGGAATCAACGGCTTC	2.08
ZmGADPH-R	GTACGGTCATGTAGTCCGTGGTGA	
ZmEIF4-F	ACCACCGACCTGCTTGCTCGT	1.92
ZmEIF4-R	GATGTCGAACAGCATCCGCTCG	
ZmCYCA1 -F	CGAGCAGCAGATCATGGAAG	2.05
ZmCYCA1-R	GCGAACTCAACCAAATCCCT	
ZmEXPB4-F	ATGTCCTTCTTCCCTCCCTG	2.03
ZmEXPB4-R	CAACGGGCATGCTTTGTAGT	
ZmIAA4-F	CTGCTTGTAAAAAGTCCCGAGT	1.88
ZmIAA4-R	TATGCCCCAAAACAGAGACC	
ZmIAA17-F	ATCAAGGCAATAGTTTGGTGGT	2.00
ZmIAA17-R	CACATCGGCAAATCTCCAA	
ZmASN1-F	GCCTCTGCTGATCCTGTCTC	2.01
ZmASN1-R	GAAGCACAAGCATGTCTCCA	
ZmIVR2-F	ACCGCAACAAATTTTCCAAC	1.88
ZmIVR2-R	ATTTGCATTGGTGTGGTGTG	
ZmSUS1-F	TGCTGCTCTTTGCTTCAAGA	2.01
ZmSUS1-R	CAACATCCCATCCAGGAAAC	

2 Results of multi-scale analysis

2.1 Early lateral root development: analysis of the variations in lateral root *primordium* development

2.1.1 Longitudinal development of lateral root *primordia*

Development of lateral root *primordia* was observed on cleared primary root segments of 15-d plants imaged after Schiff staining (see section **1.1** for a detailed description of methods). The position of each detectable *primordium* and lateral root within the rootward 20 cm of the primary root was recorded. To describe more accurately the development of lateral root *primordia*, the primary root was divided into three zones (**Figure IV-8**). Zone 1 was defined as the root segment from the root tip to the youngest *primordium* detected (closest to the root tip). This zone is supposed to contain the *primordia* at stages under the limit of detection of our method. Zone 2 extended from the youngest visible lateral root *primordium* to the most rootward emerged lateral root (usually around 0.4 mm long). Zone 3 was defined as the root segment shootward from the first emerged lateral root. This zone was considered a part of the branched zone) containing all emerged lateral roots. In contrast, zones 1 and 2, containing exclusively non-emerged *primordia*, actually correspond to the unbranched zone).

In order to estimate the development of *primordia* in terms of change in size, from their initiation to their emergence, we looked at the profile of *primordium* basal diameters within zone 2 (**Figure IV-7**). Since we did not perform any temporal tracking of lateral root *primordium* development, it is mostly a conjectural analysis, but it seems reasonable to assume that spatial trends contain some information on the developmental history of lateral root *primordia*. From preliminary observations, the basal diameter appeared to increase linearly with the distance to root tip, which was well confirmed by the linear regressions estimated separately on each plant (**Table IV-2**). The only exception was plant C1 for which the R^2 was particularly low. This plant presented a 90° bend at the root extremity. We thus chose to discard this plant for further analyses. Average rate of diameter increase with distance was 14 µm cm^{-1} (n=3). The linear model could account for 50% of total variance only (R^2 ranging from 0.42 to 0.5), in accordance with a high dispersion of lateral root *primordia* diameters within this zone.

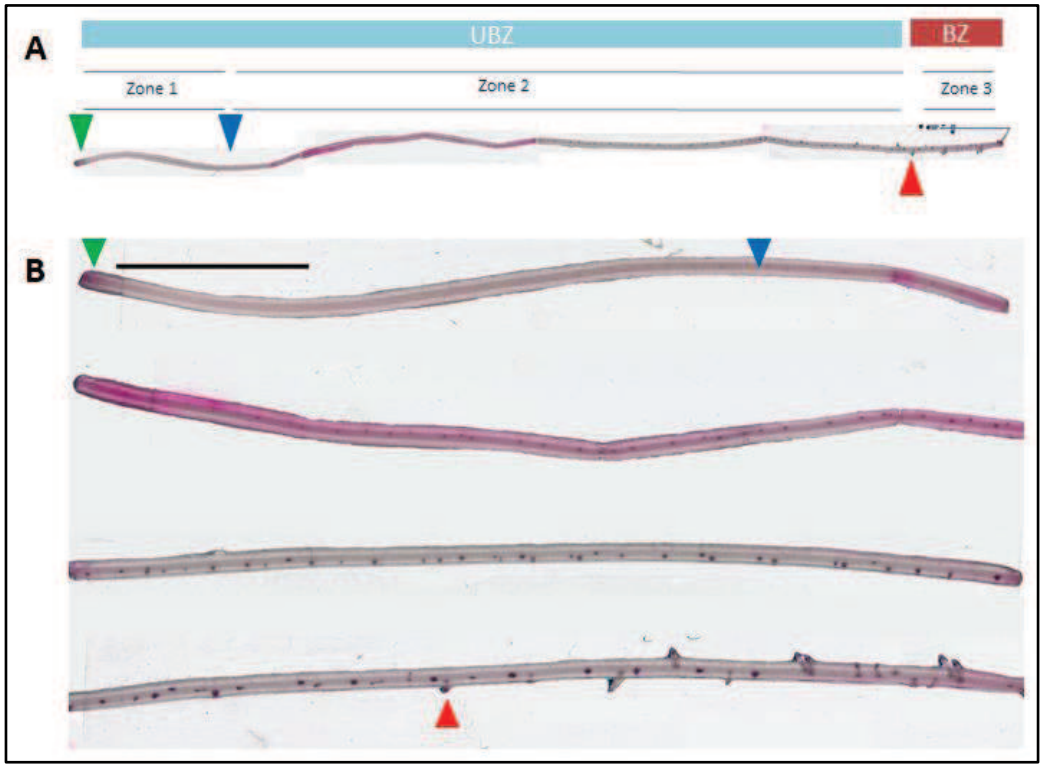

Figure IV-8. Zones defined along the rootward 20 cm region of the maize primary root for the analysis of LRP development. (**A**) Zone 1 extends from the primary root tip (green arrowhead) to the to the youngest *primordium* detected (blue arrowhead). Zone 2 extends from this point to the earliest emerged lateral root imaged visible in imaged roots (red arrowhead). Both Zone 1 and 2 form the unbranched zone (UBZ) of the root. Zone 3 situates shootward to the first emerged lateral root, considered a part of the branched zone (BZ). Note the presence of a mix of lateral root *primordia* and LRs within this zone. (**B**) Zoom on each of the 5-cm segments used to build the composite image in A. Scale-bar: 1 cm.

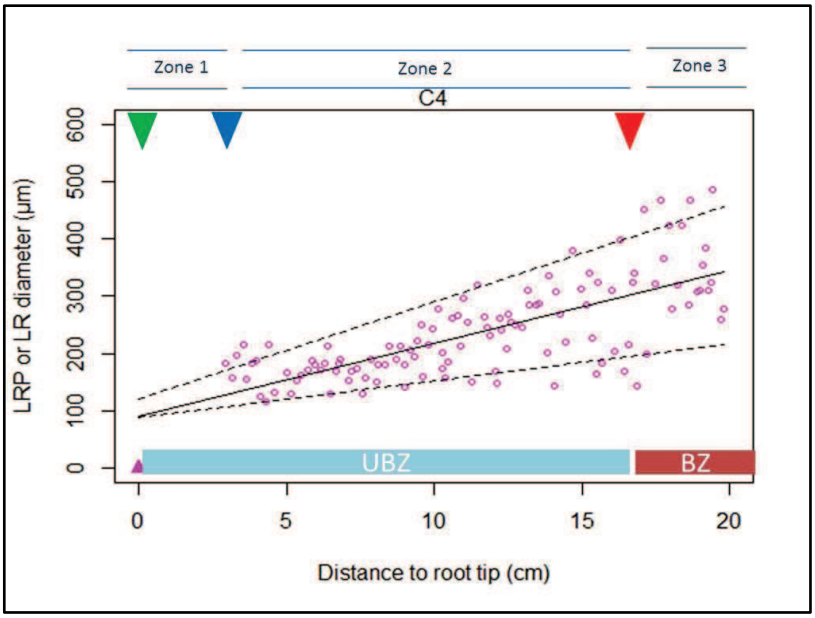

Figure IV-7. Longitudinal profile of basal diameters of lateral roots *primordia* (LRPs) and emerged lateral roots (LRs) along the rootward 20 cm of the primary root in a control plant (C4). Lines indicate the 50% (solid), 10% (dashed bottomost) and 90% (dashed uppermost) quantile; estimated by the linear quantile regression method. Zones are the ones defined in Figure IV-8.

We used these linear models to extrapolate the behaviour of a canonical lateral root *primordium* from its early initiation (considered to occur nearly at the root apex (Dubrovsky *et al*., 2000, 2006) to its emergence and exit of the zone of lateral root *primordium* development. Considering the average intercept of linear models, the size of a *primordium* at its initiation is predicted to be 88 µm. The earliest emerged lateral root in wild-type plants was found at an average distance of 13.22 cm from the root tip, which we can consider to be the average unbranched zone length . At this distance, the predicted diameter value for an emerging *primordium* was 271 µm. Based on the average unbranched zone length and on the average rate of root growth between days 14 and 15 (4 cm day^{-1}), the residence time of an average lateral root *primordium* would be approximately 3.3 days. The canonical developmental profile of a primodium in our growing conditions would then consist of a gradual 3-fold increase in diameter from its initiation at the root tip to its emergence a bit more than 3 days later.

However, this is just a simplistic view as it clearly exists a high degree of individual variability in the development of lateral root *primordia*. Indeed, if we look at the spread of diameter values for a given plant, as the one shown in **Figure IV-7**, it suggests) marked differences in the rate of development among individual *primordia*. In order to estimate the lower and higher rates of lateral root *primordia* development, we applied the quantile regression method to the lateral root *primordium* basal diameter as a function of the distance to the root tip (package 'quantreg' in R software (Koenker, 2015)), using respectively the 0.1 and 0.9 quantiles (**Table IV-2**). We found respective quantile slopes of 7.82 and 18.82 µm cm^{-1} and a median slope (0.5 quantile) of 10.46 µm cm^{-1}. The 0.1-quantile regression line (44% inferior to the median rate) suggests that there exists slowly developing lateral root *primordia* while other fast growing lateral root *primordia* could well develop following the upper trend (30% greater to the median rate). Another clue conforting this view comes from the qualitative comparison of the distribution of organ diameters in Zones 2 and 3 (**Figure IV-9**), showing a shift towards higher diameter values in zone 3 relatively to zone 2, while the minimal values tend to remain the same. This suggests that the variations in basal diameters of lateral root *primordia* increase with time. In summary, our findings highlight that differences in lateral root development can already be observed since the early steps of their history, more precisely, at the *primordium* stage.

Table IV-2. Ouput of quantile regressions of basal diameters vs. distance to root tip within Zone 2 and Zones 2 and 3 performed separately in 4 control plants (C1,C2, C3 and C4). Intercepts are expressed in µm, slopes in µm cm^{-1}, regression coefficients (R^2) are adimensional. The positions of the earliest lateral root *primordium* (LRP) and earliest emerged lateral root (LR) used for the delimitation of these zones are also given (in cm). Zones are the ones defined in Figure IV-8.

Plant	Zone 2				Zones 2+3		
	Earliest LRP position	Earliest lateral root position	Intercept	Slope (R^2)	Slope	Slope using the lowest 10%	Slope using the upper 10%
C1	1.75	10.87	159	7.49 (0.11*)	-	-	-
C2	2.38	11.25	87	13.28 (0.47)	15.60	8.63	18.54
C3	4.95	12.91	65	18.01 (0.51)	16.87	11.37	23.33
C4	2.94	15.50	111	10.47 (0.42)	12.33	5.45	16.85

Table IV-3. Summary of some characteristics of the distribution of lateral organs per zone. Provided values are median and absolute range (minimum-maximum). Lateral organs can be either lateral root *primordia* (LRPs) or lateral roots (LRs). Zones are the ones defined in Figure IV-8.

Parameter	Schiff Zone 2 only LRPs	Schiff Zone 3 LRPs and LRs	SmartRoot only LRs
Organ diameter (µm)	195 (79-380)	341 (149-565)	399 (295-536)
Inter-lateral organ distance (mm)	1.43 (0.28-4.24)	1.43 (0.0-4.19)	1.52 (0.05-7.73)
Average organ density* (cm-1)	6.7	7.0	6.7
No. of organs / No. of plants	198/3	131/3	1005/3

(*) Average organ density was calculated as the inverse of the average inter-lateral organ distance.

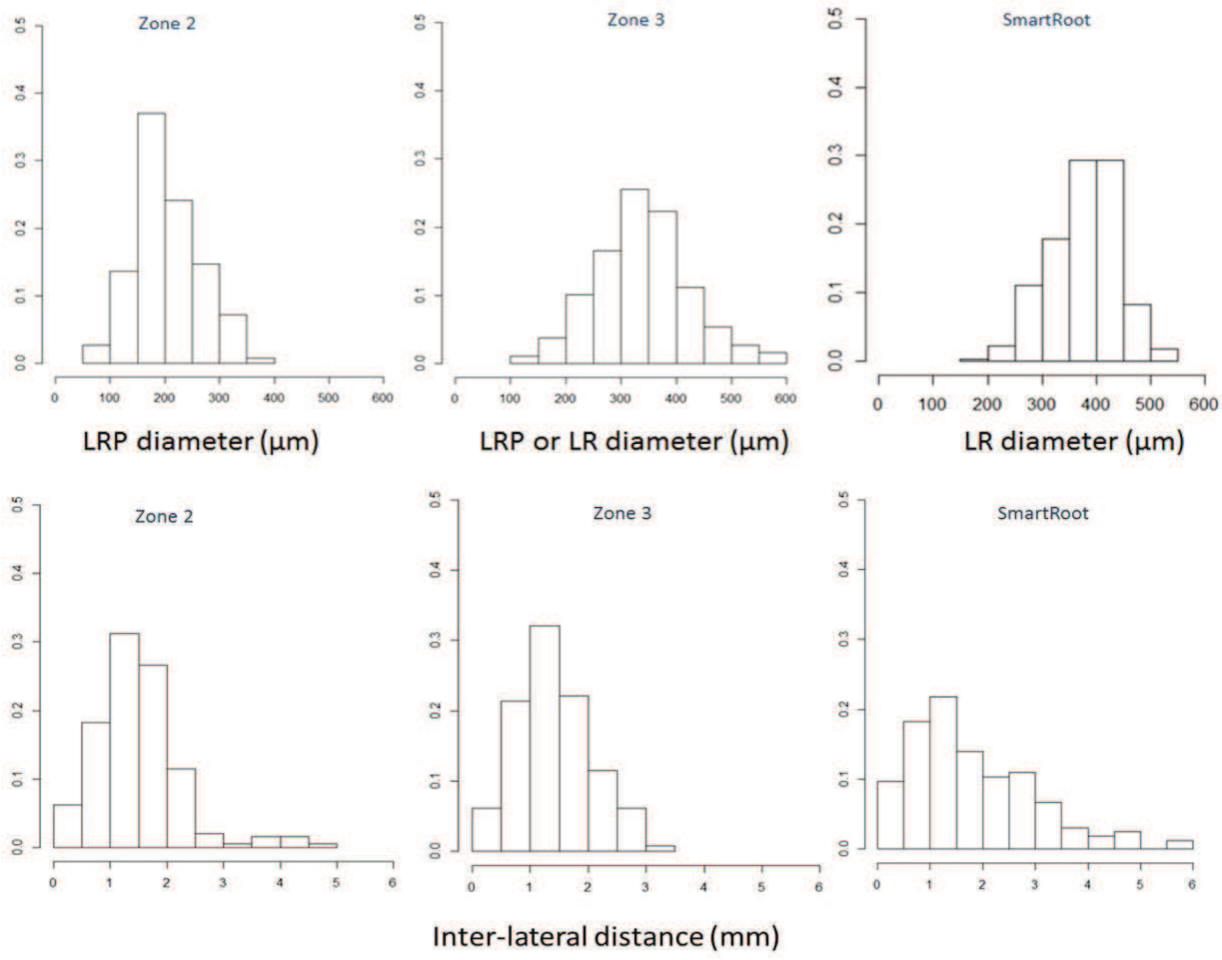

Figure IV-9. Organ diameter distribution (**A-C**) and inter-lateral organ distance distribution (**D-E**) within the Zone 1(**A, D**), Zone 2 (**B, E**) and SmartRoot region containing lateral roots (**C**, **E**). For each plot, we used data from the same maize seedlings (n=3). Lateral organs can be either lateral root *primordia* (LRPs) or lateral roots (LRs). Zones are the ones defined in Figure IV-8.

2.1.2 Longitudinal window for the initiation of lateral root *primordia*

In order to determine whether spatial rules dictate where a *primordium* is initiated, we examined the longitudinal spacing between successive lateral organs (either *primordia* or emerged roots). This inter-lateral organ distance was computed as the distance of a given organ relative to the one previously initiated (located immediately shootward). A summary of the distributions of inter-lateral organ distance within zones 2 and 3 is given in **Table IV-3**.

Overall, inter-lateral organ distance distributions were very similar for zones 2 and 3. The fact that lateral root *primordium* density did not increase with distance to root tip indirectly indicates that no new initiation events occurs between these zones and that most observed

lateral organs were initiated before zone 2, most probably zone 1. The width of the lateral root initiation window was therefore relatively restricted (at most 3 cm estimated from our data).

2.1.3 Relationship between inter-lateral organ distance and lateral root primordium development

Inter-lateral organ distance was very variable. The overall distribution was right-skewed to the, as indicated by the significant coefficient of skewness for *primordia* distances within Zone 2 (value=1.3, $p<0.001$, computed using the 'moments' R package (Komsta and Novomestky, 2015)). This distribution thus indicated that smaller distances were found more frequently than larger distances.

That led us to wonder whether such marked variations in lateral organ spacing could influence the rate of lateral root *primordium* development. Examining the relationship between the inter-lateral organ distance and lateral root *primordium* diameter, no clear patterns were revealed (**Figure IV-10**). We therefore had to stick to the hypothesis that the initiation and development of lateral root *primordia* are two processes regulated independently in the root.

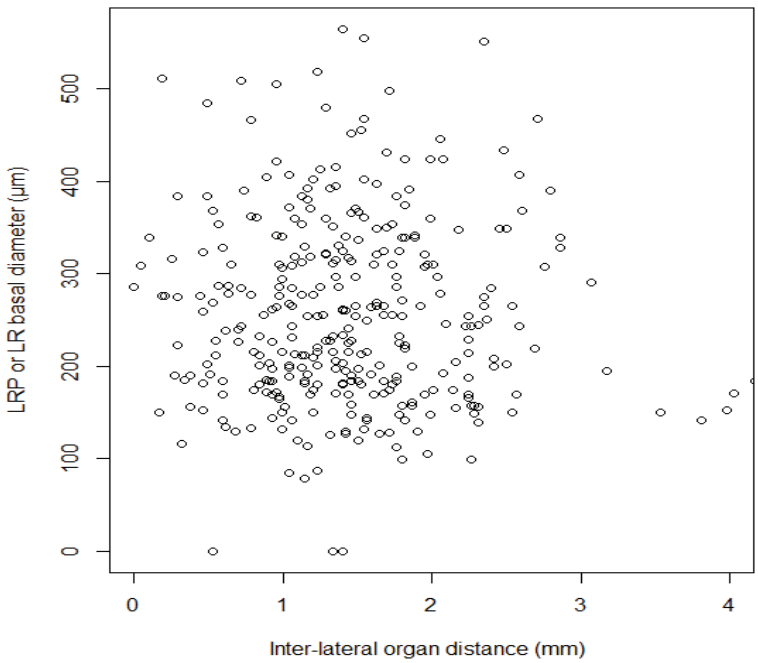

Figure IV-10. Relationship between the basal diameter and the longitudinal spacing measured through the inter-lateral organ distance.

2.1.4 Lateral root emergence

Thanks to Schiff staining, we were able to identify a zone in the primary root region containing a mixture of lateral root and lateral root *primordia* (see Zone 3 in **Figure IV-8**). If our assumption of a narrow apical window of lateral root initiation is correct, the existence of lateral root *primordia* and lateral root in the same root zone is an evidence of a non-strict acropetal development of lateral root *primordia* along the root, likely due to differences in the rate of lateral root *primordium* development.

The question we addressed next was whether these slow developing LRP would eventually emerge or not. If all the lateral root *primordia* present in the unbranched zone ultimately emerge, the density of emerged lateral roots (or branching density) should be equal to the density of lateral root *primordia*. However, if some *primordia* fail to emerge, branching density should be lower than density of lateral root *primordia*. Thus, to estimate the proportion of aborted lateral root *primordia*, we compared the distribution of lateral branching densities of 15-d old plants obtained with SmartRoot to the density of lateral root *primordia* within the unbranched zone (Zone 2) by means of an appropriate statistical test. This analysis showed that, at a significance level of 0.01, lateral root branching density was not different to the density of lateral root *primordia* within the unbranched zone (Kruskal-Wallis rank sum test, $p=0.04$). Consequently, the most likely hypothesis is that nearly all *primordia* managed to emerge with time, though at various distance from the root tip. In other words, the abortion of lateral root *primordia* in maize, if it exists, is a marginal phenomenon, at least in our growing conditions.

2.1.5 Summary

- *Key Results* Lateral root *primordia* exhibit in average a gradual 3-fold increase in diameter from their initiation at the root tip to their emergence. This process takes a little more than 3 days. However, lateral root *primordia* do not develop at the same rate. Slowly developing *primordia* have rates of diameter increase close to 8 µm cm^{-1}, while fast developing *primordia* could reach rates of 20 µm cm^{-1}. The longitudinal spacing between root *primordia* is highly variable, with smaller distances found more frequently than larger distances, but it has no visible influence in the rate of *primordium* development. The density of lateral root *primordia* within the studied zones does not increase with distance to the root tip. Lateral root branching density obtained from SmartRoot analysis was very similar to *primordium* density estimated using Schiff staining.

- *Conclusions* Differences in lateral root development can already be observed since the early steps of their history, more precisely, at the *primordium* stage. The overall constant

lateral organ densities among the unbranched and branched zones suggest that (i) no de novo lateral root *primordium* initiation occurs after a few centimetres (~3) from the root tip and that (ii) all lateral root *primordia* emerge, even if at different rates.

2.2 Anatomical lateral root structure

The second aspect that we looked at was the anatomical root structure and how its variations can be related to differences in root growth. To do so, we examined the anatomical structure of lateral roots with contrasting length in root cross sections at apical, subapical and basal regions (see section **1.2** for technical details).

2.2.1 Root labeling and growth profiles associated to anatomical samples

Sampled lateral roots were assigned three expert growth classes, namely "fast-growing", "slow-growing" or "early arrested" roots, based on root length and morphology criteria applied to the root apex at harvesting time as explained in section **1.4**. The corresponding root lengths at harvesting are shown in **Figure IV-11A**. The growth rate profiles obtained *a posteriori* for sampled roots were reasonably consistent with the expert root labeling used at harvesting (**Figure IV-11B**). 'Early arrested' roots, for instance, presented the lowest initial growth rates and very short growth durations (1-2 days), with root lengths lower than 1 cm. 'Slow-growing' roots presented relatively high initial growth rates that tended to decrease with root age, with longer growth duration (3-7 d). Finally, 'fast-growing roots' presented the highest initial growth rates with a steady (or even increasing) trend, so that their growth continued at the end of the observation period (up to 7 d). These differences in growth rate profiles were partly reflected in root lengths measured at harvesting, since all sampled roots were close to each other and therefore of similar ages. Accordingly, the root length was highly dependent on the expert growth class (Kruskal-Wallis test, $p<10^{-8}$).

Radial root anatomy was characterized using the diameter of the root (D), stele (D_{ST}) and pith (D_P) and the number of xylem poles (N_{XP}) and vessels (N_{XV}), as summarized in **Table IV-4.** A series of root cross-sections corresponding to selected root examples for each expert root growth class is shown in **Figure IV-12**. The three root classes were characterized by a large range of root diameters and anatomical characteristics with a manifest overlap between classes (**Table IV-4**). For instance, the measured ranges for the stele diameter were 145-195 µm; 146-198 µm and 125-186 µm in A, B and C roots respectively. Similar overlaps were found for all variables. The independence of all the measured anatomical variables on the expert growth class was confirmed by a Kruskal-Wallis test at a 0.01 significance level.

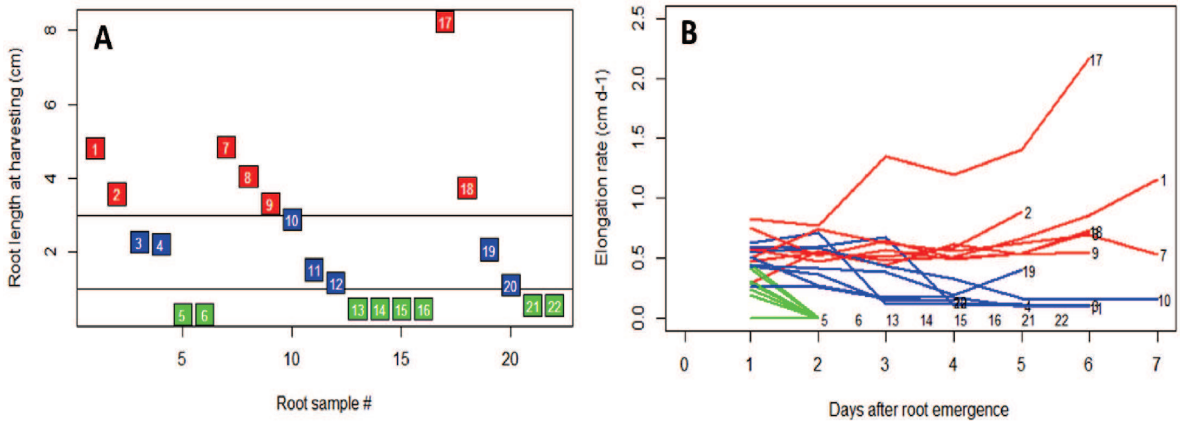

Figure IV-11. Root kinetics associated to anatomical samples. (**A**) Root length at harvesting for each sampled root. Sampled roots originated from 3 different plants: roots 1-6 from plant 1; roots 7-16 from plant 2 and roots 17-22 from plant 3. (**B**) Root growth profiles associated to root anatomical samples. Within the first week after root emergence, "A" roots appear to be either in a stationary or acceleration phase, while "B" roots seem to be in a deceleration phase. Notice "C" roots stop their growth within 2 days after emergence.

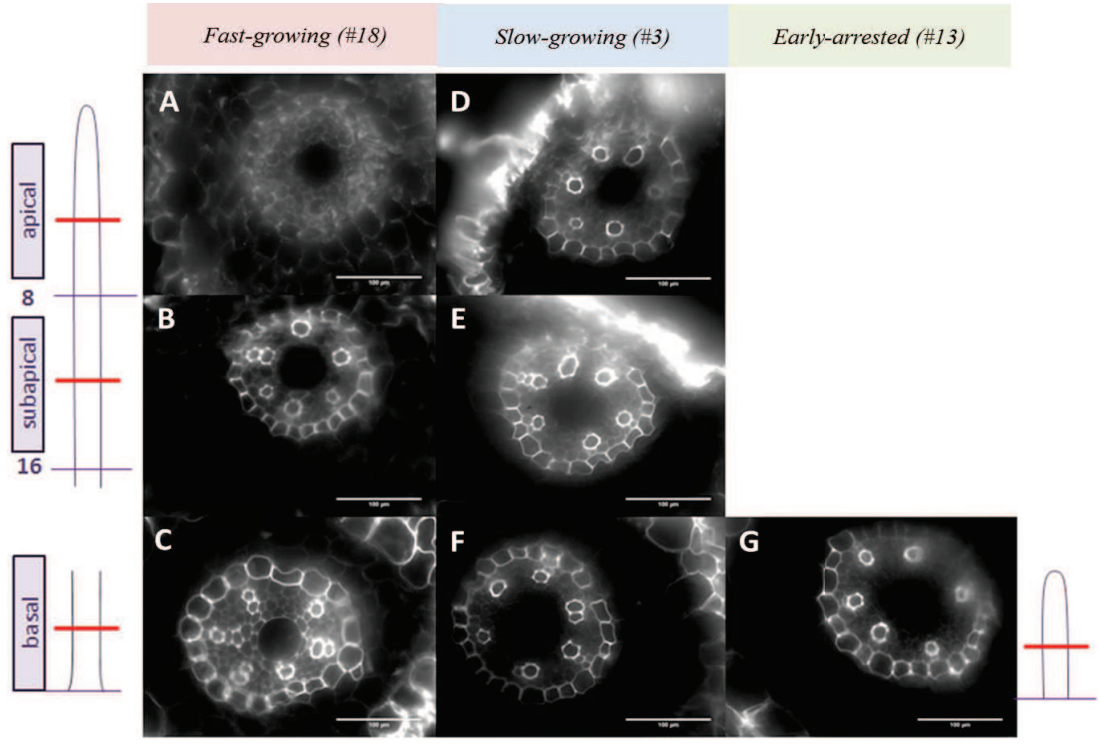

Figure IV-12. Selected examples of root cross sections for a fast-growing root (**A-C**), a slow-growing root (**D-F**) and an early arrested root (**G**) at an apical (**A,D**), subapical (**B,E**) and basal (**C,F,G**) root segments. Numbers indicates distance from apex (mm). Basal segment corresponds to the most basal 8 mm root segment. Scale-bars: 100 µm.

Table IV-4. Root anatomical traits. Mean and absolute range (minimum and maximum values, in brackets) obtained for each root growth class (A, B or C) at a given longitudinal position (apical -api-, subapical -sap- or basal -bas-).

Root type	Sample size	Final root length cm	Root zone	Root diameter μm	Stele diameter μm	Pith diameter μm	Xylem poles	Xylem vessels
A	7	4,7 (3,3-8,2)	api	488 (420-643)	163 (135-192)	74 (51-105)	0 (0-0)	0 (0-0)
			sap	530 (442-709)	173 (132-240)	74 (56-95)	5 (0-7)	6 (0-8)
			bas	534 (453-570)	173 (145-195)	68 (51-87)	7 (6-7)	9 (7-11)
B	7	1,9 (1,1-3,4)	api	472 (454-497)	147 (131-169)	53 (42-79)	6 (5-7)	6 (5-8)
			sap	485 (471-506)	135 (132-140)	56 (52-59)	6 (5-6)	7 (7-8)
			bas	553 (526-586)	165 (146-198)	72 (53-103)	7 (6-8)	9 (7-10)
C	9	0,4 (0,3-0,5)	bas	495 (396-621)	148 (125-186)	53 (34-82)	6 (4-8)	7 (4-12)

2.2.2 Root anatomical features are tightly correlated, but much less to root elongation

We wanted to explore the influence of overall root anatomy in root growth, by analyzing the potential correlations between anatomy-related traits and root growth measurements. In this analysis, two variables were used as proxy for root elongation: root length and elongation rate at harvesting, hereafter referred as $L_{harvest}$ and $ER_{harvest}$.

We found highly significant correlations between a majority of anatomical traits measured in this study, including the root, stele, and pith diameters and the number of xylem poles (correlation coefficients greater than 0.60 and p-values <0.001 for all variable combinations). The exception to this was the number of xylem vessels, presenting weaker correlations (**Table IV-5**). Scatter plots of these tightly correlated anatomical traits (D, D_{ST}, D_P and N_{XP}) are presented in **Figure IV-14.** Since D_{ST} showed the highest correlations with the remaining traits, it was used on the abscissa. Root diameter, meta-xylem diameter and number of xylem poles increased with increasing stele diameter, whatever the root segment at which these variables had been measured. *This indicates that, at any root position, there exists a scaling effect between the size of root structures such as the stele or the pith and the width of the root itself*. Consequently, root diameter can be used as a representative measure of root radial dimension.

Table IV-5. Pairwise correlations between anatomy-related traits and elongation-related variables. The Spearman correlation coefficient between each pair of variables was computed using all complete pairs of observations on those variables and indicated below the diagonal. P-values are indicated upper the diagonal using the following key: ns for P>0.05, * for P ≤ 0.05, ** for P ≤ 0.01 and *** for P ≤0.001. N_{XP} and N_{XV} for root sections without any mature xylem vessels (0 values) were excluded from the analysis. Color intensity refers to the correlation strength 0 1. Highly significant correlations between anatomical traits (see the text) are framed inside a black rectangle. Scatterplots of the correlations highlighted in yellow are presented in Figure IV-13 below.

	$ER_{harvest}$	$L_{harvest}$	D	D_{ST}	D_P	N_{XP}	N_{XV}
$ER_{harvest}$	***	***	ns	*	*	ns	ns
$L_{harvest}$	0.89	***	ns	*	**	ns	ns
D	0.05	0.19	***	***	***	***	ns
D_{ST}	0.32	0.40	0.81	***	***	***	**
D_P	0.39	0.46	0.65	0.78	***	***	*
N_{XP}	0.18	0.09	0.60	0.82	0.68	***	***
N_{XV}	0.22	0.17	0.37	0.50	0.43	0.64	***

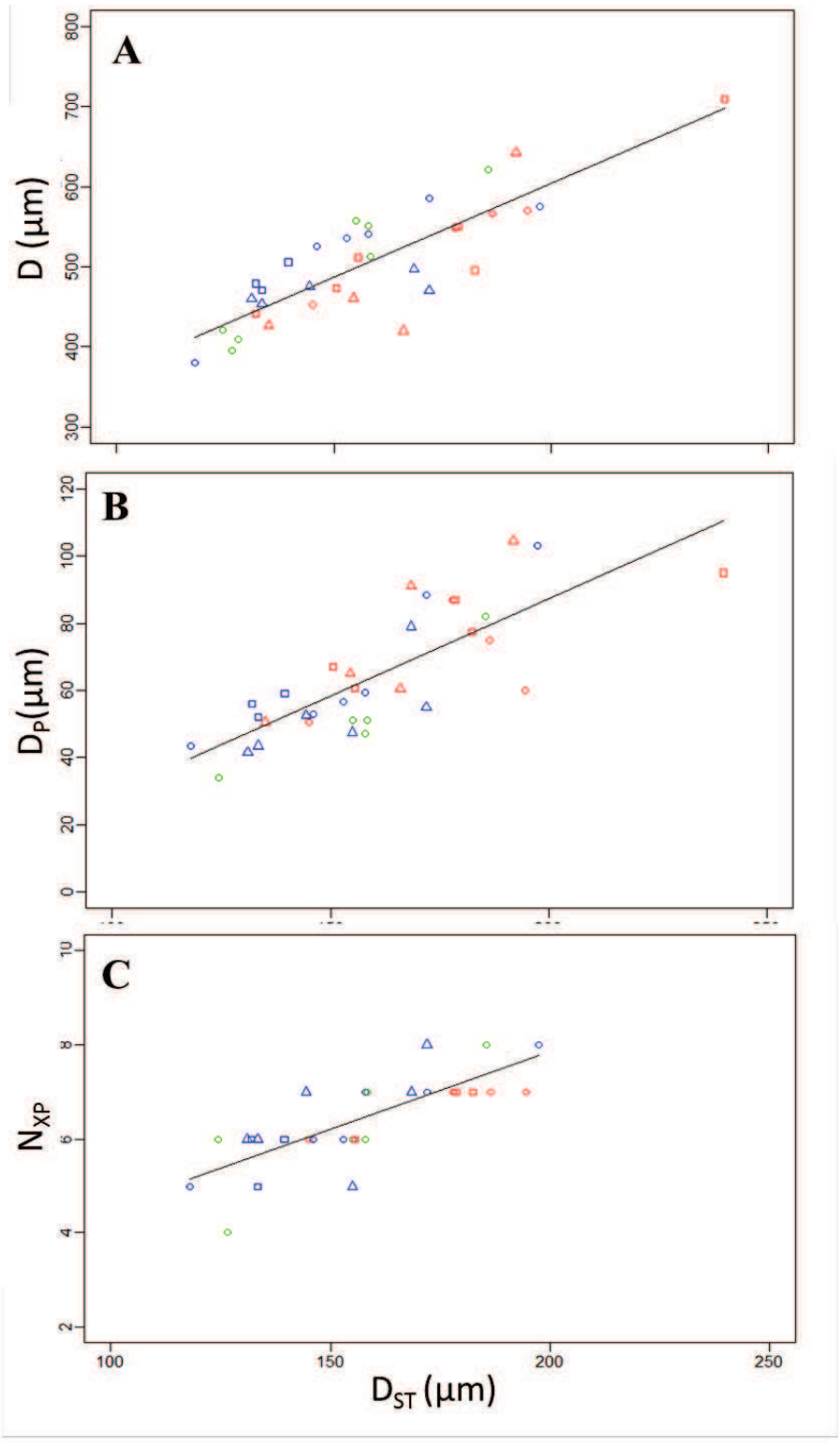

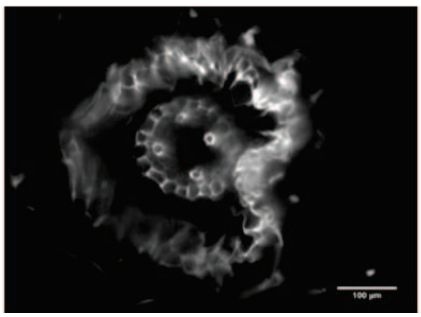

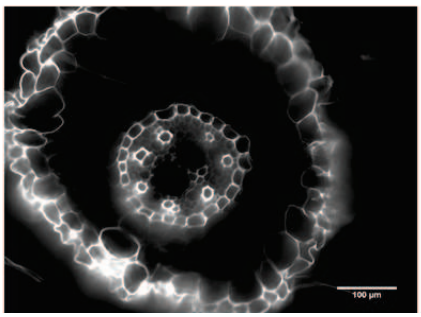

Figure IV-14 Main correlations between anatomy-related traits. (**A**) Root diameter (D), (**B**) diameter of the root central pith (D_P) and (**C**) number of xylem poles (N_{XP}) in relation to the root stele diameter (D_{ST}). N_{XP} values were excluded from the analysis for root sections without any mature xylem vessels. Colors indicate the expert root class (red for fast-growing, blue for slow-growing and green for early-arrested roots). Symbols indicate the root segment (triangle for apical, square for subapical, circle for basal). Images at the bottom show root cross-sections of a thin (left) and a thick (right) maize lateral root. Scale-bars: 100µm.

However, the link between the root anatomical structure and root elongation was not so obvious. Even if the correlation between elongation-related variables ($L_{harvest}$ and $ER_{harvest}$) was very strong ($r=0.89$, $p<10^{-16}$), their correlation with anatomy-related traits was significant but not very tight (**Table IV-5**). The weakness of this correlation might be related to the significant overlap in the range of stele diameter and other structures for roots of the different growth classes (**Figure IV-14**).

To better understand the link of root anatomy and elongation, we examined more closely the relationship of root length and root diameter, respectively taken as simple indicators of the global root elongation and radial dimension (**Figure IV-16**). The emerging triangular shape suggested that there is a maximal root length reachable by roots of a given diameter, which increases with root diameter. *In other words, our results suggest that the maximal* (*potential*) *root length is limited by the root diameter*. This potential length was not reached by all roots, especially not for roots in the early-arrested class. *Thus, root elongation, while limited, is not determined by root diameter*.

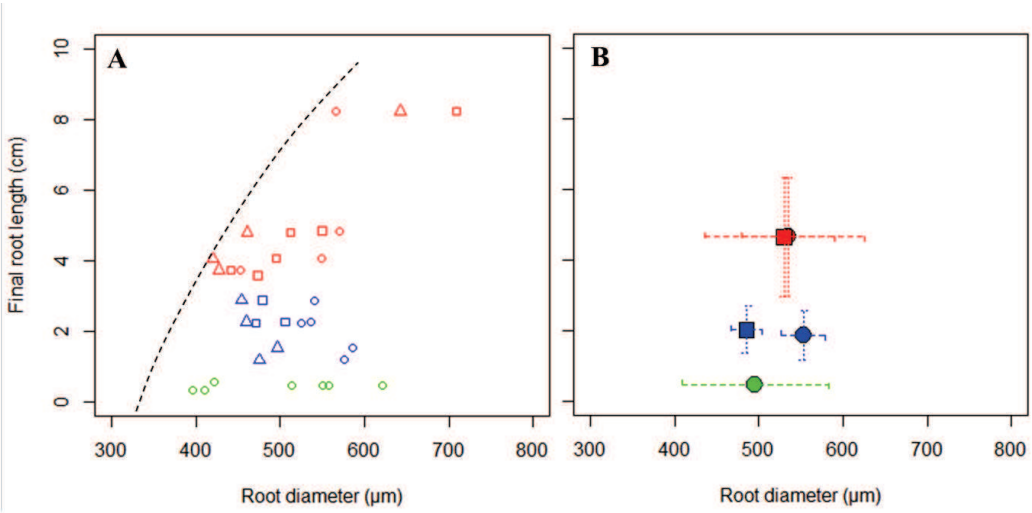

Figure IV-15. Relationship between root diameter and root length. (**A**) The hand-drawn line (upper limit of the scatterplot)) illustrates the maximal root length that might be reached for roots with a given root diameter. (**B**) Data were grouped in function of their location along the longitudinal roots axis (circles for basal, square for subapical) and expert root class (red for A, blue for B, green for C)). Symbols indicate mean values, bars indicate standard deviation values. For sake of clarity, data from apical cross-sections was not represented here.

2.2.3 Longitudinal variations in lateral root anatomy

We observed that the anatomical structure varied longitudinally along maize lateral roots (see some examples in **Figure IV-12**). For instance, the number of mature (lignified) xylem

vessels tended to increase towards the root base (**Figure IV-16B**). Moreover, a complete lack of mature xylem vessels was observed in some apical (root samples #1, #8, #17 and #18) and one subapical locations (#17). In all cases where xylem vessels were immature at the apical section, it corresponded to fast-growing roots. In contrast, all slow-growing and early-arrested roots presented mature xylem vessels at the most apical section (*i.e*. at distances lower than 8 mm from root tip) (**Table IV-4**). *Such pattern of xylem maturation suggest that the position at which xylem maturation begins depends on the rate of root elongation*

In addition, the number of mature xylem vessels could vary substantially between the distinct portions of a given root (**Figure IV-16B**). This was mainly due to the multiple-vessel xylem poles characteristic of root basal segments (see one example in **Figure IV-12C**), since the number of xylem poles remained most often constant (**Figure IV-16A**). *These observations indicate that the completion of xylem maturation occurred in some cases at distances greater than 16 mm from the root tip, and suggest that the maturation processes could extend over all the root length*. To validate this hypothesis, it would be interesting to perform contiguous cross sections covering all the root length and determine whether xylem maturation complete at the root base or at some intermediate point between the base and the root apex.

Longitudinal variations in root diameter were also commonly observed (**Figure IV-16 C**). Different trends in root diameter were observed among individual roots. Most roots presented a decrease in root diameter at more apical positions, but stable or increasing trends were also observed. Moreover, the longitudinal trend observed in root diameter seemed to be related to the temporal trend in growth rates. Indeed, data from **Figure IV-16C** suggest that fast-growing roots had rather stable or slowly decreasing trends in root diameters, whereas for slow-growing, root diameters decreased much more steeply. This trend also applied for the diameter of other root structures, such as the stele (**Figure IV-16D**), suggesting the longitudinal change in radial root anatomy could be related to the growth rate profile of the root.

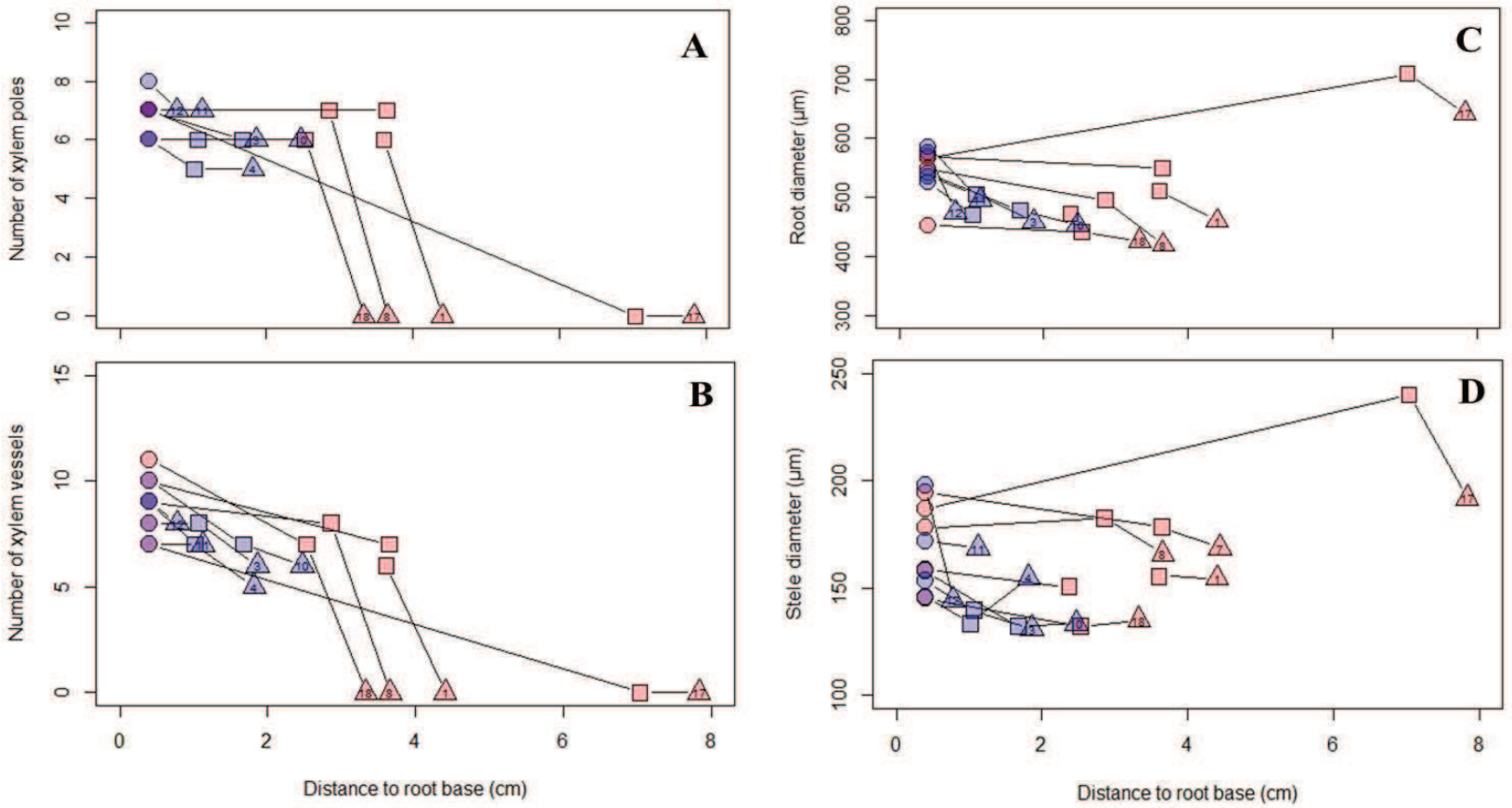

Figure IV-16. Longitudinal change in (**A**) the number of xylem poles, (**B**) number of mature xylem vessels, (**C**) the diameter of the stele and (**D**) the root diameter measured for individual roots. Fast-growing roots are colored in red, slow-growing roots in blue. Early arrested roots were excluded from the analysis.

Table IV-6. Pairwise correlations between elongation-related variables ($L_{harvest}$ and $ER_{harvest}$ for length and ER at harvesting) and anatomy-related traits at each recorded root location. The Spearman correlation coefficient between each pair of variables was computed using all complete pairs of observations on those variables. Both mature and immature cross-sections were used. Colors refer to the sign and strength of the correlation -1 1. P-values are indicated using the following key: ns for P>0.05, * for P ≤ 0.05, ** for P ≤ 0.01 and *** for P ≤0.001.

	$ER_{harvest}$		$L_{harvest}$	
apiD	-0.08	ns	-0.22	ns
sapD	0.30	ns	0.70	*
basD	-0.20	ns	-0.05	ns
$apiD_{ST}$	0.29	ns	0.22	ns
$sapD_{ST}$	0.51	ns	0.75	*
$basD_{ST}$	0.13	ns	0.21	ns
$apiD_{P}$	0.48	ns	0.46	ns
$sapD_{P}$	0.56	ns	0.84	**
$basD_{P}$	-0.14	ns	-0.09	ns
$apiN_{XP}$	-0.69	*	-0.89	***
$sapN_{XP}$	-0.15	ns	0.14	ns
$basN_{XP}$	0.11	ns	0.07	ns
$apiN_{XV}$	-0.66	*	-0.89	***
$sapN_{XV}$	-0.70	ns	-0.56	ns
$basN_{XV}$	0.11	ns	0.29	ns
$ER_{harvest}$	1.00	***	0.80	***
$L_{harvest}$	0.80	***	1.00	***

2.2.4 Relationship between longitudinal variations in root anatomy and root elongation

To investigate more deeply the relationship between longitudinal variations in root anatomy and elongation, we explored the correlations between all anatomy-related traits *at each root segment* and root elongation-related variables ($L_{harvest}$ and $ER_{harvest}$). Interestingly, a very regular pattern could be observed (**Table IV-6**). While anatomy-related traits at basal positions did not correlate with $L_{harvest}$, the correlations between D, D_{ST}, D_P at the subapical segment and $L_{harvest}$ were remarkably high (r greater than 0.70 and p-value <0.05 for all variable combinations).

N_{XP} and N_{XV} at apical positions correlated negatively with root length likely because of the characteristic distant xylem differentiation for fast-growing roots (see previous section). Again, no significant correlations were found for basal segments. Overall, these results indicate that (i) root behavior cannot be predicted from early (basal) anatomical features. A more physiological interpretation of the lack of correlation between root length and basal diameters is that the initial anatomical structure did not seem to determine the root growth profile. However, (ii) the subapical root diameter, related to the anatomical structure of the more recently formed tissues, is a good marker for the elongation capacity of the growing root, being generally thicker for fast growing roots and thinner for slow-growing roots (**Figure IV-15B**).

2.2.5 Summary

- *Key results* We found longitudinal variations in the diameter of the root, the root stele, the number of mature xylem vessels and poles taking place during lateral root growth. The degree of xylem maturation increases shootward with tissue aging, the patterning of maturation depending on root growth dynamics. Root diameter can either decrease, remain stable or even increase rootward with root age. The diameter of the root itself at any position is tightly correlated with the size of different inner root structures, such as the root stele and pith. A large overlap in the range of stele diameter and other root structures exists for lateral roots with different lengths. However, the maximal root length appeared to be limited by the global root radial dimension.

- *Conclusions* The anatomical structure of maize lateral roots varies longitudinally. A scaling effect exists between the diameter of the root itself and the diameter of different inner root structures, such as the root stele and pith. Even if the initial root anatomy does not determine the root growth profile, the anatomical structure of more recently formed tissues (typically the root subapical 8-16 mm segment) is tightly related to the elongation capacity of the root, suggesting that there exists some link between root anatomy and root growth. In view of these results, an “upper-limit” hypothesis, where the root structure

limits but does not determine root growth, seems the best way to resume the relationship between the structure and growth of the root.

2.3 Epidermal cell length pattern in the growing zone of lateral roots

2.3.1 Root labeling

Sampled lateral roots (n=21) were assigned to one of the three expert growth classes, namely "fast-growing", "slow-growing" or "early arrested" roots, based on root length and morphology criteria applied to the root apex at harvesting time as described in section **1.4**. The corresponding growth profiles and root lengths at harvesting were not available, since the experiment was designed to tune in the technique for visualization of cell walls within lateral roots. Lateral root were sampled all along the primary root. Consequently, root ages of sampled lateral roots were not comparable.

2.3.2 Analysis of longitudinal cell length profiles reveals a large range of lengths of the growing zone

Qualitatively, a common pattern was observed in most epidermal cell length profiles. Starting at the root cap function and moving shootward, the average cell length remained constant, then started to increase with position first gradually, then steeply, and finally became constant, indicating the end of the growing zone. The position at which root hairs are initiated is usually located close to the *plateau* of final cell length. Consequently, we used the distance between the most rootward root hair bulge and the root cap function (referred from now on as distance of root hair initiation) as a first approximation of the length of the growing zone (L_{GZ}) for analyzed roots.

For growing roots (A or B classes, n=15), the L_{GZ} ranged from a few µm (minimum value equal to 430 µm) to more than 2 mm (maximum value equal to 2318 µm). Despite some overlap, fast-growing roots presented *on average* longer growing zones than slow-growing roots. This suggested that the length of the growing zone was related to the root growth rate. Finally, all arrested roots (C class, n=6) presented root hair initiation very close to the root tip (up to 197 µm), suggesting that a minimal L_{GZ} might be required for root growth.

Then we tested the hypothesis that the longitudinal root growth could be related to the root radial dimension. We therefore explored the relationship between the L_{GZ}, estimated through the position of root hair initiation, and root diameter measured at the root cap junction. Root diameters increased roughly linearly with the distance from root hair initiation ($r=0.81$, $p<0.01$), revealing some positive link between the radial and longitudinal root dimensions.

However, we observed that roots with a similar range of root diameters at the root cap junction presented very different L_{GZ}, suggesting that the length of the growing zone is not determined by the diameter. The direct relationship between root growth and L_{GZ} could not be investigated because of the lack of the growth rate profiles for roots from which cell length profiles were obtained.

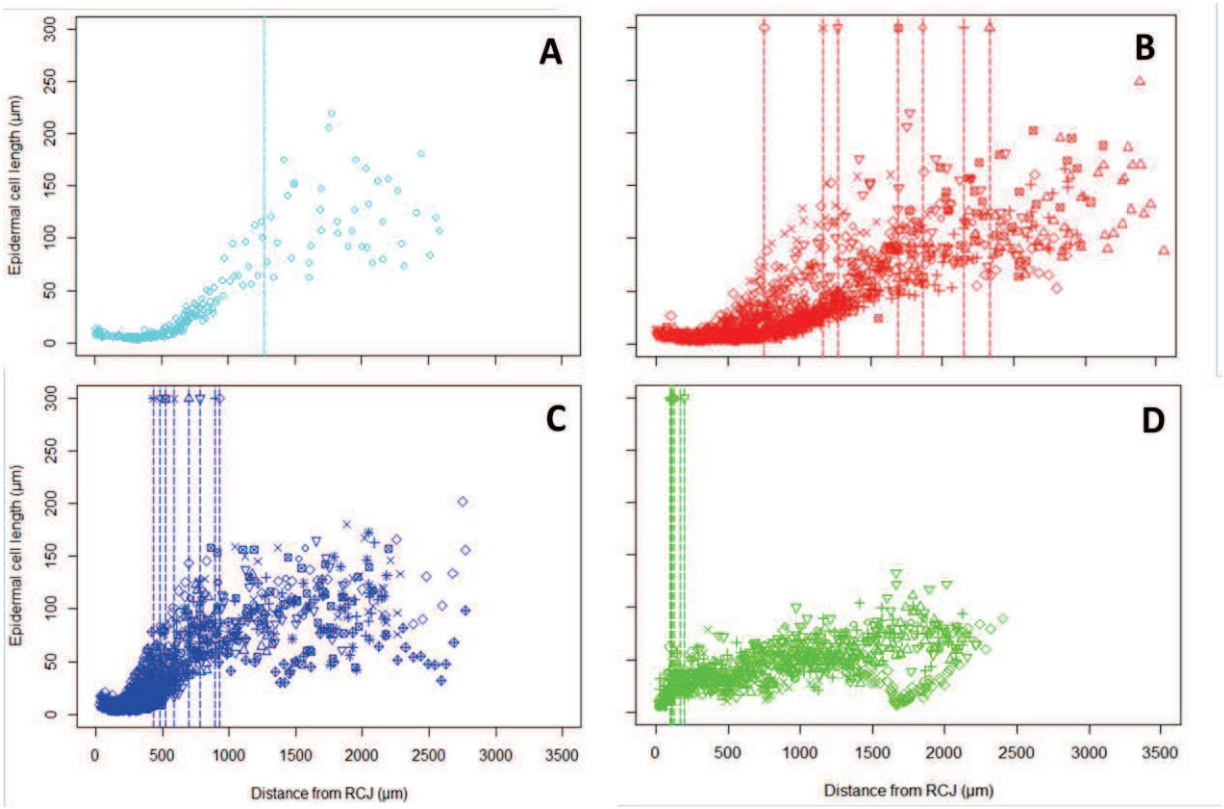

Figure IV-17 (**A**) Illustration of the pattern observed in epidermal cell length profiles on one individual root (light blue). Note that root hair initiation (dashed line) starts close to the plateau of mature cell length. (**B, C**) A scaling effect of the pattern presented in (A) is observed when comparing fast (red) and slow growing (blue) roots, accompanied by a shift in the position of root hair initiation towards the end of the plateau of mature cell length. (**D**) Arrested roots (green) present root hair differentiation very close to the root tip. Each data point represents a single epidermal cell length measurement. Symbols refer to lateral root ID.

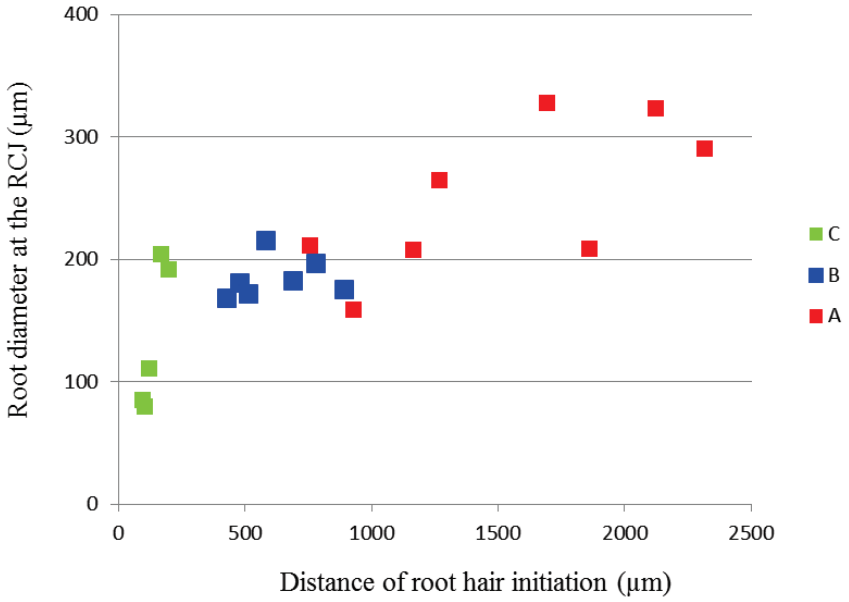

Figure IV-18 Scatterplot of root diameter measured at the root cap junction (RCJ) (in µm) versus the distance of root hair initiation to RCJ (in µm).

In **Chapter III**, a more detailed analysis of the epidermal cell length data is provided. This deeper analysis consists in an attempt to identify longitudinal root zones along cell length profiles using heteroscedastic piecewise linear models. Results obtained from this segmentation analysis are covered in the article entitled 'Identifying developmental zones in maize lateral root cell lengths profiles' submitted for publication to the Journal of Experimental Botany, and were therefore omitted from this section.

2.3.3 Summary

- *Key results* We found a 4-fold range in the length of the root growth zone (apical distance to root hair initiation) for maize lateral roots. Fast-growing roots presented longer growing zones, while minimal growing zones were found for early arrested roots. The length of the growing zone was correlated but not determined by the root apical diameter.
- *Conclusions* The spread distribution in the length of the growing zone (apical distance to root hair initiation) could be at the origin of the spread distribution in growth rates observed in lateral roots of maize.

2.4 Glucose concentration and its distribution in lateral root apices

2.4.1 Glucose concentration

Glucose concentration in sampled lateral root apices was examined separately for fast-growing, slow-growing and arrested roots in a variety of situations. These included control and no-control plants in several independent experiments, grown on rhizotrons or using aeroponics (see section **2.1** of **Chapter II**). Since the highest number of apical sugar samples was harvested at the UCL experiment, it was used as example. In this experiment, two repetitions were harvested for each root class in 7 different conditions (1: CTRL, 2: OMB, 3: EXC, 4: EXC: ENDO, 5: B73inbred, 6:RUM1, 7: RTCS).

Among the 3 soluble sugars analyzed (glucose, fructose and sucrose, noted Glc, Fru and Suc respectively), Glc was the most abundant, Fru was lower and linearly related to Glc while Suc was hardly detectable in most samples (results not shown). For sake of simplicity, only Glc results are therefore presented. **Figure IV-19** shows the Glc concentration (hereafter referred as Glc_{conc}) obtained for each independent sample of lateral roots at the UCL experiment. Within all conditions, we observed a gradient of Glc_{conc} of samples ranging from maximal values reached by fast-growing roots to minimal values corresponding to early-arrested roots. This gradient translates into a ranking of Glc_{conc} with respect to the expert growth class, being *on average* higher for A than for B and C roots of a same condition.

However, differences of Glc_{conc} between repetitions of the same growth class were often more important than differences across samples from different growth classes (for instance, Glc_{conc} for the two repetitions of B roots in condition 5 was 0.3 and 0.5 mg/g FW, and of 0.1 and 0.3 mg/g FW for C roots). This evidences an overlap of expert growth classes in terms of Glc_{conc}. This overlap has two main possible explanations, illustrated in **Figure IV-20**: either there is a significant dispersion in Glc_{conc} for roots that grow in a similar way, or the overlap is already present in the attribution of expert classes with Glc_{con} being more tightly correlated to growth. In this case, the uncertainty on the expert attribution could be explained by a continuity in the growth rate spectrum, of which the expert growth classes would constitute a (somewhat arbitrary) discretization. In any case, the fact that the gradient of Glc_{conc} for a given condition aligns at a macroscopic scale with the gradient of growth rates represented by the expert growth classes suggests a strong correlation between Glc_{conc} and growth rate, even if it can not be precisely quantified.

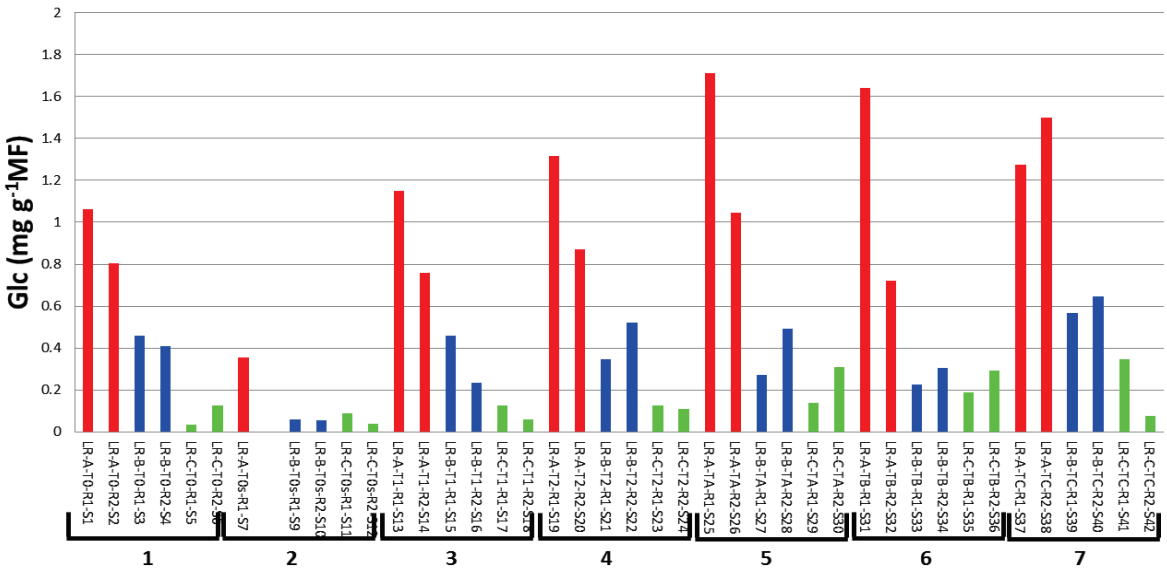

Figure IV-19 Glucose concentration measured in lateral root samples from the UCL experiment. Colors refer to the expert growth class (A: red, B: blue, C: green). Numbered brackets gather root samples of plants grown in a given condition (1: CTRL, 2: OMB, 3: EXC, 4: EXC-ENDO, 5: B73inbred, 6:RUM1, 7: RTCS).

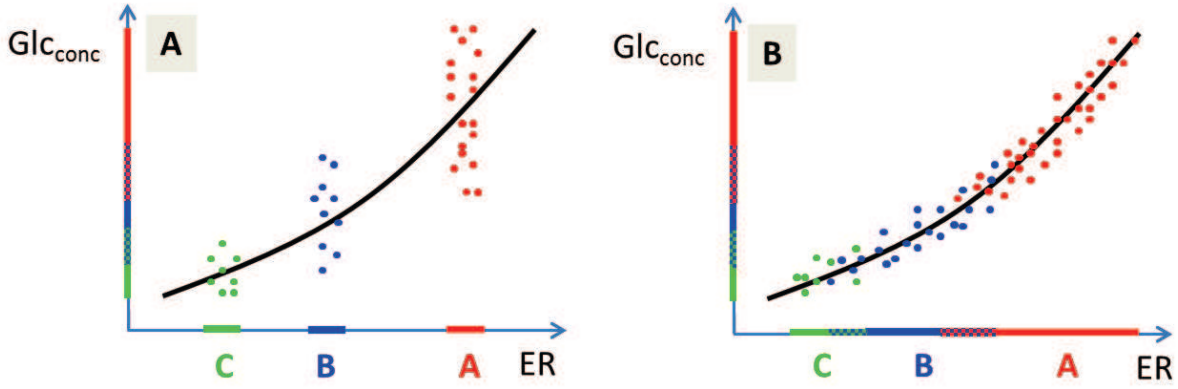

Figure IV-20. Two possible situations explaining the overlap in glucose concentrations observed for expert growth classes. (**A**) There is a significant dispersion in Glc_{conc} for roots growing at similar growth rates (**B**) There is a tight correlation between ER and Glc_{conc} but expert growth classes are overlapping in terms of growth rate.

2.4.2 Longitudinal gradient in glucose concentration

Glucose peak likely occurs at the site of phloem unloading

We studied the longitudinal distribution of Glc by dividing the apical region of lateral roots into ten consecutive 3 mm segments to obtain a longitudinal profile of concentrations. This analysis was performed in several experiments on plants grown in different conditions, separately for each expert growth class. We first show results from BMFS experiment, including samples for CTRL, END, EXCA, OMB and RTCS conditions.

In most profiles, Glc was not uniformly distributed along the apical 30 mm of the root, being highest in the meristem and declining sharply and then more slowly with distance from tip (**Figure IV-21**).The maximal Glc_{conc} were found usually in the most apical segment about 3 mm from the root tip. For a reduced number of profiles, the Glc_{conc} increased steeply in the first 3 mm and peaked further to the tip, at 6-9 mm.

In summary, the peak of glucose concentration in longitudinal profiles of root samples analyzed in this study occurred at distances of 0-9 mm, most often 3 mm, from the root tip (**Figure IV-21**). Paradoxically, it locates near the root meristem, the zone of maximal consumption. A reasonable hypothesis to explain the apical glucose peak is that it could indicate the location at which the phloem unloading takes place. Previous studies locate phloem unloading at the end of the growing zone of the root (Oparka *et al*., 1994), found to be up to 3 mm from the root cap junction in maize lateral roots in our conditions (see **Chapter III**). The former hypothesis is still compatible with our results because the root cap was not removed for sugar measurements. Hence, the 0-3 or 0-6 mm region in samples peaking at 6-9 mm from tip could indeed correspond to the root cap region.

Glucose decline could be explained by passive diffusion

Another feature needing explanation is the gradual decline of glucose concentration shootward to the peak, in a zone where root growth no longer takes place. One possibility is that it might be caused by a consumption of glucose in mature regions. While it is possible that some glucose consumption takes place in this region for the synthesis of cell wall components (cellulose, lignin and suberin) in maturing tissues, it is unlikely to be responsible of the 4-fold glucose decrease from apical maximum to basal values observed for most profiles. A complementary hypothesis would consist of the establishment of a glucose gradient at equilibrium driven by the diffusion of this metabolite from the end of the phloem to nearby tissues trough plasmodesmata. Since symplasmic diffusivity is known to be relatively high at the root tip (Bret-Harte and Silk, 1994), glucose diffusion probably occurs shootward from its unloading, therefore being consistent with the glucose decline observed with distance from root tip.

Differences at the plant root system scale alter the repeatability of experiments

Similarly to apical concentrations, maximal Glc_{conc} in longitudinal profiles cover a continuous range of values between 0 and 4 mg gFW^{-1}, and the repetitions (same conditions in different experiments) show a large dispersion for a given growth class as illustrated by the comparison of profiles in GFBM1 and BMEC1 experiment in **Figure IV-22**. Yet, the overall ordering of Glc_{conc} values with A, B and C expert classes was still observable, along with the trend to decrease more slowly from higher concentrations.

We explored the different sources of variation that could explain not reproducible results of glucose concentrations among GFBM1 and BMEC1 experiments, the former being roughly 2-fold higher. The origin of fluctuations in sugar content could relate to differences at the scale of the organ, but could also concern plant vigour or age (harvest date) or undesired fluctuations in environmental parameters from one experiment to another (questioning the status of so-called repetitions). These hypotheses were tested comparing a set of variables related to global environment and plant (aerial and root) growth on control plants for the two presented experiments (**Table IV-7**). Plants from the same experiment were supposed to be homogeneous. Data in **Table IV-7** suggest that lateral roots in GFBM1 were on average faster and older at the end of the harvesting period. Moreover, primary roots of plants in GFBM1 experiment grew more slowly, maybe reducing the competition of carbon resources for growing lateral roots. No differences were noticed for environment-related variables (temperature, light incidence and photoperiod). In summary, we can conclude that both differences in primary and lateral root growth kinetics between experiments could impact the carbon balance in lateral roots, observed to vary from one experiment to another.

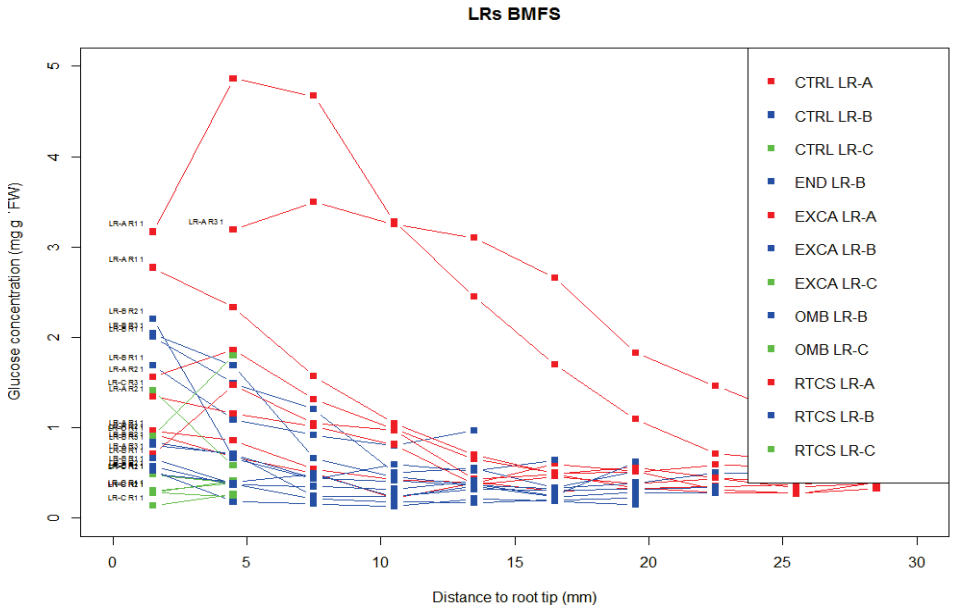

Figure IV-21 Longitudinal profiles of Glc concentration obtained at the BMFS experiment. Each line corresponds to the longitudinal Glc profile obtained for a pool of (~30) roots of the same root class. One or two replicates of each root class (A: red, B: blue, C: green) was pooled for each condition. No distinction is made between different conditions here in this graph.

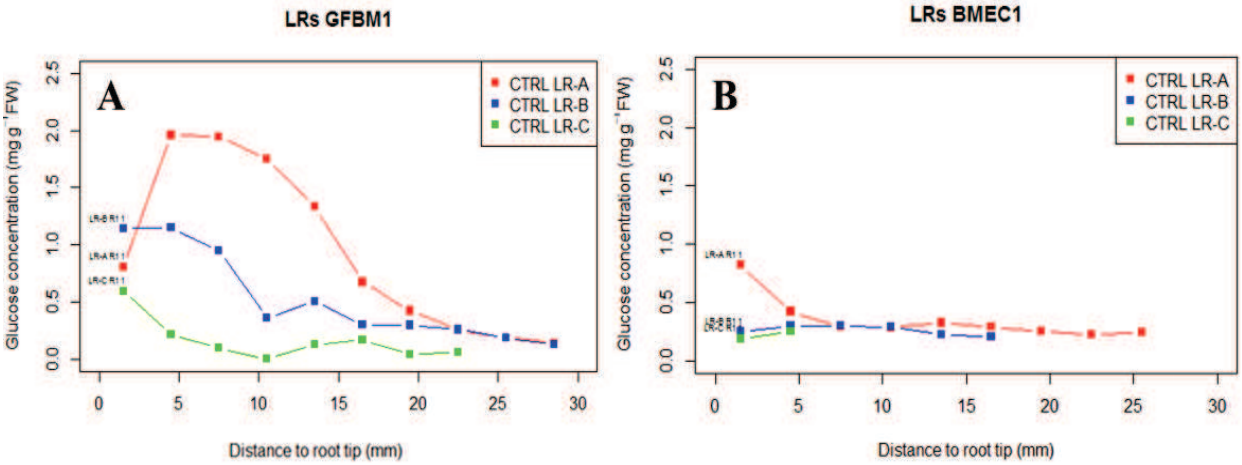

Figure IV-22 Longitudinal profiles of glc concentration obtained for plants grown in control conditions in two independent experiments: GFBM1 (A) and BMEC1 (B).

Table IV-7 Main parameters describing root growth at the organ and plant scales and environment of B73H maize control plants in GFBM1 and BMEC1 experiments.

Parameter		Experiment	
		GFBM1 (N=7)	BMEC1 (N=3)
Organ-scale	growth rate (mm/d)	2.1 (+-3.9) // 5.0 (+-4.5)	2.4 (+- 3.0)// 4.0 (+-2.9)
	basal root diameters (µm)	342 (+-86)// 370 (+-83)	368 (+-63)// 380 (+-60)
	apical root diameters (µm)	281 (+-90)// 304 (+- 94)	333(+- 53)// 342 (+-52)
Plant-scale	End of harvesting period (DAS)	31	16
	Length of the branching zone at 15 DAS (cm)	28	36

Left: all lateral roots // Right: growing lateral roots only

2.4.3 Summary

- *Key results* Variations in apical Glc_{conc} were found both within lateral roots of maize plants grown in a same condition (up to 15-fold) as well as in different conditions (up to 5-fold). Across the conditions, the Glc_{conc} seemed to be strongly related to root elongation, since higher glucose concentrations were found systematically in fast-growing roots (see **Figure IV-19**).
- *Conclusions* The absolute range of glucose concentration found for maize lateral roots was variable among conditions and experiments. Nevertheless, in relative terms, higher glucose concentrations were found systematically in fast-growing roots (see **Figure IV-19**), consuming it at much higher rates because of a faster construction of tissue. If concentration is considered as the balance between the input and the consumption, we can deduce that the rate of sugar arrival must also be higher for fast-growing roots to compensate their higher rates of consumption. Anatomically, it is reasonable to think that these roots present larger diameters with wider phloem vessels (since their xylem vessels are) that would increase their capacity for sugar transport relatively to slower, thinner roots. Altogether, these findings indicate that plant carbon resources are allocated in priority to fat-growing roots.

2.5 Gene expression in lateral root apices

2.5.1 Gene description

The aim of this study was to identify genetic markers associated with the different elongation patterns observed for lateral roots. For that, we analyzed the expression of a number of candidate genes in lateral roots of the reference genotype B73H related to cell division, cell expansion, or that might reflect the auxin or sugar status of the roots.

We first studied the expression of the ***ZmCYCA1*** (cyclin-A1) gene coding for an A-type cyclin protein. The expression of this cell-cycle regulatory protein in *Arabidopsis* is cell stage-specific with the transcript levels peaking at the S phase (Dehghan Nayeri, 2014). Thus, the expression of the *ZmCYCA1* was used as a marker of the cell division activity in the root tissue.

A second gene of interest was the ***ZmEXPB4*** (expansin-B4) gene coding for a member of the β–expansin family. These proteins are known to regulate cell wall extensibility and cell enlargement in maize leaves (Muller *et al*., 2006; Wu *et al*., 2001). In rice, the highest levels of expansin transcripts levels were observed in the most rapidly growing regions of leaf and root tissues (Rice *et al*., 2002). Thus, one would expect to find an abundance of *ZmEXPB4* transcripts in actively elongating maize lateral roots, and low or no expression for already stunted roots.

In a third position, we studied the expression of the ***ZmIAA4*** (Aux/IAA-transcription factor 4) gene, a maize homologs of the *AtIAA4* protein in *Arabidopsis* that acts as a repressor of early auxin response. This gene was shown to be rapidly induced in maize roots upon IAA treatment compared to untreated plants in an independent experiment of maize plants grown in hydroponics. In addition, the polar auxin transport inhibitor TIBA slightly inhibited *ZmIAA4* transcript levels (**Figure IV-24**). Thus, *ZmIAA4* expression was considered a first marker of the auxin response in this study.

The ***ZmIAA17*** (Aux/IAA-transcription factor 17) gene showed a pattern of expression very similar to *ZmIAA4* in the screening experiment (**Figure IV-24**), and was therefore used as a second marker of the auxin response in the root.

Then, we selected 3 three genes involved in carbon metabolism.

ZmASN1 gene coded for an asparagine synthetase enzyme involved in protein catabolism processes. The amount of this enzyme was reported to increase in excised maize primary root tips submitted to glucose starvation (Brouquisse, 1992). Conversely, a strong repression of

ZmASN1 transcripts was observed in presence of glucose (Chevalier *et al*., 1996). We therefore selected the *ZmASN1* gene as a marker of sugar starvation.

ZmSUS1 gene coded for a cytosolic sucrose synthase protein. Despite its name, this enzyme operates primarily in the degradative direction of the reversible reaction of sucrose synthesis, been responsible for sucrose cleavage in the cell. The expression of *ZmSUS1* in primary roots was found to be maximal under conditions of high glucose supply (**Figure IV-25**) (Koch *et al*., 1992; Xu *et al*., 1996). For this reason, we selected *ZmSUS1* as a first marker gene of glucose availability.

ZmIVR2 gene coded for a vacuolar invertase. Invertases are key enzymes in carbohydrate metabolism since they generate hexoses from incoming sucrose that are required for cell energy production (Smeekens, 1998; Trouverie *et al*., 2004). Previous studies have reported maximal *ZmIVR2* transcript levels in excised primary roots at high glucose concentrations (**Figure IV-25**) (Xu *et al*., 1996). In consequence, *ZmIVR2* gene was chosen as a second marker of glucose availability.

Finally, ***ZmEIF4*** (eukaryotic initiation factor 4) and ***ZmGAPDH*** (glyceraldehyde-3-phosphate dehydrogenase) were selected as potential reference genes for a better comparison of RNA samples. A list of the nine selected genes and their assumed physiological significance is given in **Table IV-8**.

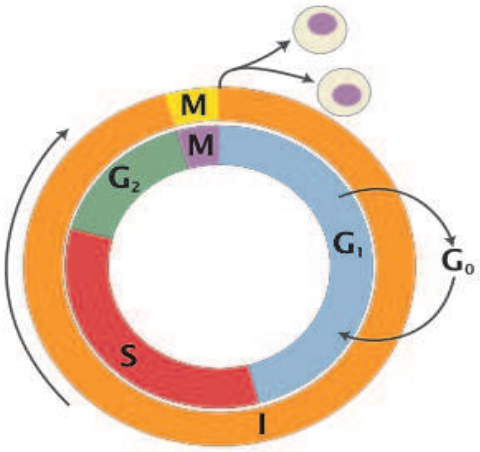

Figure IV-23 The cell cycle. The mitotic phase (M) is a relatively short period of the cell cycle. It alternates with the much longer interphase, where the cell prepares itself for the process of cell division. The interphase is divided into three phases: G1 (fist gap), S (synthesis) and G2 (second gap). All transitions from one phase to another are regulated by cyclins and other cell cycle proteins. Cells may also leave the cell cycle to enter G0 (resting phase) and stop dividing. Source: Wikipedia (public domain).

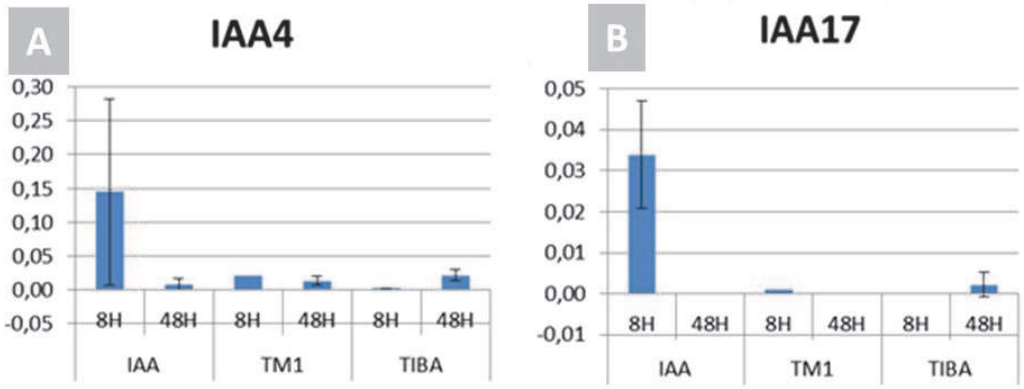

Figure IV-24 Auxin-responsive genes. Absolute transcript levels of ZmIAA4 (**A**) and ZmIAA17 (**B**) measured at the screening experiment. Maize seedlings (10 days old) were treated either with IAA 0.1 µM or TIBA 20µM or remained untreated (TM1) at time zero of the experiment. Samples of the entire root system were collected either after eight hours (8H) or 2 days (48H) to evaluate early and late potential responsiveness to IAA.

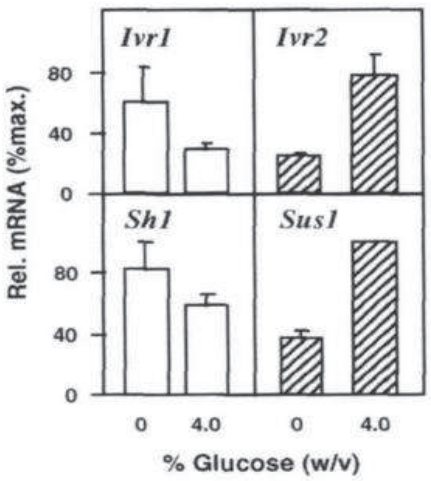

Figure IV-25 Sugar modulated expression of the *ZmIVR2* invertase and *ZmSUS1* sucrose synthase from (Xu *et al*., 1996).

Table IV-8 List of candidate genes.

Gene name	Gene product	Responsiveness
ZmEIF4	eukaryotic initiation factor 4	reference gene (1)
ZmGADPH	glyceraldehyde-3-phosphate dehydrogenase	reference gene (2)
ZmCYCA1	cyclin-A1	cell division
ZmEXPB4	expansin-B4	cell elongation
ZmIAA4	Aux/IAA-transcription factor 4	auxin induced (1)
ZmIAA17	Aux/IAA-transcription factor 17	auxin induced (2)
ZmASN1	asparagine synthetase	glucose repressed
ZmIVR2	vacuolar invertase	glucose induced (1)
ZmSUS1	cytosolic sucrose synthase	glucose induced (2)

2.5.2 Gene expression pattern associated to lateral root classes

To investigate potential gene expression patterns associated with root elongation, the transcription of *ZmCYCA1*, *ZmEXPB4*, *ZmIAA4*, *ZmIAA17*, *ZmASN1*, *ZmIVR2* and *ZmSUS1* was quantified in lateral root apices annotated either fast-growing (A), slow-growing (B) or early-arrested (C) following an expert classification established at harvesting (see **section 1.4**). This analysis included at least 4 biological repetitions for each growth class.

The transcripts levels were measured by real-time PCR and expressed in fold change relative to *ZmEIF4*, as this gene was shown to present a stable expression in maize across different tissue types and conditions (Lin *et al*., 2014). Normalization by the combination of *ZmEIF4* and *ZmGAPDH* expression was avoided as *ZmGAPDH* expression was rather unstable across growth classes. **Figure IV-26** shows the resulting comparison of gene expression levels for the growth classes. Eight among nine genes present ranked values of expression for expert growth classes. The relative abundance of *ZmGADPH*, *ZmCYCA1* and *ZmEXPB4* transcripts was higher in fast-growing roots than in arrested roots. Conversely, *ZmIAA4*, *ZmASN1* and *ZmSUS1* were more strongly expressed in arrested roots. No clear pattern was found for *ZmIAA17* expression.

We further studied the correlation among the expression levels of all the selected genes so as the possibility of common expression profiles for similarly growing roots. A centered and normalized principal component analysis (PCA) was applied to the expression of the selected genes (listed in **Table IV-8**) as PCA variables (10 variables), each individual of the dataset

being an independent RNA sample (15 samples) extracted from a pool of root tips of a given growth class (A, B or C classes).

The first axis of this PCA (**Figure IV-27**) accounted 45% of variance and was mainly correlated with *ZmGAPDH*, *ZmEXPB4* and *ZmCYCA1* expression on the positive side and *ZmIAA4* and *ZmSUS1* expression on the negative. Projection of individuals (**Figure IV-27B**) shows that this axis sorts individual samples according to their growth class. Samples of the early arrested class are on the negative side, fast-growing root samples are mainly on the positive side, and slow-growing root samples have intermediate coordinate values on this axis. The second axis extracted 25% of variance and was mainly determined by *ZmASN1* and *ZmIVR2* expression. Nevertheless, this axis did not contribute to the separation of growth classes, as it can be seen in the projection of the centroids of each growth class in **Figure IV-27B**.

The correlation between the *ZmGAPDH*, *ZmEXPB4* and *ZmCYCA1* gene expressions on one hand and *ZmIAA4* and *ZmSUS1* on the other was confirmed independently of the PCA by computing the pairwise correlation coefficients for all variable pairs presented in **Table IV-9**. In addition, the correlation between the expression of each gene and the ordinal variable 'root class' is provided in **Table IV-10**.

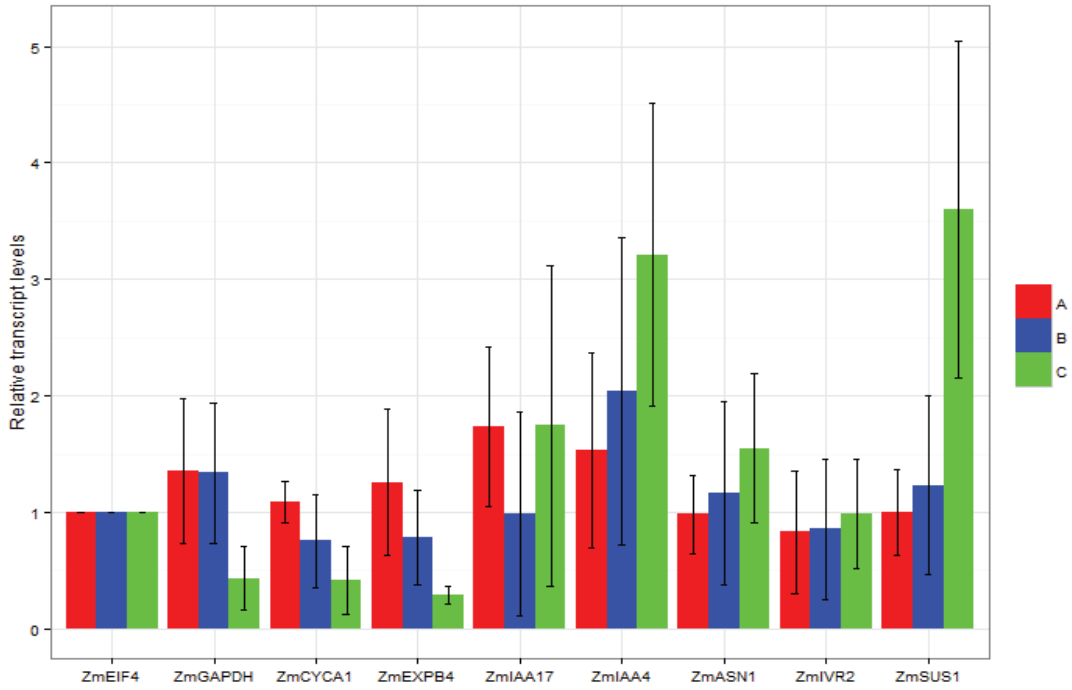

Figure IV-26 Relative expression levels of selected Zea mays genes as quantified by real time PCR in lateral roots of 15 d plants. The transcript levels are expressed in fold change as compared to EIF4 expression. See **Table IV-8** for the names of the genes.

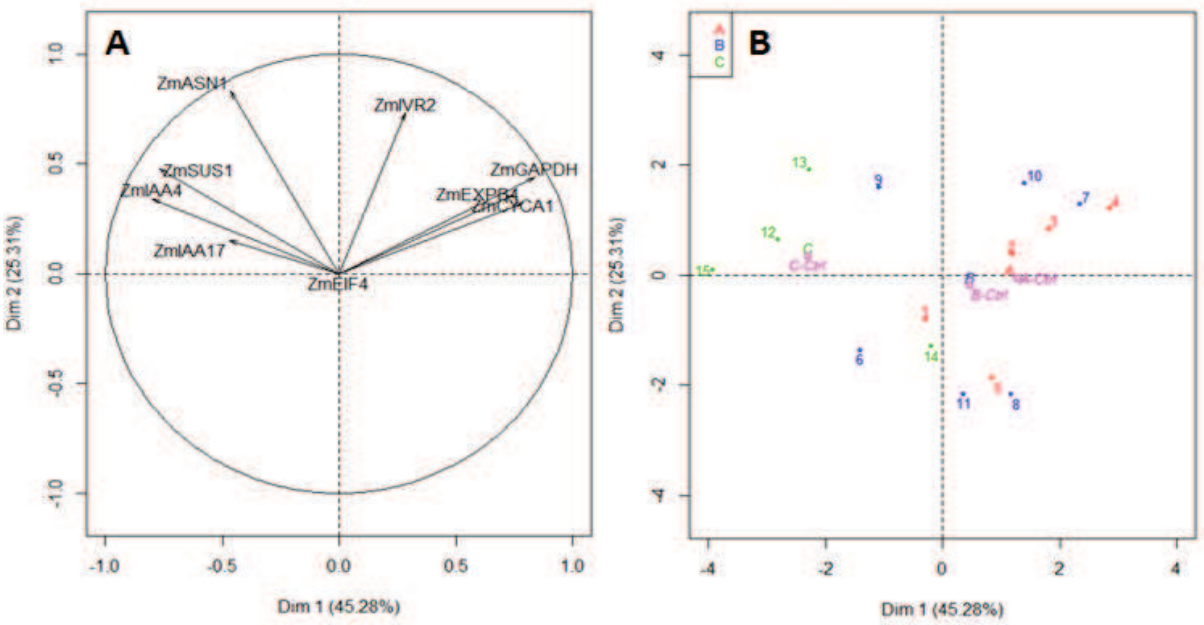

Figure IV-27 Principal component analysis. (**A**) Variables (gene transcript levels) located on the plane defined by component 1 (horizontally) and 2 (vertically). See **Table IV-8** for the names of the genes. (**B**) Projection of individuals and centroids of each growth class.

Table IV-9 Pairwise Spearman correlation coefficients between the expression of the selected genes. P-values are indicated using the following key: ns for P>0.05, * for P ≤ 0.05, ** for P ≤ 0.01 and *** for P ≤0.001.). See **Table IV-8** for the names of the genes.

	ZmCYCA1	ZmEXPB4	ZmIAA17	ZmIAA4	ZmASN1	ZmIVR2	ZmSUS1	ZmGAPDH
ZmCYCA1	***	**	ns	ns	ns	ns	ns	**
ZmEXPB4	0.73	***	ns	ns	ns	ns	ns	***
ZmIAA17	0.06	-0.17	***	*	ns	ns	ns	ns
ZmIAA4	-0.29	-0.46	0.58	***	*	ns	*	ns
ZmASN1	0.04	-0.15	0.34	0.63	***	ns	*	ns
ZmIVR2	0.25	0.33	-0.24	-0.17	0.33	***	ns	ns
ZmSUS1	-0.43	-0.45	0.07	0.60	0.61	0.26	***	ns
ZmGAPDH	0.75	0.86	-0.36	-0.43	0.06	0.45	-0.37	***

Table IV-10 Pairwise Spearman correlation coefficients between the expression of the selected genes and the ordinal variable expert lateral root class (1 for C, 2 for B and 3 for A). P-values are indicated using the following key: ns for P>0.05, * for P ≤ 0.05, ** for P ≤ 0.01 and *** for P ≤0.001. See **Table IV-8** for the names of the genes.

	Lateral root class	
ZmCYCA1	0.74	**
ZmEXPB4	0.75	**
ZmIAA17	0.03	ns
ZmIAA4	-0.48	ns
ZmASN1	-0.33	ns
ZmIVR2	-0.10	ns
ZmSUS1	-0.60	*
ZmGAPDH	0.61	*

2.5.3 Summary

- *Key results* We found a higher transcript abundance of glyceraldehyde-3-phosphate dehydrogenase (*ZmGADPH*), cyclin-A1 (*ZmCYCA1*) and expansin-B4 (*ZmEXPB4*) in fast-growing roots relatively to arrested roots. Expression levels of the cytosolic sucrose synthase-1 (*ZmSUS1*) were also ranked with the lateral root growth class, being higher in arrested roots.
- *Conclusions* We found experimental evidence for the co-expression of cyclin-A1 and expansin-B4 genes with one candidate gene related to carbon metabolism, the *ZmGADPH* coding for the glyceraldehyde-3-phosphate dehydrogenase. On the contrary, no other gene

candidates expected to be glucose induced showed a significant correlation with cell regulatory genes, found to be unregulated in fast-growing roots. Finally, no auxin responsive genes in relation to lateral growth classes could be clearly identified in this study.

Chapter references

Bingham I. J. (1998). Relationships between tissue sugar content, phloem import and lateral root initiation in wheat. *Physiol. Plant*. 103, 107–113.

Bret-Harte, M. S., and Silk, W. K. (1994). Nonvascular, Symplasmic Diffusion of Sucrose Cannot Satisfy the Carbon Demands of Growth in the Primary Root Tip of Zea mays L. *Plant Physiol*. 105, 19–33. doi:10.1104/pp.105.1.19.

Brouquisse, R. (1992). Asparagine metabolism and nitrogen distribution during protein degradation in sugar-starved root tips. *Planta* 188, 384–95.

Chevalier, C., Bourgeois, E., Just, D., and Raymond, P. (1996). Metabolic regulation of asparagine synthetase gene expression in maize (Zea mays L.) root tips. *Plant J*. 9, 1–11. Available at: http://www.ncbi.nlm.nih.gov/pubmed/8580967.

Cross, J. M., von Korff, M., Altmann, T., Bartzetko, L., Sulpice, R., Gibon, Y., *et al*. (2006). Variation of enzyme activities and metabolite levels in 24 *Arabidopsis* accessions growing in carbon-limited conditions. *Plant Physiol*. 142, 1574–1588. doi:10.1104/pp.106.086629.

Dehghan Nayeri, F. (2014). Identification of transcription factors linked to cell cycle regulation in *Arabidopsis*. *Plant Signal. Behav*. 9, e972864. doi:10.4161/15592316.2014.972864.

Dubrovsky, J. G., Doerner, P. W., Colón-Carmona, A., and Rost, T. L. (2000). Pericycle cell proliferation and lateral root initiation in *Arabidopsis*. *Plant Physiol*. 124, 1648–1657. doi:10.1104/pp.124.4.1648.

Dubrovsky, J. G., Gambetta, G. A., Hernández-Barrera, A., Shishkova, S., and González, I. (2006). Lateral root initiation in *Arabidopsis*: developmental window, spatial patterning, density and predictability. *Ann. Bot*. 97, 903–915. doi:10.1093/aob/mcj604.

Koch, K. E., Nolte, K. D., Duke, E. R., McCarty, D. R., and Avigne, W. T. (1992). Sugar Levels Modulate Differential Expression of Maize Sucrose Synthase Genes. *Plant Cell* 4, 59–69. doi:10.1105/tpc.4.1.59.

Koenker, R. (2015). Package " quantreg" . Quantile regression in R: a vignette.

Komsta, L., and Novomestky, F. (2015). Package " moments ". Moments, cumulants, skewness, kurtosis and related tests. Version 0.14.

Lin, Y., Zhang, C., Lan, H., Gao, S., Liu, H., Liu, J., *et al*. (2014). Validation of potential reference genes for qPCR in maize across abiotic stresses, hormone treatments, and tissue types. *PLoS One* 9. doi:10.1371/journal.pone.0095445.

Muller, B., Bourdais, G., Reidy, B., Bencivenni, C., Massonneau, A., Condamine, P., *et al*. (2006). Association of Specific Expansins with Growth in Maize Leaves Is Maintained under Environmental, Genetic, and Developmental Sources of Variation. *Plant Physiol*. 143, 278–290. doi:10.1104/pp.106.087494.

Oparka, K. J., Duckett, C. M., Prior, O. A. M., and Fisher, D. B. (1994). Real-time imaging of phloem unloading in the root tip of *Arabidopsis*. *Plant J*. 6, 759–766. doi:10.1046/j.1365-313X.1994.6050759.x.

Rice, D., Lee, Y., and Kende, H. (2002). Expression of ⎵ -Expansin and Expansin-Like Genes in. 130, 1396–1405. doi:10.1104/pp.008888.the.

Smeekens, S. (1998). Sugar regulation of gene expression in plants. *Curr*. *Opin*. *Plant Biol*. 1, 230–234. doi:10.1016/S1369-5266(98)80109-X.

Trouverie, J., Chateau-Joubert, S., Thévenot, C., Jacquemot, M. P., and Prioul, J. L. (2004). Regulation of vacuolar invertase by abscisic acid or glucose in leaves and roots from maize plantlets. *Planta* 219, 894–905. doi:10.1007/s00425-004-1289-3.

Wu, Y., Meeley, R. B., and Cosgrove, D. J. (2001). Analysis and expression of the α-expansin and β-expansin gene families in maize. *Plant Physiol*. 126, 222–232. doi:10.1104/pp.126.1.222.

Xu, J., Avigne, W., McCarty, D., and Koch, K. (1996). A Similar Dichotomy of Sugar Modulation and Developmental Expression Affects Both Paths of Sucrose Metabolism: Evidence from a Maize Invertase Gene Family. *Plant Cell* 8, 1209–1220. doi:10.1105/tpc.8.7.1209.

CHAPTER V. GENERAL DISCUSSION AND PERSPECTIVES

The objective of this work was to characterize the variations observable among the lateral roots of maize, taking into account different scales of analysis, from the root system to the cell level. We aimed at exploring the potential physiological, developmental and architectural factors influencing lateral root growth to unravel the endogenous origin of such root diversity.

The culture system used during the experiments (rhizotrons) aimed at maintaining a stable environment to limit any external influence on root growth. To maintain uniform conditions, the rhizotrons were placed in a growth chamber with controlled environment, filled uniformly with a soil substrate and watered daily with a nutrient solution (even during week-ends). Despite these precautions, we have systematically observed large variations in growth rates not only among individual lateral roots of a given root system but also along the lifetime of a given root. Consequently, we can assume that a large part of these measured variations are clear manifestations of the root developmental instability, providing the ideal conditions to study its intrinsic sources.

1 Lateral root growth variations: structured in time, random in space

In this study, a novel pipeline combining a dedicated image analysis system and statistical models was developed to explore the diversity of lateral root growth rate profiles in maize and pearl millet Basically, our approach relies on semi-Markov switching linear models (Guédon, 2003) to identify trends in the change in lateral growth rate with time, referred as 'growth patterns' and leading to the definition of lateral root growth classes. Lateral roots were then assigned to one of these classes based on their individual growth rate profiles, enabling a further analysis of individual growth variations at the population scale. To do so, it was necessary to record thousands of individual root growth profiles.

Two important aspects of lateral root growth variations were evidenced by this analysis. First, lateral root growth rate profiles appear to be structured in a limited number of 'growth trends' (three for the two studied cereal species in our control growth conditions) presenting similar growth trajectories. Although lateral roots of these two species presented differences in terms of absolute growth rates, growth rate profiles were structured in three classes with similar characteristics, i.e. roots with high and on average increasing growth rates and a long growth duration (named A); roots with low and decreasing growth rates ending up in early root arrest (named C) and, in between, roots with intermediate growth rates with a late growth arrest (named B). Second, the classification of lateral roots enabled to study the repartition of lateral root types along the primary root or 'branching pattern'. We found in a first step that the distance between successive lateral roots was not affected by the types of the shootward and rootward lateral roots that delimit it. We also found no local dependencies in the succession of lateral root types along the primary root, indicating that the branching pattern is random.

Lateral root growth variability has been repeatedly reported in various species, annuals, perenials, mono or dicots (Forde, 2009; Freixes *et al*., 2002; Pagès, 1995). However, such a variability has not been so far studied on the basis of growth rate profiles, but rather using morphological or anatomical features (Henry *et al*., 2016; Passot *et al*., 2016; Rebouillat *et al*., 2009; Varney *et al*., 1991). One advantage of our longitudinal approach is that, by modeling the intra-individual growth rate change, it enables the analysis of the between-individual root growth variations and their repartition in space. Moreover, this modeling approach provides a framework to explore the factors influencing the spatio-temporal structure of lateral root growth pattern (and thus to question the functional hypotheses associated with it).

However, the identified growth patterns may not be directly transposable to plants placed in other growth conditions, even less so to other plant species. First of all, the generality of growth patterns should be verified by applying SMS-LM to the considered data, and ensuring the resulting growth trends are similar (ideally plant-wise). Under this condition, differences in the structure of lateral root growth would translate into variations of the proportion and/or spatial repartition of lateral root classes, enabling quantitative comparisons. This condition was satisfied for instance when comparing *wild-type* and *rtcs* plants in our study. Otherwise, quantitative analyses would be hampered by the fact that trends are not comparable. In the latter case, only qualitative comparisons are suitable, as illustrated by the comparative study between the lateral root types of maize and pearl millet species presented in **Chapter III.**

Nevertheless, even if comparisons are only qualitative, the relative abundance of lateral root types was globally preserved among the different species considered in this work, with a majority of short roots and only a few long roots even if the absolute growth rates differed. This characteristic, non-uniform distribution has also been reported in several other species. For instance, the distribution of length in lateral roots of sunflower shows a marked skewness with a majority of small roots, a long tail of roots with increasing length and a length threshold above which growth cessation did not occur (Aguirrezabal and Tardieu, 1996). In oak, three groups of lateral roots were differentiated based on their sensitivity to defoliation (Willaume and Pagès, 2006). Similar skewed distributions were reported in other species (*e.g*. banana (Draye, 2002); pine tree (Wilcox, 1968) or even *Arabidopsis* (Chevalier *et al*., 2003)), suggesting the repartition of lateral roots into different types observed in this work might be a general rule across species.

The identification of such divergent growth patterns raises questions on the potential utility for the plant of these different lateral root growth classes. Each root type could have a preferential function in the root system (water uptake, acquisition of minerals with different soil mobility (Hodge, 2004; Barber, 1995) or even further branching) and imply a different metabolic cost for the plant. The existence of these types could be seen as a trade-off between the plant needs in terms of soil resources and the amount of carbohydrate resources from the aerial parts needed for root system construction. Testing these hypotheses requires to develop functional-structural root system models

coupling (i) the structuration of lateral root growth profiles into trends with (ii) the estimation of their metabolic cost and (iii) a model of soil structure in order to integrate the uptake functions associated to each root class.

Concerning the randomness and stationarity of the spatial repartition of lateral root types, it would be interesting to test whether it is a general feature or only a characteristic resulting from our homogeneous soil conditions. In particular, we can expect that the presence of nutrient patches induces a local root proliferation response (Drew, 1975; Hodge, 2006) and thus a disruption of the spatial randomness of root types. Finally, it should also be assessed whether this random branching pattern remain still observable in root systems developing in 3 dimensions using for instance X-ray scanner techniques. The importance of a random component in branching has already been evidenced in pioneering studies by relating it to the foraging efficiency of root systems as an optimal strategy to explore soil volume (Pagès, 2011). In this perspective, our approach provides a way to study the relationship between local soil conditions and positioning of the different root types in a quantitative way.

2 Exploring the origin of lateral root types

A significant effort has been dedicated in this PhD to study the processes at the origin of root growth diversity. More specifically: due to which factors and when in root development are these variations determined?

2.1 Lateral root fate is only partially determined before root emergence

Differences in apical root diameters were observed among root growth classes already at lateral root emergence, showing a clear ranking with fastest growing roots having on average the largest initial diameters, despite an important overlap between classes. An interpretation to this could be that roots emerging with larger diameters have more chances to elongate fast than thinner roots, meaning that the growth patterns are determined, at least partially, early in root development (even before emergence). In accordance with this hypothesis, we observed a high dispersion in the basal diameters of lateral root *primordia* within the unbranched zone of the root (**Figures IV-8** and **IV-9**), suggesting marked differences in the rate of development among individual *primordia*. Similar results have already been described in *Arabidopsis thaliana* (Dubrovsky *et al.*, 2006), tomato (Barlow and Adam, 1988), pea and fava bean (MacLeod and Thompson, 1979) and also in hydroponics grown maize (MacLeod and Thompson, 1979; MacLeod, 1990).

Differences in diameter at the lateral root *primordium* stage are likely to condition the diameter and growth rate at root emergence but do not seem enough to entirely determine lateral root fate. Indeed, our results show that the growth trajectories of two lateral roots with similar initial growth rate and diameter can diverge with time. At population scale, this indetermination is visible by the

significant overlap in initial growth rate and root diameter between roots with divergent growth trends (**Figure II-6**). Consequently, root fate does not appear as a characteristic that is completely predetermined but rather that emerges progressively throughout the life of a lateral root.

2.2 Lateral root growth variations are related to the cellular pattern in root apices

Root growth is confined to a relative small apical region specialized in the production of new cells and known as the root apical meristem (Ivanov and Dubrovsky, 2013). The analysis of cellular patterns in lateral root apices was one of the main axes of our work, with a particular focus on the determination of the number and size of root developmental zones and on the uncertainty concerning the limits between these zones. This task required a tool for the detection of objectively different zones based on the available root apical cell length profiles, using little biological assumptions. This led us to design a new segmentation method, based on multiple change-point models (Hawkins, 1976; Guédon, 2013, 2015ab), for the analysis of such profiles.

This model allowed to evidence that the differences between growth patterns are closely related to modulation in the developmental pattern at the cellular scale in the lateral root meristems. The meristem size ranked along with the growth classes, notably down to the frequent absence of proliferating cells in arrested roots. Meristem exhaustion has been reported in roots from other species presenting a determinate growth pattern, which can be either constitutive or environmentally induced (e.g. in primary roots of *Arabidopsis* under phosphorous deficiency (Dubrovsky, 1997; Shishkova *et al*., 2008)). Research on determinate roots have demonstrated that the maintenance of an active meristem is required for root growth (Rodriguez-Rodriguez *et al*., 2003; Sabatini *et al*., 2003) and that meristem exhaustion occurs when meristematic cells switch into a differentiation program leading to a gradual decrease in the number of meristematic cells until all cells become differentiated and no further growth is possible (Shishkova *et al*., 2008). Our results corroborate the view of a progressive meristem exhaustion since some arrested roots still presented an elongation zone when the division zone had already disappeared (**Figure III-6a**). Another piece of evidence comes from the identification of positive slopes in the mature zone of roots displaying slow or arrested growth (**Figure III-6b**).

Despite a variable number of developmental zones, a tight correlation between the length of division and elongation zones was observed in our set of growing roots, suggesting a strong coupling between the intensity of cell division and elongation processes all along the gradient of lateral root fates in maize. Another indirect evidence for this comes from our molecular analysis showing a tight and positive correlation between cyclin and expansin gene expression that could explain the actual correlation in terms of zone lengths. On the other hand, our results indicated meristematic cell length to be rather constant among roots of different growth types within a given genotype, and showed no correlation with meristem length, consistent with earlier results (Barlow

and Rathfelder, 1984). Under this assumption of cell length constancy, meristem size could be considered as a marker of the number of proliferating cells, linearly related to the growth rate according to the model of (Hof and Ying, 1964).

To investigate more precisely the relationship between root growth and meristem structure, new experiments could make use of our model to quantify the influence of the characteristics of zones in root meristems on root growth rate. This would require a precise monitoring of growth profiles, unfortunately lacking in this study. Alternatively, multiple change-points models could be applied with no major changes to other data (cell length profiles from other species, or tissues other than root epidermis). Ultimately, it is the dynamics of meristem development that should be at core of future studies to understand both the process of meristem exhaustion and the modulation of growth patterns. If some hypotheses on those processes have been elaborated based on our data, only a non-destructive monitoring of meristem length (e.g. (Bizet *et al.*, 2014)) could provide the necessary experimental evidence to confirm them.

In addition, our work allowed exploring a potential role of auxin in the regulation of cell developmental patterns via the characterization of maize genotypes with an impaired auxin signaling. The three more relevant results common for these mutants were (i) a significant increase in meristematic cell length, (ii) comparably enlarged root diameters and (iii) a relative preservation of the diversity of root types. A simple hypothesis to explain the increased root diameters would be an isotropic increase in the width of meristematic cells concurrent to the one in length (assuming the number of cell layers remains unchanged). If growth capacity is related to the number of meristematic cells, auxin mutants are expected to require longer (and wider) meristems to reach the same growth rate. This is consistent with the apical diameter profiles of growth classes observed in the case of *rtcs* mutant (**Figure II-18**), being increased by approximately 25% for this genotype compared to the *wild-type*. In contrast, auxin signaling does not seem to be involved in the determination of root types, since the proportion of root types found for *rtcs* mutant was similar to that of *wild-type* root systems. Moreover, lateral roots in this mutant showed a remarkable variation in the length of their growing zone. In conclusion, impairing auxin signaling altered the growth capacity of lateral root meristems, most probably by disturbing the equilibrium between cell division and elongation processes, but had little to no effect on the establishment of lateral root growth variations.

2.3 Carbohydrate supply emerges as an important factor for the determination of root growth variations

An important result of our study is the fact that the glucose concentration at the root apex exhibits a gradient following the ranking of growth patterns, ranging from maximal values reached systematically by fast-growing roots to minimal values corresponding to early-arrested roots. A more or less tight dependence of root elongation rate on carbohydrates availability has already been

reported in both primary (Freixes *et al*., 2002; Muller *et al*., 1998; Willaume and Pagès, 2011) and lateral roots (Freixes *et al*., 2002; Thaler and Pages, 1996; Willaume and Pagès, 2011) with some suspicion of temporal causality (Muller *et al*., 1998).

If concentration is considered as the balance between the input and the consumption, we can deduce that the rate of sugar arrival must also be much higher for fast-growing roots to compensate their higher rate of consumption associated to a faster generation of tissue. The allocation of plant assimilates to roots consequently emerges as an important factor that could explain variations in lateral root growth. Importantly, in a context where the pool of assimilates is limited as in the case of shaded plants, the maximal values of absolute growth rates of lateral roots were drastically reduced (as showed by the disappearance of the class with highest growth rate, see **Figure II-16**), as did the apical sugar content of the fastest growing roots (see **Figure IV-19**).

Proliferating and elongating cells require high amounts of energy for respiration, intense in growing root apices (Bidel *et al*., 2000), so the availability of carbohydrates might limit the number of these energy demanding units. In addition to their role as a fuel for respiration and growth, the stimulatory effect of carbohydrates in root growth could relate to their signaling functions in regulating gene expression (Smith and Stitt, 2007). There is evidence that carbohydrates act as a trigger of cell division regulatory genes (Riou-Khamlichi *et al*., 2000) and other genes involved in carbon metabolism (Koch *et al*., 1992) or organ development (Borisjuk *et al*., 2003; Koch, 2004). In that sense, we found experimental evidence for the co-expression of cyclin-A1 and expansin-B4 genes with one candidate gene related to carbon metabolism coding for a glyceraldehyde-3-phosphate dehydrogenase. On the contrary, no other gene candidates expected to be glucose induced showed a significant correlation with cell regulatory genes. Moreover, no sugar starvation gene markers could be associated with root growth arrest as we expected. This points out the need for new methods to understand the signaling role of carbohydrates (particularly, whether growth cessation is, or not, associated with sugar starvation), for instance via gene constructs allowing in vivo monitoring of sugar starvation during root deceleration. Such studies could be more easily done on the plant model *Arabidopsis thaliana*, where suitable genetic tools are far more developed (*e.g*. Feike *et al*., 2016).

Nevertheless, the observed variations in sugar content do not tell us the origin of the differences in sugar supply; in other words, why are the fastest growing roots receiving the largest part of sugar resources? A hypothesis could be that the structure of the vascular network acts as an important constraint for the transport of carbohydrates (mostly sucrose) (Pagès, 1995; Yang and Midmore, 2005). Indeed, a high correlation between vascular capacity and size of various shoot or root parts has been reported (Albrektson, 1984; Coutts, 1987) and also seen in the anatomical analysis of this study. This suggests that the size and number of vessels are determinant for assimilate supply, affecting the root growth, and in turn transport capacity, in a positive feedback loop manner. Such mechanism can be formalized using very basic rules (Yang and Midmore, 2005) and could

represent a way for the plant to favor the growth of its most contributing parts, within the limits of its global resource availability (Sprugel *et al*., 1991; Yang and Midmore, 2005).

3 Towards root system breeding through multi-scale phenotyping

Given the importance of root traits for improving the behavior of crops under low fertility conditions, root phenotyping appears as a major research challenge for the years to come. Our work supports the view that multiple scales are involved in the modulation of major root processes potentially related to nutrient efficiency and should therefore be considered in a breeding strategy. The methodological framework introduced in this thesis could be applied in such context to provide quantitative measurements on root features as diverse as growth pattern trends and proportions or meristematic zone lengths.

A lot of progress has been done in the automation of image acquisition for plant phenotyping, still automatic image processing currently remains a major bottleneck for most pipelines, even more so if multiple scales are involved. Substantial improvements also remain to be done in order to characterize soil structure, a necessary component to take root uptake functions into consideration. The integration of root characteristics at different scales (this study) together with representations of the soil environment is likely to require the use of functional-structural models. In this context, our spatio-temporal data could be suitable for calibration purposes on root development and open the way for the identification of key root traits (developmental, physiological or architectural) implied in the efficiency of plant root systems.

Chapter references

Aguirrezabal, L. A. N., and Tardieu, F. (1996). An architectural analysis of the elongation of field-grown sunflower root systems. Elements for modelling the effects of temperature and intercepted radiation. *J*. *Exp*. *Bot*. 47, 411–420. doi:10.1093/jxb/47.3.411.

Albrektson, A. (1984). Sapwood Basal Area and Needle Mass of Scots Pine (Pinus sylvestris L .) Trees in Central Sweden. *Forestry* 57, 35–43.

Barlow, P. W., and Adam, J. S. (1988). The position and growth of lateral roots on cultured root axes of tomato, Lycopersicon esculentum (Solanaceae). *Plant Syst*. *Evol*. 158, 141–154. doi:10.1007/BF00936340.

Barlow, P. W., and Rathfelder, E. L. (1984). Correlations Between the Dimensions of Different Zones of Grass Root Apices , and their Implications for Morphogenesis and Differentiation in Roots. *Ann*. *Bot*. 53, 249–260.

Bidel, L. P., Renault, P., Pagès, L., and Rivière, L. M. (2000). Mapping meristem respiration of Prunus persica (L.) Batsch seedlings: potential respiration of the meristems, O2 diffusional constraints and combined effects on root growth. *J*. *Exp*. *Bot*. 51, 755–768. doi:10.1093/jexbot/51.345.755.

Bizet, F., Hummel, I., and Bogeat-Triboulot, M.-B. (2014). Length and activity of the root apical meristem revealed in vivo by infrared imaging. *J. Exp. Bot.* 66, 1387–1395. doi:10.1093/jxb/eru488.

Borisjuk, L., Rolletschek, H., Wobus, U., and Weber, H. (2003). Differentiation of legume cotyledons as related to metabolic gradients and assimilate transport into seeds. *J. Exp. Bot.* 54, 503–512. doi:10.1093/jxb/erg051.

Chevalier, F., Pata, M., Nacry, P., Doumas, P., and Rossignol, M. (2003). Effects of phosphate availability on the root system architecture: large-scale analysis of the natural variation between *Arabidopsis* accessions. *Plant. Cell Environ.* 26, 1839–1850. doi:10.1046/j.1365-3040.2003.01100.x.

Coutts, M. P. (1987). Developmental processes in tree root systems. *Can. J. For. Res.* 17, 761–767.

Draye, X. (2002). Consequences of root growth kinetics and vascular structure on the distribution of lateral roots. *Plant, Cell Environ.* 25, 1463–1474. doi:10.1046/j.0016-8025.2002.00924.x.

Drew, M. C. (1975). Comparison of the effects of a localized supply of phosphate, nitrate, ammonium and potassium on the growth of the seminal root sytem, and the shoot, in barley. 479–490.

Dubrovsky, J. G. (1997). Determinate primary-root growth in seedlings of Sonoran Desert Cactaceae; its organization, cellular basis, and ecological significance. *Planta* 203, 85–92. doi:10.1007/s004250050168.

Dubrovsky, J. G., Gambetta, G. A., Hernández-Barrera, A., Shishkova, S., and González, I. (2006). Lateral root initiation in Arabidopsis: developmental window, spatial patterning, density and predictability. *Ann. Bot.* 97, 903–915. doi:10.1093/aob/mcj604.

Feike, D., Seung, D., Graf, A., Bischof, S., Ellick, T., Coiro, M., et al. (2016). The starch granule-associated protein EARLY STARVATION1 is required for the control of starch degradation in Arabidopsis thaliana leaves. *Plant Cell Adv.* 28, 1472–1489. doi:10.1105/tpc.16.00011.

Forde, B. G. (2009). Is it good noise? The role of developmental instability in the shaping of a root system. *J. Exp. Bot.* 60, 3989–4002. doi:10.1093/jxb/erp265.

Freixes, S., Thibaud, M.-C., Tardieu, F., and Muller, B. (2002). Root elongation and branching is related to local hexose concentration in Arabidopsis thaliana seedlings. *Plant, Cell Environ.* 25, 1357–1366. doi:10.1046/j.1365-3040.2002.00912.x.

Guédon, Y. (2003). Estimating Hidden Semi-Markov Chains From Discrete Sequences. *J. Comput. Graph. Stat.* 12, 604–639. doi:10.1198/1061860032030.

Henry, S., Divol, F., Bettembourg, M., Bureau, C., Guiderdoni, E., Périn, C., et al. (2016). Immunoprofiling of Rice Root Cortex Reveals Two Cortical Subdomains. *Front. Plant Sci.* 6, 1–9. doi:10.3389/fpls.2015.01139.

Hodge, A. (2006). Plastic plants and patchy soils. *J. Exp. Bot.* 57, 401–11. doi:10.1093/jxb/eri280.

Hof, J. V., and Ying, H.-K. (1964). Relationship Between the Duration of the Mitotic Cycle, the Rate of Cell Production and the Rate of Growth of Pisum Roots at Different Temperatures. *Cytologia (Tokyo).* 29, 399–406.

Ivanov, V. B., and Dubrovsky, J. G. (2013). Longitudinal zonation pattern in plant roots: Conflicts and solutions. *Trends Plant Sci.* 18, 237–243. doi:10.1016/j.tplants.2012.10.002.

Koch, K. (2004). Sucrose metabolism: Regulatory mechanisms and pivotal roles in sugar sensing

and plant development. *Curr*. *Opin*. *Plant Biol*. 7, 235–246. doi:10.1016/j.pbi.2004.03.014.

Koch, K. E., Nolte, K. D., Duke, E. R., McCarty, D. R., and Avigne, W. T. (1992). Sugar Levels Modulate Differential Expression of Maize Sucrose Synthase Genes. *Plant Cell* 4, 59–69. doi:10.1105/tpc.4.1.59.

MacLeod, R. D. (1990). Lateral Root Primordium inception in Zea mays. *Environ*. *Exp* 30, 225–234.

MacLeod, R. D., and Thompson, A. (1979). Development of lateral root primordia in Vicia faba, Pisum sativum, Zea mays and Phaseolus vulgaris: Rates of primordium formation and cell doubling times. *Ann*. *Bot*. 44, 435–449.

Muller, B., Stosser, M., and Tardieu, F. (1998). Spatial distributions of tissue expansion and cell division rates are related to irradiance and to sugar content in the growing zone of maize roots. *Plant, Cell Environ*. 21, 149–158. doi:10.1046/j.1365-3040.1998.00263.x.

Pagès, L. (1995). Growth patterns of the lateral roots of young oak (Quercus robur) tree seedlings Relationship with apical diameter. *New Phytol*. 130, 503–509. doi:doi: 10.1111/j.1469-8137.1995.tb04327.x.

Pagès, L. (2011). Links between root developmental traits and foraging performance. *Plant*. *Cell Environ*. 34, 1749–60. doi:10.1111/j.1365-3040.2011.02371.x.

Passot, S., Gnacko, F., Moukouanga, D., Lucas, M., Guyomarc'h, S., Moreno Ortega, B., et al. (2016). Characterization of Pearl Millet Root Architecture and Anatomy Reveals Three Types of Lateral Roots. *Front*. *Plant Sci*. 7, 1–11. doi:10.3389/fpls.2016.00829.

Rebouillat, J., Dievart, A., Verdeil, J. L., Escoute, J., Giese, G., Breitler, J. C., et al. (2009). Molecular genetics of rice root development. *Rice* 2, 15–34. doi:10.1007/s12284-008-9016-5.

Riou-Khamlichi, C., Menges, M., Healy, J. M., and Murray, J. a (2000). Sugar control of the plant cell cycle: differential regulation of Arabidopsis D-type cyclin gene expression. *Mol*. *Cell*. *Biol*. 20, 4513–21. doi:10.1128/MCB.20.13.4513-4521.2000.

Rodriguez-Rodriguez, J. F., Shishkova, S., Napsucialy-Mendivil, S., and Dubrovsky, J. G. (2003). Apical meristem organization and lack of establishment of the quiescent center in Cactaceae roots with determinate growth. *Planta* 217, 849–857. doi:10.1007/s00425-003-1055-y.

Sabatini, S., Heidstra, R., Wildwater, M., and Scheres, B. (2003). SCARECROW is involved in positioning the stem cell niche in the Arabidopsis root meristem. *Genes Dev*. 17, 354–358. doi:10.1101/gad.252503.354.

Shishkova, S., Rost, T. L., and Dubrovsky, J. G. (2008). Determinate root growth and meristem maintenance in angiosperms. *Ann*. *Bot*. 101, 319–340. doi:10.1093/aob/mcm251.

Smith, A. M., and Stitt, M. (2007). Coordination of carbon supply and plant growth. *Plant, Cell Environ*. 30, 1126–1149. doi:10.1111/j.1365-3040.2007.01708.x.

Sprugel, D., Hinckley, T., and Schaap, W. (1991). The Theory and Practice of Branch Autonomy. *Annu*. *Rev*. *Inc* 22, 309–334.

Thaler, P., and Pagès, L. (1996). Root apical diameter and root elongation rate of rubber seedlings (Hevea brasiliensis) show parallel responses to photoassimilate availability. *Physio* 97, 365–371.

Varney, G., Canny, M., Wang, X., and McCully, M. (1991). The branch roots of Zea. I. First Order Branches, Their Number, Sizes and Division into classes. *Ann*. *Bot*. 67, 357–364.

Wilcox, H. E. (1968). Morphological Studies of the Root of Red Pine, Pinus resinosa I. Growth Characteristics and Patterns of Branching. *Am. J. Bot.* 55, 247–254. doi:10.2307/2440459.

Willaume, M., and Pagès, L. (2006). How periodic growth pattern and source/sink relations affect root growth in oak tree seedlings. *J. Exp. Bot.* 57, 815–826. doi:10.1093/jxb/erj059.

Willaume, M., and Pagès, L. (2011). Correlated responses of root growth and sugar concentrations to various defoliation treatments and rhythmic shoot growth in oak tree seedlings (Quercus pubescens). *Ann. Bot.* 107, 653–662. doi:10.1093/aob/mcq270.

Yang, Z., and Midmore, D. J. (2005). Modelling plant resource allocation and growth partitioning in response to environmental heterogeneity. *Ecol. Modell.* 181, 59–77. doi:10.1016/j.ecolmodel.2004.06.023.